ESO ASTROPHYSICS SYMPOSIA



European
Southern
Observatory

A. P. Lobanov · J. A. Zensus
C. Cesarsky · P. J. Diamond
Editors

EXPLORING THE COSMIC FRONTIER

Astrophysical Instruments for the 21st Century

Springer



ESO ASTROPHYSICS SYMPOSIA
European Southern Observatory

Series Editor: Bruno Leibundgut

A.P. Lobanov J.A. Zensus C. Cesarsky
P.J. Diamond (Eds.)

Exploring the Cosmic Frontier

Astrophysical Instruments for the 21st Century

Springer

Volume Editors

Andrei P. Lobanov
J. Anton Zensus
Max-Planck-Institut für Radioastronomie
Auf dem Hügel 69
53121 Bonn, Germany

Phillip J. Diamond
Jodrell Bank Observatory
University of Manchester
Macclesfield
Cheshire SK11 9DL
United Kingdom

Catherine Cesarsky
European Southern Observatory
Karl-Schwarzschild-Str. 2
85748 Garching, Germany

Series Editor

Bruno Leibundgut
European Southern Observatory
Karl-Schwarzschild-Str. 2
85748 Garching
Germany

ISBN-10 3-540-39755-8 Springer Berlin Heidelberg New York
ISBN-13 978-3-540-39755-7 Springer Berlin Heidelberg New York

Library of Congress Control Number: 2006933138

This work is subject to copyright. All rights are reserved, whether the whole or part of the material is concerned, specifically the rights of translation, reprinting, reuse of illustrations, recitation, broadcasting, reproduction on microfilm or in any other way, and storage in data banks. Duplication of this publication or parts thereof is permitted only under the provisions of the German Copyright Law of September 9, 1965, in its current version, and permission for use must always be obtained from Springer. Violations are liable for prosecution under the German Copyright Law.

Springer is a part of Springer Science+Business Media
springer.com
© Springer-Verlag Berlin Heidelberg 2007

The use of general descriptive names, registered names, trademarks, etc. in this publication does not imply, even in the absence of a specific statement, that such names are exempt from the relevant protective laws and regulations and therefore free for general use.

Typesetting: by the authors and techbooks using a Springer LaTeX macro package
Cover design: Erich Krichner, Heidelberg

Printed on acid-free paper SPIN: 11839453 55/techbooks 5 4 3 2 1 0

Preface

In the coming decades, astrophysical science will benefit enormously from the construction and operation of several major international ground- and space-based facilities, such as ALMA, Herschel/Planck, and SKA in the far infrared to radio band, ELTs, JWST, and GAIA in the optical to near infrared regime, XEUS and Constellation-X in the X-ray, and GLAST in the Gamma-ray regime. These and other new instruments will change dramatically the entire landscape of observational astrophysics and the will become the cornerstones of astrophysical research in the 21st century. These new facilities will have a major impact in a wide range of scientific topics including the cosmological epoch of re-ionization, galactic dynamics and nuclear activity, stellar astronomy, extra-solar planets, gamma-ray bursts, X-ray binaries, and many others. Because these new facilities will each be addressing several of the key scientific problems, the synergies and coordination between them must be explored early on. An important step toward realizing this goal is to bring together leading scientists from the entire spectrum of astrophysical science, encouraging cross-field discussion and dialog to outline the most important directions of future research and to chart ways for achieving complementarity and cooperation between the various new astrophysical facilities.

From May 18 to 21, 2004, the Max-Planck-Society's Harnack-Haus in Dahlem, Berlin, hosted the international symposium "Exploring the Cosmic Frontier: Astrophysical Instruments for the 21st Century." The symposium was organized by the Max-Planck-Institut für Radioastronomie, endorsed by the International SKA Steering Committee. The European Southern Observatory, Max-Planck-Society, European Space Agency, and the EU Consortia RadioNet and OPTICON sponsored the meeting. The symposium in Berlin was dedicated to exploring the complementarity and synergies between different branches of astrophysical research, by presenting and discussing the fundamental scientific problems that will be addressed by major future astrophysical facilities in the next few decades. Over 160 scientists from more than 20 countries took part in the symposium and contributed actively to the presentations and working group discussions.

This book contains 70 papers from the meeting and is intended to give a snapshot, a lasting account of an evolving scientific discourse and interaction throughout our field of research. We especially thank all the contributors to this volume. We would like to express our sincere gratitude to all of the participants

for bringing and sharing their thoughts, ideas, and inspirations and thereby making the meeting in Berlin a success. Finally, we also thank all of those who contributed to the organizational effort, among them the members of the Scientific Advisory Committee, the Local Scientific Advisory Board, and the Event Coordination team.

Bonn, Garching, Jodrell Bank
March 2006

Andrei Lobanov
J. Anton Zensus
Catherine Cesarsky
Philip Diamond

Contents

Part I Future Astrophysical Facilities

Radio Astronomy Facilities
R.D. Ekers 3

Future Optical and Near-Infrared Facilities
R. Gilmozzi, M. Mountain, N. Panagia, P. Dierickx 19

The new 40-m Radiotelescope of OAN in Yebes
R. Bachiller and OAN Staff 35

Design of the Near-term Next Generation Space-VLBI Mission VSOP-2
H. Hirabayashi, Y. Murata, P.G. Edwards, Y. Asaki, N. Mochizuki, M. Inoue, T. Umemoto, S. Kameno, L.I. Gurvits, A.P. Lobanov 37

Synergies Between SKA and Other Future Telescopes
A. Lobanov 39

The Korean VLBI Network Project
H.-G. Kim, S.-T. Han, B.W. Sohn 41

Frequency Protection for the 21st Century
W. van Driel 43

SCUBA-2: A Large-Format CCD-Style Imager for Submillimeter Astronomy
M.D. Audley, W. Holland, D. Atkinson, M. Cliffe, M. Ellis, X. Gao, D. Gostick, T. Hodson, D. Kelly, M. MacIntosh, H. McGregor, D. Montgomery, I. Smith, I. Robson, K. Irwin, W. Duncan, R. Doriese, G. Hilton, C. Reintsema, J. Ullom, L. Vale, A. Walton, W. Parkes, C. Dunare, P. Ade, D. Bintley, F. Gannaway, C. Hunt, G. Pisano, R. Sudiwala, I. Walker, A. Woodcraft, M. Fich, M. Halpern, J. Kycia, D. Naylor, P. Bastien, G. Mitchell 45

The Large Millimeter Telescope
F.P. Schloerb, L. Carrasco, E. Brinks 47

An Overview of the Submillimeter Array Telescope
A. Peck, A. Schinckel, the SMA team 49

Tunable Heterodyne Receivers - A Promising Outlook for Future Mid-Infrared Interferometry
C. Straubmeier, R. Schieder, G. Sonnabend, D. Wirtz, V. Vetterle, M. Sornig, A. Eckart 51

ESPRIT – Exploratory Submillimeter sPace Radio Interferometric Telescope
W. Wild, L. Venema, J. Cernicharo on behalf of the ESPRIT *study team* . . 53

Fizeau Interferometry with the LBT Astronomy on the Way to ELTs
W. Gaessler, T.M. Herbst, R. Ragazzoni, A. Eckart, G. Weigelt, the LINC-NIRVANA team 55

MUSE: 3D Spectroscopy with Large Telescopes
A. Kelz, M.M. Roth, M. Steinmetz on behalf of the MUSE consortium . . . 57

Layer-Oriented MCAO Projects for 8-m Class Telescopes and Possible Scientific Outcome
M. Lombini, R. Ragazzoni, C. Arcidiacono, A. Baruffolo, G. Cresci, E. Diolaiti, R. Falomo, W. Gaessler, F. Mannucci, E. Vernet, J. Vernet, M. Xompero 59

Prospects for an Extremely Large Synthesis Array
A. Quirrenbach 61

Interferometry in the Near-Infrared: 1 Mas Resolution at the Wavelength of 1 Micron
G. Weigelt, Y. Balega, T. Beckert, T. Driebe, K.-H. Hofmann, K. Ohnaka, T. Preibisch, D. Schertl, M. Wittkowski 63

Electrical and Geometrical Characterization of the Silicon Flight Sensors of the GLAST/LAT Tracking System
M. Brigida, C. Favuzzi, P.G. Fusco, F. Gargano, N. Giglietto, F. Giordano, F. Loparco, B. Marangelli, M.N. Mazziotta, N. Mirizzi, S. Rainó, P. Spinelli, for the GLAST LAT Tracker Italian Collaboration . . 65

Environmental Testing of the GLAST Tracker Subsystem
M. Brigida, C. Favuzzi, P.G. Fusco, F. Gargano, N. Giglietto, F. Giordano, F. Loparco, B. Marangelli, M.N. Mazziotta, N. Mirizzi, S. Rainó and P. Spinelli, For The GLAST LAT Tracker Italian Collaboration 67

The Potential of a Large Cherenkov Array for Supersymmetry and Cosmology
E. Giraud, A. Falvard, J. Lavalle, S. Sajjad, G. Vasileiadis 69

MAGIC: First Observational Results and Perspectives for Future Developments
T. Hengstebeck, O. Kalekin, M. Merck, R. Mirzoyan, N. Pavel, T. Schweizer, M. Shayduk for the MAGIC Collaboration 71

LOBSTER - Astrophysics with Lobster Eye Telescopes
R. Hudec, L. Pina, A. Inneman, L. Sveda 73

Novel Light-Weight X-ray Optics for future X-ray Telescopes
R. Hudec, L. Pina, A. Inneman, V. Brožek 75

Science Prospects for the GLAST LAT
O. Reimer for the GLAST LAT Collaboration 77

Astrophysics with Astronomical Plate Archives
R. Hudec 79

Virtual Observatories and Access to Radio Interferometry Data
A.M.S. Richards, S.T. Garrington, P.A. Harrison, T.W.B. Muxlow, A.M. Stirling, N. Winstanley, M.G. Allen, B. Vollmer, T. Venturi, P. Lamb, R. Power, N.A. Walton, P. Padovani, the AVO and AstroGrid teams 81

Part II Fundamental Physics and Cosmology

Fundamental Physics with the SKA: Strong-Field Tests of Gravity Using Pulsars and Black Holes
M. Kramer 87

Measuring Variations in the Fundamental Constants with the SKA
S. Curran 91

ELT Observations of Supernovae at the Edge of the Universe
M.D. Valle, R. Gilmozzi, N. Panagia, J. Bergeron, P. Madau, J. Spyromilio, P. Dierickx 95

SKA and the Magnetic Universe
R. Beck, B. Gaensler, L. Feretti 103

SSF as a Manifestation of Protoobjects in the Dark Ages Epoch: Theory and Experiment
V.K. Dubrovich, A.T. Bajkova, V.B. Khaikin 109

Cosmic Ray Astrophysics with AMS-02
E. Lanciotti on behalf of the AMS collaboration 111

Studying the Nature of Dark Energy with Current and Future Instruments
T.H. Reiprich 113

Project ASTRAL: All-sky Space Telescope to Record Afterglow Locations
G. Tsarevsky, G. Bisnovaty-Kogan, A. Pozanenko, G.M. Beskin, S. Bondar, V. Rumyantsev 115

Part III High-redshift Universe, Galaxies, Galaxy Evolution

Overview of the Science Case for a 50–100 m Extremely Large Telescope
I. Hook, The OPTICON ELT Science Working Group 121

Distant Galaxies and Extremely Large Telescopes
M.N. Bremer, M.D. Lehnert 125

Extragalactic Science with the Allen Telescope Array
G.C. Bower 129

Spectral Aging in the Relic Radio Galaxy B2 0924+30
L. Gregorini, M. Jamrozy, U. Klein, K.-H. Mack, P. Parma 133

Study of Extragalactic Sources with Extended Radio Emission
M. Jamrozy, U. Klein, K.-H. Mack 135

The B3 VLA Sample at Low Frequencies: Results from a Survey at 74 MHz
K.-H. Mack, M. Vigotti, L. Gregorini, U. Klein, W. Tschager, R.T. Schilizzi, I.A.G. Snellen 137

Modeling the Faint Radio Population: The NanoJY Radio Sky
I. Prandoni, H.R. de Ruiter, P. Parma 139

Radio View of Merging Clusters of Galaxies
T. Venturi, S. Bardelli, D. Dallacasa, S. Giacintucci, P. Rao, E. Zucca . . . 141

Part IV AGN and Compact Objects

Active Galactic Nuclei at the Crossroads of Astrophysics
A. Lobanov, J.A. Zensus 147

New Frontiers in AGN Astrophysics: The X-ray Perspective
T. Boller, L. Gallo 163

Deep Radio Source Surveys with the SKA
K.I. Kellermann 167

e-VLBI... a Wide-field Imaging Instrument with Milliarcsecond Resolution & Microjy Sensitivity
M.A. Garrett 171

Results from Observations of AGNs with the H·E·S·S· Telescope System and Future Plans
M. Punch for the H·E·S·S· Collaboration 175

The Innermost Regions of AGN with Future mm-VLBI
I. Agudo, T.P. Krichbaum, U. Bach, A. Pagels, B.W. Sohn, D.A. Graham, A. Witzel, J.A. Zensus, J.L. Gómez, M. Bremer, M. Grewing 179

Probing the Gravitational Redshift Effect from the Relativistic Jets of Compact AGN
T.G. Arshakian 181

VLBA Surveys and Preparation of the "RADIOASTRON" Mission
A. Chuprikov, I. Guirin 183

The Radio Properties of Low Power BL Lacs
M. Giroletti, G. Giovannini 185

Probes of Jet-Disk Coupling in AGN from Combined VLBI and X-Ray Observations
M. Kadler, J.Kerp, E. Ros, K.A. Weaver, J.A. Zensus 187

Towards the Event Horizon: High Resolution VLBI Imaging of Nuclei of Active Galaxies
T.P. Krichbaum, D.A. Graham, A. Witzel, J.A. Zensus, A. Greve, M. Grewing, M. Bremer, S. Doeleman, R.B. Phillips, A.E.E. Rogers, H. Fagg, P. Strittmatter, L. Ziurys 189

Two-Component Model for the AGN Broad Line Region
L.Č. Popović 191

Part V ISM and Formation and Evolution of Stars

The Physics and Chemistry of High Mass Star Formation
T.L. Wilson 197

Building Complex Molecules During Star- and Planet Formation
E.F. van Dishoeck 201

GAIA: Composition, Formation and Evolution of Our Galaxy
G. Gilmore 205

Large–Scale Surveys with the Arecibo Multibeam System
P.F. Goldsmith 209

Preliminary Science Results from the SMA
A.B. Peck, the SMA Team 215

On the Relevance and Future of UV Astronomy
A.I.G. de Castro 219

Interrelations Between Strömgren and Vilnius Photometric Systems: An Improvement of Stellar Classification
N. Kaltcheva, J. Knude 223

HH 110 Proper Motions
R. López, A. Riera, R. Estalella, A.C. Raga 225

The Effect of the Galactic Gas Distribution on the Expected Cosmic Rays Spectrum
M. Mollá, M. Aguilar, J. Alcaraz, J. Berdugo, J. Casaus, C. Díaz, E. Lanciotti, C. Mañá, J. Marín, G. Martínez, C. Palomares, E. Sánchez, I. Sevilla, A.S. Torrentó 227

Exploring Star Formation in the Galactic Centre Region: From ISO to ALMA
F. Schuller, F. Bertoldi, M. Felli, K.M. Menten, A. Omont, L. Testi 229

Future Observations of Cosmic Masers
V. Slysh 231

Part VI Planets and Origins of Life

Detection and Characterization of Extra-Solar Planets: Future Space Missions
M.A.C. Perryman 237

Down to Earths, with OWL
O.R. Hainaut, F. Rahoui, R. Gilmozzi 253

High-Precision Radio Astrometry: The Search for Extrasolar Planets
J.C. Guirado, E. Ros 257

The CHEOPS Project: Characterizing Exoplanets by Opto-infrared Polarimetry and Spectroscopy
M. Feldt, R. Gratton, S. Hippler, H.M. Schmid, M. Turatto, R. Waters, T. Henning 261

Towards High-Precision Astrometry: Differential Delay Lines for PRIMA@VLTI
R. Launhardt, Th. Henning, D. Queloz, A. Quirrenbach 265

Author Index 267

List of Participants

Agudo, Ivan
Max-Planck-Institut für Radioastronomie, Auf dem Hügel 69, 53121 Bonn, Germany
Iagudo@mpifr-bonn.mpg.de

Alef, Walter
Max-Planck-Institut für Radioastronomie, Auf dem Hügel 69, 53121 Bonn, Germany
walef@mpifr-bonn.mpg.de

Andreani, Paola
INAF, Osservatorio Astronomico di Trieste, Via Tiepolo 11, 34131 Trieste, Italy
andreani@ts.astro.it

Anglada, Guillem
Instituto de Astrofísica de Andalucía (CSIC), Camino Bajo de Huetor 24, 18008 Granada, Spain
guillem@iaa.es

Arshakian, Tigran
Max-Planck-Institut für Radioastronomie, Auf dem Hügel 69, 53121 Bonn, Germany
tigar@mpifr-bonn.mpg.de

Audley, Michael
UK Astronomy Technology Centre, Royal Observatory, Blackford Hill, Edinburgh EH9 3HJ, UK
mda@roe.ac.uk

Baan, Willem
ASTRON, Houde Hoogeveensedijk 4, 7991 PD Dwingeloo, The Netherlands
baan@astron.nl

Bachiller, Rafael
Observatorio Astronómico Nacional, C/ Alfonso XII, 3, 28014 Madrid, Spain
r.bachiller@oan.es

Beck, Rainer
Max-Planck-Institut für Radioastronomie Auf dem Hügel 69, 53121 Bonn, Germany
rbeck@mpifr-bonn.mpg.de

Beckert, Thomas
Max-Planck-Institut für Radioastronomie, Auf dem Hügel 69, 53121 Bonn, Germany
tbeckert@mpifr-bonn.mpg.de

Beckwith, Steven
Space Telescope Science Institute, 3700 San Martin Drive, Baltimore, MD 21218, USA
svwb@stsci.edu

Bergeron, Jacqueline
Institut d'Astrophysique de Paris, 98bis Boulevard Arago, 75014 Paris, France
bergeron@iap.fr

Bertoldi, Frank
Max-Planck-Institut für Radioastronomie, Auf dem Hügel 69, 53121 Bonn, Germany
bertoldi@mpifr-bonn.mpg.de

Boller, Thomas
MPI für extraterrestrische Physik, Giessenbachstr., 85741 Garching, Germany
bol@xray.mpe.mpg.de

Bondi, Marco
Istituto di Radioastronomia, Via Gobetti 101, 40129 Bologna, Italy
bondi@ira.cnr.it

Booth, Roy S.
Onsala Space Observatory, 439 92 Onsala, Sweden
roy@oso.chalmers.se

Bower, Geoffrey
University of California, Berkeley, 601 Campbell Hall, Berkeley, CA 94720, USA
gbower@astro.berkeley.edu

Boyle, Brian J.
ATNF, PO Box 76, Epping, NSW 1710, Australia
brian.boyle@csiro.au

Bremer, Malcolm
University of Bristol, H.H. Wills Physics Laboratory, Tyndall Avenue, Bristol BS8 1TL, UK
m.bremer@bristol.ac.uk

Brinks, Elias
INAOE, Apdo. Postal 51 & 216, Puebla, Puebla 72000, Mexico
ebrinks@inaoep.mx

Britzen, Silke
Max-Planck-Institut für Radioastronomie, Auf dem Hügel 69, 53121 Bonn, Germany
sbritzen@mpifr-bonn.mpg.de

Burgarella, Denis
Observatoire Astronomique Marseille Provence — LAM, Traverse du siphon, B.P. 8, cedex 12, 13376 Marseille, France
denis.burgarella@oamp.fr

Butcher, Harvey
ASTRON, P.O. Box 2, 9301 KE Dwingeloo, The Netherlands
butcher@astron.nl

Cernicharo, José
DAMIR — CSIC, C/ Serrano 121, 28006 Madrid, Spain
cerni@damir.iem.csic.es

Cesarsky, Catherine
European Southern Observatory, Karl-Schwarzschild-Str. 2, 85748 Garching, Germany
ccesarsk@eso.org

Chuprikov, Andrey
Astro Space Center of P.N. Lebedev Physical Institute, 84/32 Profsoyuznaya street, 117997 Moscow, Russia
achupr@asc.rssi.ru

Colless, Matthew
Anglo-Australian Observatory, P.O. Box 296, Epping, NSW 1710, Australia
colless@aao.gov.au

Cotter, Garret
University of Oxford, Denys Wilkinson Building, Keble Road, Oxford OX1 3RH, UK
garret@astro.ox.ac.uk

Cox, Pierre
IRAM, 300 rue de la Piscine, 38406 St. Martin d'Heres, France
cox@iram.fr

Cuby, Jean-Gabriel
Observatoire Astronomique Marseille Provence — LAM Traverse du siphon, B.P. 8, cedex 12, 13376 Marseille, France
jean-gabriel.cuby@oamp.fr

Curran, Stephen
University of New South Wales, School of Physics, Sydney, NSW 2052, Australia
sjc@phys.unsw.edu.au

Curtef, Valentin
Max-Planck-Institut für Radioastronomie, Auf dem Hügel 69, 53121 Bonn, Germany
vcurtef@mpifr-bonn.mpg.de

Dallacasa, Daniele
Astronomy Department, Bologna University, Via Ranzani 1, 40127 Bologna, Italy
ddallaca@ira.cnr.it

Davies, John
UK Astronomy Technology Centre, Royal Observatory, Blackford Hill, Edinburgh EH9 3HJ, UK
jkd@roe.ac.uk

DeBoer, David
SETI Institute, 601 Campbell Hall, University of California, Berkeley, CA 94720, USA
ddeboer@seti.org

Della Valle, Massimo
Arcetri Astrophysical Observatory — INAD, Largo E. Fermi 5, 50125 Firenze, Italy
massimo@arcetri.astro.it

Dennefeld, Michel
Institut d'Astrophysique de Paris, 98bis Boulevard Arago, 75014 Paris, France
dennefel@iap.fr

Dettmar, Ralf-Jürgen
Astronomisches Institut, Ruhr-Universität Bochum, Universitätsstr. 150 / NA7, 44780 Bochum, Germany
dettmar@astro.rub.de

Diamond, Philip
Jodrell Bank Observatory, University of Manchester, Macclesfield, Cheshire SK11 9DL, UK
pdiamond@jb.man.ac.uk

Ekers, Ron
Australia Telescope National Facility, P.O. Box 76, Epping, NSW 1710, Australia
ron.ekers@csiro.au

Feldt, Markus
Max-Planck-Institut für Astronomie, Königstuhl 17, 69117 Heidelberg, Germany
mfeldt@mpia.de

Gaessler, Wolfgang
Max-Planck-Institut für Astronomie, Königstuhl 17, 69117 Heidelberg, Germany
gaessler@mpia.de

Gargano, Fabio
University and INFN Bari, Via Orabona 4, 70126 Bari, Italy
fabio.gargano@ba.infn.it

Garrett, Michael
Joint Institute for VLBI in Europe
P.O. Box 2, 7990 AA Dwingeloo,
The Netherlands
garrett@jive.nl

Gilmore, Gerry
Institute of Astronomy, Cambridge University, Madingley Road, Cambridge CB3 0HA, UK
gil@ast.cam.ac.uk

Gilmozzi, Roberto
European Southern Observatory,
Karl-Schwarzschild-Str. 2,
85748 Garching, Germany
rgilmozz@eso.org

Gimenez, Alvaro
ESA/ESTEC, Postbus 299, 2200 AG Noordwijk, The Netherlands
alvaro.gimenez@esa.int

Gioia, Isabella
Istituto di Radioastronomia, Via Gobetti 101, 40129 Bologna, Italy
gioia@ira.cnr.it

Giordano, Francesco
University and INFN Bari, Via Orabona 4, 70126 Bari, Italy
francesco.giordano@ba.infn.it

Giovannini, Gabriele
Dipartimento di Astronomia, Via Ranzani 1, 40127 Bologna, Italy
ggiovannini@ira.cnr.it

Giraud, Edmond
GAM, Bât. 12, Université Montpellier II, Place E. Bataillon, 34095 Montpellier, France
edmond.giraud@gamum2.in2p3.fr

Giroletti, Marcello
Istituto di Radioastronomia, Via Gobetti 101, 40129 Bologna, Italy
giroletti@ira.cnr.it

Goldsmith, Paul F.
Department of Astronomy, Cornell University, 522 Space Sciences Building,
Ithaca, NY 14853, USA
pfg@astro.cornell.edu

Gomez, José F.
LAEFF (INTA), Apartado 50727, 28080 Madrid, Spain
jfg@laeff.esa.es

Gomez, José L.
Instituto de Astrofísica de Andalucía (CSIC), Camino Bajo de Huetor 24, 18008 Granada, Spain
jlgomez@iaa.es

Gomez de Castro, Ana I.
Istituto de Astronomia y Geodesia, Fac. De CC Matematicas, Universidad Complutense de Madrid, 28040 Madrid, Spain
aig@mat.ucm.es

Gregorini, Loretta
Dept. of Physics, University of Bologna, Via Irnerio 46,40126 Bologna, Italy
gregorini@ira.cnr.it

Grewing, Michael
IRAM, 300 rue de la Piscine, 38406 St. Martin d'Heres, France
grewing@iram.fr

Guélin, Michel
IRAM, 300 rue de la Piscine, 38406 St. Martin d'Heres, France
guelin@iram.fr

Guirado, José Carlos
Universidad de Valencia,
Dr. Moliner 50, 46100 Burjassot,
Valencia, Spain
Jose.C.Guirado@uv.es

Gurvits, Leonid I.
Joint Institute for VLBI in Europe (JIVE),
P.O. Box 2, 7990 AA Dwingeloo,
The Netherlands
lgurvits@jive.nl

Hainaut, Olivier
European Southern Observatory,
Casilla 19001, Santiago 19, Chile
ohainaut@eso.org

Hartogh, Paul
Max-Planck-Institut für Aeronomie,
Max-Planck-Str. 2,
37191 Katlenburg-Lindau, Germany
hartogh@linmpi.mpg.de

Hasinger, Günther
MPI für extraterrestrische Physik,
Giessenbachstr., 85741 Garching,
Germany
ghasinger@mpe.mpg.de

Henning, Thomas
Max-Planck-Institut für Astronomie,
Königstuhl 17, 69117 Heidelberg,
Germany
henning@mpia-hd.mpg.de

Hofmann, Werner
MPI für Kernphysik, Postfach 10 39
80, 69029 Heidelberg, Germany
werner.hofmann@mpi-hd.mpg.de

Hook, Isobel
University of Oxford,
Denys Wilkinson Building,
Keble Road, Oxford OX1 3RH, UK
imh@astro.ox.ac.uk

Horns, Dieter
MPI für Kernphysik, Postfach 10 39
80, 69029 Heidelberg, Germany
Dieter.Horns@mpi-hd.mpg.de

Hudec, René
Astronomical Institute,
251 65 Ondrejov, Czech Republic
rhudec@asu.cas.cz

Jackson, Carole
CSIRO – ATNF, P.O. Box 76, Epping,
NSW 1710, Australia
Carole.Jackson@csiro.au

Jamrozy, Marek
Radioastronomisches Institut, Universität Bonn, Auf dem Hügel 71, 53121 Bonn, Germany
mjamrozy@astro.uni-bonn.de

Jonas, Justin
Hartebeesthoek Radio Astronomy Observatory, Rhodes University, P.O. Box 94, 6140 Grahamstown, South Africa
j.jonas@ru.ac.za

Junkes, Norbert
Max-Planck-Institut für Radioastronomie, Auf dem Hügel 69, 53121 Bonn, Germany
njunkes@mpifr-bonn.mpg.de

Kaltcheva, Nadejda
Dept. of Physics and Astronomy, University of Wisconsin Oshkosh, 800 Algoma Boulevard, Oshkosh, WI 54901-8644, USA
kaltchev@uwosh.edu

Kanbach, Gottfried
MPI für extraterrestrische Physik,
Giessenbachstr., 85741 Garching,
Germany
gok@mpe.mpg.de

Kellermann, Kenneth
National Radio Astronomy Observatory, 520 Edgemont Rd., Charlottesville, VA 22903, USA
kkellerm@nrao.edu

Kelz, Andreas
AIP, An der Sternwarte 16, 14482 Potsdam, Germany
akelz@aip.de

Kerp, Jürgen
Radioastronomisches Institut, Universität Bonn, Auf dem Hügel 71, 53121 Bonn, Germany
jkerp@astro.uni-bonn.de

Khaikin, Vladimir
Special Astrophysical Observatory, RAS, Pulkovskoe Shosse 65, 196140 St. Petersburg, Russia
vkh@brown.nord.nw.ru

Klare, Jens
FGAN e.V., Neuenahrer Str. 20
53343 Wachtberg, Germany
jklare@fgan.de

Kramer, Michael
Jodrell Bank Observatory, University of Manchester, Macclesfield, Cheshire SK11 9DL, UK
mkramer@jb.man.ac.uk

Krichbaum, Thomas
Max-Planck-Institut für Radioastronomie, Auf dem Hügel 69, 53121 Bonn, Germany
tkrichbaum@mpifr-bonn.mpg.de

Kudritzki, Rolf-Peter
Institute for Astronomy, University of Hawaii, 2680 Woodlawn Drive,Honolulu, HI 96822, USA
kud@ifa.hawaii.edu

Laing, Robert
European Southern Observatory, Karl-Schwarzschild-Str. 2,
85748 Garching, Germany
rlaing@eso.org

Lanciotti, Elisa
CIEMAT, Avenida Complutense 22, 28040 Madrid, Spain
Elisa.Lanciotti@ciemat.es

Launhardt, Ralf
Max-Planck-Institut für Astronomie, Königstuhl 17, 69117 Heidelberg, Germany
rl@mpia.de

Leedjärv, Laurits
Tartu Observatory, Tõravere, 61602 Tartumaa, Estonia
leed@aai.ee

Lehnert, Matthew
MPI für extraterrestrische Physik, Giessenbachstr., 85741 Garching, Germany
mlehnert@mpe.mpg.de

Leibundgut, Bruno
European Southern Observatory, Karl-Schwarzschild-Str. 2,
85748 Garching, Germany
bleibundgut@eso.org

Lilly, Simon
ETH , Hoenggerberg HPF G4.1, 8093 Zürich, Switzerland
simon.lilly@phys.ethz.ch

Lo, Fred K.Y.
National Radio Astronomy Observatory, 520 Edgemont Rd., Charlottesville, VA 22903, USA
flo@nrao.edu

Lobanov, Andrei
Max-Planck-Institut für Radioastronomie, Auf dem Hügel 69, 53121 Bonn, Germany
alobanov@mpifr-bonn.mpg.de

Lombini, Matteo
Osservatorio Astrofisica di Arcetri, Largo E. Fermi 5, 50125 Firenze, Italy
matteo@arcetri.astro.it

Lonsdale, Colin
MIT Haystack Observatory, Westford, MA 01886, USA
cjl@haystack.mit.edu

Lopez, Rosario
Dpto. Astronomia, Universidad de Barcelona, Diagonal 647, 08028 Barcelona, Spain
rosario@am.ub.es

Lorenzen, Dirk H.
Deutschlandfunk, Wildgansstr. 32c, 22145 Hamburg, Germany
Dlorenzen@Compuserve.com

Mack, Karl-Heinz
Istituto di Radioastronomia, Via Gobetti 101, 40129 Bologna, Italy
mack@ira.cnr.it

Marcaide, Jon
Universitat de Valencia, Departamento de Astronomia, Edificio de Investigacion, 46100 Burjassot, Spain
J.M.Marcaide@uv.es

Marti, Ivan
Universitat de Valencia, Departamento de Astronomia, Edificio de Investigacion, 46100 Burjassot, Spain
I.Marti-Vidal@uv.es

Mauersberger, Rainer
IRAM, Pico Veleta Observatory, Avda. Divina Pastora, 7 NC, 18012 Granada, Spain
mauers@iram.es

Melnick, Jorge
European Southern Observatory, Alonso de Cordova 3107, Santiago, Chile
jmelnick@eso.org

Mezger, Peter G.
Max-Planck-Institut für Radioastronomie, Auf dem Hügel 69, 53121 Bonn, Germany
pmezger@mpifr-bonn.mpg.de

Michalowski, Stefan
Organisation for Economic Co-operation And Development (OECD), 2 rue André Pascal, 75016 Paris, France
stefan.michalowski@oecd.org

Mollá, Mercedes
CIEMAT, Avda. Complutense 22, 28040 Madrid, Spain
mercedes.molla@ciemat.es

Monnet, Guy
European Southern Observatory, Karl-Schwarzschild-Str. 2, 85748 Garching, Germany
gmonnet@eso.org

Mould, Jeremy
NOAO, 950 N. Cherry Ave., Tucson, AZ 85719, USA
jrm@noao.edu

Osorio, Mayra
Instituto de Astrofísica de Andalucía (CSIC), Camino Bajo de Huetor 24, 18008 Granada, Spain
osorio@iaa.es

Parma, Paola
Istituto di Radioastronomia, Via Gobetti 101, 40129 Bologna, Italy
parma@ira.cnr.it

Pavel, Nikolaj A.
Humboldt University Berlin, Newtonstrasse15, 12489 Berlin, Germany
pavel@physik.hu-berlin.de

Peck, Alison
Harvard-Smithsonian CfA, SMA Project, 645 N. A'ohoku Pl, Hilo, HI 96720, USA
apeck@cfa.harvard.edu

Perryman, Michael
ESA / ESTEC, Keplerlaan 1, 2200 AG Noordwijk, The Netherlands
mperryma@rssd.esa.int

Popovic, Luka
Astronomical Observatory Belgrade, Volgina 7, 11160 Belgrade, Serbia
lpopovic@aip.de

Porcas, Richard
Max-Planck-Institut für Radioastronomie, Auf dem Hügel 69, 53121 Bonn, Germany
rporcas@mpifr-bonn.mpg.de

Prandoni, Isabella
Istituto di Radioastronomia, Via Gobetti 101, 40129 Bologna, Italy
prandoni@ira.cnr.it

Puget, Jean-Loup
Institut d'Astrophysique Spatiale, Université Paris-Sud, Bâtiment 121, 91405 Orsay Cedex, France
jean-loup.puget@ias.u-psud.fr

Punch, Michael
PCC / APC, Collége de France, 11 place Marcelin Berthelot, 75231 Paris Cedex 05, France
punch@in2p3.fr

Quirrenbach, Andreas
Sterrewacht Leiden, P.O. Box 9513, 2300 RA Leiden, The Netherlands
quirrenb@strw.leidenuniv.nl

Rawlings, Steve
University of Oxford, Astrophysics, Denys Wilkinson Building, Keble Road,
Oxford OX1 3RH, UK
sr@astro.ox.ac.uk

Reimer, Olaf
Institut für Theoretische Physik IV, Ruhr-Universität Bochum,
NB 7/68, 44797 Bochum, Germany
olr@tp4.rub.de

Reiprich, Thomas
Astronomisches Institut,
Universität Bonn, Auf dem Hügel 71, 53121 Bonn, Germany
reiprich@astro.uni-bonn.de

Richards, Anita M. S.
Jodrell Bank Observatory/AVO, University of Manchester, Macclesfield, Cheshire SK11 9DL, UK
amsr@jb.man.ac.uk

Ros, Eduardo
Max-Planck-Institut für Radioastronomie, Auf dem Hügel 69, 53121 Bonn, Germany
ros@mpifr-bonn.mpg.de

Sackett, Penny D.
Mt. Stromlo Observatory, Cotter Road, Weston, Canberra ACT 2611, Australia
director@mso.anu.edu.au

Sadler, Elaine
University of Sydney, School of Physics, Sydney, NSW 2006, Australia
ems@physics.usyd.edu.au

Salinari, Piero
INAF Arcetri Observatory, Largo E. Fermi 5, 50125 Firenze, Italy
salinari@arcetri.astro.it

Schilizzi, Richard
International SKA Project Office, c/o ASTRON, P.O. Box 3, 7990 AA Dwingeloo, The Netherlands
schilizzi@skatelescope.org

Schilling, Govert
Bloemendalsestraat 32, 3811 ES Amersfoort, The Netherlands
mail@govertschilling.nl

Schinckel, Antony
Harvard-Smithsonian CfA, SMA Project, 645 N. A'ohoku Pl, Hilo, HI 96720, USA
schinck@cfa.harvard.edu

Schuller, Frédéric
Max-Planck-Institut für Radioastronomie, Auf dem Hügel 69, 53121 Bonn, Germany
schuller@mpifr-bonn.mpg.de

Schutz, Bernhard F.
Max-Planck-Institut für Gravitationsphysik (Albert-Einstein-Institut), Am Mühlenberg 1, 14476 Potsdam, Germany
bernhard.schutz@aei.mpg.de

Schwartz, Rolf
Max-Planck-Institut für Radioastronomie, Auf dem Hügel 69, 53121 Bonn, Germany
rschwartz@mpifr-bonn.mpg.de

Schwope, Axel
Astrophysikalisches Institut Potsdam, An der Sternwarte 16, 14482 Potsdam, Germany
aschwope@iap.de

Seifahrt, Andreas
AIU, Friedrich-Schiller-Universität Jena, Schillergässchen 2, 07745 Jena, Germany
andreas@seifahrt.de

Shaver, Peter
European Southern Observatory, Karl-Schwarzschild-Str. 2, 85748 Garching, Germany
pshaver@eso.org

Sirey, Rowena
PPARC, Polaris House, North Star Avenue, Swindon SN25 1Q, UK
rowena.sirey@pparc.ac.uk

Slysh, Viacheslav
Astro Space Center of P.N. Lebedev Physical Institute, 84/32 Profsoyuznaya street, 117997 Moscow, Russia
vslysh@asc.rssi.ru

Sohn, Bong Won
Max-Planck-Institut für Radioastronomie, Auf dem Hügel 69, 53121 Bonn, Germany
bwsohn@mpifr-bonn.mpg.de

Stanghellini, Carlo
Istituto di Radioastronomia / CNR, Via Gobetti 101, 40129 Bologna, Italy
cstan@ira.cnr.it

Steinmetz, Matthias
Astrophysikalisches Institut Potsdam, An der Sternwarte 16, 14482 Potsdam, Germany
msteinmetz@aip.de

Storm, Jesper
Astrophysikalisches Institut Potsdam, An der Sternwarte 16, 14482 Potsdam, Germany
jstorm@aip.de

Strassmeier, Klaus G.
Astrophysikalisches Institut Potsdam, An der Sternwarte 16, 14482 Potsdam Germany
kstrassmeier@aip.de

Straubmeier, Christian
Universität zu Köln, Zülpicher Strasse 77, 50937 Köln, Germany
cstraubm@ph1.uni-koeln.de

Straumann, Ulrich
Universität Zürich, Winterthurerstr. 190, 8057 Zürich, Switzerland
strauman@physik.unizh.ch

Sunyaev, Rashid
MPI für Astrophysik, Karl-Schwarzschild-Str. 1, 85748 Garching, Germany
sunyaev@mpa-garching.mpg.de

Tascau, Oana
Bergische Universität Wuppertal, Vorm Holz 4, 42119 Wuppertal, Germany
andorada@yahoo.com

Torrelles, José-Maria
ICE(CSIC) — IEEC, C/ Gran Capita 2-4, 08034 Barcelona, Spain
torrelles@ieec.fcr.es

Tsarevsky, Gregory
ATNF, P.O. Box 76, Epping, NSW 1710, Australia
Gregory.Tsarevsky@atnf.csiro.au

Turon, Catherine
Observatoire de Paris, 5 Place Jules Janssen, 92195 Meudon Cedex, France
catherine.turon@obspm.fr

van Ardenne, Arnold
ASTRON, P.O. Box 2, 7990 AA Dwingeloo, The Netherlands
ardenne@astron.nl

van Dishoeck, Ewine F.
Leiden Observatory, P.O. Box 9513, 2300 RA Leiden, The Netherlands
ewine@strw.leidenuniv.nl

van Driel, Wim
Observatoire de Paris, 5 Place Jules Janssen, 92195 Meudon Cedex, France
wim.vandriel@obspm.fr

Venturi, Tiziana
Istituto di Radioastronomia / CNR, Via Gobetti 101, 40129 Bologna, Italy
tventuri@ira.cnr.it

Verdes-Montenegro, Lourdes
Instituto de Astrofísica de Andalucía (CSIC), Camino Bajo de Huetor s/n, 18008 Granada, Spain
lourdes@iaa.es

Vettolani, Giampaolo
INAF, Vialle del Parco Mellini 84, 00136 Roma, Italy
vettolani@inaf.it

Voss, Hauke
Max-Planck-Institut für Radioastronomie, Auf dem Hügel 69, 53121 Bonn, Germany
hvoss@mpifr-bonn.mpg.de

Watt, Graeme
PPARC, Polaris House, North Star Avenue, Swindon SN2 1SZ, UK
graeme.watt@pparc.ac.uk

Weber, Michael
Astrophysikalisches Institut Potsdam, An der Sternwarte 16, 14482 Potsdam, Germany
mweber@aip.de

Wiedemann, Günter
Hamburger Sternwarte, Gojenbergsweg 112, 21029 Hamburg, Germany
gwiedemann@hs.uni-hamburg.de

Wild, Wolfgang
SRON, P.O. Box 800, 9700 AV Groningen, The Netherlands
W.Wild@sron.rug.nl

Wilkinson, Peter
Jodrell Bank Observatory, University of Manchester, Macclesfield, Cheshire SK11 9DL, UK
pnw@jb.man.ac.uk

Wilson, Thomas L.
European Southern Observatory, Karl-Schwarzschild-Str. 2, 85748 Garching, Germany
twilson@eso.org

Wucknitz, Olaf
Universität Potsdam, Astrophysics, Am Neuen Palais 10, 14469 Potsdam, Germany
olaf@astro.physik.uni-potsdam.de

Zensus, J. Anton
Max-Planck-Institut für Radioastronomie, Auf dem Hügel 69, 53121 Bonn, Germany
azensus@mpifr-bonn.mpg.de

Exploring the Cosmic Frontier: Astrophysical Instruments for the 21st Century

Scientific Organizing Committee:

Steven Beckwith, Roy Booth, Chris Carilli, Catherine Cesarsky (co-chair), Philip Diamond (co-chair), Reinhard Genzel, Gerry Gilmore, Roberto Gilmozzi, Alvaro Gimenez, Fred K.Y. Lo, Andrei Lobanov (secretary), John Mather, Ewine van Dishoeck, Anton Zensus (chair).

Local Scientific Advisory Board:

Karsten Danzmann, Ralf-Jürgen Dettmar, Andreas Eckart, Guenther Hasinger, Werner Hofmann, Karl Menten, Thomas Henning, Sami Solanki, Klaus Strassmeier, Hans-Walter Rix, Gerd Weigelt.

Review Talks:

Radio Astronomy	Ron Ekers
Millimeter and Submillimeter Astronomy	Jose Cernicharo
Optical Astronomy	Roberto Gilmozzi
High-Energy Astronomy	Guenther Hasinger
Gravitational Wave Astronomy	Bernard Schutz
Fundamental Physics and Cosmology	Steve Rawlings
High-redshift Universe, Galaxies, and Galaxy Evolution	Simon Lilly
CMB and Galaxy Clusters	Rashid Sunyaev
AGN and Compact Objects	Anton Zensus
ISM and Star Formation	Thomas Henning
Planets and Origins of Life	Michael Perryman

Working Groups:

I. Fundamental Physics and Cosmology	Jean-Loup Puget
II. High-redshift Universe,Galaxies, and Galaxy Evolution	Elaine Sadler
III. AGN and Compact Objects	Robert Laing
IV. ISM, Stars, and Planets	Steven Beckwith



Part I

Future Astrophysical Facilities

Radio Astronomy Facilities

R.D. Ekers

ATNF, CSIRO, PO Box 76, Epping, NW, 2121, Australia

Abstract. Five decades ago, astronomers finally broke free of the boundaries of light when a new science, radio astronomy, was born. This new way of 'seeing' rapidly uncovered a range of unexpected objects in the cosmos. This was our first view of the non-thermal universe, and our first un obscured view of the universe. In its short life, radio astronomy has had an unequaled record of discovery, including four Nobel prizes: Big-Bang radiation, neutron stars, aperture synthesis and gravitational radiation. New technologies now make it possible to construct new and upgraded radio wavelength arrays which will provide a powerful new generation of facilities. Radio telescopes such as SKA and the upgraded VLA will have orders of magnitude greater sensitivity than existing facilities. They will be able to study thermal and non-thermal emission from a wide range of astrophysical phenomena throughout the universe as well as greatly extending the range of unique science accessible at radio wavelengths.

1 Astronomy at Radio Wave Lengths

1.1 The Exponential Growth of Radio Telescope Sensitivity

It is well known that most scientific advances follow technical innovation, Harwit [1]. De Solla Price [2], had also reached this conclusion from his application of quantitative measurement to the progress of science. His analysis also showed that the normal mode of growth of science is exponential and he gave examples from many areas. Moore's Law, describing the 18 month doubling of transistor density on semiconductor chips, is a recent example. A plot of the continuum sensitivity of telescopes used for radioastronomy shows this exponential character (Fig. 1) with an increase in sensitivity of 10^5 since 1940, doubling every three years. To maintain the extraordinary momentum of discovery of the last few decades a very large new radio telescope will be needed in the next decade.

1.2 The 3 Nobel Prizes in Radio Astronomy

This exponential development of radio astronomical instrumentation has generated an impressive list of discoveries with three of the five Nobel prizes awarded for discoveries in astrophysics coming directly from radio astronomy.

1. Cosmic microwave background radiation (1965); Nobel prize awarded to Penzias and Wilson, Bell Telephone Labs, for this technology driven serendipitous discovery.

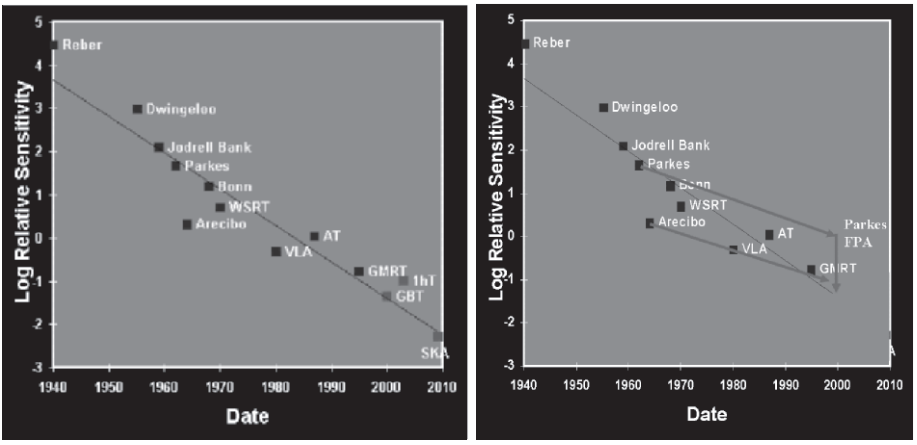


Fig. 1. (a) Radio telescope sensitivity; (b) Upgrade examples

2. Discovery of neutron stars (1974) through their radio pulsations (pulsars) by Jocelyn Bell and Tony Hewish. Another technology enabled serendipitous discovery. This Nobel prize was shared with Sir Martin Ryle for the development of the aperture synthesis technique which has been the basis for all high resolution imaging in radio astronomy.

3. Verification of Einstein's prediction of gravitational radiation (1993); Nobel prize to Taylor and Hulse using Arecibo to make precise time measurements of a binary pulsar to test the theoretical prediction of General Relativity.

1.3 Why has Radio Astronomy had So Much Impact?

The fraction of the energy output in the radio wavelength range of the electromagnetic spectrum is negligibly small but radio waves are easy to generate and they propagate with little absorption so provide unique information about the Universe. Moreover, radio observations probe a wide range of conditions - from dense gases to dilute, highly relativistic plasmas - are sensitive to magnetic fields, and yet are not affected by absorption from dust. The fundamental element hydrogen has a key transition at centimetre wavelengths (the 21-cm hyperfine transition).

- Radio astronomy provided the first evidence of non-thermal processes in astronomy.
- The discovery of the galactic nuclei and quasars drove the paradigm shift to gravitational astrophysics, black holes and AGNs .
- Radio galaxies and quasars are easily seen at high red shift and they dominate radio catalogues. The counts of these radio sources had a profound impact on cosmology giving the first evidence for strong cosmic evolution.

- The long radio wavelengths and benign atmosphere made it possible to build interferometers with very long baselines providing the highest angular resolution in astronomy.
- The low opacity has let us probe regions deep in the centers of galaxies which are often highly obscured by dust at optical and even infrared wavelengths.
- Observations of pulsars have been exploited to study some of the most extreme conditions known, e.g. the strong gravitational fields in binary pulsars.
- Finally, the microwave band is well suited to long distance communications and so is one of the most interesting wavelength for SETI searches.

1.4 Discoveries in Radio Astronomy

Radio telescopes have produced a stream of discoveries including an unusually high fraction which are serendipitous (shown in bold in the following compilation). A large fraction of these discoveries have been enabled by the largest telescopes at the time.

- **Non-thermal emission from astrophysical processes**
- **Quasars and radio galaxies**
- 21cm line of atomic hydrogen
- **Cosmological evolution required to explain steep slope of radio source counts**
- **Mercury and Venus spin rates**
- **Cosmic Microwave Background**
- **Masers and megamasers**
- Confirmation of General Relativity by time delay and bending
- **Pulsars**
- Interstellar molecules and galactic molecular clouds
- **First evidence for the need for dark matter in spiral galaxies from the 21cm HI rotation curves**
- **Superluminal motions of the jets in radio galaxies**
- Gravitational radiation from binary pulsar
- Gravitational lenses
- First extra-solar planetary system
- Mass of the black hole in NGC4258 using H_2O megamaser emission
- Size of GRB fireball
- Structure in Cosmic Microwave Background power spectrum

2 Impact of New Technology

2.1 Quantum v Classical

At radio wavelengths the relevant technology applies to the classical not the quantum limit. The number of photons per state is so high that quantum effects can be ignored and the signal streams behave classically. The ability to split signal streams with no loss in S/N leads to a big advantage in arraying technology

since interference can be measured simultaneously between all combinations of antennas. Wave-fronts can be recorded digitally and stored before detection so the whole imaging process (including detection) can be moved into software. E.g. self calibration is the exact equivalent of adaptive optics but doesn't have to be done in real time.

At these long wavelengths the telescopes are always operated at the diffraction limit. The phase stability is sufficient to make long coherent integration possible, and to make it possible to measure interference patterns between independent telescopes at large separation (VLBI).

2.2 Commercial Drivers for Technology

The advances described by Moore's Law are directly applicable to radio telescope design. MMIC (large scale integrated circuit) technology allows cheap duplication of complex circuits. This technology is driven by commercial applications such as mobile radio communications technology. Wide band optical fibre communications are becoming ubiquitous and can be used for connected telescope interferometry with wide bandwidth. The R&D needed to design new technology telescopes at radio wavelengths is directly relevant to the broader S&T research priorities in most countries today.

2.3 Radio Frequency Interference (RFI)

Ironically, the very developments in communications that drive Moore's Law and make these radio telescopes possible also generate radio interference at levels far in excess of the weak signals detectable with the next generation of telescopes. The future of observations with high sensitivity will depend on our ability to mitigate against interference but I am optimistic that a combination of adaptive cancellation, regulation and geographic protection will let us access even the faint red shifted HI signals from the early universe [3].

2.4 Conclusion

The combination of the classical signal properties and the MMIC technology generates totally new opportunities in which large dishes can be replaced by arrays of smaller elements. This not only delivers imaging capability but dramatically reduces costs of the collecting area. This is the technology driver for the ATA and SKA. A large FoV is physically easy at these long wavelength and is mainly dependent on the signal processing capability, so lets us increase FoV at the Moore's Law rate.

3 Science Opportunities

3.1 New Parameter Space at Radio Wavelengths

Radio telescopes do not have much new parameter space to explore because angular, spectral temporal resolution and polarization parameters have all been

probed at most wavelengths with the current generation of radio telescopes. However, future radio telescopes and in particular the SKA will greatly enlarge known parameter space by: i) a much greater sensitivity, over a very wide range of angular resolutions; ii) a much larger instantaneous field-of-view; iii) the potential of multiple, independently steerable beams. The sensitivity and sky coverage advances combine to provide a major step forward compared with current instruments: the volume of space accessible will be enormously increased - and hence the chances of finding intrinsically rare objects in large scale surveys will be much enhanced.

One intriguing expansion into new parameter space is negative time! See Sect. 9.4.

3.2 SKA Key Science Projects

The product of all the astronomy touched by radio, and all the opportunities opened up by the proposed new facilities, is too large to cover in this talk so I will illustrate the opportunities by describing a few of the experiments using some of the proposed facilities in the following Key Science Projects which were identified at a recent SKA workshop in Leiden [4].

- Strong Field Tests of Gravity Using Pulsars and Black Holes
- Probing the Dark Ages
- The Origin and Evolution of Cosmic magnetism
- The Cradle of Life
- The Evolution of Galaxies and Large Scale Structure

I have confined this talk to cm and metre wavelengths. Exciting developments at mm and sub-mm wavelengths are covered by other speakers.

3.3 Exploring the Unknown

The scientific challenges discussed in this meeting are today's problems – will they still be the outstanding problems that will confront astronomers in the period 2020–2050 and beyond, when the next generation of telescopes are operating? If history is any example, the excitement will not be in the old questions which are answered, but the new questions which will be raised by the new types of observations it will permit. We now plan telescopes which will be a tool for as-yet-unborn users and this realization places an onus on its designers to allow for the exploration of the unknown.

4 Future Facilities

4.1 Big Dishes or Arrays

There are major differences in implementation for the two approaches. A single dish uses optics to combine the analog signal (wave front) at the focus whereas

a modern aperture synthesis telescope uses digital signal processing. This difference leads to a very big shift in cost between mechanical structures for a big dish and computers for an aperture plane array. These two cost drivers have a very different time dependence, with the decreasing cost of digital processing shifting the most cost effective designs from big dishes to arrays. At higher frequencies the increased cost contribution of the lowest noise receivers and the cost of the backend signal processing for the larger bandwidth, shift the balance back to arrays with larger dish size. An analysis by Weinreb & D'Addario [5] shows that the optimum centimetre telescope in 2010 will be an array of 8m dishes.

There is an equivalence between focal plane arrays and aperture plane arrays. For a given number of receiver elements these two approaches are exactly equivalent for contiguous aperture. However, achieving the maximum compactness without either shadowing or geometric projection losses is only possible if the aperture plane array is on a tilting platform. For unfilled aperture arrays the synthesis approach trades resolution for brightness sensitivity.

4.2 Mass-produced Parabolas: The Allen Telescope Array

The Allen Telescope Array (ATA) being built by the SETI Institute and UC Berkeley is a modern example of an aperture plane array with 350 x 6.1 m parabolic antennas giving aperture synthesis capability with a very large primary beam (2°.5 field of view at 1.4 GHz) and the equivalent of a 100 m aperture. Taking advantage of modern electronics and wide band optical communication it will cover 0.5-11 GHz and generate 4 simultaneous beams. The planned completion date is 2005.

5 Sensitivity

The sensitivity of the future telescopes, and in particular the SKA, means that for the first time many objects which dominate the science done at other wavebands (stars, galaxies, star forming regions, proto-galaxies, galaxy clusters) become readily observed at radio wavelengths. The EVLA and SKA will be leading members of a complementary group of next-generation photon collectors including: ground-based optical telescopes in the 30–50 m class; the JWST (near- and mid-IR); ALMA (mm- and sub-mm wave); next-generation X-ray and gamma-ray observatories (XEUS; Constellation-X; GLAST). All of these will provide imaging information on the scale 0.1 arcsec or better and all will provide unique views of the universe.

5.1 Faint Radio Source Population

At the high radio flux levels in catalogues such as 3C, (Fig. 2), the radio sky is dominated by radio galaxies and quasars which are so bright in the radio that they can be seen at any redshift. Extragalactic continuum radio astronomy was very much the domain of the AGN and observations of the same objects at

other wavebands was often difficult because they were so faint. As surveys went fainter, e.g. the B2 catalogue, the average redshift stayed about the same but the fraction of low luminosity radio galaxies increased. Going even deeper, the radio galaxies and quasars start to run out and the average redshift starts to decrease as the nearby normal galaxies are detected. Towards the flux limit of the VLA (Kellermann - this symposium) the population of normal star forming galaxies starts to dominate.

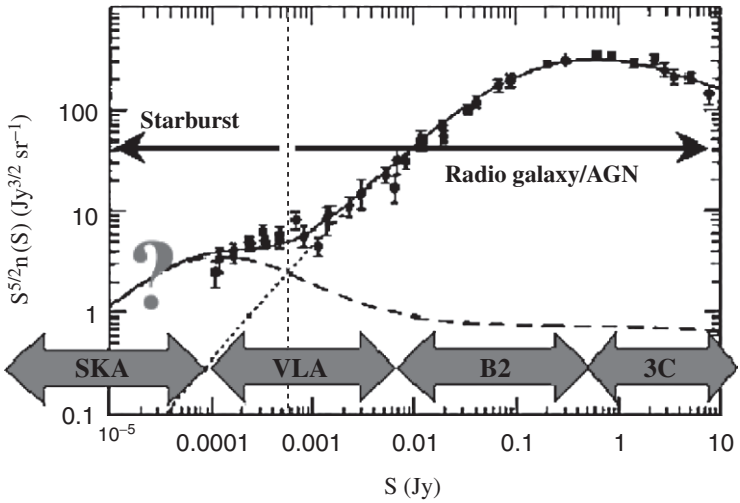


Fig. 2. Radio source counts

5.2 Star Formation and the Far Infra-Red - Radio Continuum Correlation

The radio continuum emission from normal galaxies is an excellent tracer of star formation [6] and it is unaffected by dust absorption. The connection between the diffuse continuum radio emission in the disk of a galaxy and its star formation rate is a result of the FIR-radio continuum correlation discovered serendipitously by Dickey & Salpeter [7] while searching for hydrogen gas in the Hercules cluster of galaxies. They found that the 60 μm far infra-red flux measured, by the then new IRAS satellite, was strongly correlated with the radio continuum emission from the cosmic ray electrons. A broad correlation is to be expected on the grounds that galaxies dominated by star formation will heat dust, making it radiate in the far infra-red, and this star formation also results in supernovae whose remnants will accelerate cosmic rays which produce synchrotron radio emission. However, it is the tightness of the correlation, still not satisfactorily explained, that makes the radio continuum such an excellent measure of the star formation rate.

5.3 The Micro Jansky Sky

It is interesting to note that, just as for the Hubble deep field, a radio continuum image at micro Jansky sensitivity - is dominated by normal galaxies - the radio galaxies and quasars have already all been seen at higher flux levels out to the beginning of the universe. Imaging normal galaxies at high z is a basic goal of the higher sensitivity and it will be possible to make radio images of star forming galaxies seen at other wavebands out to redshifts of at least 4 with the SKA. These radio observations can be applied to galaxies in the early universe now accessible through the Hubble Space Telescope (HST) and, later in the decade, through the New Generation Space Telescope (NGST) and ALMA.

By combining sub-mm and cm observations, Carilli [8] has been able to use the far infra-red - radio correlation to obtain radiometric redshifts for starburst galaxies in the early universe.

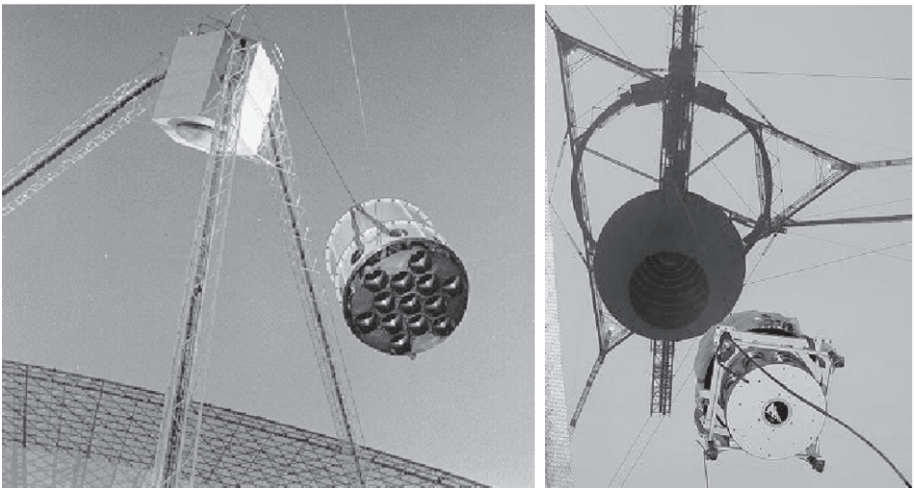


Fig. 3. (a) Installing the Parkes 21cm Multibeam Receiver (b) Installing Arecibo Multibeam (ALFA)

5.4 The Origin and Evolution of Cosmic Magnetism

Radio astronomy is uniquely placed in its capability to study magnetic fields at large distances, through studies of Faraday rotation, polarized synchrotron emission and the Zeeman effect. Through an all-sky continuum survey, a telescope with the sensitivity of the SKA could measure tens of millions rotation measures of polarized extragalactic sources. The sheer weight of statistics in these data, combined with deep polarimetric observations of nearby galaxies and clusters, would allow us to completely characterize the evolution of magnetic fields in galaxies and clusters from redshifts $z > 3$ to the present.

6 Field of View (FoV)

6.1 Focal Plane Arrays

A number of big single dishes are increasing their FoV by using focal plane arrays. Parkes, Jodrell Bank and Arecibo all now have 21 cm arrays as do many of the mm and sub-mm telescopes (IRAM, JCMT) (Fig. 3). The new 100 m GBT which is just being brought into operation in Green Bank, West Virginia, will have a 64 pixel bolometer array operating at 3 mm.

6.2 The Aperture Arrays (THEA and LOFAR)

In the extreme aperture plane array with element size comparable to a wavelength it is possible, with no moving parts, to electronically steer beams to any part of the sky. It is also possible to generate simultaneous independent beams anywhere in the sky.

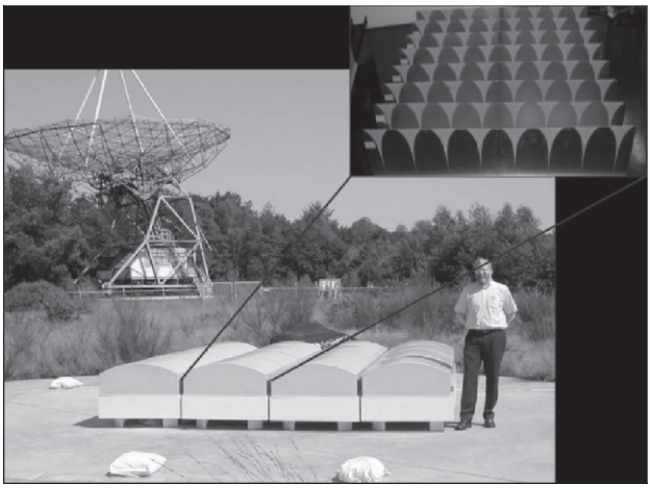


Fig. 4. NFRA phased array with director Harvey Butcher and the Dwingeloo 25m dish in the background

The Netherlands have now produced a pure phased array with significant collecting area and no moving parts. (Fig. 4). The juxtaposition of the 25m dish and the phased array nicely illustrates 50 years of technology development. This technology is particularly effective at lower frequencies and will be exploited in the LOFAR array working in the 15–200 MHz range.

6.3 Probing the Dark Ages

By the end of this decade one of the biggest questions remaining in astronomy will be the state of the Universe when the neutral hydrogen which recombined

after the Big Bang is being re-ionized by the first sources of ionizing radiation. This epoch of the Universe is totally opaque to optical radiation but can be probed by the 21-cm H line redshifted to the hundred MHz frequency range accessible by LOFAR. The first structures will appear as inhomogeneities in the primordial hydrogen, heated by infalling gas or the first generation of stars and quasars. A patchwork of either 21-cm emission or absorption against the cosmic background radiation will result. This structure and its evolution with z will look completely different for different re-ionization sources. A large population of low mass stars will be completely different from a small number of QSOs. For $z \sim 6$ we expect to see a growing 'cosmic web' of neutral hydrogen and galaxy halos forming and evolving (e.g. [9,10]). A radio telescope with a square kilometre of collecting area operating in the 100–200 MHz frequency range will have the sensitivity to detect and study this web in HI emission!

But the FM radio transmission band corresponds to HI at redshift = 10–11 so this will not be accessible from most countries and it will be essential to identify and protect some regions on Earth which are protected for radio astronomy. The OECD Global Science Forum has set up a Task Force to study this issue [11].

6.4 Even More FoV!

Because a radio wavelength is long, a large FoV is natural but changing technology may enable even greater increases. The SKA design goal has specified a FoV of at least $1\,\mathrm{deg}^2$ at a wavelength of 21 cm. In some concepts actively being pursued this may rise to as much as $100\,\mathrm{deg}^2$ or more.

Phased arrays make total FoV a signal processing rather than a physical limitation so the FoV becomes limited only by the cost of the signal transport and processing and it can expand with Moore's Law! However, aperture phased arrays are still expensive at higher frequencies but phased arrays in the focal planes of the elements of an array of dishes provide an intermediate solution with acceptable cost. $100\,\mathrm{deg}^2$ FoV at 1 GHz is possible now!

7 The Evolution of Galaxies and Large Scale Structure

With the SKA sensitivity it will be possible to detect typical galaxies at redshift z = 3 via 21 cm emission. The cosmic history of neutral hydrogen is a critical ingredient of galaxy evolution about which almost nothing is presently known. An HI emission-line survey is able to map out galaxies independently of dust extinction, with one additional advantage: once the galaxy has been located on the sky, the observed wavelength of the emission line automatically provides an accurate redshift, locating the object's position in the three-dimensional cosmic web.

Simulations indicate that with a wide enough field-of-view ($> 10\,\mathrm{deg}^2$) the SKA can survey the entire visible sky in a year of operation, locating a billion HI emission galaxies over a vast volume stretching to redshift $z = 1.5$.

The result would be the most accurate measurement of the clustering pattern of galaxies ever achieved, testing theoretical models for the growth of structure in the Universe and pinpointing the cosmological parameters (in conjunction with Cosmic Microwave Background data from the Planck satellite). For example, this survey would permit an accurate quantification of the properties of the mysterious "dark energy", which is believed to compose 70 % of the current energy density of the Universe, and which is driving the cosmic expansion to accelerate (as evidenced by observations of distant supernovae). One of the cleanest methods of measuring dark energy in the Universe is by accurately delineating the small-amplitude "acoustic oscillations" in the clustering power spectrum. This baryonic signature has an identical physical origin to the acoustic peaks already identified in the Cosmic Microwave Background, which act as an accurate standard ruler for the experiment. Their recovery in the SKA HI survey, as a function of redshift, permits an extremely accurate determination of the rate of evolution of the equation of state of dark energy with cosmic time, discriminating between theoretical dark energy models. Thus an SKA cosmic structure survey can potentially disprove Einstein's cosmological constant.

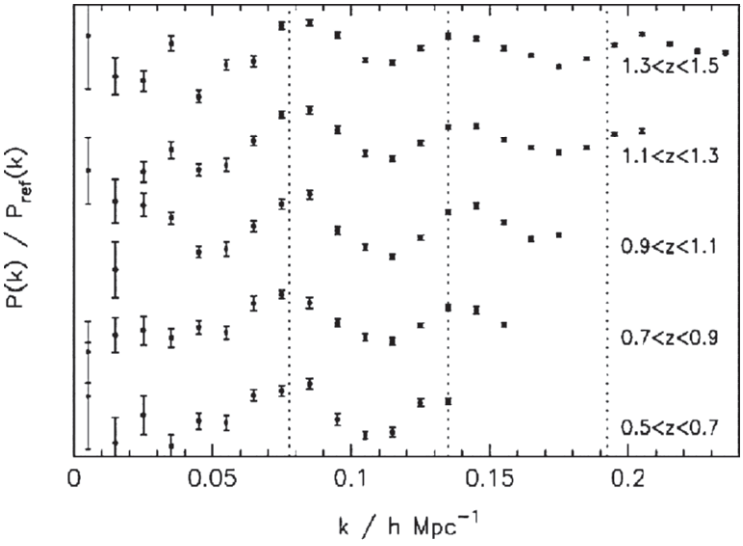


Fig. 5. Simulation of baryonic oscillations in the power spectrum of the clustering of HI emission galaxies as a function of redshift. Credit: Chris Blake

7.1 Strong Field Tests of Gravity Using Pulsars and Black Holes

Pulsar surveys with a large FoV and the sensitivity of the SKA can discover tens of thousands of pulsars, amongst which we expect to find a pulsar in orbit around a stellar-mass black hole, thousands of millisecond pulsars which can form an

immense pulsar timing array, and pulsars in close orbit around the supermassive black hole at the Galactic Center. These data can be used to provide fundamental and detailed tests of our understanding of gravity, in regimes that cannot be probed by any other experiment.

8 Multiple Beams

The reduction in the cost and size of the electronics in telescopes of the future will allow radio astronomers to take increasing advantage of multibeaming through either focal plane or aperture plane arrays. In the extreme aperture plane array with element size comparable to a wavelength it is possible to generate simultaneous independent beams anywhere in the sky, changing the whole sociology of big telescope astronomy. (Fig. 6)

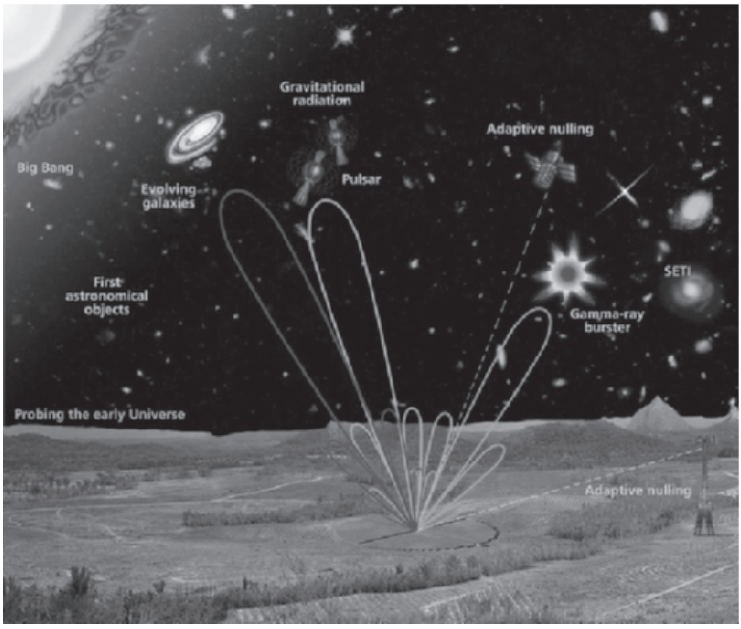


Fig. 6. SKA Multibeaming

8.1 Interstellar Scintillation

A nice example of the value of multiple beams is the determination of the size and expansion rate of the GRB fireball. Frail & Kulkarni [12] using the VLA at 8 GHz observed interstellar scintillation and estimated sizes in the $\theta \approx 10\,\mu$as range. However, there has been only 1 GRB strong enough in 4 years for the VLA

to observe the scintillation. These experiments take many days observing using the most sensitive telescopes, an opportunity greatly enhanced if simultaneous multiple beams are available.

9 Surprising Science

9.1 Searching for Redshifted CO

If an upper frequency of 22 GHz can be achieved the 1–0 transition of CO is redshifted into the band for $z \geq 4$. Even though the 1–0 line may be as much 100 times weaker than the higher order lines seen at mm wavelengths, the larger field of view, sensitivity and relative bandwidth makes the SKA 1–200 times faster than even the ALMA array for a blind CO survey of galaxies.

9.2 Measuring CMB Anisotropy and the Sunyaev-Zeldovich Effect at cm Wavelengths

Although the SKA will only operate at cm wavelengths, where discrete source confusion dominates the CMB anisotropy, its extreme sensitivity to point sources will make it possible to subtract the source contamination at these wavelengths and thereby image the low surface brightness CMB anisotropies on small angular scales. The SKA, operating at 10–20 GHz, will be able to make high-l observations of the CMB anisotropy spectrum and survey the sky for Sunyaev-Zeldovich decrements with unprecedented sensitivity [13].

9.3 High Energy Neutrinos

A wide range of astrophysical models predict the existence of neutrinos in the energy range 10^{19}–10^{22} eV, e.g. Protheroe [14]. These high energy neutrinos produce an observable pulse of Cherenkov emission at radio frequencies if they interact in the front surface of the moon [15]. A patch of SKA antennas operating in the continuum between 1–2 GHz could be configured to detect such pulses with sensitivity 3 orders of magnitude better than any existing experiment [16,17].

9.4 Observing Transients Before They Happen

Entirely new ways of doing astronomy may be possible with the SKA. With an array that is pointed electronically, the raw, 'undetected' signals can be recorded in memory. These stored signals could be used to construct beams pointing anywhere in the sky. Using such beams astronomers could literally go back in time and use the full collecting area to study pulsar glitches, supernovae and gamma-ray bursts or SETI candidate signals, following a trigger from a subarray or other wavelength domain.

9.5 The Cradle of Life

The SKA has the unique potential for finding evidence of extra-solar planets and of other life like us. At 20 GHz, the SKA will provide thermal imaging at 0.15 au resolution out to a distance of 150 pc, encompassing many of the best studied Galactic star forming regions. Such observations will allow us to study the process of terrestrial planet formation; such systems will evolve on timescales of months.

For the first time with the SKA, we will have the capability of detecting leakage radiation from ETI transmitters out to a few hundred parsecs, involving of order a million solar type stars.

10 Future Facilities

10.1 EVLA – The Expanded Very Large Array

The VLA is an array of 27 25-meter diameter antennas which was built in the 1970's and has been in full operations since 1980. It is one of the most successful telescopes ever built with more publications than any other telescope except the HST. The EVLA will incorporate state-of-the-art electronics to replace present equipment dating to the 1970s and it may also include approximately eight new stations as distant as 250 kilometers from the current array. These features will improve the scientific capabilities of the instrument by a factor of 10 in all key observational parameters.

The Phase I EVLA consists of : wideband receiver systems, a state-of-the-art, flexible correlator, a fiber-optic data transmission system, all new digital electronics, a new powerful on-line control system, and the 27 existing VLA antennas. Completion is expected by 2012.

In Phase II of the EVLA both higher and lower resolution will be added. Approximately 8 new stations at distances of up to 300 km from the VLA will be added increasing the angular resolution to 0.004 arcsec at 50 GHz to 0.2 arcsec at 1 GHz. This bridges the gap in resolution between the VLA and the VLBA. The new antennas, and some of the inner VLBA antennas, will be connected directly to the VLA by fiber-optics links. Additional stations will be added inside the current most compact configuration to provide a compact configuration with much higher brightness sensitivity.

Many of the technical developments being undertaken for the EVLA (correlator, real time links, wideband feeds, software) will be part of the development path for the SKA.

10.2 The Square Kilometre Array (SKA)

The exponential improvement in Fig. 1 is obtained by the successive introduction of new design concepts. Upgrades to existing systems (illustrated for Arecibo and Parkes in Fig. 1(b)) are impressive but it's hard to maintain the same exponential improvement. An increase in sensitivity of the order needed to maintain this

exponential growth until 2010 cannot be achieved by improving the electronics or receiver systems in existing telescopes but only by *increasing the total effective collecting area of radio telescopes to about a million square metres*. The project has therefore acquired the appellation, the Square Kilometre Array.

10.3 The Concept

The SKA is a unique radio telescope now being planned by an international consortium. Extensive discussion of the science drivers and of the evolving technical possibilities led to a set of design goals for the Square Kilometre Array [18]. Some of the basic system parameters required to meet these goals are summarized in Table 1. Over the last year a completely updated and expanded science case has been prepared by the International SKA Science Advisory Committee and this is about to go to press [4]. The same SKA technology is also under consideration by NASA-DSN for its next generation deep space communications system,

Table 1. SKA Design Goals

Parameter	Design Goal
Sensitivity: 50–100 × VLA	
Total Frequency Range	0.15 – 22 GHz
Imaging Field of View	1 square deg. @ 1.4 GHz
Angular Resolution	<0.1 arcsec @ 1.4 GHz
Surface Brightness Sensitivity	1 K @ 0.1 arcsec (continuum)
Instantaneous Bandwidth	$0.5 + \nu/5$ GHz
Number of Spectral Channels	10^4
Number of Instantaneous Pencil Beams	100 (at lower frequencies)

11 Achieving the Vision - International Collaboration

Even with the dramatic reduction in cost of unit aperture, a telescope such as the SKA will be expensive. One path to achieving this vision is through international collaboration, to build facilities which no single nation can afford. While the additional overhead of a collaborative project is a penalty, the advantages are also great. It can avoid wasteful duplication and competition; provide access to a broader knowledge base; generate innovation through cross fertilisation; and create wealth for the nations involved. An analysis of successful international collaborations has shown the importance of starting the collaboration early. This has been the case for the SKA, starting with an URSI/IAU Working Group on large facilities in 1993, and an agreement between a number of observatories for joint technology development.

References

1. M. Harwit: *Cosmic Discovery* (New York: Basic Books, Inc, 1981)
2. D.J. de Solla Price: *Little Science, Big Science* (Columbia University Press, 1963)
3. R.D. Ekers, J.F. Bell: In *IAU Symp. 196, Preserving the Astronomical Sky, Vienna, 2001*. ed. by R.J. Cohen, W.T. Sullivan (San Francisco: ASP)
4. *Astrophysics with the SKA*. ed. C. Carilli, S. Rawlings (New Astronomy Reviews, in press 2004)
5. S. Weinreb, L.D'Addario: *The SKA Cost Equation* (www.skatelescope/documents/skamemo1.html) (2001)
6. J. Condon: ARAA **30**, 576 (1992)
7. J. Dickey, E. Salpeter: ApJ **284**, 461 (1984)
8. C. Carilli, M.S. Yun: ApJ **513**, 13 (1999)
9. P. Tozzi, P. Madau, A. Meiksin, M.J. Rees: Appl. J Phys. **528**, 597-606 (2000)
10. M. Zaldarriaga, S.R. Furlanetto, L. Hernquist: ApJ **608**, 622 (2004)
11. *Report of the Task Force on Radio Astronomy and the Radio Spectrum*, OECD Global Science Forum 2004
12. D.A. Frail, S.R. Kulkarni, S.R. Nicastro, M. Feroci, G.B. Taylor: Nature, 389, 261 (1997)
13. R. Subrahmanyan, R.D. Ekers: In *URSI General Assembly, Maastricht, 2002*
14. R.J. Protheroe: In *Neutrino 98, Takayama 1998* Nuclear Physics B Proc. Suppl. **77**, pp. 465–473 (1999)
15. R.D.Dagkesamanskij, I.M. Zheleznyak: JETP **50**, 233 (1989)
16. T.H. Hankins, R.D. Ekers, J.D. O'Sullivan: MNRAS **283**, 1027 (1996)
17. P.W. Gorham, K.M. Liewer, C.J. Naudet, D.P. Salzburg, D. Williams: In *Radhep 2000, Los Angeles, 2001*.ed. by D. Salzburg, P. Gorham (AIP Conference Proceedings 579) pp. 177–188
18. A.R. Taylor, R. Braun: In *Science with the Square Kilometre Array* http://waw.skatelescope.org/science/node1.html (1999)

Future Optical and Near-Infrared Facilities

R. Gilmozzi[1], M. Mountain[2], N. Panagia[3], and P. Dierickx[1]

[1] European Southern Observatory, Garching D-85748 Germany
[2] Gemini Observatory, Hilo HI 96720, USA
[3] Space Telescope Science Institute, Baltimore MD 21218, USA

Abstract. Several projects and studies are being prepared for the second decade of the third millennium, both in space and on the ground. Here we review the status of optical / near infrared facilities now on the drawing board, with particular emphasis on the *James Webb Space Telescope* (JWST), the *Thirty Meter Telescope* (TMT), and the *OverWhelmingly Large* 100m telescope (OWL).

1 Introduction

The decade 2010-2020 will see the maturity of the current generation of telescopes (VLT, Keck, Gemini, Subaru, LBT, GTC, HET, SALT, Magellan etc) equipped with a second generation of instruments often performing at the diffraction limit through advanced Adaptive Optics (AO) systems. Interferometry will have come out of its infancy to operate in the faint object regime and to produce astrometric result in the μas range. ALMA will provide mm and submm astronomers with a facility 'equivalent' to optical ones (both in terms of service offered to the community and of resolution and sensitivity). And a new generation of ground based optical/NIR 30 to 100m telescopes now on the drawing board (CELT+GSMT+VLOT=TMT, GMT, Euro-50, OWL etc) may open a completely new window on the Universe and produce unprecedented results (with resolution $\sim$ mas and sensitivity hundreds or even thousands of times beyond what is available today).

JWST, XEUS, TPF/Darwin precursor missions and others will explore the heavens from above the atmosphere, exploiting the freedom from turbulence, sky absorption and gravity. In this paper, we review the status of three major projects, the JWST, TMT and OWL.

2 The James Webb Space Telescope

The James Webb Space Telescope (*JWST*), formerly the Next Generation Space Telescope (*NGST*), is a cooperative program of the National Aeronautics and Space Administration (*NASA*), the European Space Agency (*ESA*) and the Canadian Space Agency (*CSA*) to develop and operate a large, near- and mid-infrared optimized space telescope by the end of this decade that can build and expand on the science opened up by the highly successful Hubble Space Telescope (*HST*). Jointly, *NASA*, *ESA*, and *CSA* will build *JWST*.

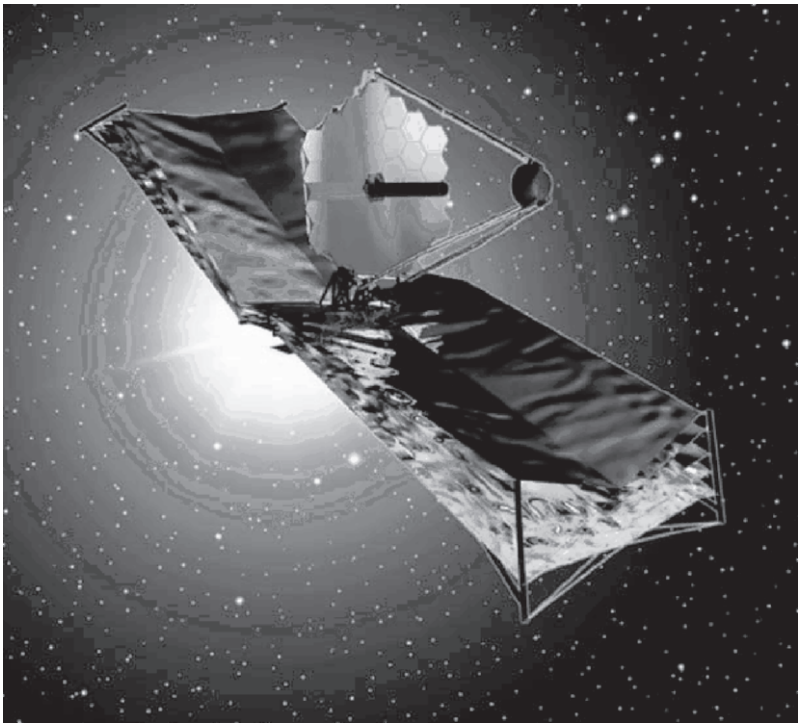


Fig. 1. The Northrop Grumman design for *JWST*. Easily recognizable are the Optical Telescope Element (OTE), *i.e.* the cylindrical structure between the primary and the secondary mirror, and the multi-layered deployable sunshield. [Copyright & Credit: Northrop Grumman Corporation 2000]

JWST has the goal of understanding the formation of galaxies, stars, planets and ultimately, life. *JWST* is specifically designed for discovering and understanding the formation of the first stars and galaxies, measuring the geometry of the Universe and the distribution of dark matter, investigating the evolution of galaxies and the production of elements by stars, and the process of star and planet formation.

JWST has been under study since 1995 and is planned to be launched around 2011, nearly 400 years after Galileo discovered the moons of Jupiter, over 60 years after Lyman Spitzer proposed space telescopes, and about 20 years after the launch of *HST*.

JWST has been conceived as a 6 m class deployable, radiatively cooled telescope, optimized for the 1–5 μm band, with background limited sensitivity from 0.6 to 10 μm or beyond, operating for 10 years near the Earth-Sun second Lagrange point (L2), about 1.5 million km from Earth. It will be a general-purpose observatory, operated by the STScI for competitively selected observers from the international astronomy community.

JWST is a unique scientific tool, with excellent angular resolution (about 0.05 arcsec at 2 μm) over a large field of view (at least 10 arcmin^2), deep sensitivity and a low infrared background. As a cold space telescope, *JWST* will achieve far better sensitivities than ground-based telescopes. Among the advantages of *JWST* over potentially competing telescopes are:

- *JWST* will observe with background levels much lower than possible from the best sites on Earth: for example, the background will be one to six orders of magnitude lower than for Mauna Kea, depending on wavelength, the biggest gain occurring around 5 μm.
- *JWST* will have diffraction limited resolution at 2 μm, and will achieve much higher Strehl ratios and wider fields of view than anticipated from ground-based telescopes using adaptive optics.
- *JWST*'s aperture is an order of magnitude larger than *SIRTF*'s (now Spitzer Space Telescope), with a factor of 100 better sensitivity.

JWST will indeed be able to observe the first generations of stars and galaxies, including individual starburst regions, protogalactic fragments, and supernovae out to redshifts of z=5–20. *JWST* will resolve individual solar mass stars in nearby galaxies, penetrate dust-clouds around star-forming regions, and discover thousands of isolated substellar and Kuiper Belt objects.

The *JWST* Mission Concept

The science goals for *JWST* require a telescope with high sensitivity covering the wavelength range from 0.6 μm to 10 μm, with capability out to 28 μm, and with NIR resolution comparable to that of HST in the optical. Figure 1 shows the observatory that will be built by the Space Technology division of Northrop Grumman (cleverly named *NGST*) and will include the Optical Telescope Element (OTE), the Integrated Science Instruments Module (ISIM) Element, and the Spacecraft Element (Spacecraft Bus and Sunshield).

The Integrated Science Instrument Module (ISIM) consists of a cryogenic instrument module integrated with the OTE, and processors, software, and other electronics located in the Spacecraft Support Module (SMM). The instrument suite will include:

– A near IR camera (NIRCam), built by US institutions, covering 0.6–5 μm, critically sampled at 2 μm. The field of about 10 arcmin^2 is apportioned over two sub-cameras each covering a field of $2\farcm3 \times 2\farcm3$.
– A near IR multi-object spectrometer (NIRSpec), provided by ESA, with spectral resolutions 1000 and possibly 100, and a spatial resolution of 100 mas, covering a field of view of $3' \times 3'$ and capable of observing more than 100 objects simultaneously.
– A mid-IR camera/spectrometer (MIRI), built in a 50/50 collaboration between NASA and European institutions, covering a field of $2' \times 2'$ with a spectral range of 5–28 μm using a long-slit cross-dispersed grism with a resolution of 1000.
– A Fine Guidance Sensor (FGS), provided by CSA, that enables stable pointing at the milli-arcsecond level and have sensitivity and field of view to allow guiding with 95% probability at any point on the sky.

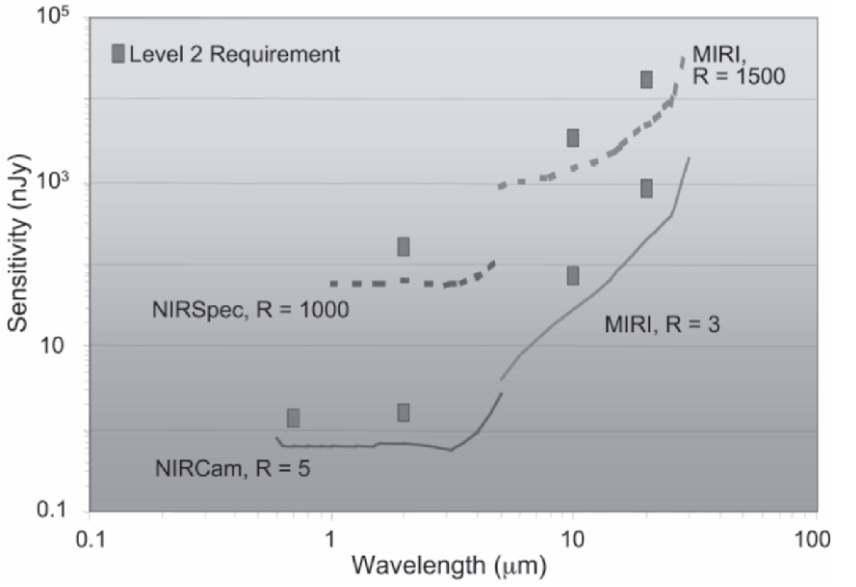


Fig. 2. The JWST instruments sensitivity, exceeding the level 2 requirements

The *JWST* design solve the problem of passively cooling to the cryogenic temperatures required for NIR and MIR operation by *(a)* protecting the observatory from the Sun with a multi-layer shield, *(b)* using a heliocentric orbit to decrease the Earth's thermal input, and *(c)* configuring the telescope to have a large area exposed to space to improve radiative cooling.

With these general characteristics, *JWST* will have an enormous discovery potential both at 0.6–10 μm and at longer wavelengths. In particular, *JWST* enjoys a considerable background advantage over the ground at all wavelengths, a larger field of view over which high-resolution images can be obtained and a significant aperture advantage over the Spitzer Space Telescope. The shorter times required to reach a given threshold can translate into larger fields observed (more targets) and/or greater sensitivities.

Details and updates can be found at http://www.stsci.edu/jwst/overview/ and linked URLs.

3 Extremely Large Telescopes

Figure 3 (top) shows the history of the telescope diameter, with a few future telescopes (TMT and OWL) added for reference. There are two aspects that are immediately evident: (1) "local" scatter notwithstanding, the trend of diameter increase has remained substantially constant since Galileo (doubling every 50 years or so) and (2) the quantum jump between a 10 and a 100m telescope is similar to that between the night-adapted naked eye and the first telescope,

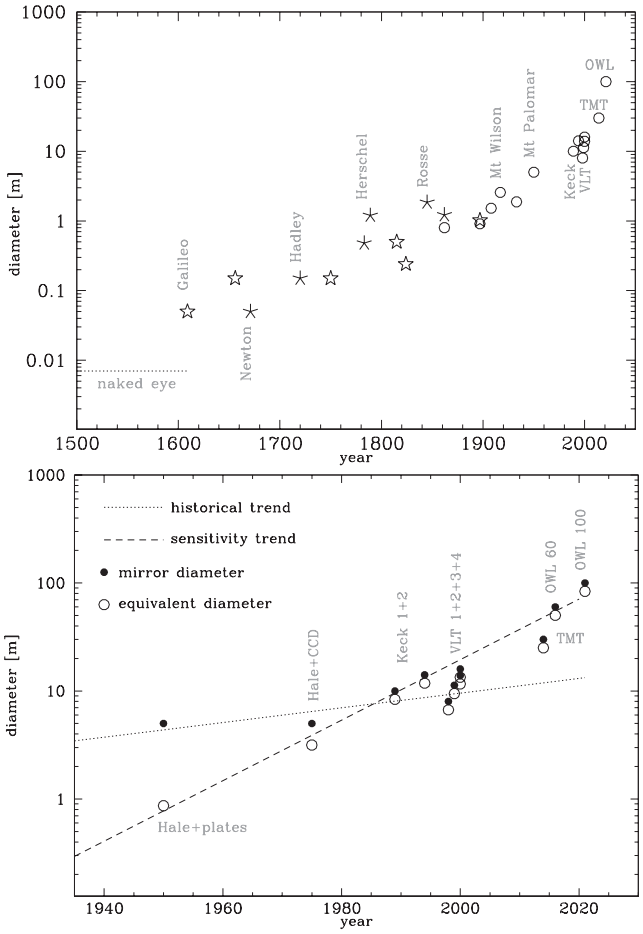


Fig. 3. (**top**) Brief history of telescope. Stars: refractors, asterisks: speculum reflectors, circles: glass reflectors. Some specific telescopes are named. The trend to the present is a doubling in size every ~ 50 years (35 during the 20th century). The quantum jump between a 10m and a 100m telescope is equivalent to the one between the naked eye and the first telescope by Galileo. (**bottom**) Recent history of improvement in sensitivity of telescopes expressed in 'equivalent diameter of a perfect telescope' $= \sqrt{\eta D^2}$, with η the telescope overall efficiency (the dashed line is an aid to the eye, not a fit). Over the last 50 years the increase in sensitivity has been mostly due to increase in detector efficiency. Now that detectors approach 100% efficiencies, large improvements require large increases in diameter (i.e. larger than a factor of two).

which certainly bodes well for the potential for new discoveries. During the 20th century there has been some acceleration, with the doubling happening every 35 years, (see e.g. the 'California progression' with the Hooker [2.5m, 1917], Hale [5m, 1948], and Keck [10m, 1992] telescopes).



Fig. 4. The three independent ELT studies undertaken by the TMT partnership

One point that perhaps is not immediately evident, though, is that in the last 50 years there has been a larger increase in telescope sensitivity due to improvements in detectors than to increases in diameter (figure 4, bottom). Now that detectors are at efficiencies close to 100%, large improvements can be obtained only through large increases in diameter. For example, at the times of photographic plates, with efficiency of a few percent, even the 5-meter Hale telescope was only equivalent to a 1-meter 'perfect' telescope (i.e. one with 100% efficiency).

This is the rationale for breaking the "factor-of-two increase in diameter every 50 year" law. The advances in technology in the last decades (fostered in part by the present generation of telescopes) provide the means to achieve this goal. In the following we describe the status of two ELT designs, the TMT and the OWL.

3.1 The Thirty Meter Telescope

In response to the US National Academy of Sciences recommendation that a thirty meter telescope should be the top priority for the US astronomy projects in this decade, the thirty meter telescope (TMT) project was formed as a public-private partnership between the University of California, Caltech, the Association of Universities for Research in Astronomy (AURA) and ACURA, the Association of Canadian Universities for Research in Astronomy. The genesis of this partnership were three independently conceived and reviewed ELT design studies undertaken over two years; the CELT, GSMT and VLOT concept studies.

In 2003 the Gordon & Betty Moore Foundation donated $35M to the Design and Development Phase (DDP), and the TMT Project Office was established in 2004, which will have a staff of approximately 35. Matching contributions are now being sought from the NSF and Canadian government to bring this DDP funding to ∼$70M. The science case for the TMT has been explored in depth by the Science Advisory Committee (SAC), which is composed of representatives of all four partners. The high level goals of TMT are to explore:

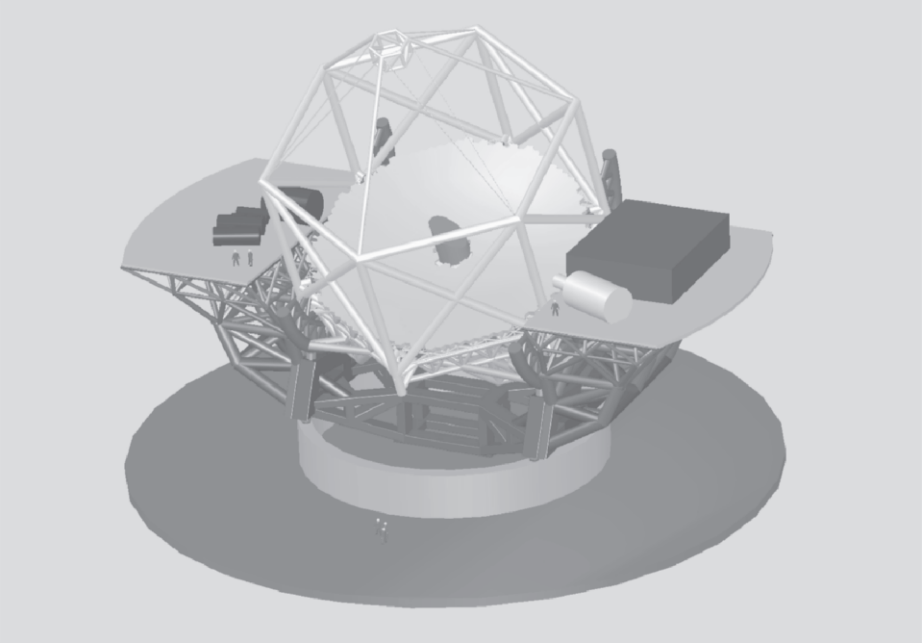


Fig. 5. The Thirty Meter Telescope reference design engineering model

- The origin of large scale structure in the Universe
- The assembly of galaxies in the early universe ($z > 3$)
- Extra solar planet detection and characterization
- The processes governing star and planet formation

To respond to these science objectives, the TMT Project studied the various technical options explored in the independent studies and have now synthesized these into a single TMT Reference Design. Following a detailed engineering study, the partnership has agreed on a single TMT reference design:

- 30m filled aperture, highly segmented primary
- aplanatic Gregorian (AO M2 capable) two mirror telescope
- f/1 primary
- f/15 final focus
- Field of view 20 arcmin
- Elevation axis in front of the primary
- Wavelength coverage 0.31–28 μm
- Operational zenith angle range 1°–65°
- Both seeing-limited and adaptive optics observing modes
- First generation instrument requirements defined
- AO system requirements defined

Instrument	Spectral Resolution	Science Case
Near-IR DL Spectrometer & Imager	<4000	• Assembly of galaxies at large redshift • Black holes/AGN/Galactic Center • Resolved stellar populations in crowded fields
Wide-field Optical Spectrometer	300 - 5000	• IGM structure and composition 2<z<6 • High-quality spectra of z>1.5 galaxies suitable for measuring stellar pops, chemistry, energetics
Multi-IFU, near-DL, near-IR Spectrometer	2000 - 10000	• Near-IR spectroscopic diagnostics of the faintest objects • JWST followup
Mid-IR Echelle Spectrometer & Imager	5000 - 100000	• Physical structure and kinematics of protostellar envelopes • Physical diagnostics of circumstellar/protoplanetary
ExAO I (PFI)	50 - 300	• Direct detection and spectroscopic characterization of extra-solar planets
Optical Echelle (MTHR)	30000 - 50000	• Stellar abundance studies throughout the Local Group • ISM abundances/kinematics • IGM characterization to z~6
MCAO imager	5 - 100	• Galactic center astrometry • Stellar populations to 10Mpc
Near-IR, DL Echelle	5000 - 30000	• Precision radial velocities of M-stars and detection of low-mass planets • IGM characterizations for z>5.5

Fig. 6. Table 1: The first pass TMT Instrument summary.

The current high priority studies underway in the DDP are:

- Primary mirror segment fabrication/cost & schedule
- Development of required AO technologies
- Instrumentation concepts and prototyping/development (The first pass instrument concepts are shown in Table 1)
- Site selection
- Operational model & costs

One of the key science objectives of TMT, which is a principle driver behind the TMT schedule, is to be contemporary with NASA's James Webb Space Telescope. This is to allow the TMT partnership to exploit the scientific synergies between these two world-class capabilities (see table 2) Hence the partnership is pursuing an aggressive schedule, aiming at a construction start in 2008, with a goal of the first fully phased telescope in 2014, and the start of science operations in 2015. The TMT operational approach is to phase in each capability and instrument to build up TMT's capabilities between 2014–2016:

Wavelength range	JWST	TMT
$< 1.0\mu m$	• wide-field high spatial resolution imaging to $0.6\mu m$ • low-R* spectroscopy	• extended wavelength coverage to $0.31\mu m$ • faint-object spectroscopy
$1.0\mu m < \lambda < 2.5\mu m$	• wide-field high spatial resolution imaging • low-R spectroscopy	• higher spatial resolution over small fields •R > 3000 spectroscopy
$\lambda > 2.5\mu m$	low-background gives significant sensitivity gains over ground-based facilities for imaging and spectroscopy**	• 3000 < R < 100,000 spectroscopy • higher spatial resolution imaging over small fields

Fig. 7. Table 2: TMT complements JWST, as called for in the US NAS Decadal Survey

Install 1st science instrument	Jul 2014
Start science (seeing limited)	Jan 2015
1st light, first AO system	Jan 2015
Install first diffraction-limited inst	Jul 2015
Begin AO based science	Jan 2016
Install 3rd instrument	Jul 2016
Install additional instruments	(1 per 2 year)

3.2 The 100m OWL

Since 1997, ESO is developing the concept of a ground-based 100-m class optical telescope. It has been christened OWL for its keen night vision: this also stands for *OverWhelmingly Large* (showing either the *hubris* of astronomers or their distorted sense of humor). The challenge and the science potential are formidable – and highly stimulating: a 100-m diffraction-limited optical telescope would offer 40 times the collecting power of the whole VLT with the milliarcsecond imaging resolution of the VLTI.

A few principles, mostly borrowed from recent developments in the art of telescope making, hold the key to meet these harsh requirements: optical segmentation as pioneered by the Keck, massive production of standardized mirrors from the Hobby-Eberly, active optics control and system aspects from the VLT. The most critical aspect is to develop the means to reach diffraction-limited images in "large" fields (a few arcminutes in the near-IR). This is the goal of the so-called multi-conjugate adaptive optics concept, whose principles and applications have been already demonstrated (ESO is building MAD, an MCAO demonstrator, to see first light at the VLT in 2006). Tremendous pressure is

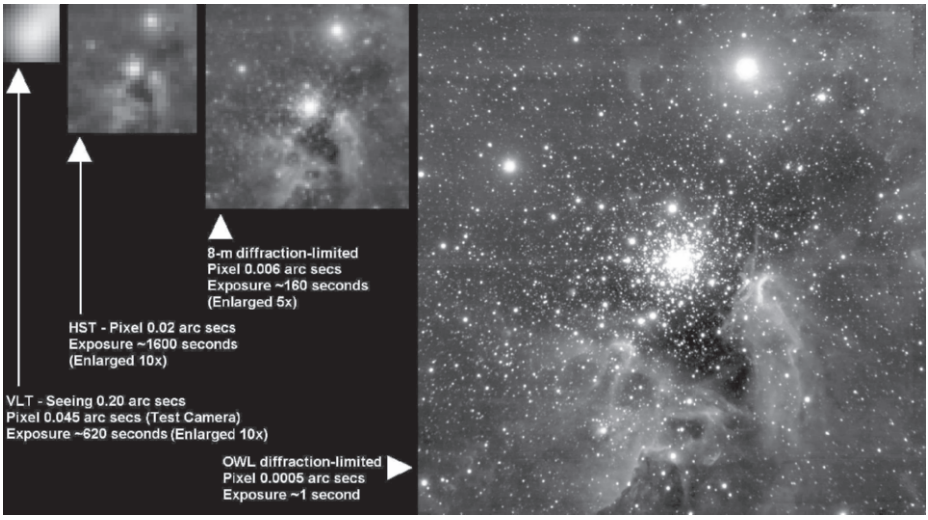


Fig. 8. Resolution, from 0.2 arc seconds seeing to diffraction-limited with 100-m. All images 0.6×0.6 arc seconds^2

building up to implement such a capability into existing large telescopes, and rapid progress in the underlying technologies is taking place, *e.g.* to fabricate low-cost deformable mirrors with tens of thousands actuators from integrated circuits techniques.

Succeeding with OWL means breaking time-honored trends like doubling the diameter D only every 30 years, with a $D^{2.6}$ cost law and primary mirror production speed of 1m linear per year. An especially encouraging case concerns the primary (and secondary) mirror fabrication: industry indicated a baseline of 6-8 years for producing the full 100-m mosaic at affordable cost. One of our main challenges is to achieve such a huge reduction in time and cost for *all* major components of the Telescope. There are vocal supporters for a more "conservative" approach in any Extremely Large Telescopes Meeting; the burden of the proof is clearly in our camp and a major item for our Concept Study (to be reviewed in 2005).

Angular resolution and sensitivity are the highest priority requirements. Figure 8 illustrates the effect of increased resolution by showing the same hypothetical 0.6×0.6 arc seconds field, as seen by a seeing-limited telescope under best conditions ($\sim$ 0.2 arc sec), HST, an 8-m diffraction-limited telescope and OWL. There are also technical reasons for striving for high spatial resolution. Instruments designed for a seeing-limited 100-m would be impossibly large or wholly inefficient or both. There are exceptions, e.g. a mosaic of multi-band imagers, but none covering core OWL science cases. The price to pay to get efficient instruments is of course the exacting adaptive optics system which must be incorporated in the overall concept right from the start.

At ten times the combined collecting area of every telescope ever built, a 100m filled aperture telescope would open new horizons in observational astronomy – going from 10m to 100m represents a "quantum" jump similar to that from the naked eye to Galileo's telescope. Simulations show that V=38 point sources can be detected in 10 hours assuming diffraction-limited quality, more than a 1000-fold improvement over the VLT. OWL is very complementary to JWST. JWST has unmatched capability in the thermal IR, while OWL is better for imagery at $\lambda < 2.5\,\mu$m and spectrography ($R \geq 5,000$) at $\lambda < 5\,\mu$m. Sensitivity-wise, OWL could not compete in the thermal IR, but has a much higher spatial resolution. OWL would also have a synergetic role with ALMA (e.g. in finding and/or studying proto-planets) and with VLBI (the radio astronomers have been waiting for us optical/IR people to catch up in spatial resolution for decades!)

The OWL Science Case

A 100-m telescope working at the diffraction limit (e.g. 1 mill-arcsecond at V $\sim$ 37) has an unprecedented scientific potential (not least for new discoveries). In contrast, a seeing-limited 100-m telescope (deprecatingly named a "light-bucket") would probably be scientifically unjustified. Discussion on science cases in the framework of the OPTICON working group on science with ELTs has been recently published in an extensive book. Here we summarize some recently developed cases for OWL, in particular those that take full advantage of its capabilities: the spectroscopy of exo-earths to look for signs of life, and some of the cosmological science cases.

Spectroscopy of earth-like exoplanets. Searching for exo-biospheres could be defined as the holy grail of today's astronomy. This science case depends very strongly on the telescope diameter. First of all, the volume accessible to a telescope is proportional to D^3 (since resolution is $\propto D$). For example, the number of accessible G stars in the solar neighbourhood where an earth at 1 AU could be detected would be 20, 165 and 750 respectively for a 30-, 50- and 100-m telescope (assuming minimum resolvable separation 5 λ/D). From the point of view of the sensitivity, the time to achieve the same S/N in the planet (for objects in common, of course) is $\propto D^4$ (the planet is $\sim 10^{10}$ times fainter than the parent star, and even at many λ/D from the star we are definitely in the background-limited regime). This means that a 30-m telescope would need $\sim$ 120 times longer than OWL to detect the same object. Our simulations indicate that for a solar system analogue at 10 parsec the earth would be detected in about one hour with OWL, opening up the possibility of doing spectroscopy for D > 80m. A recent study by Angel (2003) confirmed that spectroscopy of exo-earths is within the reach of a 100-m in the optical/near-IR, while in the thermal infrared space interferometers (à la Darwin/TPF) are moderately better unless the 100-m is placed in Antarctica. Sophisticated coronagraphic techniques, able to suppress by factors upward of 10^6 the light of the parent star may allow to resolve closer separations, at the same time expanding the accessible volume and decreasing the necessary exposure times.

Measure of cosmological parameters with primary distance indicators (note: H, not H-not!) Beyond the local universe, distances are determined today

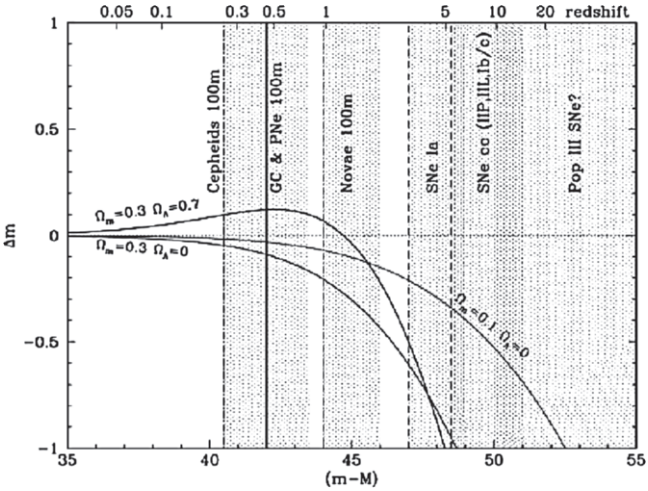


Fig. 9. Using primary distance indicators to disentangle cosmological models. Regions of application for various methods with OWL are indicated.

using derived standard candles (e.g. SNe Ia) whose calibration is not always completely reliable. OWL will allow the measurement of distances using primary indicators in the redshift range where the difference between cosmological models is more pronounced. Using Cepheids and Novae, as well as the planetary nebulae and globular clusters luminosity functions, accurate measurements of distances can be obtained out to z $\sim$ 1 and these will allow to disentangle the various models, including those alternative to Λ. Beyond z $\sim$ 1, Type Ia SNe can be detected up to z $\sim$ 5 (although Ia's are the second brightest explosions in he universe after GRBs they do not emit in the UV and K being the last useful band they are not detected beyond that z), core-collapse SNe out to z $\sim$ 10, and alleged Pop III SNe even beyond. While SNe may be more useful to determine the cosmic supernova rate, and from this the early universe star formation history, than in disentangling cosmologies, they will provide critical cosmological information up to redshift $\sim$ 10 (e.g. quintessence).

Primordial stellar populations. WMAP sets the recombination epoch at z between 10 and 20. Pop III stars are strong candidates as possible re-ionization sources. Pop III stars are hot and massive, and form before re-ionization possibly in dwarf-galaxy sized over-densities ($10^6 - 10^7$ M$\odot$). Strong emission lines of H and He, and strong nebular continuum characterize their spectra. Both the continuum and line spectrum can accurately be studied with OWL at high z, thus detecting and characterizing the first-light objects in the Universe. OWL would be about 10 times more efficient than JWST for these observations.

Direct measurement of the cosmic acceleration/deceleration. Enormous collecting areas together with extreme instrumental stability open also the very exciting prospect of measuring the acceleration (or the deceleration) of the Uni-

verse in a direct way. Recent results on Type Ia supernovae indicate that our universe has undergone a phase of acceleration following one of deceleration. In some cases the interpretative process has been based on the very models the data were supposed to support (or disprove). Not that there were alternatives: a direct measurement of the change in recession velocity of cosmological objects has always been considered impossible for the present generation of telescopes. However, it has been shown that with a sufficient flux of photons, and with a spectrograph stability of the order of 10 cm s^{-1} over 10 years, changes in the recession velocity of absorption lines in the Lyman-α forest of bright quasars out to $z \sim 5$ can be detected. This would allow a real physics experiment to be carried out with an ELT, whose results would be unequivocal, model-independent and assumptions-free. ESO is designing an instrument, called CODEX (for COsmic Deceleration [or Dynamics] Experiment) to carry out these observations with OWL. (A stability of 10 cm s^{-1} is achieved already today, e.g. the HARPS instrument at the ESO 3.6m telescope; maintaining this stability over a long period of time is the challenge here).

OWL telescope design

New generations of telescopes built over the last century, from the Hooker to VLT and Keck have generally relied on extensive R&D programs, in particular in the area of optics fabrication. Optical configurations basically did not change: with few exceptions, telescopes were designed on the basis of a Ritchey-Chrétien solution. The new emphasis has been put on solving optical scalability problems (new materials, active optics, segmentation), reducing cost (e.g. enclosure costs: alt-az-mount, faster primary mirror hence shorter telescope length), relaxing tolerances and improving performance (active optics).

NTT, VLT, HET and, to a lower extent, Keck, embody a certain re-thinking of system aspects of telescope design and construction. To a great extent, these projects have relied on industry for the design and fabrication of crucial components, while developing expertise and solutions at system level. OWL could be seen as a step further in the direction of an industrial approach: its design shifts the balance in the direction of proven subsystem technology, hence low industrial risk, while allowing for some (limited) system innovation, e.g. the combination of active and segmented optics, and modular mechanical design. This approach has already led to a positive response of industry to the OWL concept.

A crucial objective pursued in the design of OWL is predictability, i.e. reliable optical, mechanical and control solutions. The experience derived from VLT (performance and reliability of active optics), Keck (virtually unlimited optical scalability), and HET (spherical primary solution) ensures that this objective can be met in the field of telescope optics, as the associated processes and design solutions are fully demonstrated.

The design, fabrication and integration of mechanical structures are inherently predictable, as accurate modeling is possible. The same may be said of control systems (the number of degrees of freedom to control in a telescope like OWL –a few thousands, at modest frequencies– may appear unusual for an astronomical telescope but does not require any technology breakthrough).

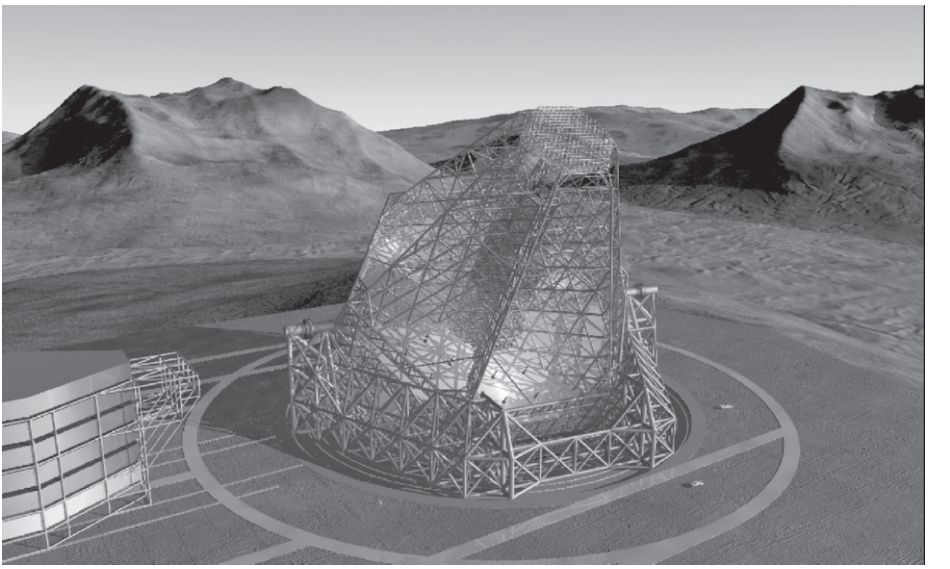


Fig. 10. Layout of the OWL facility. On the left, primary mirror covers. A sliding enclosure (not shown) is foreseen to shield the telescope.

Under these conditions, it appears that the scalability of telescope diameter is no longer set by optical fabrication processes, but most likely by structural characteristics and cost. Our estimate is that the technical limit for a fully steerable telescope is (today) ∼130-150-m, possibly more if high performance (and prohibitively expensive) materials are used for the telescope structure.

As of today, the evident exception to suitable predictability is adaptive optics. The fact that the principle of multi-conjugate adaptive optics has been verified on the sky, together with the pressure implied by its promises, and potential spin-off from consumer applications (MEMs), leave room for (cautious) optimism.

OWL design evolution

The evolution of the telescope design has been marked by a few key trade-offs and subsequent decisions: (i) Segmented primary and secondary mirrors, segment dimension ∼ 2-m; (ii) Optical design, spherical primary mirror solution; (iii) Non-adaptive main telescope optics (2 mirrors in the corrector, however, have been identified as adaptive mirrors, conjugated at 0 and 8km) (iv) Implementation of active optics and field stabilization; (v) Alt-az mount.

Several optical designs have been explored, from Ritchey-Chrétien solutions to siderostat with relatively slow primary mirror. It has been found that cost, reliability, fabrication and telescopes functionality considerations point towards a spherical primary mirror solution. In terms of fabrication, all-identical spherical segments are ideally suited for mass-production and suitable fabrication processes recommended by potential suppliers are fully demonstrated. In a modified version, these processes could also be applied to aspheric segments, however

with a substantial cost overshoot (more complex polishing, lower predictability, tighter material requirements). It can be shown that an aspherical solution also implies faster primary mirror for equivalent structure height, thereby exacerbating telescope alignment and mirror fabrication issues. The secondary mirror becomes a critical issue as well. If convex (e.g. Ritchey-Chrétien solution), it must be small (∼2-3-m) in order to be feasible (optical testing), which again implies tight alignment tolerances (at a location where they are the least achievable). A Gregorian solution solves the secondary mirror feasibility problem, however at the cost of a longer telescope structure.

The current baseline design is based on a spherical primary mirror solution, with flat secondary mirror and aspheric, active corrector. The flat secondary mirror has also major advantage in terms of decenters (cm rather than μm), which are evidently crucial with a structure the size of OWL's.

Several mount options have been assessed, from a classical alt-az solution to de-coupled primary and secondary mirror structures. Cost and performance considerations point clearly towards the alt-az solution (see observatory layout in figure 10). The current baseline design is modular i.e. the structure is made of (nearly) all-identical, pre-assembled modules. This crucial feature allows for major cost savings.

There is no provision for a co-rotating enclosure, the advantage of which is anyway dubious in view of the enormous opening such enclosure would have. Protection against adverse environmental conditions and excessive day-time heating would be ensured by a sliding hangar, whose dimensions may be unusual in astronomy but actually comparable to or lower than those of large movable enclosures built for a variety of applications. Mirror covers sliding into the structure would provide segments cleaning and handling facilities, and local air conditioning if required.

Relevant site aspects are more complex than with previous telescope generations, mainly because of multi-conjugate adaptive optics (MCAO), telescope size, and the higher impact of seismic activity on cost and safety. MCAO implies, in particular, that the function of merit of the atmosphere cannot be described by a single parameter (seeing). Better understanding of site quality in relation to climatology is also essential. A positive development is the availability of databases providing suitable worldwide coverage. Indeed, the screening of these databases with respect to relevant parameters is under way.

Cost and schedule

Cost estimates (half of which supported by Industrial studies) indicate that the required capital investment could be around 1 billion Euros, including contingency. Compared to "classical" telescope cost factors, substantial cost reduction occurs with the main optics (fabrication processes adapted to mass-production), the telescope structure (very low mass in proportion to dimensions, mass-produced modules), and the enclosure (reduced functionality, no air conditioning).

Preliminary schedule estimates indicate that technical first light could occur within 8-9 years after project funding. Allowing for 2.5 years integration and

verification of the IR adaptive module(s) and 3.5 years for integration and verification of the visible adaptive module(s), the telescope could already deliver science data in the IR and in the visible within 10.5-11.5 and 11.5-12.5 years after project go-ahead, with unmatched resolution and collecting power. Full completion would occur ∼15 years after project start.

4 Conclusions

Several projects in the optical and near infrared, both in space and on the ground, are currently underway for deployment in the second decade of the third millennium. Their scientific goals open new and exciting avenues of research which are outside the reach of current instrumentation. The detection of earth-like exo-planets and possibly of biospheres, the study of the first building blocks of stars and galaxies and their evolution, the direct measure of the deceleration of the Universe, all have driven the technical requirements to unprecedented levels, and the sensitivity increase of the new generation of instruments with respect to the previous one will be one never seen before in astronomy.

Large collaborations will probably be needed to achieve these lofty goals. These are either already set up or being set up. NASA and ESA collaborate on space ventures, and the JWST will certainly be built. International, transatlantic and even global exchanges of information are the first steps that have already been taken on the ELT path, with formal agreements to pursue a common project a definite possibility. It may be that not all the projects now on the drawing board will be transformed in glass and steel, but a decade from now it is very likely that at least one ELT and the JWST will complement each other in the pursuit of the secrets of the Universe.

References

Up to date references for these projects are kept at their respective web sites. Here we give some that can be useful. More links can be found at each site.

JWST: http://www.stsci.edu/jwst/overview/
TMT: http://tmt.ucolick.org/
OWL: http://www.eso.org/projects/owl/
Euro50: http://www.astro.lu.se/∼torben/Euro50/
OPTICON: http://www.astro-opticon.org/

The New 40-m Radiotelescope of OAN in Yebes, Spain

R. Bachiller and OAN Staff

Observatorio Astronómico Nacional (OAN, Instituto Geográfi= co Nacional),
C/ Alfonso XII, 3, 28014 Madrid, Spain

Abstract. This report describes the new 40-meter radiotelescope which is currently close to the end of its construction phase at Yebes, near Guadalajara, Spain.

1 Introduction

The Observatorio Astronómico Nacional (OAN) of Spain is operating a 14-meter radiotelescope at Yebes, near Guadalajara, 80 km Northeast from Madrid. The observatory is located at an altitude of 1000 m and is protected by law against harmful radio interference. Studies are being conducted to connect the Yebes site to GEANT, the high speed transeuropean data network.

The observatory is a full member of the European VLBI Network (EVN). The 14-meter radiotelescope is also a network station of the International VLBI Service (IVS), and participates regularly in the geodetic VLBI campaigns to study the tectonic plate motions in Europe (project EUROPE), Earth rotation, and pole motion.

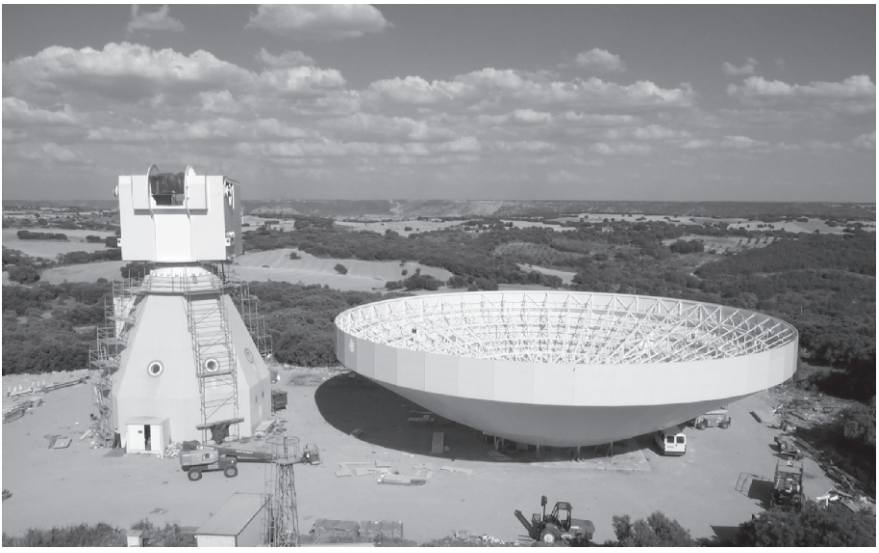


Fig. 1. Status of the new 40-meter radiotelescope of OAN in Yebes, Spain

2 The New 40-meter Radiotelescope

The current major project of OAN is the construction of a 40-meter radiotelescope in Yebes. The new instrument will be the most important large scale facility for Radioastronomy at a national level and will significantly increase the performance of the EVN.

The antenna consists of a homologous parabolic reflector and an hyperbolic subreflector on a quadrupode. It is mounted on a concrete pedestal which serves also as control building and workshop, and is designed to operate in Nasmyth focus configuration.

The main reflector has a diameter of 40 m (F/D=3D7.9) and a weight of about 400 tons. Moreover it consists of 420 stretched aluminium panels (1.8 mm thick)that will be adjusted using holographic techniques. The specification for the primary dish overall surface rms error is 158 μm which leads to antenna aperture efficiencies equal to 70% at 7 mm, and 50% at 3 mm. The antenna pointing error specification is 3.″7 under wind speeds of 10 m/s.

The large receiver cabin (8×9×3.5 m) will move in azimuth together with the telescope and keep a constant temperature in a range of (20 ± 3)°C. The receiver which will be used for holography measurements at 12 GHz will be placed at the primary focus. All other receivers will be located in the secondary focus cabin (so that several of them can be used simultaneously), arranged in a high frequency branch, for $\nu > 30$ GHz, and a low frequency branch for $\nu < 30$ GHz.

The radiotelescope will operate in several bands from 13 cm (2.3 GHz) to 2.6 mm (115 GHz) both as a single dish antenna and as an element of a VLBI array. Table 1 lists the receivers under construction at OAN. The new 40 meter radiotelescope will replace the current Yebes 14-meter dish in all VLBI projects in which OAN/IGN is involved for Astronomy and Geodesy, using the Mark-5 VLBI data acquisition system developed by Haystack (Ma,USA). It should then become an important partner in most VLBI networks at cm and mm wavelengths.

More information at http://www.oan.es/

Table 1. Receivers under construction at OAN

Band	**ν (GHz)**	**Focus**	**T_{rec}**	**Polarization**
S/X	2.3/8.4	S	15-20	RCP
C	5-6	S	45	DUAL
K	21-24	S	45	DUAL
Q	40-50	S	75	DUAL
W	86-115	S	100	DUAL

Design of the Near-term Next Generation Space-VLBI Mission VSOP-2

H. Hirabayashi[1], Y. Murata[1], P.G. Edwards[1], Y. Asaki[1], N. Mochizuki[1], M. Inoue[2], T. Umemoto[2], S. Kameno[2], L.I. Gurvits[3], and A.P. Lobanov[4]

[1] Institute of Space and Astronautical Science, Japan Aerospace Exploration Agency
[2] National Astronomical Observatory of Japan
[3] Joint Institute for VLBI in Europe, The Netherlands
[4] Max-Planck Institute for Radioastronomy, Germany

Abstract. A second generation space VLBI mission, VSOP-2, is being planned for a launch in 2010 or soon after. The scientific objectives are very high angular resolution imaging of astrophysically exotic regions, including the cores, jets, and accretion disks of active galactic nuclei (AGN), water maser emissions, micro-quasars, coronae of young stellar objects, etc. A highest angular resolution of about 40 μas is achieved in the 43 GHz band. Engineering developments are in progress for the deployable antenna, high data rate transmission, cryogenic receivers, antenna pointing, accurate orbit determination, etc., to realize this mission. International collaboration will be as important as it has been for VSOP.

1 VSOP-2 Science Goals

Following the successes of VSOP (the VLBI Space Observatory Programme), a near-term next generation Japanese space VLBI mission, currently referred to as VSOP-2 [1,2], is being planned in collaboration with international partners. The VSOP-2 website is http://www.vsop.isas.jaxa.jp/vsop2/ .

The VSOP-2 science goals include: study of emission mechanisms in conjunction with the next generation of X-ray and gamma-ray satellites; full polarization studies of magnetic field orientation and evolution in jets, and measurements of Faraday rotation towards AGN cores; high linear resolution observations of nearby AGN to probe the formation and collimation of jets and the environment around supermassive black holes; and the highest resolution studies of spectral line masers and mega-masers, and circum-nuclear disks. Higher observing frequencies, cooled receivers, increased bandwidths and larger telescope diameters will result in gains in resolution and interferometer sensitivity by factors of $\sim$10 over the VSOP mission.

2 The VSOP-2 Satellite

The VSOP-2 spacecraft will employ a 9 m off-axis paraboloid antenna. The observing bands will be 8, 22, and 43 GHz. It is assumed the VSOP-2 satellite will be launched on a M-V rocket and placed in an elliptical orbit with an apogee height of $\sim$25,000 km and a perigee height of $\sim$1,000 km, resulting in a period

of ∼7.5 hours. Unlike HALCA, the VSOP-2 satellite will receive both LCP and RCP, and use cryogenic coolers for the two higher frequency bands to reduce the system temperature. Observing requires a two-way link between the satellite and a tracking station, for a wideband down link at 1 Gbps, and with the uplink used to transfer a reference signal. The current spacecraft mass estimate is 910 kg, with a generated power of 1800 W.

3 New Technical Aspects for VSOP-2

The on-board radio astronomy antenna is one of the most critical parts of the spacecraft. The development of an off-axis mesh antenna with a segmented (modular) radial rib design has been in progress over the last four years at ISAS. The radio astronomy receivers for the 22 GHz and 43 GHz bands will be cooled.

The frequency band for the 1 Gbps VLBI data down-link is 37–38 GHz, and the up-link reference frequency is 40 GHz. Studies and trade-offs have been done taking into account both the quantization loss, circuitry complexity, and down-link power.

Nodding of the whole spacecraft quickly between the calibrator and target sources is possible with the addition of 2 Control Moment Gyroscopes (CMGs) to the 4 momentum reaction wheels (RWs). For such phase-referencing observations, orbit determination accuracy of a few cm is required, and this could be achieved by adding GPS receivers with a high precision 3-dimensional accelerometer, or by using both GPS and Galileo receivers, according to simulations performed at JPL for the VSOP-2 orbit.

4 VSOP-2 Proposal Status

The VSOP-2 proposal was submitted to ISAS' Science Steering Committee in October 2003, at the same time as the X-ray mission NeXT. Both missions were highly ranked, but ultimately, due to ISAS' near-term budget profile for the next few years, neither was included in the budget request for the 2005 fiscal year. ISAS is preparing a long-term plan to outline a coherent strategy for future missions connected with future budget requests.

The ongoing support and assistance from the domestic and international communities will be required for the submission of an even more competitive proposal.

References

1. H. Hirabayashi, et al.: In *Galaxies and their Constituents at the Highest Angular Resolutions*, IAU Symposium 205, eds. R.T. Schilizzi, S.N. Vogel, F. Paresce and M. Elvis, p. 428 (2001)
2. H. Hirabayashi: In: *Future Directions in High Resolution Astronomy: A Celebration of the 10th Anniversary of the VLBA* (ASP Conf. Ser.) eds. J.D. Romney & M.J. Reid (in press)

Imaging Across the Spectrum: Synergies Between SKA and Other Future Telescopes

A. Lobanov

Max-Planck-Institut für Radioastronomie, Auf dem Hügel 69, 53121 Bonn, Germany

Abstract. SKA[1] will be operating at the same time with several new large optical, X–ray and Γ–ray facilities currently under construction or planned. Fostering synergies in astrophysical research made across different spectral bands presents a compelling argument for designing the SKA such that it would offer imaging capabilities similar to those of other future telescopes. Imaging capabilities of the SKA are compared here with those of the major future astrophysical facilities.

1 Imaging Performance of SKA and Other Future Telescopes

A first order comparison of imaging performance of different instruments can be made by comparing their respective spatial dynamic ranges (SDR, the ratio between the maximum and the minimum detectable angular scales) and resolutions.

The resolution of the SKA is compared in Figure 1 with the resolutions of various existing and future telescopes. The resolution of SKA is close to the resolution of the largest projected optical telescopes, but it may be inferior to the resolution of the proposed X–ray interferometer mission MAXIM. For the optical telescopes, the SKA would be able to present a reasonable match provided that the SKA reaches a ≤ 1 mas resolution at its highest observing frequency (see [1] for more details).

The SDR of the different SKA designs is compared in Figure 1 with the SDR of other instruments. For a radio interferometer, the SDR is affected by the observing bandwidth, $\Delta\nu$, averaging time, τ, and filling factor of the Fourier domain, $\Delta u/u$ [1] (analogies of these quantities can be found for all instruments working in other spectral bands).

For most of the high–dynamic range observations with the SKA the bandwidth and integration time may have to be significantly reduced, if one would require to reach SDR similar to that of the largest optical instruments. These two corrections can be introduced at the stage of observation preparation, and their worst effect is the increased observing time needed to reach the required sensitivity. The Fourier space sampling, described by the $\Delta u/u$ ratio, is however "hard–wired" into the array design, and can only be improved by adding new

[1] The Square Kilometer Array, a next generation interferometric instrument for centimeter-wave radio astronomy. See http://www.skatelescope.org for a detailed description.

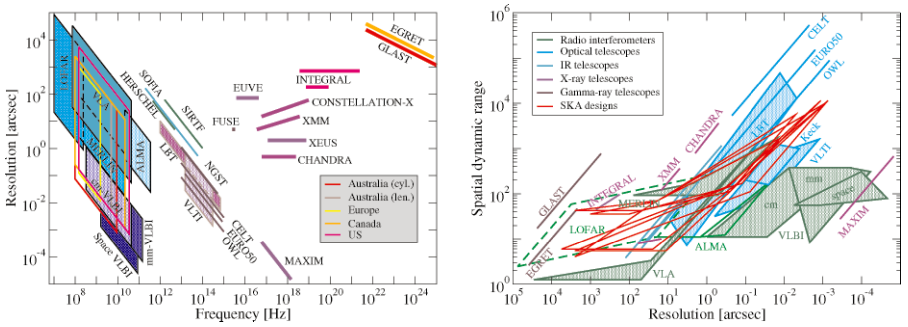


Fig. 1. Left: Resolution of the SKA compared with the resolution of other main existing and future astronomical instruments. **Right:** Spatial dynamic range of the SKA designs for observations with $\Delta\nu$=1 MHz and τ=1 s) compared to other major instruments [1].

stations. For an inhomogeneous array in which $\Delta u/u$ varies depending on the baseline length, the reduction of spatial and even conventional dynamic range may be substantial. This dictates the need to optimize this parameter at the earliest possibles stages of the array design. In addition to that, optimization of $\Delta u/u$ is also required by high–fidelity imaging at low SNR levels. The lowest SNR of "trustable" pixel in an interferometric image is given by

$$\ln(\mathrm{SNR_{low}}) = \left[\frac{\pi}{4}\left(\frac{\Delta \mathrm{u}}{\mathrm{u}} + 1\right)\right]^2 \frac{1}{\ln 2}\,. \tag{1}$$

The SDR reduction due to poor Fourier space sampling becomes significant at $\Delta u/u \geq 0.4$, and it is negligible at $\Delta u/u \leq 0.2$. It should therefore be possible to reach the maximum SDR levels in an array configuration that provides $\Delta u/u \leq 0.2$ at all baselines. If multifrequency synthesis is used for imaging, this condition becomes $\Delta u/u \leq 0.2 + \Delta\nu_{\mathrm{mfs}}$ ($\Delta\nu_{\mathrm{mfs}}$ is the fractional bandwidth over which the synthesis is performed). Therefore, this requirement must be considered as one of the basic requirements for the design of the SKA.

To make the SKA a competitive imaging instrument that would match the capabilities of future optical and X-ray telescopes, two basic conditions must be fulfilled:

1. Resolution of ≤ 1 mas at the highest observing frequency.
2. Fourier plane filling factor $\Delta u/u \leq 0.2$ over the entire range of uv–coverage.

References

1. A.P. Lobanov, SKA Memo No. 38 (2003)
`http://www.skatelescope.org/PDF/ska_memo38.pdf`

The Korean VLBI Network Project

H.-G. Kim[1], S.-T. Han[1], and B.W. Sohn[2]

[1] Korea Astronomy Observatory, 61-1 Hwaam, Yuseong, Daejeon 305-348, Korea
[2] MPI for Radio Astronomy, Auf dem Hügel 69, 53121 Bonn, Germany

Introduction Korean VLBI Network (KVN) is a mm-VLBI network construction project of Korea Astronomy Observatory. During the (first) project period (2001 - 2007), three observatories are going to be constructed at Seoul (Yonsei Univ.), Ulsan (Univ. of Ulsan), and Jeju (Tamna Univ.). All possible baselines and the sites of the observatories are listed in Table 1. Scientific goals are various, e.g. continuum observation of AGNs, of star forming regions, of microquasars, spectroscopy of stars, of star forming regions, and of Galactic centre region as well as geodetic observation. The antenna specifications of KVN are described in Table 2.

KVN system KVN distinguishes itself from other VLBI networks by its simultaneous multi-frequency observation capability at mm wavelength and by its flexible wideband data acquisition system (KVN DAS) [1]. KVN is going to install a multi-frequency receiver system which employs perforated plate filters within a quasi-optical beam transportation system. This system enables simultaneous multi-frequency on-source phase referencing and simultaneous multi-frequency observation [1,2]. Significant increase of phase coherent time at mm wavelength is expected as a result of this concept. Frequency which is covered by KVN receiver system ranges from 2/8 GHz to 150 GHz. KVN is also going to install water-vapor radiometer for the atmospheric phase correction e.g. [2,3]. This technique is known to be not as accurate as the on-source phase referencing [2]. However the phase correction of weak sources benefits from this technique in the dry weather condition. In order to enable simultaneous multi-frequency observation, KVN DAS consists of four high speed samplers for each system and each sampler is to be operated at 1 Gsps and 2 bits per sample (Tab. 3). FIR digital filters are designed to manage 16 channels of 8 MHz to 32 MHz and of 2 bits/sample data. KVN started the conceptual design of the new KVN correlator; this new correlator is planed to process multi-frequency data in e-VLBI mode.

References

1. Y.C. Minh et al: in *New Technologies in VLBI* , ed. by Y.C. Minh (A.S.P. Conf. Ser. Vol 306, 2003) pp. 373–381
2. T. Sasao: in *New Technologies in VLBI* , pp. 53–74
3. W. Alef et al: in *New Technologies in VLBI* , pp. 75–92

Table 1. Sites and baselines of KVN observatories and Taeduk Radio Astronomy Observatory (TRAO)

KVN	Longitude	Latitude	Baseline			
Site	° ′ ″ E	° ′ ″ N	Yonsei	Ulsan	Tamna	TRAO
Yonsei (Seoul)	126 56 35	37 33 44	–	305.2	477.7	135.1
Ulsan (Ulsan)	129 15 04	35 32 33	305.2	–	358.5	194.2
Tamna (Jeju)	126 27 43	33 17 18	477.7	358.5	–	356.0
TRAO (Daejeon)	127 22 19	36 23 53	135.1	194.2	356.0	–

Table 2. KVN antenna specifications

Type	AZ/EL, Cassegrain
Diameter	21 m
f/D Ratio	4.7
Total Surface Tolerance	≤ 150 μm at wind speed of 10 m/s
Pointing Accuracy	≤ 4 arcsec at wind speed of 10 m/s
Slewing Speed	3°/s (in AZ,EL)
Acceleration	$3^\circ/s^2$ (in AZ,EL)
AZ Oper. Range	$-270^\circ \sim +270^\circ$
EL Oper. Range	$0^\circ \sim 90^\circ$
Tolerable Wind Speed	
- Precision Operation	$\leq$ 10m/s
- Maximum Survival	90 m/s

Table 3. KVN DAS specifications

IF Inputs	selectable 4 IF streams of wide bandwidth
Samplers	4 streams at 1 Gsps, 2 bits/sample
Digital Filters	16 channels, 8/16/32 MHz bandwidths, 2 bits/sample
Recorder	Mark 5, 1 Gbps recording rate

Frequency Protection for the 21st Century

W. van Driel[1,2]

[1] Observatoire de Paris, GEPI, 92195 Meudon, France
[2] Scientif. Comm. on Frequency Allocations for Radio Astronomy and Space Science (IUCAF)

The electromagnetic (radio) spectrum is a very valuable natural resource that is finite and shared by an increasing number of users vying for the allocation of frequency bands. As a result, the electromagnetic environment in which astronomical observations are made is getting increasingly polluted, driven by commercial interests. In general, non-scientific spectrum use emits radiation at levels that far exceed those emitted by the cosmic sources in which astronomers are interested.

On the other hand, the sensitivity (and cost) of astronomical instruments is ever increasing, driven by scientific and technological progress, and their fruitful operation requires the ability to perform observations down to the increasingly fainter levels, and, in the regulated (radio) frequency domain, increasingly outside the frequency bands allocated for astronomical use (basically due to the redshift of spectral lines). Radio telescopes can pick up interference emitted from positions on the horizon or in the sky that are far away from the telescope's pointing direction, at frequencies well outside the observed band.

In principle, two ways are available to enable high-sensitivity observations: interference mitigation (technical approach) that identifies and removes unwanted man-made interference signals, and spectrum management (regulatory approach) that accommodates all competing services and systems within the finite usable range of the radio spectrum, which includes setting limits on unwanted emissions (interference) by other spectrum users into frequency bands allocated for astronomical research. The saying "Prevention is better than a cure" is also self-evident in this case: the stricter the regulatory limits set on interference levels, the weaker the unwanted signals to be removed will be.

Astronomical spectrum management requires different kinds of interactions with quite different organisations, ranging from town- and county councils, through national spectrum management Administrations and regional coordinating commissions, to global forums like the International Telecommunication Union (ITU). The ITU provides the global framework for spectrum management in its Radio Regulations, that contain the international Frequency Allocation Table and provide rules to national Administrations for the regulation of equitable access to the radio spectrum. The Radio Regulations are revised at World Radiocommunication Conferences (WRCs) once every three years on

average. National Administrations regulate, e.g., the implementation of Radio Quiet Zones or exclusion- and coordination zones around radio observatories.

IUCAF (the Scientific Committee on Frequency Allocations for Radio Astronomy and Space Science of ICSU) is the international organisation representing the interests of astronomers in the use of the spectrum at the ITU. It is sponsored by COSPAR, the IAU and URSI. IUCAF is organising an expansion in its regional (African, American, ...) coverage and in its frequency (optical/infrared) coverage, to respond to the ITU decision to expand its regulation of spectrum use to the sub-millimetre, infrared and optical wavelength domains.

The protection of future giant radio telescopes: the key scientific goals of ALMA, LOFAR and the SKA will require ultra-sensitive observations outside the frequency bands currently allocated to the Radio Astronomy Service by the ITU, where we cannot claim protection from interference, which will be many orders of magnitudes stronger than the cosmic signals we will try to detect. The aim of IUCAF, in cooperation with national Administrations, is an ITU Recommendation on Radio Quiet Zones for the sites of these giant telescopes, to provide guidance to national Administrations on their implementation. A key problem remains the emissions by communication satellites outside our bands, which cannot be limited or controlled by the Administration on whose territory a radio telescope is located, unlike those of terrestrial transmitters.

Towards regulation at higher frequencies (sub-millimetre, infrared, optical...): hitherto, the ITU concerned itself only with regulating spectrum use at radio frequencies, up to 275 GHz (or 1 mm wavelength), but its role will in principle be extended over the entire electromagnetic spectrum, as required – e.g., at the WRC in 2010 frequency allocations are expected to be considered between 275 GHz and 3000 GHz (100 μm wavelength). IUCAF is organising a group of Correspondents from observatories operating at infrared and optical wavelengths – specifically, the astronomical community should express itself at the ITU on the possibility and relevance of the regulation of the spectrum below 100 μm wavelength.

Space-borne observations: IUCAF is coordinating efforts towards the drafting of a new ITU Recommendation on protection criteria for radio astronomical observations from space made at frequencies covered by the ITU Radio Regulations ($\leq$275 GHz); high-frequency space telescopes will be considered under the expansion of the scope of the ITU Radio Regulations towards higher frequencies (see above).

Another route - the OECD Global Science Forum: initiating discussions outside the well-established Administrations/ITU spectrum management circuit, this Forum organised a Task Force on Radio Astronomy and the Radio Spectrum to examine the spectrum use requirements of the astronomical and satellite telecommunications communities, which resulted in a Report with recommendations on consultation and collaboration between both communities, e.g. on the establishment of "Controlled Emission Zones" around future giant radio telescopes (based on agreed technical and economic feasibility). Their practical implementations need to be examined further.

SCUBA-2: A Large-Format CCD-Style Imager for Submillimeter Astronomy

M.D. Audley[1], W. Holland[1], D. Atkinson[1], M. Cliffe[1], M. Ellis[1], X. Gao[1], D. Gostick[1], T. Hodson[1], D. Kelly[1], M. MacIntosh[1], H. McGregor[1], D. Montgomery[1], I. Smith[1], I. Robson[1], K. Irwin[2], W. Duncan[2], R. Doriese[2], G. Hilton[2], C. Reintsema[2], J. Ullom[2], L. Vale[2], A. Walton[3], W. Parkes[3], C. Dunare[3], P. Ade[4], D. Bintley[4], F. Gannaway[4], C. Hunt[4], G. Pisano[4], R. Sudiwala[4], I. Walker[4], A. Woodcraft[4], M. Fich[5], M. Halpern[5], J. Kycia[5], D. Naylor[5], P. Bastien[5], and G. Mitchell[5]

[1] UK Astronomy Technology Centre, Blackford Hill, Edinburgh EH9 3HJ, UK
[2] National Institute of Standards and Technology, 325 Broadway, Boulder, CO 80305, USA
[3] The Scottish Microelectronics Centre, University of Edinburgh, Edinburgh, EH9 3JF, UK
[4] Cardiff University, Cardiff, CF24 3YB, UK
[5] Canadian SCUBA-2 Consortium

Abstract. We describe the capabilities of SCUBA-2, the first CCD-like imager for submillimeter astronomy, and the technologies that make it possible. Unlike previous detectors using discrete bolometers, SCUBA-2 has two dc-coupled, monolithic arrays with a total of ∼10,000 bolometers. SCUBA-2's absorber-coupled pixels use superconducting transition edge sensors operating at $\sim$ 120 mK for photon-noise limited performance and a SQUID time-domain multiplexer for readout. It will offer simultaneous imaging of an 8×8 arcmin field of view at wavelengths of 850 μm and 450 μm. SCUBA-2 is expected to have a huge impact on the study of galaxy formation and evolution in the early Universe as well as star and planet formation in our own Galaxy. Mapping the sky to the same S/N up to 1000 times faster than SCUBA, SCUBA-2 will also act as a pathfinder for submillimeter interferometers such as ALMA. SCUBA-2 will begin operation on the JCMT in 2006.

1 Introduction

SCUBA (the Submillimeter Common User Bolometer Array) on the James Clerk Maxwell Telescope has been one of the most successful instruments ever built for a ground-based telescope [1]. SCUBA-2 will leverage new technologies for a revolutionary improvement in sensitivity and mapping speed. The science case for SCUBA-2 is discussed in detail elsewhere [2].

SCUBA-2 is expected to be delivered to the JCMT in February 2006. The first prototype sub-array has been successfully fabricated and is being integrated for testing at the time of writing [3].

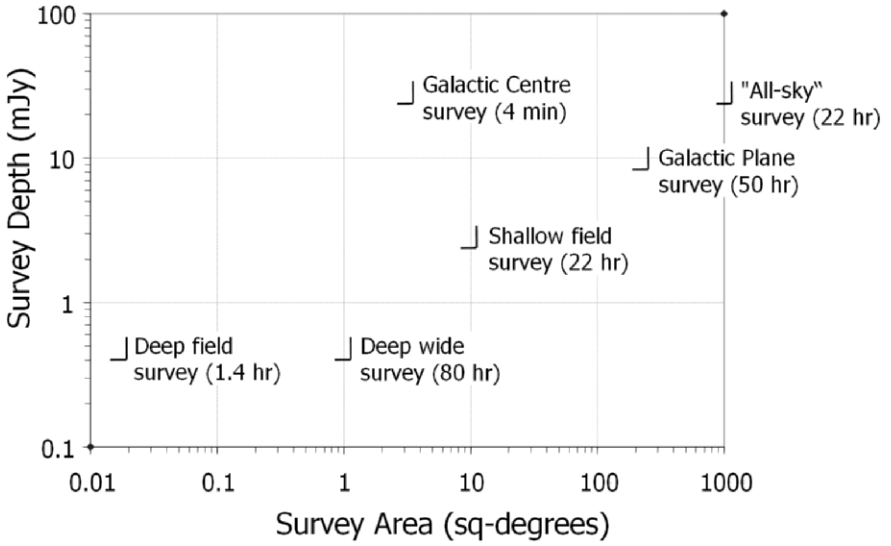


Fig. 1. A selection of possible SCUBA-2 surveys at 850 μm. The time estimates assume an observing efficiency of 70%.

2 SCUBA-2 Surveys

Less than 1 square degree of sky has been mapped in the sub-millimeter to any great depth (e.g. close the the extragalactic confusion limit). SCUBA-2 will be primarily a survey instrument that will map large areas of sky about 1000 times faster than SCUBA. The new sub-millimeter interferometers like ALMA and the SMA are limited as survey instruments by their narrow fields of view. SCUBA-2 will act as a pathfinder for these instruments, filling the JCMT's 8×8-arcmin field of view with dc-coupled pixels. Figure 1 shows some of the surveys that will be possible with SCUBA-2.

References

1. W.S. Holland, E.I. Robson, W.K. Gear, C.R. Cunningham, J.F. Lightfoot, T. Jenness, R.J. Ivison, J.A. Stevens, P.A.R. Ade, M.J. Griffin, W.D. Duncan, J.A. Murphy, D.A. Naylor: MNRAS **303**, 659 (1999)
2. W.S. Holland, W. Duncan, B.D. Kelly, K.D. Irwin, A.J. Walton, P.A.R. Ade, and E.I. Robson: Proc. SPIE **4855**, 1 (2003)
3. M.D. Audley, W.S. Holland, T. Hodson, M.J. MacIntosh, I. Robson, K.D. Irwin, G.C. Hilton, W.D. Duncan, A. Walton, W. Parkes, P.A.R. Ade, I. Walker, M. Fich, J. Kycia, M. Halpern, D.A. Naylor, G. Mitchell, and P. Bastien: In: *Millimeter and Submillimeter Detectors for Astronomy II, ed. by J. Zmuidzinas and W. S. Holland*, Proc. SPIE **5490**, in press (2004)

The Large Millimeter Telescope

F.P. Schloerb[1], L. Carrasco[2], and E. Brinks[2]

[1] Department of Astronomy, University of Massachusetts, Amherst MA 01003, USA
[2] Instituto Nacional de Astrofísica Óptica y Electrónica, Tonantzintla, Pue 72840, Mexico

Abstract. The LMT is a 50m–diameter millimeter-wave antenna designed for performance in the 1–4 mm band. Erection is expected to be completed by the end of 2004, with outfitting running through 2006. The LMT will have nearly 2000 m^2 of collecting area with an overall surface accuracy of 70 μm rms. Its sensitivity will exceed that of existing millimeter–wavelength telescopes by a significant margin. As a completely filled aperture, the LMT will have optimum sensitivity to low surface brightness emission at angular resolutions of 6–15 arcsec, which is comparable to that of maps made with today's interferometric arrays. Consequently, we expect the LMT to become one of the premier instruments to explore the cosmic frontier.

1 The Telescope and Site

The LMT Project is the joint effort of the University of Massachusetts (UMass) and the Instituto Nacional de Astrofísica, Óptica, y Electrónica (INAOE), Mexico. The telescope is being built atop Volcán Sierra Negra, an extinct volcanic peak in the state of Puebla located approximately 100 km east of the city of Puebla and 8 km SW of Mexico's highest peak, Pico de Orizaba. Figure 1 shows the appearance of the site in May 2004.

The Sierra Negra site was selected in 1997 following radiometric site tests at a number of potential mountain sites in Mexico. The site's elevation is 4600m



Fig. 1. LMT Steel Structure Assembly at Sierra Negra: (Left) Alidade, with portions of one counterweight in the foreground; (Right) Backup Structure.

and its latitude is 19 degree, hence the LMT's coverage of the southern sky will be very good, with the Galactic center culminating at an elevation of about 45 degrees. The meteorological conditions at the site are relatively mild for such a high altitude. Snow fall is generally light during the year. The diurnal temperature cycle is typically only 5K; the median wind speed is only $\sim 5\,\mathrm{m\,s^{-1}}$, and the telescope has been designed with the goal of meeting its specifications in all winds below $10\,\mathrm{m\,s^{-1}}$. These conditions occur $\sim$90% of the time. The LMT approach to mitigate the effects of insulation, wind load, gravity, etc., is to create an "active" telescope which measures properties of the antenna in real time and uses the predictions of finite element models of the structure to improve its performance.

2 The Instruments

The LMT will initially be equipped with the following instruments that are being developed at UMass' Five College Radio Astronomy Observatory (FCRAO):

SEQUOIA: The FCRAO's 32-pixel focal plane array for the 85–115 GHz frequency band.

Bolocam II: Bolocam II will be a second realization of the Bolocam I instrument; it provides 144 pixels and is designed to operate in the 2.1, 1.4, or 1.1 millimeter bands.

SPEED: The Spectral Energy Distribution Camera (SPEED) is designed to complement Bolocam II by enabling efficient measurements of the complete SED of objects using all the LMT millimeter and submillimeter bands. SPEED will use 16 frequency selective bolometers (FSB) to sample the 2.1, 1.4, 1.1, and 0.86 mm bands *simultaneously* at four sky positions. This novel bolometer technique will enable improved removal of atmospheric fluctuations, resulting in a factor of two improvement in sensitivity over conventional bolometer arrays.

Redshift Receiver: The FCRAO has begun final design of an ultrawideband Redshift Search Receiver that allows distant objects to be observed at low (25 MHz) resolution over the entire 75–111 GHz frequency band in a single observation.

1mm receiver: The FCRAO labs are building a dual-polarization SIS receiver for the 210–275 GHz frequency band as a precursor to an eventual focal plane array. The wideband characteristics of this receiver allow it to be used effectively with the redshift receiver's spectrometer to carry out efficient redshift searches for galaxies at $z \lesssim 3$.

Acknowledgements

Financial support in Mexico is provided by the INAOE and the Consejo Nacional de Ciencia y Tecnologia (CONACyT) and in the USA by the Commonwealth of Massachusetts and the Advanced Research Project Agency, Sensor Technology Office DARPA Order No. C134 Program Code No. 63226E Issued by DARPA/CMO under contract #MDA972-95-C-0004. Funding for LMT instrumentation is also supported by National Science Foundation grants AST0228993, AST0096854, and AST0215916.

An Overview of the Submillimeter Array Telescope

A. Peck[1], A. Schinckel[2], and the SMA team[2,3]

[1] Harvard-Smithsonian CfA
[2] Smithsonian Astrophysical Observatory, USA
[3] Academia Sinica Institute of Astronomy & Astrophysics of Taiwan

Abstract. The Submillimeter Array (SMA) is a new interferometer dedicated to observations in millimeter and sub-millimeter wavelengths. It is located on Mauna Kea, Hawaii, near the CSO and JCMT facilities and was commissioned in November 2003 [2]. The array consists of eight 6-meter diameter antennas which can be moved among 24 pads on the sides of four Reuleaux triangles, producing a maximum angular resolution of 0.″1. Each antenna is equipped with a cryostat at its Nasmyth focus which will accept eight receivers covering all usable bands from 175 GHz to 920 GHz. Signal processing is performed on a special purpose XF correlator, which is based on an ASIC developed at the Haystack Observatory and the NASA/SERC for VLSI Design. The highly flexible correlator will accept two channels of 2 GHz bandwidth from each antenna, making possible either dual polarization or simultaneous dual frequency operation. A pilot program to include the 15 m JCMT and 10.4 m CSO as part of the SMA will begin in 2005.

The SMA is a collaborative project of the Smithsonian Astrophysical Observatory and the Academia Sinica Institute of Astronomy and Astrophysics of Taiwan.

The SMA antennas use a traditional alt-azimuth mount, with steel base structure and a carbon fiber reflector support structure with machined aluminium surface panels. Total weight including counterweights is 43,200 kg. The backup structure is composed of 648 carbon fiber tubes connected at stainless steel nodes. The tube lay-up, epoxy, and stainless steel material were all selected to minimize the coefficient of thermal expansion for the overall structure. The reflectors were assembled in the antenna maintenance facility on Mauna Kea, using a mechanical template. This allowed reflectors with an RMS of around 50 μm to be produced in about 10 weeks. The reflector surface is measured using holography with near-field beacons; one at 232.4 GHz and one at 680 GHz using artificial beacons on a neighboring observatory dome [3].

The SMA receivers are double sideband, SIS mixer heterodyne systems [1]. They use room temperature local oscillators which consist of Gunn oscillators and multipliers with multiplication factors of between 3 and 6. The cryostat is a circular dewar, "top" illuminated, which can hold up to 8 separate receiver inserts. Pairs of inserts can be illuminated simultaneously, allowing either 2 frequency (for example 230 GHz and 690 GHz) or dual polarization observations. Each insert consists of a Teflon window, lens at about 80 K, feed horn, mixer block, and first stage amplifier. The cooling is done entirely via closed-cycle systems, obviating the need for any liquid cryogens. The Daikin compressor provides

3 levels of cooling; approximately 4.0 K (mixer block), 16 K (second stage amplifier) and 66 K (shields etc.). The Niobium SIS junctions are fabricated at the Center for Space Microelectronics at JPL. Typical DSB receiver temperatures are 70 K (230 GHz), 90 K (345 GHz) and 450 K (690 GHz).

The distribution of local oscillator signals to the antennas and the return of the intermediate frequency (centered at 5.0 GHz) signal is performed on Sumitomo LTCD single mode fiber optic cable. These fibers have an extremely low coefficient of thermal expansion; it effectively goes through a "null" at the typical sub-ground temperature on Mauna Kea, ensuring stability of the fiber lengths over the entire site to better than 10 μm over periods of an hour or more. Thus there is no need to perform closed-loop delay measurements. The LOs in each antenna are derived from a common 5.5–8.5 GHz master reference generator. Direct Digital Synthesizers for each receiver provide the changes required for Walsh cycles, Doppler tracking and fringe stopping. This lower frequency signal (∼109 MHz) is sent to each antenna on the same fiber that is used to return the IF.

The correlator is a hybrid XF design, using extensive analog filtering and splitting before the digitizing. Each 2 GHz IF band is returned from the antennas over temperature stable single mode fibers and split into 24 "chunks" of 104 MHz at 82 MHz intervals. These 104 MHz chunks are digitized (2 bit digitizers running at an effective clock of 208 MHz) and the resultant 384 data streams (as there are two 2 GHz IFs per antenna) are fed to the correlator. There are 32 custom ASIC correlator chips per board, with 90 boards in 12 expanded VME crates for a total of 2880 correlator chips clocked at 52 MHz. This produces 1,474,560 lags, which is effectively 2.3×10^{14} operations/second. There is a great deal of flexibility in signal routing, so a wide range of resolution and bandwidth combinations are possible, including combining widely differing resolutions in the same spectrum. Standard resolution values range from 1.0 MHz/channel to 25 kHz/channel. The chip was designed by the M.I.T Haystack Observatory and the NASA/UNM Microelectronics Research Center for a consortium of 5 Institutions - the SMA, USNO, NASA, NRFA and IfAG.

References

1. R. Blundell: In: *Fifteenth International Symposium on Space Terahertz Technology*, Northhampton, MA (2004)
2. P.T.P. Ho, J.M. Moran, K.Y. Lo: ApJL, (in press), astro-ph/0406352 (2004)
3. T.K. Sridharan, M. Saito, N.A. Patel, R.D. Christensen: Proc. SPIE **5495** *Astronomical Structures and Mechanisms Technology*, Eds. J. Antebi & D. Lemke (2004)

Tunable Heterodyne Receivers - A Promising Outlook for Future Mid-Infrared Interferometry

C. Straubmeier[1], R. Schieder[1], G. Sonnabend[2], D. Wirtz[1], V. Vetterle[1], M. Sornig[1], and A. Eckart[1]

[1] I. Physikalisches Institut, University of Cologne, Zülpicher Straße 77, 50937 Cologne, Germany
[2] Goddard Space Flight Center, Greenbelt, MD 20771, USA

1 Principle of Operation

Sketching the beam layout of the Cologne Tunable Heterodyne Infrared Spectrometer (THIS), the basic principle of operation of a heterodyne receiver is illustrated in Fig. 1 [1,2]. A local oscillator (LO) is precisely locked to a frequency close to the observing wavelength by the resonance of a Fabry-Perot diplexer, which itself is stabilised to a resonance of a special HeNe laser. The LO radiation with its known frequency is then superimposed onto the signal of the observed science source (or hot or cold calibration sources) and both get mixed via a HgCdTe (MCT) detector, what generates a beat frequency (intermediate frequency; IF) at a much lower (and therefore easier to process) frequency of about 1 GHz. This broadband low frequency signal, which still contains all the spectral information of the science source, can then be analysed using common broadband Acousto Optical Spectrometers (AOS).

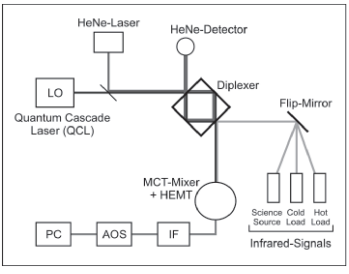


Fig. 1. Beam layout of the Cologne Tunable Heterodyne Infrared System (*THIS*).

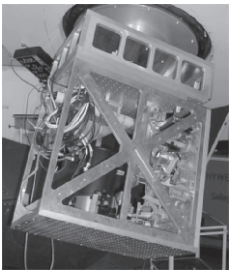


Fig. 2. *THIS* mounted to the Cass. focus of the *TIRGO* telescope on Gornergrat.

2 Existing Systems and First Scientific Results

Fig. 2 shows the *THIS* instrument of the I. Physikalisches Institut of the University of Cologne mounted to the Cassegrain focus of the *TIRGO* telescope on Gornergrat (CH). The receiver is designed as a flexible and transportable system (volume $\sim 60 \times 60 \times 45\,\mathrm{cm}^3$, weight $\sim 80\,\mathrm{kg}$) that can be adapted easily to

various telescope configurations. Since 1998 the system has been operated successfully at the *TIRGO* telescope on Gornergrat, the Hainberg Solar Tower at Göttingen, the *IRSOL* Solar Telescope at Locarno, the Hoher List Observatory at Daun, and the McMath-Pierce Solar Telescope at Kitt Peak. The obtained scientific measurements include height profiles of stratospheric Ozone [1,2], SiO and water absorption in sunspots, CO_2 emission of Venus, and Ozone absorption and CO_2 emission on Mars. A long term objective of *THIS* is the installation of the detector system on board of the airborne *SOFIA* telescope.

3 Heterodyne Receivers for Mid-IR Interferometry

At large interferometers like the VLTI heterodyne systems might prove superior over genuine mid-infrared cameras because of several technical reasons [3]. By installing one heterodyne detector at each telescope, the observed mid-infrared signal is converted to the radio domain directly at each station, what removes the need of sensitive optical delay lines and allows to perform the geometrical delay compensation at radio wavelengths. Especially if a high number of baselines shall be correlated, this is technically much simpler to achieve at lower frequencies. Furthermore, the single dish signals can easily be amplified before the transmission to the interferometry station, so that the correlation of all $n(n-1)/2$ baselines can be performed without loss in sensitivity.

However, an interferometric setup like this with distributed heterodyne receivers requires a common local oscillator signal, which has to be transmitted from a single reference source to each telescope station. Thinking of heterodyne systems at currently existing optical interferometers, the distribution of this LO signal could be accomplished for example by using the optical delay lines in a fixed geometry. Since this task does not require precise movement over large distances, the respective technical requirements of the delay lines are much easier to achieve and maintain, therefore increasing the uptime of the system.

Regarding the demandingly high technical requirements of current NIR and MIR interferometers, which sometimes are close to the limit of feasibility, the introduction of heterodyne receiver technology might offer a promising opportunity to reduce complexity, and therefore increase system availability and scientific return.

References

1. G. Sonnabend, D. Wirtz, F. Schmülling, R. Schieder: Applied Optics **41**, 15, 2978 (2002)
2. D. Wirtz, G. Sonnabend, R. Schieder: Spectrochimica Acta Part A **58**, 2457 (2002)
3. G. Sonnabend, D. Wirtz, R. Schieder, A. Eckart: "Proposal for a VLT Multichannel Infrared Heterodyne Instrument based on THIS (Tunable Heterodyne Infrared Spectrometer)". In: *Proceedings of the ESO Workshop: Scientific Drivers for ESO Future VLT/VLTI Instrumentation*, p. 225 (2001)

ESPRIT – Exploratory Submillimeter sPace Radio Interferometric Telescope

W. Wild[1], L. Venema[2], and J. Cernicharo[3] on behalf of the ESPRIT study team

[1] SRON, Landleven 12, 9747 AD Groningen, The Netherlands,
http://www.sron.rug.nl/esprit
[2] ASTRON, Postbus 2, NL-7990 AA, Dwingeloo, The Netherlands
[3] CSIC-IEM, C/. Serrano 113&121 28006 Madrid, Spain

Abstract. The far-infrared (FIR) wavelength regime is of prime importance for astrophysics. The study of ionic, atomic and molecular lines, many of them present in the FIR, provides important and unique information on the star and planet formation process occurring in interstellar clouds, and the lifecycle of gas and dust in general. As these regions are heavily obscured by dust, FIR observations are the only means of getting insight in the physical conditions and chemistry. These investigations require high spectral as well as high angular resolution in order to match the small angular sizes of star forming cores and circumstellar disks. ESPRIT provides *both*, in a wavelength regime not accessible to ALMA (Atacama Large Millimeter Array) nor to JWST (James Webb Space Telescope).

1 Science case

One of the key questions of modern astrophysics is the birth of stars and planets. Important questions include: What are the physical conditions for star-formation to occur; How do the circumstellar disks evolve; How do the proto-planetary regions decouple from the gas; and what is the chemistry that led to the prebiotic conditions of the early Earth? Finally, we also would like to know what role star-formation (in particular star-bursts) plays in external galaxies and how it interacts with the general interstellar medium.

Observations of spectral lines in the FIR domain will contribute to answer these questions. Due to the small angular size of star forming regions, and the narrow line widths, very high spatial (0.″02 to 0.″1) and spectral resolution (<1 km/s at 100μm) is required. In particular, ESPRIT will observe:

- Water, its isotopomers and other hydrides,
- Oxygen bearing species, such as [OIII], [OI], OH, and H_3O^+, and
- Cooling lines (like C^+ and N^+) of the ISM in our Galaxy and other galaxies,

Not only allows this for a complete oxygen inventory to be made, but the widely spaced energy ladders of water and the other (deuterated) hydrides (with their best or main spectral lines in the (far-)infrared) allow for probing very special regions from heavily depleted star-formation regions, to diffuse photon-dominated regions.

2 ESPRIT Mission Concept

ESPRIT will consist of 6 to 8 telescopes, about 3.5m diameter each, passively cooled to $\sim$ 80K. They will work as an interferometer in a free-flying configuration with a distributed correlator linked by fast optical data links. Baselines will range from a very close configuration ($\sim$ 10m) to about 1000m. This will result in a spatial resolution of $2''$ to $0\farcs02$. Each telescope will be equipped with heterodyne frontends (cooled to 4K), e.g. Hot-Electron-Bolometer (HEB) mixers, pumped with Quantum-Cascade-Laser (QCL) local oscillators (LOs), operating between 1 to 6 THz (50 to 300 μm) and solid-state LOs at 557 GHz, both with an instantaneous bandwidth of at least 4GHz. Phase calibration is not possible on celestial sources so self-calibration techniques will have to be applied making use of exact knowledge on the positions of the satellites and phase locked LOs. Most of the technology needed to realize ESPRIT is either available, or will be available in the near future. Using the Darwin-studies we can safely assume that formation flying will be possible in 10 years from now. HEB mixers have been demonstrated above 4 THz, and QCLs are either available or under development for the planned frequencies. Space qualified frontend-coolers are under development or tested at various places. The optical design will use SWAS, ODIN and Herschel-HIFI knowledge. Nevertheless, some further technology development is needed. Items include control of the free-flying formation, phase-locking of FIR LOs, increasing the instantaneous bandwidth of HEBs, wider tuning range of QCLs, and a low-power distributed correlator.

3 Advantages of ESPRIT Over Other Missions

ESPRIT will fill an important observational gap which is not covered by other existing or planned instruments or missions. ISO, Spitzer and Herschel lack(ed) the high spatial resolution, JWST-MIRI and ALMA the wavelength coverage. ESPRIT is therefore unique for FIR astronomy in combining very high spectral *and* spatial resolution.

ESPRIT has some major advantages over Darwin, because the coherence length of an heterodyne interferometer at 100μm is about 30m. This means that all delay compensations are possible within the correlator and complex, physical, instantaneous delay line corrections are not needed. ESPRIT can also observe while the telescopes move and it can image in spectral lines. ESPRIT is, however, not suited for nulling like Darwin is. The metrology requirements for ESPRIT are much more relaxed than for the SPECS concept. SPECS (combining photons), also doesn't have the advantage of heterodyne detection where the signal can be divided and amplified after conversion. Moreover, its capabilities as a spectrometer are limited. SPECS, however, is likely better in detecting continua of objects at the end of the Universe.

Fizeau Interferometry with the LBT Astronomy on the Way to ELTs

W. Gaessler[1], T.M. Herbst[1], R. Ragazzoni[1,2], A. Eckart[3], G. Weigelt[4], and the LINC-NIRVANA team[1,2,3,4]

[1] Max-Planck-Institut für Astronomie, Königstuhl 14, D-69117 Heidelberg, Germany
[2] INAF Osservatorio Astrofisico di Arcetri, Largo E. Fermi 5, I-50125 Firenze, Italy
[3] 1. Physikalisches Institut der Universität Köln, Zuelpicher Str. 77, D-50937 Köln, Germany,
[4] Max-Planck-Institut für Radioastronomie, Auf dem Hügel 69, D-53121 Bonn, Germany

Abstract. The Large Binocular Telescope (LBT) consists of two 8.4 m mirrors on one mechanical mounting, with a center to center separation of 14.4 m. In the combined, focus the LBT provides the spatial resolution of a 23 m telescope and the sensitivity of a 12 m telescope. We are building an instrument called LINC-NIRVANA using the capability of LBT in Fizeau mode (imaging interferometry), leading to a unique combination of spatial resolution, sensitivity and field of view. The instrument will prove technology, such as Multi-Conjugated Adaptive Optics, which is needed for the next generation of Extremely Large Telescopes (ELT) (20 to 100 m diameter). The capabilities of LINC-NIRVANA will extend science, especially for extragalactic programs, building a bridge between current 10 m class telescopes and ELTs.

1 Instrument Overview

LINC-NIRVANA (Fig. 1) consists of an interferometric IR science camera with a $10'' \times 10''$ FoV, operating in the J, H and K bands with a spatial resolution of 10mas at J and 20mas at K.

A Fringe and Flexure Tracker corrects the optical path difference between the right and the left arms of the telescope. It uses one guide star in a $1\farcm5 \times 1'$ field and observers in the J,H or K band. The measurement is done by fitting the point spread function of the guide star.

The Multi-Conjugated Adaptive Optics with 2 Ground Layer Wavefront Sensors (GWS) uses 12 natural guide star pyramid sensors optically co-added over a $2'$ to $6'$ annular field. The GWS drives the adaptive secondary mirror with 672 actuators. The two Mid- and High Layer Wavefront Sensors (MHWS) use 8 natural guide star pyramid sensors optically co-added over a $2'$ circular central field. Each MHWS drives a 349 element deformable piezo-stack mirror.

2 Image Reconstruction

The astronomical target is observed at different parallactic angles. With a minimum of 3 images, the full 23m resolution can be reconstructed [1]. A point like

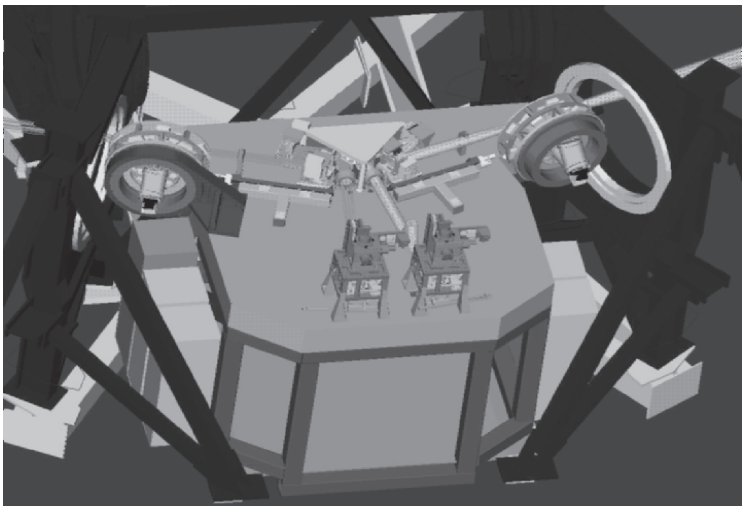


Fig. 1. Overview of LN. The round structure to the right and left are the GWS. Below the triangular shaped plate in the middle, the piston mirror for optical path difference correction is placed folding the beam into the cryostat below the bench. The MHWS can be seen on the top front of the bench

source shows the diffraction pattern of a 23 m telescope in horizontal and of a 8.4 m telescope in the vertical direction.

3 Science Cases

LINC-NIRVANA [2] gains from the combination of field of view, spatial resolution and sensitivity. It will be able to resolve stellar populations in galaxies out to 20 Mpc and detect Jupiter-like planets at the distance of 5 AU through astrometric wobble of stars out to 100pc. The surface of Titan could be resolved down to 130km per pixel (40 pixel across, with HST 4 pixels across).

Acknowledgments

This work is partially funded by the Alexander von Humboldt Foundation through the Wolfgang Paul Prize.

References

1. M. Carbillet, et al.: A&A **387**, 744 (2002)
2. H. -W. Rix and T. M Herbst: 'A Near Infrared Beam Combiner for the LBT', Response to: *Level II call for in-kind instrument contributions, September 1998* http://www.mpia.de/LINC/Files.html

MUSE: 3D Spectroscopy with Large Telescopes

A. Kelz[1], M.M. Roth[1], and M. Steinmetz[1]
on behalf of the MUSE consortium[2]

[1] Astrophysikalisches Institut Potsdam, Sternwarte 16, D-14482 Potsdam, Germany
[2] P.I.: Roland Bacon, Centre de Recherche Atronomique de Lyon, F-69230, France

1 Project Overview

The Multi Unit Spectroscopic Explorer (MUSE) is a second generation instrument [1] in development for the Very Large Telescope (VLT) of the European Southern Observatory (ESO). It is a panoramic integral-field spectrograph operating in the visible wavelength range. It combines a wide field of view with the improved spatial resolution provided by adaptive optics and covers a large simultaneous spectral range. MUSE couples the discovery potential of an imaging device to the measuring capabilities of a spectrograph, while taking advantage of the increased spatial resolution provided by adaptive optics. This makes it a unique and powerful tool for discovering objects that cannot be found in imaging surveys. MUSE is optimized for the study of the progenitors of normal nearby galaxies out to very high redshift. It will also allow detailed studies of nearby normal, starburst and interacting galaxies, and of galactic star formation regions.

MUSE is a project of 7 European institutes: Astrophysikalisches Institut Potsdam (AIP), ETH Zürich, Laboratoire d'Astrophysique de Toulouse, Sterrewachte Leiden, University of Oxford, the European Southern Observatory and is led by the Centre de Recherche Atronomique de Lyon (CRAL). In April 2004, ESO reviewed the phase A study and approved the continuation of the project.

2 Scientific Motivation

MUSE will provide the critical spectral information for the understanding of high-z galaxies. In particular **3D deep fields** will advance the knowledge of galaxy formation, from the epoch of reionization and the birth of the first stellar lumps, to the effects of feedback on the IGM and the dynamics of high-redshift galaxies. It is worth to emphasize that the power of MUSE will lie in its capacity for serendipity. The information content of a MUSE data cube is huge, and provides mining resources for unexpected discoveries.

MUSE will make key contributions to the understanding of **nearby galaxies**, both in its high-resolution AO assisted mode and in its wide-field mode. The former mode will focus on resolving the complex morphology, dynamics and stellar populations in galactic nuclei, active or not. The latter will bring an unprecedented combination of sub-arcsecond spatial resolution and a wide field of view which will allow probing high spatial frequency structures in the central few kiloparsecs of nearby galaxies or the study of galaxy mergers.

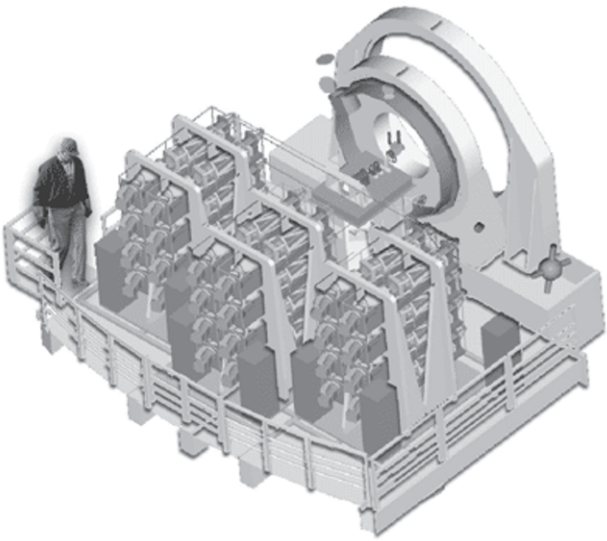


Fig. 1. MUSE at the VLT Nasmyth platform: The instrument features an AO-system, a calibration unit, an image de-rotator and atmospheric dispersion compensator. The fore-optics slices the image into 24 sub-fields, that feed as many spectrograph units.

MUSE will provide a unique opportunity to pursue **extragalactic stellar astrophysics** in galaxies up to several Mpc distance, pioneering a research field and a technique that will be fundamental for the development of both the scientific background and the instrumentation for Extremely Large Telescopes.

3 Instrumental Capabilities

MUSE features 90,000 spatial elements, either with a sampling of $0\farcs2$/spaxel for the $60'' \times 60''$ wide-field mode or with $0\farcs025$/spaxel and a resulting FoV of $7\farcs5 \times 7\farcs5$ in high-resolution mode (with AO). The wavelength range is from $465-930$ nm with corresponding resolutions between 2000 and 4000 respectively. To record this amount of information, the field-of-view is split and directed to 24 identical spectrographs. The instrument design aims at high throughput (of 20% including atmosphere plus telescope), and limiting magnitudes of $I_{AB} = 25.0$ ($I_{AB} = 26.7$) at R=3500 (R=180) for an 80-hour exposure at the VLT.

The AIP contributions include the entire calibration unit, the data reduction software, and the spectrograph-detector assembly, integration and test.

References

1. R. Bacon: 'The 2nd generation VLT instrument MUSE'. In: *Astronomical Telescopes and Instrumentation, SPIE Conference at Glasgow, UK, June 21–25, 2004*, ed. by A. Moorwood, M. Iye, 2004, 5492-51

Layer-Oriented MCAO Projects for 8-m Class Telescopes and Possible Scientific Outcome

M. Lombini[1], R. Ragazzoni[2], C. Arcidiacono[4], A. Baruffolo[5], G. Cresci[2], E. Diolaiti[1], R. Falomo[5], W. Gaessler[3], F. Mannucci[2], E. Vernet[2], J. Vernet[2], and M. Xompero[2]

[1] INAF- Osservatorio Astronomico di Bologna - Via Ranzani 1, I-40127 Bologna, Italy,
[2] INAF-Osservatorio Astrofisico di Arcetri - Largo E.Fermi 5, I-50125 Firenze, Italy,
[3] Max-Planck-Institut für Astronomie, Konigstuhl 17, D69000 Heidelberg, Germany,
[4] Dipartimento di Astronomia, Univ. Di Firenze - Largo E. Fermi 5, I-50127 Firenze, Italy,
[5] INAF-Osservatorio Astronomico di Padova - vic. Osservatorio 5, I-35100 Padova, Italy

Abstract. Four projects exploiting Multi Conjugate Adaptive Optics with Layer-Oriented wavefront sensing technique are being developed by our group in this period. The purpose of these projects is, in some cases, to give experimental evidence to the Layer-Oriented concept, developed in the last few years. In some other cases, to build real facilities to be used in 8-m class telescopes, like VLT in Chile or LBT in Arizona. A brief description of these project will be given while indeed an analysis of the possible scientific outcome which can be obtained when reaching diffraction limit images in the near infrared using MCAO will be performed.

1 MCAO Projects

All the four WFS projects described below are conceived for a LO approach of the wave front sensing. It means that each detector is conjugated to a specific height and that the reference stars light is co-added. For the WF sensing the pyramid approach [5] is used.

The LOWFS prototype [1] (Manu-Chao) will be mounted at the TNG replacing the actual single pyramid sensor, only for the period of the experiment. It can test up to 4 guide stars (GS).

The LOWFS for MAD [2] is fully integrated and it is being tested in the laboratory. It is an ESO demonstrator to test in the sky the MCAO concept. It can sense up to 8 GSs in a circular Field of View (FoV) of $2'$. The conjugation heights will be the ground level and 8.5 km above the telescope aperture. It will be installed in Paranal at the end of 2005.

The LINC-Nirvana [6] the LBT WFS module. It is in the fase of final design. For each arm of the telescope there will be a ground WFS testing up to 12 GSs in an annular FoV of $6'$ and a high WFS in a circular FoV of $2'$. The system can be upgraded conjugating a third deformable mirror (DM) to an intermediate height. By inserting a beam splitter in the high WFS half of the splitted light

can be re-imagined by another objective onto a detector conjugated to that given height.

The single arm experiment [3] will be performed using one of the two mid-high LOWFS for the LBT. The pupil re-imagers of the two sensors their optical designs was made in order to have a good optical quality also if they are conjugated to a different height. The experiment will consist in mounting two pupil re-imagers in the same sensor that will become a copy of the LOWFS for MAD.

2 Scientific Outcome

We have started to simulate the scientific outcome that can be retrieved using the LOWFS for MAD. It is not a study of the LO approach performance but simply we want to choose some scientific targets for the observations during our guaranteed time at the telescope (at least 6 nights). The scientific camera will operate in the K-band and will have a FoV of $1'$x $1'$. The first case we took under consideration is a deep field survey in which we can take advantage of the wide field in which the correction id done. The PSF above the field is simulated by LOST code [4] choosing real asterisms. We are investigating the differences in detection rate of galaxies between the LO case and the one without adaptive optics (ISAAC). The results do not carry an important improvement in using the MCAO but we are now studying the gain in morphological structure detection of galaxies due to the better angular resolution.

References

1. E. Vernet, R. Ragazzoni, E. Diolaiti, J. Farinato, A. Bariffolo, C. Arcidiacono, G. Crimi, M. Ghigo, R. Tomelleri, F. Rossettini: 'Layer Oriented WFS Prototype Test Report'. *Doc. No.: OWL-TRE-INA-600000-0054, Issue:2.0*
2. E. Marchetti, N. Hubin, E. Fedrigo, J. Brynnel, B. Delabre, R. Donaldson, F. Franza, R. Conan, M. Le Louarn, C. Cavadore, A. Balestra, D. Baade, J.-L. Lison, R. Gilmozzi, G. Monnet, R. Ragazzoni, C. Arcidiacono, A. Baruffolo, E. Diolaiti, J. Farinato, E. Viard, D. Butler, S. Hippler, A. Amorim: Proc. SPIE **4839**, 317, (2003)
3. E. Egner, W. Gaessler, T.M. Herbst, R. Ragazzoni, D. R. Andersen, H. Baumeister, P. Bizenberger, H. Boehnhardt, S. Ligori, H. Rix, R. Soci, R. Rohloff, R. Weiss, W. Xu, C. Arcidiacono, J. Farinato, E. Diolaiti, P. Salinari, E. Vernet, A. Eckart, T. Bertram, C. Straubmeier.: Proc. SPIE **5490**, 175, (2004)
4. C. Arcidiacono, et al.: Applied Optics **42**, 22 (2004)
5. R. Ragazzoni: Journal of Modern Optics **43**, 289, (1996)
6. T. Herbst, R. Ragazzoni, D. Andersen, H. Boehnhardt, P. Bizenberger, A. Eckart, W. Gaessler, H. Rix, R. Rohloff, P. Salinari, R. Soci, C. Straubmeier, W. Xu: 'LINC-NIRVANA: a Fizeau beam combiner for the large binocular telescope'. In: *SPIE conference 2003, Proceeding 4838, pp. 456-465* (2003)

Prospects for an Extremely Large Synthesis Array

A. Quirrenbach

Sterrewacht Leiden, Postbus 9513, NL-2300 RA Leiden, The Netherlands

1 ELSA: Concept for an Extremely Large Synthesis Array

The present article attempts to address the question of the role of optical and infrared interferometry in the era of Extremely Large Telescopes (ELTs). A strawman concept for an Extremely Large Synthesis Array (ELSA) could consist of 27 ten-meter telescopes and baselines of up to 10 km [1] (see also Tab. 1). It appears that ELSA could be built today with existing technologies, but the cost would probably be prohibitively high. A technology roadmap for ELSA must therefore provide solutions that are not only *technically feasible*, but also *affordable*. In this context it will be interesting to explore to which extent cost-reduction approaches that are being investigated for the design and construction of large monolithic telescopes – such as the OWL concept – can also be applied to ELSA.

2 Science with ELSA

With baselines up to $B = 10\,\mathrm{km}$ and operating at wavelengths down to $\lambda = 0.5\,\mu\mathrm{m}$, ELSA would deliver images with $10\,\mu\mathrm{as}$ resolution, two orders of magnitude better than any other telescope contemplated at the moment. Combined with a sensitivity (for compact objects) that equals or surpasses present-day large monolithic telescopes, this spectacular angular resolution enables a wealth of completely new observing programs in many different areas of astrophysics:

- Imaging of Jupiter-size objects at a distance of $\sim 10\,\mathrm{pc}$ with 16 resolution elements across the disk.
- High-quality images of stellar surfaces (90 resolution elements across the disk of Solar-type stars at 10 pc).
- Pre-main-sequence disks (temperature and density laws, vertical structure, flaring, magnetic fields, jets and outflows, gaps created by planets).
- Binary stars (Roche lobe overflow, mass transfer, accretion).
- Three-dimensional motions of stars in globular clusters.
- General-relativistic precession of orbits of stars near the Galactic Center.
- Baade-Wesselink distances of pulsating stars, novae, and supernovae.
- Extragalactic stellar populations in crowded regions.
- Detailed images of broad-line regions in active galaxies and geometric distances of quasars.
- Shapes and Doppler factors of the afterglows of gamma-ray bursts.

Table 1. Summary of strawman ELSA parameters and characteristics.

Parameter	Value	Comment
Number of telescopes	27	Needed for snapshot imaging
Telescope phasing	Autonomous	Adaptive optics
Array co-phasing	External	Dual-star operation
Sky coverage	$\gtrsim 10\%$	At R band, near Galactic pole
Telescope diameter	10 m	Needed to get sky coverage
Efficiency	25%	To limit telescope size
Wavelength range	$0.5 \ldots 20\,\mu$m	Could be reduced to $0.5 \ldots 2.2\,\mu$m
Cost	$\lesssim 400$ M€	Design-to-cost target figure

3 Key Technologies for ELSA

To achieve good sky coverage, array elements with ~ 10 m diameter are needed for ELSA. Allocating half of the project cost to the telescopes would mean that each telescope should not cost more than about 7.5 M€, including enclosures and the adaptive optics system. It will therefore be necessary to capitalize on advances such as those needed by OWL and ALMA: cheap mass production of primary mirror segments, standardized elements for the mechanical structure, and minimization of non-recurrent design and engineering effort through replication of identical elements. The interferometer elements will need only a small field-of-view, which should be achievable with a spherical primary mirror; this minimizes the cost of the mirror segments. 27-fold reproduction would reduce the price of the AO systems. Applying the $D^{2.7}$ scaling law of telescope cost with diameter to the OWL concept (100 m for 1,000 M€) suggests a price of only 2 M€ for a 10 m telescope built with the same design and construction principles. A target of 7.5 M€ for the ELSA elements thus appears to be reasonable.

Because of diffraction effects and the desired field size, the minimum diameter of the optical elements increases with the length of a classical beam train. For a propagation length of 10 km, field of $2''$, and operation in the near-infrared, a beam diameter of 50 cm is needed. The optics and vacuum system are clearly a cost driver for large interferometric arrays. Another problem is the poor transmission due to the many optical elements between the telescope and the beam combiner. These difficulties could be solved by coupling the light from the target and the reference star into optical fibers in the prime focus of the telescope, and relaying the light to a fiber delay compensator consisting of fiber segments with lengths of 1 m, 2 m, 4 m, ...; selecting an appropriate chain of these segments can thus provide any desired delay in steps of 1 m. The remaining delay could be taken out in a fiber which is stretched mechanically to the desired length. The largest challenge for this concept is the development of fibers with extremely low dispersion, or of dispersion compensation schemes. In addition, nearly lossless switches would be needed for selecting the sets of discrete fibers.

References

1. A. Quirrenbach: 'Design Considerations for an Extremely Large Synthesis Array'. In: *New Frontiers in Stellar Interferometry*, Proc. SPIE **5491**, in press

Interferometry in the Near-Infrared: 1 Mas Resolution at the Wavelength of 1 Micron

G. Weigelt[1], Y. Balega[2], T. Beckert[1], T. Driebe[1], K.-H. Hofmann[1], K. Ohnaka[1], T. Preibisch[1], D. Schertl[1], and M. Wittkowski[3]

[1] MPI für Radioastronomie, Bonn, Germany
[2] Special Astrophysical Observatory, Nizhnij Arkhyz, Russia
[3] European Southern Observatory, Garching, Germany

High-resolution interferometric imaging at optical and infrared wavelengths provides unique information for the study of many different classes of astronomical objects. A large number of key objects have been resolved with unprecedented resolution using bispectrum speckle interferometry or infrared long-baseline interferometry. IR interferometry allows the study of, for example, disks and outflows of YSOs (e.g., [1]), the wavelength and phase-dependent size of evolved stars (e.g., [2]), as well as the structure of AGN. The ESO Very Large Telescope Interferometer with its AMBER phase-closure instrument will enable us to achieve the spectacular resolution of 1 mas at the wavelength of 1 micron. The science goals of AMBER include studies of the jet structure of YSOs, the interferometric detection of extra-solar planets as well as the resolution of tori and broad-line regions of AGN.

The nucleus of the Seyfert Galaxy NGC 1068 has been resolved by both NIR bispectrum speckle interferometry [3,4] and K- band long-baseline interferometry using the the ESO VLTI [5]. A diffraction-limited K'-band image with 74 mas resolution and the first H-band image with 57 mas resolution were reconstructed from speckle interferograms obtained with the SAO 6 m telescope. The compact core has a north-western, tail-shaped extension as well as a fainter, south-eastern extension (Fig. 1). The K'-band FWHM diameter of this resolved compact core is $\sim 18 \times 39$ mas or 1.3×2.8 pc (the diameter errors are $\pm\,4$ mas), and the position angle (P.A.) of the north-western extension is $-16 \pm 4°$. In the H band, the FWHM diameter of the compact core is approximately 18×45 mas ($\pm\,4$ mas). The P.A. of $-16 \pm 4°$ of the compact 18×39 mas core is very similar to that of the western wall of the bright region of the ionization cone. This suggests that the H- and K'-band emission from the compact core is both thermal emission and scattered light from dust near the western wall of a low-density, conical cavity or from the innermost region of a dusty torus heated by the central source. (the dust sublimation radius of NGC 1068 is approximately 0.1 – 1 pc).

The first K-band long-baseline interferometry of the nucleus of NGC 1068 with resolution $\lambda/B \sim 10$ mas was obtained with the VLT interferometer [5]. A squared visibility amplitude of 16.3 ± 4.3 % was measured for NGC 1068 at a sky-projected baseline length of 45.8 m and azimuth angle 44.9 deg. This value corresponds to a FWHM size of the observed K-band structure of 5.0 ± 0.5 mas if it consists of a single Gaussian component. Taking into account the speckle

interferometry observations, we favor a multi-component model, where one part of the flux originates from scales clearly smaller than ~ 5 mas (≤ 0.4 pc) and the other part from larger scales. The K-band emission from the small (≤ 5 mas) scales might arise from the substructure of the dusty torus or directly from the central accretion flow viewed through low extinction.

To explain the implied substructure of the torus in NGC 1068, the existence of cold and dusty clouds in a geometrically thick torus is required. We have applied the radiative transfer treatment in a clumpy medium [6] to our dynamical model of clouds in the torus [7]. The resulting images allow a comparison with the structures seen in Fig. 1.

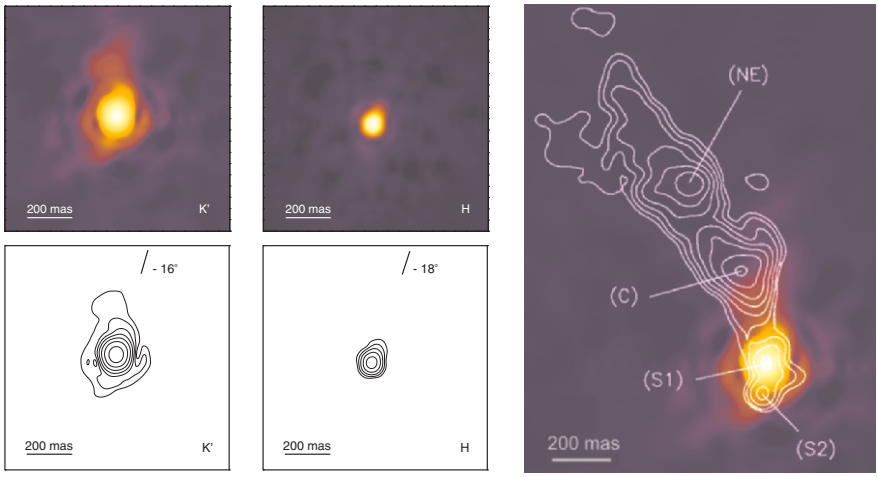


Fig. 1. Left, top, and bottom: Diffraction-limited K'-band image of NGC 1068 reconstructed by bispectrum speckle interferometry. The image shows the compact core (yellow) with its tail-shaped, north-western extension at a P.A. of $\sim$–16° as well as the northern and south-eastern extended components (red). **Middle, top, and bottom:** Diffraction-limited H-band image, which also shows the tail-shaped, north-western extension. **Right:** MERLIN 5 GHz contour map from [8] superposed on our K' image. The center of the radio component S1 coincides with the center of the K' peak. The northern extended 400 mas structure (red) aligns with the direction of the inner radio jet (S1 – C).

References

1. R. Millan-Gabet, F. P. Schloerb, W. A. Traub: ApJ 546, 358 (2001)
2. H. C. Woodruff, M. Eberhardt, T. Driebe, et al.: A&A 421, 703 (2004)
3. M. Wittkowski, Y. Balega, T. Beckert, et al.: A&A 329, L45 (1998)
4. G. Weigelt, M. Wittkowski, Y. Balega, et al.: A&A accepted (2004)
5. M. Wittkowski, P. Kervella, R. Arsenault, et al.: A&A 418, L39 (2004)
6. M. Nenkova, Ž. Ivezić, M. Elitzur: ApJ 570, L9 (2002)
7. T. Beckert, W. J. Duschl: A&A accepted (2004)
8. J. F. Gallimore, S. A. Baum, C. P. O'Dea: ApJ 464, 198 (1996)

Electrical and Geometrical Characterization of the Silicon Flight Sensors of the GLAST/LAT Tracking System

M. Brigida, C. Favuzzi, P.G. Fusco, F. Gargano[1], N. Giglietto, F. Giordano, F. Loparco, B. Marangelli, M.N. Mazziotta, N. Mirizzi, S. Rainó, and P. Spinelli, for the GLAST LAT Tracker Italian Collaboration

Dipartimento Interateneo di Fisica and INFN Bari Via Orabona 4 - 70126 Bari Italy
[1] Corresponding author. E-mail: fabio.gargano@ba.infn.it tel: 0039-080544317

Abstract. GLAST-LAT is a telescope for gamma rays in the range 20 MeV÷300 GeV. It consists of a Silicon Strip Detectors (SSDs) Tracker, a CsI calorimeter and an anticoincidence detector. The total surface of silicon detectors is almost 80 m^2 so it will have the largest equipped area among all space experiments. In this paper will be presented the electrical and dimensional tests performed on all the flight SSDs and the ladders assembly procedures and the electrical and geometrical tests on the first flight sensor produced.

1 Introduction

The Gamma-ray Large Area Space Telescope [1] is the next high-energy gamma ray mission, scheduled for launch by NASA in 2006. GLAST will cover the energetic range 5 keV÷300 GeV with capabilities up to 1TeV. The GLAST-LAT is essentially a silicon tracker devoted to the reconstruction of the e^+/e^- pairs produced by incident gammas. It also has a CsI calorimeter to measure the total energy of the gamma induced event and a scintillator-based anticoincidence detector to reject charged particle entering into the silicon tracker. The silicon sensors (wafers) are produced by Hamamatsu with a strip pitch of 228 µm, 400 µm thick and with a surface of 8.9×8.9 cm^2. The active sensor (ladder) consists of 4 wafers glued head-to-head. Electrical acceptance tests are scheduled for every every sensor, both at wafer [2] and ladder [3] assembly level; a database is continuously being updated recording all detectors characteristics [4].

2 Wafers Tests

All the wafers ($\sim$ 10000) needed to build the GLAST/LAT silicon tracker have been received and fully tested, both geometrically and electrically. To perform the electrical test on wafers we use a Semi-automatic Probe Station (KarlSuss PA200) connected to calibrated instruments (V-source & p-ammeter; LCR) and completely controlled and read through a LabView code. The data are automatically stored in the Construction DataBase. To measure the I-V and C-V curve we keep the Bias ring at ground potential and the back plane (n) at variable

V(+). To measure the single strip defect we connect the bias ring at ground, the strips AC-pad at +100 V and the detector is in conduction by means of a light spot. The mean measured leakage current is 110 nA at 150 V (i.e. 0.3 nA per strip) and only 51 SSDs have been rejected (less than 0.5% of the total produced). The strip failure rate is less than 10^{-4}.

3 Ladders Tests

The ladders are assembled manually with a tool that helps in obtaining a very good alignment of the wafers, with an error less then 5 μm. After the encapsulation of the bonds, the ladders are electrical tested. Also in this case an I-V and a C-V scan is performed on each ladder to measure the leakage current, the bulk capacitance and the depletion voltage [5]. At the present ∼ 900 flight ladders have been already fully tested. The mean leakage current is 600 nA (i.e. 1.5 nA per strip). Every single ladder strip is tested in order to check the integrity of all the bonds. The bonds failure rate is almost 0.03%. Less than 2% of the whole tested sample of the ladders have been rejected.

3.1 Effect of Ladder Leakage Current on Electrical Noise

The TKR front end electronics consists of a charge preamplifier followed by a shaper. The electronic chain and the noise have been simulated with a code that takes into account the transfer functions of both signal and noise. The electronic noise is due both to the detector and to the electronic front-end. The main noise sources are the following: the leakage current of the semiconductor detector, the noise due to the bias resistor, the noise from the feedback resistor, the electronic noise of the amplifier. The total evaluated noise is $1500e^-$ (i.e. ∼5.5 keV)

4 Conclusion

The whole GLAST/LAT TKR will consist of 10368 SSDs, and all of them have already been delivered from manufacturer and tested. The ladders assembly procedure is now completely reliable and the first 900 flight ladders (∼ 40% of the total) have been produced and fully tested. The rejection level is 2%. The mass production is started and it is going on quickly with good results. All the ladders will be assembled on schedule.

References

1. GLAST - Scientific and Technical Plan, AO 99-OSS-03 (http://glast.gsfc.nasa.gov/)
2. A. Brez: LAT-TD-00527, GLAST TKR Technical Doc
3. A. Brez: LAT-PS-00635, GLAST TKR Technical Doc
4. L. Latronico: LAT-TD-00914, GLAST TKR Technical Doc
5. F. Gargano, L. Latronico: LAT-TD-01166, GLAST TKR Technical Doc

Environmental Testing of the GLAST Tracker Subsystem

M. Brigida, C. Favuzzi, P.G. Fusco, F. Gargano, N. Giglietto, F. Giordano[1], F. Loparco, B. Marangelli, M.N. Mazziotta, N. Mirizzi, S. Rainó and P. Spinelli, For The GLAST LAT Tracker Italian Collaboration

Dipartimento Interateneo di Fisica and INFN - Sez. Bari Via Orabona 4 - 70126 Bari Italy
[1] Corresponding author. E-mail: francesco.giordano@ba.infn.it, tel: 0039-0805443168

Abstract. A test sequence that involves functional verification and mechanical - thermal properties of the GLAST LAT Tracker has been done, first on Engineering model prototypes, and it will continue on flight hardware. The results of vibration and thermal vacuum tests on the Engineering Model Tower of the GLAST LAT Tracker are presented. The performance expected for silicon detectors as a function of operating temperatures in the mission environment have also been investigated and described.

1 Introduction

Before starting the flight production, an Engineering Model (EM) prototype of a LAT tracker tower [1] has been assembled and submitted to the environmental tests needed to qualify the tracker design. Vibration and thermal-vacuum tests have been performed at Alenia I&T clean laboratories in Rome. The results are discussed in the following sections.

2 Vibration Test

The goal of dynamic tests is to qualify the design and at the same time verify the workmanship of the TKR Towers. The EM tower has been subjected to qualification test levels exceeding the maximum loads expected during launch and ascent dynamic environments [2]. The fundamental frequency of the Tower has been measured by studying the response to low level signature sweep tests at $0.15\,g$ input level from 5 Hz to 2000 Hz. The dynamic environments are usually simulated by sinusoidal vibration ($5 \div 50$ Hz at $8\,g$) and random vibration (at workmanship level of $6.8\,g_{\rm rms}$). The response under dynamic excitation has been studied both along the thrust axis first and lateral directions successively: the first mode frequency of the EM TKR tower was of 376 Hz along the z axis and of 150 Hz along both the lateral axis. These results together with the absence of shifts in the resonance frequencies during the test represent a very encouraging success for the flight hardware production start-up.

3 Thermal Vacuum Test

The goal of the test was to correlate the EM GLAST Tracker Tower internal temperatures with those measured by the thermistors located on the tower flex cables and also with those predicted by the thermal math model. This was accomplished by placing thermocouples throughout the tower and then measuring the temperature distribution in it, by using a combination of three tracker power levels (8 W, 10 W, 12 W) and three controlled temperatures at the base of the tower (20°, 0°, -15°C). It has been found that the mean temperature gradient for the nominal tracker power level of 10 W between the top and the bottom of the tower is about 6°C. Moreover, the analysis on the thermistors data has shown a very good agreement with the thermocouples measurements [3].

3.1 Silicon Detectors Performance: S/N Dependence on Temperature

A preliminary study of the temperature dependence of silicon strip detectors operation has also been done: MIPs crossing 400 μm silicon at normal incidence have been simulated. The dependence on temperature of the number of electron-hole pairs produced in Si and the noise sources have been evaluated [4]. On the average we have evaluated a signal to noise ratio of 21.5 at 300 K that decreases to 17 if the temperature rises up to 350 K, which are the temperature margins expected for the on orbit operational regime of the TKR.

4 Conclusion

A complete campaign of environmental tests and preliminary functional verification on the EM TKR tower has been conducted successfully. The design has been qualified mechanically; the thermal math model has been verified. On the basis of the results obtained, a preliminary study on the prediction of Silicon Sensors performance has been developed, concerning the S/N ratio dependence on temperature. The first flight trays have already been assembled and tested; the first flight tower will be assembled and tested in September.

References

1. O. Reimer: “The GLAST Large Area Telescope science prospects”, this volume
2. Vibration test: Bari web page http://www.ba.infn.it/ glast/alenia.htm
3. Thermal Vacuum Tests: Bari web page http://www.ba.infn.it/∼glast/EM_TV.htm
4. M.N. Mazziotta, et al.: ‘Signal to Noise Ratio Temperature dependence’. LAT-TD-03715, GLAST Technical Document

The Potential of a Large Cherenkov Array for Supersymmetry and Cosmology

E. Giraud, A. Falvard, J. Lavalle, S. Sajjad, and G. Vasileiadis

GAM, Université Montpellier II, Montpellier, France

Abstract. The Large Cherenkov Array is a concept for a γ-ray instrument in the 15 GeV to 1 TeV energy range, optimized for Fundamental Physics and Cosmology, with significant capabilities in Astrophysics. It is based on a 16-20 Cherenkov telescope array, with $\sim$ 18 m diameter, located at high altitude (5000 m; possibly on Chajnantor).

1 Scientific Rationale

This project is proposed with the following objectives:

1. Exploring a significant fraction of the supersymmetric parameter space by detecting high energy annihilation photons coming from Galactic structures.

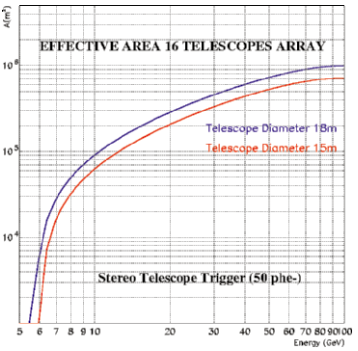
2. Serving as a major instrument in Observational Cosmology and High Energy Astrophysics above 15-20 GeV to TeV energies. It will obtain images and spectra of sources detected by GLAST, at lower energies, namely AGNs, BL Lacs, FSRQs, SNRs, microquasars, pulsars, as well as GRBs and galaxy clusters. It will see the bulk of AGNs, and will address the questions of the Cosmological γ-ray horizon and of the IR background.

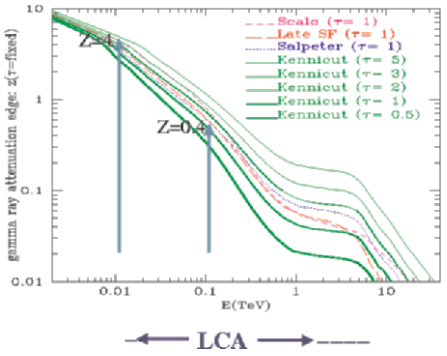
2 Instrument Capabilities

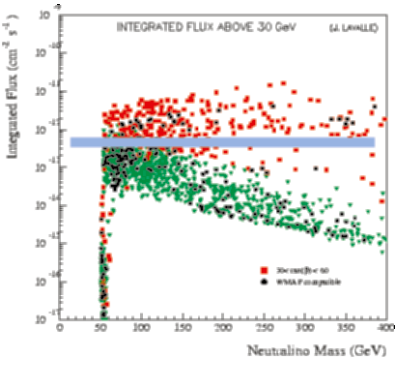
High energy particles interacting with the atmosphere produce relativistic showers which induce Cherenkov cones of UBVR light emission. Reflectors with prime focus large angle PMT cameras associated with very fast electronics provide images in UBV of the Cherenkov flash. The telescope diameter determines the minimum energy of showers that can be detected at a given altitude. The number of telescopes provides the effective area, i.e.the flux limit at a given energy. Groups of N telescopes in stereoscopy provide several images of the same shower allowing improved resolution, higher S(γ)/N(e-) ratio, and better rejection of muon false images and protons.

Positioning Cherenkov telescopes at high altitude result in the following characteristics: 1) a gain by a factor 2 in the density of Cherenkov photons due to the shower geometry, 2) a significant gain in U and B band absorptions and Rayleigh scattering, 3) the absence of low altitude aerosol layers. The same energy threshold and effective area as those of an $\sim$ 18 m reflector located at 5000 m requires to have a $\sim$ 28 m reflector at 2000 m. The main limitations of high altitude are: 1) the shower images are more extended, i.e. a large opening angle is necessary, 2) high energy showers at $\sim$ 1 TeV are truncated. An array of 16-20 telescopes with 18 m diameters can provide effective detection areas $> 10^5$ m^2 at 15 GeV

Fig. 1a (up right): Effective area for a grid of 16 telescopes at 5000m, in a square configuration. **1b** (bottom left): The model curves from astro-ph/0011475 give distance limits for γ detection due to e^+e^- pair production by γ - IR background interaction. **1c** (bottom right): Expected flux at E > 30 GeV from the Sagittarius dwarf assuming a NFW profile. L.o.s. int.: $8 \times 10^{23} \mathrm{GeV}^2/\mathrm{c}^4/\mathrm{cm}^5$. The flux limit (thick line) is for 400 h of integration.







(Fig. 1a). Showers above 50 GeV can be detected by an increasingly number of telescopes improving the angular resolution, and the energy of showers detected by a large number of telescopes is measured with improved energy resolution. The large effective area allows an efficient rejection of hadronic showers and subshowers.

3 Efficiency for SUSY Dark Matter and Cosmology

Probing a significant fraction of the SUSY parameter space by assuming that some of the galactic structures are made of neutralinos is one of the present day major scientific issues. A Cherenkov array can explore large tan β SUSY models through γ production in the GC and in the most massive dSphs (Fig. 1c)

At energies below 100 GeV the Universe becomes progessively transparent to γ-rays and observations up to high redshift become feasible (Fig. 1b). The predicted number of blazar-type objects visible to GLAST should be of the order of a thousand to a few thousand, depending on the luminosity evolution. A large Cherenkov array has the potential of studying the bulk of cosmological AGNs. It will allow to understand the origin of the IR and γ extra-galactic backgrounds and determine the contributions of AGNs, BL Lacs, FSRQs, topological defects. Physics of nearby objects like supernova remnants can be studied with unprecedented statistics, as well as micro-quasars and distant GRBs.

MAGIC: First Observational Results and Perspectives for Future Developments

T. Hengstebeck[1], O. Kalekin[1], M. Merck[2], R. Mirzoyan[3], N. Pavel[1], T. Schweizer[1], and M. Shayduk[1] for the MAGIC Collaboration

[1] Humboldt Universität zu Berlin
[2] Würzburg Universität
[3] Max-Plank-Institut für Physik, München

1 Introduction

The MAGIC (Major Atmospheric Gamma Imaging Cherenkov) telescope was designed to close the energy gap ($\sim$ 10–250 GeV) between ground based and satellite gamma detectors. It is situated on the Roque de los Muchachos, La Palma, Canary Islands at altitude of 2200 m. The main subjects of the investigations with the telescope are: Gamma Ray Bursts, Supernova Remnants, Plerions, Pulsars, Active Galactic Nuclei (AGNs), unidentified EGRET sources, Dark matter and Quantum gravity. More details about physics with a low threshold gamma ray telescope one can find in [2]. The telescope hardware installation was finished in October 2003. Since that time the observations of the different classes of objects have been carried out but the experiment is still in the commission phase.

2 Telescope Design and First Observational Results

The MAGIC telescope is the largest ground based imaging Cherenkov detector. It consists of a mirror dish with a diameter of 17 m, a collecting area of 240 m^2, and a 577-channel imaging camera with $3.^{\circ}5$ field of view. The telescope has an increased sensitivity and a lower trigger threshold of about 40 GeV compared to the old generation telescopes. Because of using such innovations as a carbon fiber frame, signal transmission via optical fibers the weight of the telescope is only 65 tons. Due to it the telescope has a very short repositioning time of $\sim$ 22 s permitting gamma burst hunting. The detailed design and performance of the MAGIC telescope are described in [3]. The Crab nebula and the AGN Mkn 421 were first object observed with the MAGIC telescope. Both objects were detected with high confidence level. The results are presented in the Table 1.

3 Future Plans

3.1 MAGIC II

For phase II it is planed to build a clone of the existing MAGIC telescope 80 m away from the telescope which is already operating. This will allow us to improve background suppression by stereoscopic observations and therefore increase the

Table 1. The results of first observations

Object	Date	Obs. time	Significance	Gamma rate
Crab Nebula	15 Feb 2004	55 min	9.7 σ	5.2 min^{-1}
Mkn 421	15 Feb 2004	102 min	27 σ	13 min^{-1}

sensitivity. In addition it enables simultaneous observations of two objects and increase the observation throughput. The construction of the foundation will start this summer 2004 and the second telescope will be operable in 2006.

In parallel, a high quantum efficiency camera, consisting of HPDs (Hybrid Photo detectors), is developed and constructed which will lower the threshold to 15–20 GeV.

3.2 ECO–1000

To extend the IACT technique down to still lower thresholds, we are studying the concept of a 1000 m^2 telescope with an enhanced quantum efficiency camera [1]. This telescope design, called ECO-1000, shall be capable to detect gamma-rays below 10 GeV, an energy where the background from charged cosmic ray particles should be substantially reduced due to the geomagnetic rigidity cutoff of 12 GeV for vertical incidence at a location like La Palma. The performance of the proposed project as well as sensitivities of other experiments are presented in Fig. 1.

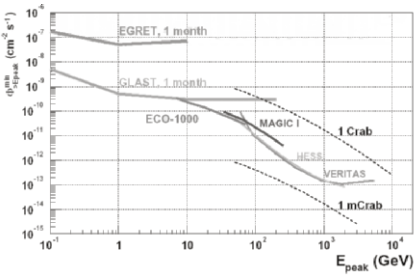


Fig. 1. Integral flux sensitivities, 5 σ in 50 h. $E^{-2.5}$ differential source spectrum. Zenith angle of observations smaller 30° (ground based experiments)

References

1. C. Baixeras, D. Bastieri, W. Bednarek, et al.: astro-ph/0403180 (2004)
2. C. Baixeras, D. Bastieri, W. Bednarek, et al.: submitted to Astr. J. (2004)
3. C. Baixeras, D. Bastieri, C. Bigongiari, et al.: Nucl. Instrum. Meth. A **518**, 188 (2004)

LOBSTER - Astrophysics with Lobster Eye Telescopes

R. Hudec[1], L. Pina[2], A. Inneman[3], and L. Sveda[2]

[1] Astronomical Institute of the Academy of Sciences of the Czech Republic, Fricova 298, 251 65, Ondrejov, Czech Republic
[2] Czech Technical University in Prague, Faculty of Nuclear Sciences and Physical Engineering, V Holesovickach 2, 180 00 Praha 8, Czech Republic
[3] Centre for Advanced X-ray Technologies, Reflex, Novodvorska 994, 142 00 Praha 4, Czech Republic

Abstract. We refer on the project of a Lobster Eye (LE) X–ray All Sky Monitor (ASM) and on the related developments of the innovative Lobster Eye X–ray telescopes. The related scientific issues will be also in detail presented and discussed.

1 The ASM

We propose a focusing wide–field X–ray optics for the All-Sky Monitor (ASM), such as a Multi–Foil optic (MFO) [1–4] in Schmidt [5] arrangement (Fig. 1). Multi–foil optic (MFO) in general is an X–ray optic based on the thin glass foils.

The dimensions of the plates can be optimized for a given focal length, plate spacing, photon energy, and surface quality. The spacing between the reflecting plates changes the angular resolution substantially. If a wide energy range response is needed, the gain in the whole energy range should be optimized. We have simulated various LE MFO samples designed for various energies.

The most interesting design suitable for an orbital scanning experiment, based on current simulations, seems to be: $78.0 \times 11.5 \times 0.1\,\mathrm{mm}^3$ gold coated plates, 0.3 mm spacing between plates, and focal length $f = 375\,\mathrm{mm}$. Field of view of such an optic is approximately $6 \times 6\,\mathrm{deg}$ (FWHM).

The optic, together with the planar detector $4{\times}4\,\mathrm{cm}^2$ large with $150{\times}150\,\mu\mathrm{m}^2$ pixel size, necessary electronic, and the casing will create a single LE module. A number of modules suitably arranged will create a whole ASM. An example of such an arrangement is plotted in Fig. 2.

The ASM built from the modules will have a Field of View (FOV) $180 \times 6\,\mathrm{deg}^2$. It will scan the sky once per orbit ($\sim 90\,\mathrm{min}$) and hence will cover the whole sky several times per day. The limiting detectable flux after a one–day operations depends on the position on the sky relative to the orbit and can be $\sim 10^{-12}\,\mathrm{erg/s/cm}^2$) near the orbit and can reach $\sim 4 \times 10^{-13}\,\mathrm{erg/s/cm}^2$) near the orbit poles. The angular resolution will be $\sim 3 - 4\,\mathrm{arc\ min}$.

We acknowledge the support from the Ministry of Industry and Trade of the Czech Republic, projects FB–C3/29/00 and FD–K3/052.

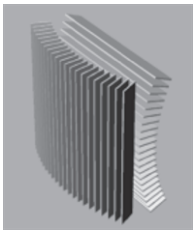


Fig. 1. Schematic view of the MFO sample in Schmidt arrangement. Two perpendicular sets of reflecting surfaces are clearly visible

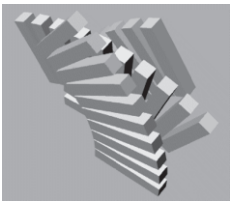


Fig. 2. Example of LE module assembly strategy. The modules are divided into three groups each covering 60 × 6 deg. Total FOV of 180 × 6 deg is covered.

2 Scientific Objectives

Soft X–Ray ASM scientific targets can be obviously divided into two work modes.

The first work mode is the fast discovery of new X–Ray sources and/or discovery of sudden flux changes of known sources. Prompt emission study, precise positioning, and alert system for narrow field instruments will be an important output in this work mode.

GRBs study (20 − 60 triggers per year), X-Ray flashes (> 8 triggers per year), supernovae prompt X–Ray emission (10 − 20 triggers per year), X–Ray binaries and cataclysmic variables sudden flux/spectra changes, and stellar events at the nearby stars will be observable targets. All these sources are relatively bright and are above the daily detection limit, hence can be detected much faster.

The second work mode is the long–term monitoring of large number of X–Ray sources with sampling rate from hours to days (depending on the actual source flux). Light curves and rough spectra will be gathered during the whole mission lifetime for X–Ray binaries (∼ 700 in the Milky Way galaxy), cataclysmic variables (∼ 200), nearby stars (∼ 600), and AGN (∼ 4000).

The LE ASM is expected to play an important role in the X–ray astrophysics of the 21. century. For the first time, sensitive X–ray ASM will be provided with numerous scientific implications.

References

1. R. Hudec, et al.: Proc. SPIE **4012**, 432 (2000)
2. R. Hudec, et al.: Proc. SPIE **4851**, 578 (2003)
3. A. Inneman, et al.: Proc. SPIE **3766**, 72 (1999)
4. A. Inneman, et al.: Proc. SPIE **4138**, 94 (2000)
5. W.K.H. Schmidt: Nucl. Instrum. Meth. **127**, 285 (1975)

Novel Light-Weight X-ray Optics for Future X-ray Telescopes

R. Hudec[1], L. Pina[2], A. Inneman[3], and V. Brožek[4]

[1] Astronomical Institute Academy of Sciences of the Czech Republic, CZ-251 65 Ondrejov, Czech Republic
[2] Czech Technical University, Faculty of Nuclear Science, Prague, Czech Republic
[3] Center for Advanced X- ray Technologies, Reflex sro, Prague, Czech Republic
[4] Institute of Plasma Physics, Academy of Sciences of the Czech Republic, Prague, Czech Republic

Abstract. The future X–ray astrophysics missions (such as the ESA XEUS) require light-weight but large and precise X-ray mirror shells. We discuss the possible alternative techniques with focus on the technologies and experience available in the Czech Republic.

The light-weight imaging X–ray mirrors represent a key component of future X–ray astrophysics missions. Various technologies for their production exist, but the future X-ray astrophysics missions such as the ESA's XEUS [1] will however require innovative technologies and approaches resulting in even lighter mirror shells in order to achieve high sensitivity and high angular resolutions at a still reasonable weight of the mirror assembly.

We have analysed the available possibilities of the suitable alternative technology to recently widely used electroforming replication.

Glass. This is a promising material since it has 4 times less volume density if compared with nickel in common use. Highly flat and highly smooth thin glass foils may serve in various X-ray astrophysics experiments [2]. The recently developed advanced Lobster Eye X-ray optics modules are based on gold-coated foils, only 100 microns thick, spaced at 300 microns. The developed mirror test assembly module is based on 50 30 x 30 cm gold-coated glass foils 0.75 mm thick, spaced at 12 mm, with possible thickness decrease up to 0.1 mm in future. The plates are bent to achieve the parabolic shape.

Recently, we have successfully produced test mirrors from glass of various origin (DESAG, BOROFLOAT, MARIENFELD) by thermal forming. The modified technology, the optimized choice and manufacture process of the mandrels, and the optimised thermal forming process have lead to significant improvements. While the original fine surface microroughness (typically 0.5 nm) of the glass foils is maintained in the process, the resulting slope deviations (from the desired profile) are now below 1 microns. The further improvements are in progress as well as plans to continue on larger samples.

Composites. We have developed double-sided X-ray reflecting foils and flats of various thickness within the US - Czech Science and Technology Program. They are based either on a combination of composite and electroforming technologies, or on gold-coated composites, and exhibit a low weight and a very

smooth surface. Analogous flats and foils may find applications in future X-ray optics experiments.

Ceramics. The ceramics materials can be considered as carriers or shell material of the X-ray mirrors. Their volume density may be up to four times less than electroformed nickel. However, due to the large number of materials possible, an careful optimization must be made.

Amorphous-glossy metals. Mechanical properties of amorphous alloys are comparable with those of high strength steel. As an example, the mechanical properties of amorphous Ni/Fe alloy are nearly four times better than those of crystalline Ni. The preparation of amorphous metallic layers can be accomplished by a special electrodeposition process. The following Ni containing amorphous layers were prepared: Ni1-xPx , (Fe0.5Ni0.5)1-xPx, (Co0.5Ni0.5)1-xPx, where x is from interval 0.13 up to 0.25. The layer thickness varies from 0.1 to 100 microns.

Glossy carbon. Glass-like carbons are known to be typical, more or less isotropic, non-graphitizable carbons. The recent evolutions indicate that the structures of thermosetting resins can be effectively modified to control the structure of resultant glass-like carbon. This material has been never discussed and studied before for this type of application, but we consider it also very promising. While the preparation of thick, glass-like carbon products is still difficult, the thin layers and films are much easier to be produced. In the thin film glass carbon techniques, the resin is coated on to a silica-glass plate, cured, peeled, and carbonised, and, if necessary, it can be graphitized. It is obvious that this may be considered as one of promising completely new techniques to be exploited as a possible alternative for future large segmented X-ray mirrors/foil telescopes. The structure of glass-like carbons has been studied over many years.

Conclusion. There are several promising alternative methods to produce large precise and lightweight X-ray mirror shells for future X-ray astronomy satellite missions. The first prototypes and tests have indicated that the glass foils (especially those thermally formed), double-sided composite flats, light ceramics, glossy carbon as well as amorphous metal alloys all belongs to the suitable techniques to be further exploited and analysed. **Acknowledgements.** We appreciate the support provided by the Grant Agency of the Czech Republic, grant 102/99/1546 and by the Ministry of Industry and Trade of the Czech Republic, project FB–C3/29 “Centre of Advanced X–ray Technologies”, and project FD–K3/052.

References

1. B. Aschenbach, et al.: ESA-SP 1253 (2001).
2. R. Hudec, et al.: Proc. SPIE **4012**, 422 (2000).

GLAST LAT Science Prospects

O. Reimer[1] for the GLAST LAT Collaboration[2]

[1] Ruhr-Universität Bochum, Institut für Theoretische Physik IV, 44780 Bochum
[2] http://glast.stanford.edu/people.html

Abstract. The Large Area Telescope (LAT), a pair-conversion telescope that provides coverage over the approximate energy range 20 MeV to 300 GeV, is GLAST's principal instrument. The LAT will provide an unprecedented capability for high-energy astrophysics, superseding the sensitivity of EGRET by more than 40 times. Highlights of the physics and astrophysics opportunities the LAT will provide are summarized.

The Universe is largely transparent to gamma rays in the energy range of GLAST. Energetic sources near the edge of the visible Universe can be detected by the light of their gamma rays. There is good reason to expect that GLAST will see known classes of sources to redshifts of 5, or even greater if the sources existed at earlier times. The small interaction cross sections for gamma rays also means that gamma rays can provide a direct view into nature's highest-energy acceleration processes.

- Blazars and Active Galactic Nuclei

The bulk of the luminosity for many blazars is emitted in GLAST's energy range. GLAST will increase the number of known gamma-ray AGN sources to thousands. Moreover, it will be scanning the full sky every three hours and thus greatly decrease the minimum time scale for detection of variability.

- Unidentified Sources

The majority of the sources on the gamma-ray sky remain unidentified. GLAST will enable identification of sources for which no counterparts are known at other wavelengths by providing much smaller error boxes and the capability to directly search for periods in sources at least down to EGRET's flux limit.

- New Particle Physics

GLAST's large area and low instrumental background will allow searches for decays of exotic particles in the early Universe and for annihilations of postulated weakly-interacting massive particles in the halo of the Milky Way.

- Extragalactic Background Light

GLAST will also permit study of the extragalactic background light by measurement of the attenuation of AGN spectra at high energies. The measured attenuation as a function of AGN redshift will relate directly to the star formation history of the Universe.

- Gamma-Ray Bursts

GLAST will be able of time-resolved measuring GRB spectra from keV to GeV energies. This will permit the determination of the minimum Lorentz factors and baryon fractions for the emitting regions, and distinguish between internal and external shocks as the mechanism for gamma-ray production, and may also permit gamma-ray-only distance determinations. GLAST will detect more than 200 bursts per year and provide near-real-time location information to other observatories for afterglow searches and will have the capability to slew autonomously toward bursts to monitor for delayed emission with the LAT.

- Pulsars

GLAST will discover many gamma-ray pulsars, and will provide definitive spectral measurements that will distinguish between the two primary models proposed to explain particle acceleration and gamma-ray generation. Because the gamma-ray beams of pulsars are apparently broader than their radio beams, many radio-quiet pulsars likely remain to be discovered.

- Cosmic Rays and Interstellar Emission

GLAST will spatially resolve some supernova remnants and precisely measure their spectra, and investigate whether remnants are sources of cosmic-ray nuclei. Cosmic rays produce the pervasive diffuse gamma-ray emission in the Milky Way via their collisions with interstellar nuclei and photons. GLAST will also be able to detect the diffuse emission from a number of local group and starburst galaxies, and map the emission within the largest of these, for the first time. Spatial and spectral studies of the gamma-ray emission will permit the distributions of cosmic-ray protons and electrons to be measured separately and will test cosmic-ray production and diffusion theories.

- Solar Flares

GLAST will be able to determine where the acceleration in solar flares takes place, and whether protons are accelerated along with the electrons. GLAST will be the only mission observing high-energy photons from solar flares during Cycle 24.

- Complementarity with Ground-Based Gamma-Ray Telescopes

GLAST in orbit will complement the capabilities of the next-generation atmospheric Cherenkov and shower gamma-ray telescopes that are planned, under construction, or operational. GLAST will monitor the whole sky on timescales of hours and will provide flare alerts. For the first time, a broad useful range of overlap in energy between some of the next-generation Cherenkov telescopes and GLAST will become reality.

For further information, visit http://glast.stanford.edu/ or obtain the GLAST science brochure "GLAST: Exploring Nature's Highest Energy Processes with the Gamma-ray Large Area Space Telescope", NASA/NP-2000-9-107-GSFC, via http://glast.gsfc.nasa.gov.

Astrophysics with Astronomical Plate Archives

R. Hudec

Astronomical Institute, Academy of Sciences of the Czech Republic, CZ-251 65 Ondrejov, Czech Republic

Abstract. The digitised astronomical plate archives represent a source of unique data for various scientific projects including analyses of objects such as AGN, blazars, cataclysmic variables, galactic X-ray sources, various transients, and other objects. These data may easily provide very long term monitoring over very extended time intervals (up to more than 100 years) with limiting magnitudes between $12^{\rm m}$ and $23^{\rm m}$.

The archival astronomical plates represent a unique database for various scientific projects, and, after digitization, can be easily implemented into the Virtual Observatories. They can provide thousands of exposures for any celestial position, reaching monitoring intervals of up to few years of continuous monitoring - i.e. tens of thousands of hours. There are nearly 3 millions astronomical archival plates located at different observatories [1].

The recent efforts to digitise the plates and the corresponding software development significantly facilitate the extraction of unique scientific data from archival records and related reductions and analyses. The photographic sky monitoring is available for more than 100 years. However, only the recent development of photographic scanners and powerful computers allows an efficient extraction of scientific data. Some of the archives have very high quality plates achieving limiting magnitudes of up to $20^{\rm m}$–$23^{\rm m}$ (direct imaging) and /or $17^{\rm m}$–$19^{\rm m}$ (spectral with objective prism). Recent efforts focus on digitisation and automated evaluation. Some of the archives already have devices for digitisation of plates and few of them have already started extended digitisation of the plates (e.g. Sonneberg Observatory - about 60 000 plates already scanned). Some of the archives have started projects to develop high quality scanners to convert all plates into files/CD ROMs (e.g. The Royal Observatory Brussels). There are efforts to use these data for automated evaluation of objects on the plates and creating their light curves. There are attempts to create an European Plate Centre in Brussels, Belgium (the UDAPAC project, for more details see http://midasf.oma.be/fido/project.html) - all interested people can contact us at rhudec@asu.cas.cz.

Most of the sky patrol programs are already closed. However, two of the photographic sky patrols are still in operation, regularly taking photographic patrol images every clear night. The Ondrejov all sky patrol operated for monitoring of bright meteors has a sensitivity of $12^{\rm m}$ in the best case and a very large sky coverage (full visible sky hemisphere). The Sonneberg sky patrol is operated for variable stars simultaneously in two colours with limits $14^{\rm m}$–$15^{\rm m}$ but with a less

extended sky coverage. Both programs exhibit suitable scanners to digitise and to evaluate the patrol images.

Archival and sky patrol plates represent a valuable tool in investigations of various types of high energy sources such as blazars/quasars, X-ray binaries, X- and gamma-ray transients, etc. It is obvious that the automated evaluation of sky patrol plates has large potential in:

- providing extended (more than 10 years) monitoring intervals with good (daily or weekly measurements) sampling,
- allowing long-term evolution and changes to be studied
- searching for optically variable AGNs-QSOs-blazars and other objects
- providing their light curves with good sampling
- searching for their flares
- providing simultaneous and quasi-simultaneous optical data for satellite campaigns, even back in time
- monitoring of objects as base for proposals for ToO (Target of Opportunity) for satellite high energy observations
- providing extended database for identification and classification of sources

The detection and investigation of very large amplitude flares from AGNs may serve as an example. There is increasing evidence that some AGNs may exhibit very large amplitude flares exceeding 10^{m} [2]. These large flares are however rare so very large fractions of monitoring times (of order of thousands hrs or more) are required to detect them. This can be accessed easily on plates but hardly by other methods.

The importance of the plate archives for recent astrophysical projects is that for objects optically brighter than 23^{m}, there is a chance that the light changes of the object can be analysed over years and often even over decades. This can provide valuable additional scientific data for complex analyses and for better understanding of evolutions of the objects as well as of underlying physical processes. The chance for availability of archival data increases with optical brightness of the object.

Acknowledgements

We acknowledge the support provided by the Grant Agency of the Academy of Sciences of the Czech Republic, grant A3003206.

References

1. R. Hudec: Acta Historica Astronomiae **6**, 28 (1999)
2. R. Hudec, F.J. Vrba, C.B. Luginbuhl: 'Large Amplitude Frales in AGN'. In: *BL Lac Phenomenon*, ed. L.O. Takala, A. Sillanpää, ASP Conf. Ser. **159**, pp. 115–118 (1999)

Virtual Observatories and Access to Radio Interferometry Data

A.M.S. Richards[1], S.T. Garrington[1], P.A. Harrison[1], T.W.B. Muxlow[1], A.M. Stirling[1], N. Winstanley[1], M.G. Allen[2], B. Vollmer[2], T. Venturi[3], P. Lamb[4], R. Power[4], N.A. Walton[5], P. Padovani[6], and the AVO and AstroGrid teams

[1] MERLIN/VLBI National Facility, JBO, Univ. Manchester, SK11 9DL, UK.
[2] CDS, 11 rue de l'Université, F-67000 Strasbourg, France.
[3] EVN/IRA (CNR), via P. Gobetti 101, 40129 Bologna, Italy.
[4] CSIRO, ANU, GPO Box 664, Canberra ACT 2601, Australia.
[5] AstroGrid/IoA, University of Cambridge, Cambridge CB3 0HA, UK
[6] AVO, ESO, Karl-Scwarzchild-Straße 2, 85748 Garching, Germany

1 Radio Interferometry

Radio interferometry produces visibility data which can be processed flexibly to achieve higher resolution or better surface brightness sensitivity. These results are now within the reach of any astronomer as radio archives appear on-line and pipelines and other user-friendly data reduction tools become common. All raw VLA data are now available by ftp via a web form offering many search parameters. Images from the MERLIN archive, the NVSS, SUMSS and other surveys and many radio catalogues are already published electronically directly and via CDS. However a typical 1024×1024-pixel image covers less than one percent of the typical potential field of view. The ideal solution is to store calibrated visibility data and produce images or other products on demand to user specifications. Prototypes have been developed to do this via web interfaces (not requiring any specialised radio astronomy knowledge) for the MERLIN and ATCA archives.

Nine radio observatories (ALMA, ATNF, BIMA, CARMA, IRAM, JCMT, JIVE, MERLIN, NRAO) responded to an IVOA (International Virtual Observatory Alliance) questionnaire, covering metre to sub-mm waves, real-time correlation and VLBI. Data providers and users want:

- Clean images for analysis/multiwavelength comparison;
- High spatial and spectral resolution datacubes;
- Images from any part of the field of view;
- Images of combined visibilities from different arrays;
- Visibility 'light curves' for variable objects;
- Standard metadata for VO use;
- VO tools which understand radio units, field of view etc.;
- Full history and quality characterisation;
- Standardised export product format, not observatory software-dependent;
- Remote friendly-interface access to user-driven pipelines;
- Options depending on user experience.

2 Virtual Observatories

Virtual Observatories provide a single interface to compare radio data with results from across the electromagnetic spectrum. This means being able to select data of matched resolution, transform galactic, equatorial and other coordinates and understand flux and energy units from 10 MHz to 10 MeV. The AVO (European Virtual Observatory) has developed a prototype based on Aladdin for displaying and measuring spectra and datacubes, source extraction, cross-matching and a variety of other services. The work of VOs around the world is coordinated through the IVOA. A vital part of its work is establishing a common language to describe data – metadata. The work of AstroGrid (UK) includes developing a user-driven tool to build complex workflows and testing IVOA Registry standards in practice at real data centres.

The first challenge in analysis is to identify sources from different images and catalogues with a range of resolutions and accuracies. The typical non-thermal spectral index of bright radio sources has allowed [1] to cross-ID these sources for inclusion in the SIMBAD data base as well as providing spectral indices for VO use. The first VO science paper [2] used VO tools to search for optically faint AGN using published CHANDRA, HST and ESO images, spectra and catalogues for the GOODS fields (a.k.a. the regions around the HDF(N) and CDF(S)). They found 68 candidate obscured AGN including 31 sources powerful enough to be type 2 QSO, suggesting that current models underestimate their surface density at redshifts ≥ 3. About 20% of the AGN in the HDF(N) have radio counterparts [3,4] and, surprisingly, the radio emission appears to be of starburst origin in the majority of sources. A further AVO project is investigating this by comparing radio and x-ray data.

3 Data Transport

The next generation of radio interferometers are described elsewhere in these proceedings. The e-MERLIN and VLA upgrades will increase sensitivity by over an order of magnitude by using dedicated optical fibre connections. The EVN is already testing real-time correlation using the Dante European academic network. A typical experiment raises the traffic tenfold from it normal level to 0.5 Gbps. These rates will be far exceeded by LOFAR, ALMA and eventually the SKA which will produce Pb or more data every day. Such developments add urgency to the VO mantra *move the results, not the users nor the data* and the need for specialised interferometry data centres.

References

1. B. Vollmer, et al.: A&A, submitted (2004)
2. P. Padovani, et al.: A&A, accepted (astro-ph/0406056) (2004)
3. D.M. Alexander: AJ **341**, 539 (2003)
4. T.W.B. Muxlow, et al.: MNRAS, accepted (2004)





Bringing issues out in the open





Breaking out for a glimpse of the sun

Part II

Fundamental Physics and Cosmology

Fundamental Physics with the SKA: Strong-Field Tests of Gravity Using Pulsars and Black Holes

M. Kramer

University of Manchester, Jodrell Bank Observatory, Cheshire SK11 9DL, UK

Abstract. The Square-Kilometre-Array (SKA) will be a radio telescope with a collecting area that will exceed that of existing telescopes by a factor of a hundred or so. This contribution summarises one of the key-science projects selected for the SKA.

The sensitivity of the SKA allows us to perform a Galactic Census of pulsars which will discover a large fraction of active pulsars beamed to us, including the long-sought for pulsar-black hole systems. These systems are unique in their capability to probe the ultra-strong field limit of relativistic gravity. By using pulsar timing we can determine the properties of stellar and massive black holes, thereby testing the Cosmic Censorship Conjecture and the No-Hair theorem. The large number of millisecond pulsars discovered with the SKA will also provide us with a dense array of precision clocks on the sky. These clocks will act as the multiple arms of a huge gravitational wave detector, which can be used to detect and measure the stochastic cosmological gravitational wave background that is expected from a number of sources.

1 Introduction

Solar system tests provide a number of very stringent tests of Einstein's theory of general relativity (GR), and to date GR has passed all observational tests with flying colours. Nevertheless, the fundamental question remains as to whether Einstein has the last word in our understanding of gravity or not. Solar-system experiments are all made in the weak-field regime and will never be able to provide tests in the strong-field limit which is largely unexplored. Tests involving the observations of X-ray binaries may help, but the interpretation of these results depends to some extent on models which are known with only limited precision. In contrast, pulsars represent accurate clocks which can, in a binary orbit, allow us to perform high precision tests of gravitational theories. In the following we describe a key-science project developed for the SKA with a number of colleagues, namely Don Backer, Jim Cordes, Simon Johnston, Joe Lazio and Ben Stappers. Details can be found in [8,2].

2 Strong-field Tests of Gravity

Through its sensitivity, sky and frequency coverage, the SKA will discover a very large fraction of the pulsars in the Galaxy, resulting in about 20,000 pulsars. This number represents essentially all active pulsars that are beamed toward Earth

and includes the discovery of more than 1,000 millisecond pulsars (MSPs). This impressive yield effectively samples every possible outcome of the evolution of massive binary stars. The sensitivity of the SKA allows much shorter integration times, so that searches for compact binary pulsars will no longer be limited. Among the discovered sources, pulsar-black hole (PSR-BH) systems are to be expected. Being timed with the SKA, a PSR-BH system would be an amazing probe of relativistic gravity with a discriminating power that surpasses all of its present and foreseeable competitors [3].

2.1 Black Hole Properties

As stars rotate, astrophysicists also expect BHs to rotate, giving rise to both a BH spin and quadrupole moment. The resulting gravito-magnetic field causes a relativistic frame-dragging in the BH vicinity, leading the orbit of any test mass about the BH to precess if the orbit deviates from the equatorial plane. The consequences for timing a pulsar around a BH have been studied in detail by Wex & Kopeikin (1999 [13]), who showed that the study of the orbital dynamics allows us to use the orbiting pulsar to probe the properties of the rotating BH. Not only can the mass of the BH be measured with very high accuracy, but the spin of the BH can also be determined precisely using the nonlinear-in-time, secular changes in the observable quantities due to *relativistic* spin-orbit coupling. The anisotropic nature of the quadrupole moment of the external gravitational field will produce characteristic short-term periodicities due to *classical* spin-orbit coupling, every time the pulsar gets close to the oblate BH companion [12,13]. Therefore, the mass, M, and both the dimensionless spin χ and quadrupole q,

$$\chi \equiv \frac{c}{G}\,\frac{S}{M^2} \qquad \text{and} \qquad q = \frac{c^4}{G^2}\,\frac{Q}{M^3} \tag{1}$$

of the BH can be determined, where S is the angular momentum and Q the quadrupole moment. These measured properties of a BH can be confronted with predictions of GR.

In GR, the curvature of space-time diverges at the centre of a BH, producing a singularity, which physical behaviour is unknown. The Cosmic Censorship Conjecture was invoked by Penrose in 1969 (see e.g., [6]) to resolve the fundamental concern that if singularities could be seen from the rest of space-time, the resulting physics may be unpredictable. The Cosmic Censorship Conjecture proposes that singularities are always hidden within the event horizons of BHs, so that they cannot be seen by a distant observer. A singularity that is found not to be hidden but "naked" would contradict this Cosmic Censorship. In other words, the complete gravitational collapse of a body always results in a BH rather than a naked singularity (e.g., [11]). We can test this conjecture by measuring the spin of a rotating BH: In GR we expect $\chi \leq 1$. If, however, SKA observations uncover a massive, compact object with $\chi > 1$, two important conclusions may be drawn. Either we finally probe a region where GR is wrong, or we have discovered a collapsed object where the event horizon has vanished and where the singularity is exposed to the outside world.

One may expect a complicated relationship between the spin of the BH, χ, and its quadrupole moment, q. However, for a rotating Kerr BH in GR, both properties share a simple, fundamental relationship [10], i.e. $q = -\chi^2$. This equation reflects the "No-hair" theorem which implies that the external gravitational field of an astrophysical (uncharged) BH is fully determined by its mass and spin. Therefore, by determining q and χ from timing measurements with the SKA, we can confront this fundamental prediction of GR for the very first time.

The best timing precision would be provided by a PSR-BH system with a MSP companion. Such systems do not evolve in standard scenarios, but they can be created in regions of high stellar density due to exchange interactions. Prime survey targets would therefore be the innermost regions of our Galaxy and Globular Clusters. Finding pulsars in orbits around massive or super-massive BHs would allow us to apply the same techniques for determining their properties as for the stellar counterpart [13]. Since the spin and quadrupole moment of a BH scale with its mass squared and mass cubed, respectively, relativistic effects would be measured much easier.

2.2 Gravitational Wave Background

The SKA will discover a dense array of MSPs distributed across the sky. Being timed to very high precision (<100 ns), this "Pulsar Timing Array" (PTA) acts as a cosmic gravitational wave (GW) detector. Each pulsar and the Earth can be considered as free masses whose positions respond to changes in the space-time metric. A passing gravitational wave perturbs the metric and hence affects the pulse travel time and the measured arrival time at Earth [4,5,9]. With observing

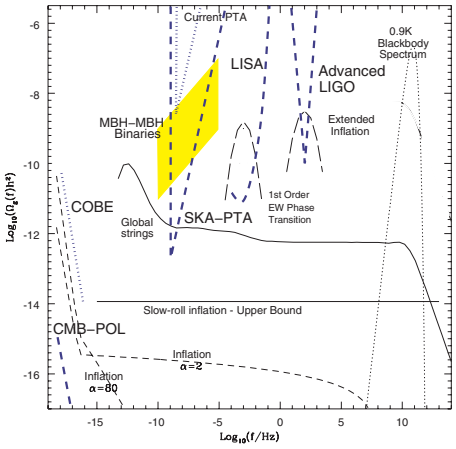


Fig. 1. Summary of the potential cosmological sources of a stochastic gravitational background as presented by Battye & Shellard (1996) and sensitivity curves for various experiments (see text).

times of a few years, pulsars are sensitive to GWs frequencies of $f > 1/T$, hence in the ∼nHz range. Consequently, the SKA can detect the signal of a stochastic background of GW emission in a frequency range that is complementary to that covered by LISA and LIGO.

A stochastic gravitational wave background should arise from a variety of sources. Cosmological sources include inflation, string cosmology, cosmic strings and phase transitions (see Figure 1). We can write the intensity of this GW background as

$$\Omega_{\rm gw}(f) = \frac{1}{\rho_c}\frac{d\rho_{gw}}{d\log f} \tag{2}$$

where $\rho_{\rm gw}$ is the energy density of the stochastic background and ρ_c is the present value of the critical energy density for closure of the Universe, $\rho_c = 3H_0^2/8\pi G$ with $H_0 \equiv h_0 \times 100$ km s^{-1} Mpc^{-1} as the Hubble constant. A contribution to the GW background is also expected from astrophysical processes, i.e. the coalescence of massive BH binaries during early galaxy evolution [9,7]. The amplitude of this signal depends on the mass function of the massive BHs and their merger rate [7]. Measuring the slope of the spectrum would allow us to discriminate between this foreground signal and the cosmological sources. The wedge-like sensitivity curve of the PTA is shown in Fig. 1. For timing precision that is only limited by radiometer noise, the RMS is expected to scale with the collecting area of the observing telescope. In reality, the precision is also affected by other effects. Their limiting influence and the application of correction schemes will need to be determined on a case by case basis. However, extrapolating from the experience with the best performing MSPs today, we can expect the SKA to improve on the current limit on $h_0^2\Omega_{\rm gw}$ by a factor $\sim 10^4$!

References

1. R.A. Battye, E.P.S. Shellard: Class. Quant. Grav. **13** pp. A239–A246 (1996)
2. J.M. Cordes, M. Kramer, T.J.W. Lazio, et al.: New Astron. Rev. **48**, 1413 (2004)
3. T. Damour, G. Esposito-Farèse: Phys. Rev. D **58**, 1 (1998)
4. S. Detweiler: ApJ **234**, 1100 (1979)
5. R.S. Foster, D.C. Backer: ApJ **361**, 300 (1990)
6. S.W. Hawking, R. Penrose, Proc. Royal Soc. of London, Ser. A **314**, 529 (1970)
7. A.H. Jaffe, D.C. Backer: ApJ **583**, 616 (2003)
8. M. Kramer, D.C. Backer, J.M. Cordes, et al.: New Astron. Rev. **48**, 993 (2004)
9. M. Rajagopal, R.W. Romani: ApJ **446**, 543 (1995)
10. K.S. Thorne, R.H. Price, D.A. Macdonald: 'Black Holes: The Membrane Paradigm' (Yale Univ. Press, New Haven 1986)
11. R.M. Wald: 'General relativity' (University of Chicago Press, Chicago 1984)
12. N. Wex: MNRAS **298**, 997 (1998)
13. N. Wex, S. Kopeikin: ApJ **513**, 388 (1999)

Measuring Variations in the Fundamental Constants with the Square Kilometre Array

S. Curran[1]

School of Physics, University of New South Wales, Sydney NSW 2052, Australia

1 Introduction

Recent theories of the fundamental interactions *naturally predict* space-time variations of the fundamental constants. In these theories (e.g. superstring and M-theory), the constants naturally emerge as functions of the scale-lengths of the extra dimensions (e.g., [1,2]). At present, no mechanism has been found for keeping the compactified scale-lengths fixed and so, if extra dimensions exist and their sizes undergo any cosmological evolution, our 3-D coupling constants may vary in time. Several other modern theories also provide strong motivation for an experimental search for variation in the fine structure constant, $\alpha \equiv e^2/\hbar c$. Interestingly, varying constants can provide alternative solutions to the "cosmological problems", e.g. flatness, horizon, etc. The most effective and well understood method of measuring variations in α is by observing absorption lines due to gas clouds along the line-of-sight to distant quasars. Recent detailed studies of the relative positions of heavy element optical transitions and comparison with present day (laboratory) wavelengths, may indeed suggest that the α may have evolved with time [3,4], although this consensus is be no means universal [5]. It is therefore clear that an independent check is required, which can refute or confirm the optical results, thus providing a sound experimental test of possible unified theories. The study of redshifted radio absorption lines offers the best test of cosmological changes in the fundamental constants, although presently, the paucity of systems exhibiting HI 21-cm and molecular absorption severely limits our ability to carry out statistically sound comparisons.

2 Measurements Using Radio Absorption Lines

2.1 Atomic Lines

The comparison between optical and radio absorption lines can provide a considerably more precise determination of $\Delta\alpha/\alpha$ than pure intra-optical techniques: For the frequency of the optical transition, where the interaction is Coulombic, $\nu_{\rm opt} \propto 1 + 0.03\alpha^2$. For the 21 cm spin-flip transition of H I, which is produced by the interaction of the electron magnetic moment, the frequency is $\nu_{21} \propto g_{\rm p}\mu\alpha^2$, where $g_{\rm p}$ is the proton g-factor and $\mu \equiv m_{\rm e}/m_{\rm p}$ is the electron–proton mass ratio. Therefore for a constant $g_{\rm p}$ and μ, this is ≈ 30 times more sensitive than the

optical transition to a given change in α [6]. From this, the ratio of the H I and optical frequencies is (e.g., [7])

$$\frac{\nu_{21}}{\nu_{\rm opt}} \propto \mu\alpha^2 g_p. \tag{1}$$

2.2 Molecular Lines

1. Centimetre-wave OH lines: These are a combination of Λ-doubling and hyperfine splitting, giving each state 4 lines which have various dependencies on α, $m_{\rm e}/m_{\rm p}$ and $g_{\rm p}$. For example, from the 1612, 1665, 1667 and 1720 MHz lines of the ground state (18-cm) transition [8,9]:

$$\nu_{1665} + \nu_{1667} \propto \mu^{2.57}\alpha^{-1.14}, \tag{2}$$
$$\nu_{1667} - \nu_{1665} \propto \mu^{2.44}\alpha^{-0.88} g_{\rm p}, \tag{3}$$
$$\nu_{1720} - \nu_{1612} \propto \mu^{0.72}\alpha^{2.56} g_{\rm p}. \tag{4}$$

2. Millimetre-wave (e.g. CO, HCO^+, HCN, etc.) lines: These arise from rotational transitions and the line frequencies are proportional to μ only, making these very useful reference lines with which to compare the centimetre transitions. Specifically, for the H I 21-cm, OH 18-cm and 6-cm lines [10,8,11], respectively:

$$\frac{\nu_{21}}{\nu_{\rm mm}} \propto \alpha^2 g_p, \frac{\nu_{1667}}{\nu_{\rm mm}} \propto \mu^{1.57}\alpha^{-1.14}, \frac{\nu_{4750}}{\nu_{\rm mm}} \propto \mu^{-0.49}\alpha^{2.98}, \tag{5}$$

   the latter two of which, like (2), contain no contribution from g_p.

Note finally that many more constraints are available from other excited OH ($\lambda \leq 6$ cm) transitions [8,9], none of which have yet been detected at high redshift.

3 Radio Absorption Lines with the SKA

3.1 SKA Parameters

1. Coverage: The SKA will offer continuous frequency coverage from 0.1 to 25 GHz, with an instantaneous bandwidth of 25% of the band centre frequency. An unprecented wide field of view is also expected (see [12]).
2. Sensitivity: After 1 hour of integration, at a spectral resolution of 1 km s^{-1}, the SKA will reach r.m.s noise levels of $\sigma \approx 0.2$ mJy at 0.2 GHz, $\sigma \approx 0.04$ mJy at 0.5–5 GHz and $\sigma \approx 0.01$ mJy at 25 GHz [12].

3.2 H I 21-cm Absorption

H I 21-cm absorption at high redshift is currently only found in systems with very high neutral hydrogen column densities ($N_{\rm HI} \gtrsim 10^{20}$ cm^{-2}). Damped Lyman-alpha absorption systems (DLAs) constitute a large fraction of these and represent a class of high column density absorbers of accurately determined redshifts which exhibit a plethora of optical (heavy element, Sect. 1) absorption lines. From the above parameters, the SKA will be able to detect 21-cm absorption at redshifts of $z \leq 13$. In the most sensitive regime ($\gtrsim 200$ MHz or $z_{\rm HI} \lesssim 6$), for a continuum flux density[1] of 0.5 Jy, a 3σ sensitivity to a column density of

$$N_{\rm HI} \approx 2 - 20 \times 10^{14}.\frac{T_{\rm spin}}{f} \text{ cm}^{-2} \text{ per unit km s}^{-1} \text{ line width,} \qquad (6)$$

will be obtained after one hour of integration, where $T_{\rm spin}$ is the spin temperature of the gas (K) and f is the covering factor of the continuum flux. For DLAs this gives $\frac{T_{\rm spin}}{f} \sim 10^5$ for a typical 10 km s^{-1} line width, thus covering an unprecedented range of spin temperatures and covering factors. This is more than an order of magnitude more sensitive those currently measured and is expected to yield many more 21-cm detections in the known DLAs (see [13] for a detailed discussion). For more nominal values ($T_{\rm spin} \approx 100$ K and $f \approx 1$), Eq. 6 suggests that 21-cm absorption will be detectable to $N_{\rm HI} \sim 10^{17}$ cm^{-2}, i.e. in Lyman-limit systems, thus increasing the number of known redshifted 21-cm absorbers by 3 orders of magnitude, over and above the DLAs with high $T_{\rm spin}/f$ ratios and weak radio illumination which currently remain undetected.

3.3 Molecular Absorption

Redshifted molecular absorption systems are currently very rare, with only 10 H_2 (in high redshift DLAs, e.g., [14]) and 4 millimetre/OH (e.g., [15]) systems known. The tuning range of the SKA (Sect. 3.1) will permit searches at redshifts of $z_{\rm OH} \lesssim 16$, $z_{\rm CO} \gtrsim 3.6$ and $z_{\rm HCO^+\ \&\ HCN} \gtrsim 2.6$. Using the parameters above (Sect. 3.2) and continuum flux densities of 0.5 Jy (cm) and 0.1 Jy (mm) gives:

$$N_{\rm OH} \approx 3 - 60 \times 10^{11} \text{ cm}^{-2},\ \nu_{\rm rest} = 1667 \text{ MHz over } 0 \geq z_{\rm abs} \geq 16, \qquad (7)$$

$$N_{\rm CO} \sim 10^{13}\ (z_{\rm abs} \approx 3.6),\ N_{\rm HCO^+\ \&\ HCN} \sim 10^{10}\ (z_{\rm abs} \approx 2.6) \qquad (8)$$

cm^{-2} per unit km s^{-1} line width for an excitation temperature of 10 K at $z_{\rm abs} = 0$ (see [16]). In the low redshift regime, this corresponds to molecular hydrogen fraction sensitivities of $f(H_2) \gtrsim 10^{-2}$ for OH & HCO^+ and $\gtrsim 10^{-4}$ for CO in high column density absorbers (see [17] for details). Due to the steep cosmological evolution of the molecular hydrogen fraction in apparent in H_2-bearing DLAs [18], values of $f(H_2) \lesssim 10^{-4}$ are expected at the redshifts were the SKA can observe millimetre transitions ($z \gtrsim 2.6$). Note, however, that the 4 known millimetre/OH absorbers have $f(H_2) \approx 0.3-1.0$ and visual magnitudes of $V > 20$, confirming that non-optically selected objects provide the best targets for molecular absorption searches.

[1] The minimum flux density illuminating a DLA currently detected in H I absorption.

4 Summary

Radio absorption lines provide by far the best means with which to unambiguously determine the cosmological evolution of several dimensionless fundamental "constants", thus providing a physical test of current Grand Unified Theories. However, such studies are severely hampered by the rarity of H I 21-cm, OH 18-cm and millimetre absorption systems currently known in the distant Universe.

- With the SKA we will for the first time be able to detect 21-cm absorption in a large fraction of known DLAs as well as in Lyman-limit systems, thus providing an extremely large sample of absorbers at known redshift.
- Due to its unprecedented large field of view and instantaneous bandwidth the SKA will be ideal for surveys for new H I and OH absorbers, which are unbiased by dust extinction, again vastly increasing the sample of high redshift absorbers.
- Finally, although the SKA's 25 GHz frequency cut-off may rule out the direct detection of millimetre absorption systems, the blind surveys for OH will provide an excellent diagnostic with which to search for molecules in millimetre lines, which would prove inefficient using the next generation of millimetre telescopes due to the much smaller fields of view.

References

1. W. Marciano: Phys. Rev. Lett. **52**, 489 (1984)
2. T. Damour, A.M. Polyakov: Nucl. Phys. B **423**, 596 (1994)
3. J.K. Webb et al.: Phys. Rev. Lett. **87**, 091301 (2001)
4. M.T. Murphy, J.K. Webb, V.V. Flambaum: MNRAS **345**, 609 (2003)
5. H. Chand et al.: A&A **417**, 853 (2004)
6. V.A. Dzuba, V.V. Flambaum, J.K. Webb: Phys. Rev. A **59**, 230 (1999)
7. L.L. Cowie, A. Songaila: ApJ **453**, 596 (1995)
8. J. Darling: Phys. Rev. Lett. **91**, 011301 (2003)
9. J.N. Chengalur, N. Kanekar: Phys. Rev. Lett. **91**, 241302 (2003)
10. M.J. Drinkwater, et al.: MNRAS **295**, 457 (1998)
11. N. Kanekar, J.N. Chengalur: MNRAS **350**, L17 (2004)
12. D.L. Jones: SKA Memo 45 (2004)
13. S.J. Curran, et al.: MNRAS, in preparation (2004)
14. D. Reimers, et al.: A&A **410**, 785 (2003)
15. F. Combes, T. Wiklind: ESO Messenger **91**, 29 (1998)
16. S.J. Curran, et al.: MNRAS **352**, 563 (2004)
17. S.J. Curran, N. Kanekar, J.K. Darling: New Astron. Rev. **48**, 1095 (2004)
18. S.J. Curran, et al.: MNRAS **351**, L24 (2004)

ELT Observations of Supernovae at the Edge of the Universe

M.D. Valle[1], R. Gilmozzi[2], N. Panagia[3], J. Bergeron[4], P. Madau[5], J. Spyromilio[2], and P. Dierickx[2]

[1] INAF-Arcetri Astrophysical Observatory, Largo E. Fermi 5, 50125, Firenze, Italy
[2] European Southern Observatory, 3107 Alonso de Cordova, Santiago, Chile
[3] ESA/Space Telescope Science Institute, 3700 San Martin Drive, Baltimore, MD 21218, USA
[4] Institut d'Astrophysique de Paris - CNRS, 98bis Boulevard Arago, 75014 Paris, France
[5] Department of Astronomy and Astrophysics, University of California, 1156 High Street, Santa Cruz, CA 95064, USA
[6] European Southern Observatory, Karl-Schwarzschild-Strasse 2, Garching D-85748, Germany

Abstract. In this paper we discuss the possibility of using Supernovae as tracers of the star formation history of the Universe for the range of stellar masses $\sim 3-30$ $M_\odot$ and possibly beyond. We simulate the observations of 400 SNe, up to $z \sim 15$, made with OWL (100m) telescope.

1 Introduction

The detection and the study of Supernovae (SNe) is important for at least two reasons: *1.* the use of *local* SNe (both type Ia and II) as 'calibrated' standard candles [9,10,23] provides a direct measurement of the expansion rate of the Universe $H_\circ$, whereas their detection at $z > 0.3$ allows to measure its deceleration parameter $q_\circ$ and to probe different cosmological models [24,25,27]; *2.* the evolution of the cosmic SN rate provides a direct measurement of the cosmic star formation rate (SFR). Indeed the rate of core-collapse SN explsions (SN II, Ib/c) is a direct measurement of the death of stars with masses in the range 8–30 $M_\odot$ (although it is still debated if stars more massive than 30 $M_\odot$ make "normal" type II/Ibc SNe, or collapse forming a BH with no explosion at all, or just make a different kind of explosion like GRBs; see, e.g., [11]). Similarly, type Ia SNe may provide the history of star formation of moderate mass stars, 3–8 $M_\odot$, i.e. their most likely progenitors provided that the SNe Ia explosion process is unambiguously identified (e.g., [18]). In addition the evolution of the SN-Ia rate with redshift helps to clarify the nature of their progenitors (e.g., [5,14,30]).

2 SNe as Tracers of Star Formation

For a Salpeter Initial Mass Function (IMF) with an upper cutoff at 100 $M_\odot$ we find that half of all SNII is produced by stars with masses between 8 and 13 $M_\odot$

and half of the mass in SN-producing stars is in the interval of mass $\sim$ 8–22 $M_\odot$. A main sequence star with 13 $M_\odot$ has approximately a luminosity of 8000 $L_\odot$ and a temperature of 22000 K and one with 22 $M_\odot$ has $L \sim 3.5 \times 10^4$ $L_\odot$ and $T_{\rm eff} \sim 27000$ K. This means that more than half of the SN producing stars are rather poor sources of ionizing photons and of UV continuum photons, while the bulk of the UV radiation, both in the Balmer and in the Lyman continuum is produced by much more massive stars. Actually, starburst models (e.g., [13]) suggest us that stars above 30 $M_\odot$ produce 90% of the Lyman continuum photons and 70% of the 912-2000Å UV continuum. It follows that the bulk of the UV radiation both in the Balmer and Lyman continuum is produced by stars more massive than 30 $M_\odot$, so that the Hα and UV fluxes measure **only** the very upper part of the IMF (stars with masses $> 30\,M_\odot$ are only 13% of the stars with masses larger than $> 8\,M_\odot$). Therefore, Hα and UV flux are not ideal indicators of star formation rate because: *a)* they require a huge extrapolation to lower masses and *b)* the extrapolation depends on the value of minimum mass to make a SNII, $M_{\rm up}$, which is not well known and may be different in different environments [3] or at different redshifts [11]. On the other hand, SNe can provide a measurement of the star formation rate which is: *i)* independent of other SFR determinations; *ii)* more direct because the IMF extrapolation is appreciably smaller; *iii)* more reliable because it is based on counting SN explosions rather than relying on identifying and measuring the sources of ionization or of UV continuum. A possible drawback for this approach is the fact that a number of SNe may be missed because of extinction in their parent galaxies [15].

3 The Ingredients of the Simulation

Our simulation is based on a number of assumptions:

1. ELT performance. We have assumed ELT= OWL, i.e. a 100 m telescope. The imaging and spectroscopic limits are a function of the S/N ratio as derived from the ELT exposure time calculator (www-astro.physics.ox.ac.uk/ imh/ELT).

2. OWL field. A reasonable extrapolation of the current technological standards let us presume that a 2×2 arcmin field, corrected for adaptive optic (K band), is within the technological possibilities in the next decade (Ragazzoni, private communication).

3. Number of SNe expected in a single OWL frame. By extrapolating at higher redshifts the result obtained by Madau et al. [14], Miralda Escudé & Rees [19] and Heger et al. [11], we estimate up to 8 SNe per OWL field per year. Here we are including the very powerful Pop III SNe that are expected to be produced by pair-creation in zero-metallicity massive stars, in the range $140 - 260 M_\odot$ [11]

4. Spectral energy distribution (=SED) of SNe (see Fig. 1). We have assumed as templates for type Ia and II : SN 1992A, SN 1999em and SN 1998S [20,28]. The SED for SNe originating from Pop III stellar population has been obtained from [11].

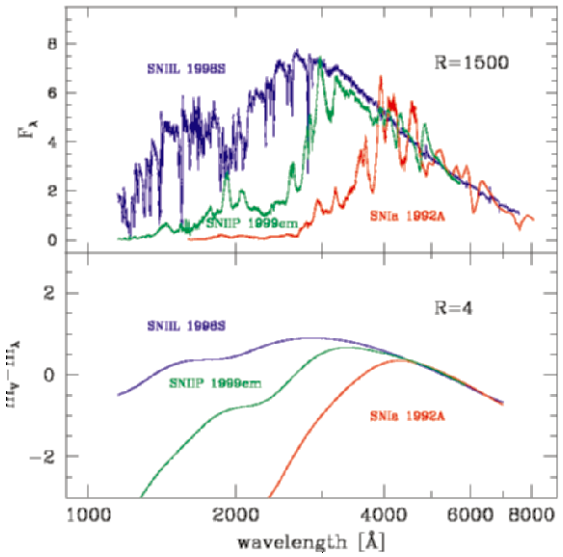


Fig. 1. Spectral Energy Distribution adopted for type I and type II SNe. (Adapted from [20])

5. Observational strategy. It is based on the control time methodology [32]. The morphology of the light curves and the absolute magnitudes at maximum of SNe have been obtained from [2,8,22,29].

6. Distribution of SNe into spectroscopic types. These data have come from [4,6,11,17,26]. We have estimated about 63% of SNe to be of type II, of which about 3/4 regular and 1/4 bright (a few SNe-II are expected to be observed during the UV shock breakout, that at z$\sim$ 7 − 8 should last about 4-5 days in the observer rest frame), about 20% type Ia, 15% type Ib/c, less than 0.5% hypernovae and about 1.5% SNe from Pop III.

7. Cosmology ($\Omega_{\rm m} = 0.3$, $\Omega_{\Lambda} = 0.7$); e.g., [12,28].

4 Redshift Thresholds

Fig. 2-5 represent the spectroscopic templates for SNeI-a, SNeII, and from Pop III at different redshifts as viewed in the observer rest-frame. The three solid lines denote the fluxes, at different resolution factors, corresponding to S/N=10 for OWL exposures of 10^5 sec. The dashed line is the threshold for JWST [21]. Scaling the data in Figures 2-5 reveals that SNe are well detectable with OWL in 1h exposure. SNe-Ia are detectable up to $z \sim 5$ while SNe-II (bright) up to $z \sim 7$–8. Pop III SNe, which in principle would be easily detectable up to $z \sim 20$ [11] are unlikely observable beyond $z \sim 15$, due to the Lyman forest absorption.

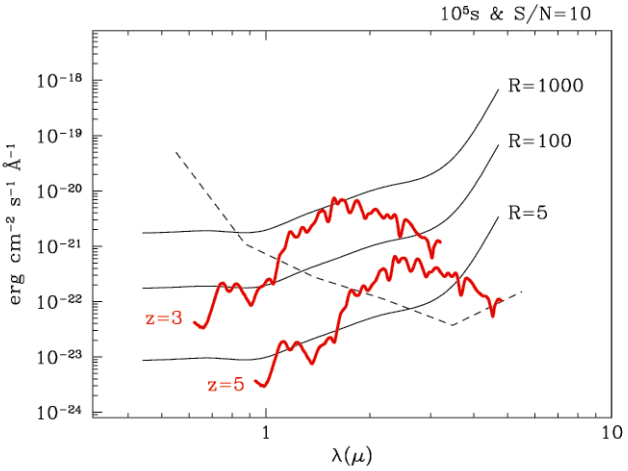


Fig. 2. The spectroscopic template for type Ia SNe as viewed in the rest-frame of the observer, at different redshifts. The three solid lines denote the fluxes corresponding to a S/N=10 for OWL exposures of 10^5 sec at different resolution. The dashed line is the threshold (R=5) for JWST.

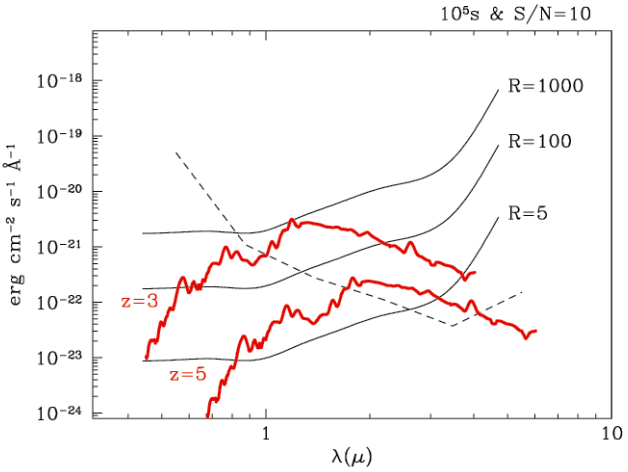


Fig. 3. The same as Fig. 2, for SNe-II (regular).

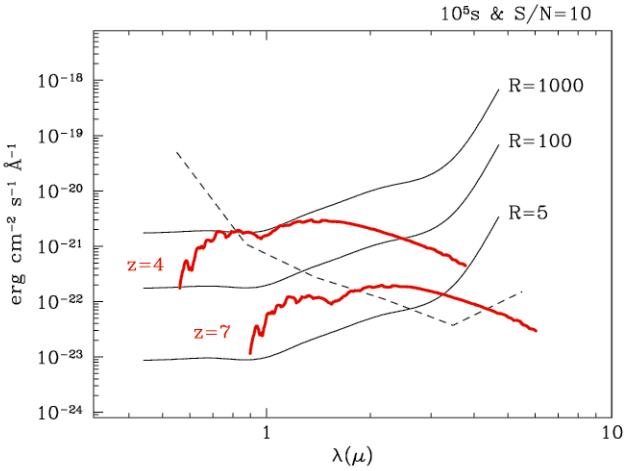


Fig. 4. The same as Fig. 2, for SNe-II (bright).

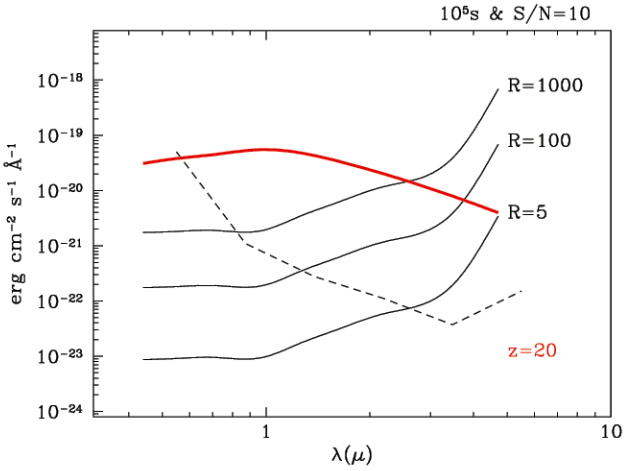


Fig. 5. The same as Fig. 2, for SNe originating from Pop III stellar population. The template has been derived from Heger et al. [11] (their Fig. 3).

5 The Simulation

An ELT project devoted to the study the evolution of the cosmic SN rate up to $z \sim 15$ requires an important (although not huge, as we shall see) investment of telescope time. We plan to carry out the SN search on 50 OWL fields in the J, H and K bands (1 hour each) at 4 different epochs over an interval of time of 1 year. This strategy is justified by the following considerations. The typical light curve width around maximum light is 15-20 days in the SN rest frame and most SNe will occur (see Fig. 2-5) at $z < 5$. Therefore, the light curve widths in the observer rest frame lasts about 100-120 days, so that 4 exposures obtained 3 months apart will cover all events occurring within 1 year. In addition we need 3 more epochs (1h each) in the K band for the photometric follow-up and 1 spectroscopic epoch (4h for each SN discovered at $z < 5$) for the spectroscopic classification. At very high redshifts, $z \sim 7$–8, only bright type II SNe may be used as standard candles (due to their strong UV emission, while SNe Ia are basically blind below 2400 Å and therefore they are detectable 'only' up to $z \sim 5$). Bright type II SNe can be standardized via "expanding photosphere method" [9] or alternatively via expansion velocity vs. bolometric luminosities relationship at the plateau stage [10]. This task can be accomplished by securing a second and possibly a third spectroscopic epoch, and this requires about 200 hours of observing time. Finally, we need 4 h for each SN of Pop III to obtain medium/high resolution spectroscopy.

In summary, this programme needs a "grand total" of 1270 h, i.e. 600 h are for the SN search, 150 h for the photometric follow-up (K band) and 200 h for the spectroscopy of type Ia, Ib/c and II SNe. 200 additional hours for the second and third spectroscopic epochs of bright type II SNe and finally 120 h for the spectroscopy of Pop III SNe. All of this corresponds to about 160 nights, which will allow us to study about 400 SNe. This is certainly an important investment in terms of telescope time, however we note that this corresponds to about three times as much the size of a current Treasury programme (450 orbits) and it is comparable with SNAP (now Joint Dark Energy Mission) which is expected to study about 2000 SNe Ia (at $z < 2$) in 2 years [1]. In Fig. 6 we show the 'virtual' SNe discovered by OWL: pink dots are type Ia SNe, black dots type II (+Ib/c), blue and green dots are Ia SNe 'actually' discovered by ground based telescopes [12,24,27,31] and from HST [28]. The SNe have been distributed around the track $\Omega_{\rm m} = 0.3$, $\Omega_{\Lambda} = 0.7$ after taking into account the intrinsic dispersion of the peak of the luminosity of type Ia and II SN populations, while the photometric errors have been derived from the signal to noise which has been computed for each simulated observation. Grey and red dots represent SNe from Pop III star population, the latter ones are SNe caught at maximum light. The explosion rate for Pop III SNe was taken from Heger et al. [11]. However, recently Lilly (private communication) found that Heger et al.'s rates may be too high and may have to be reduced by about an order of magnitude.

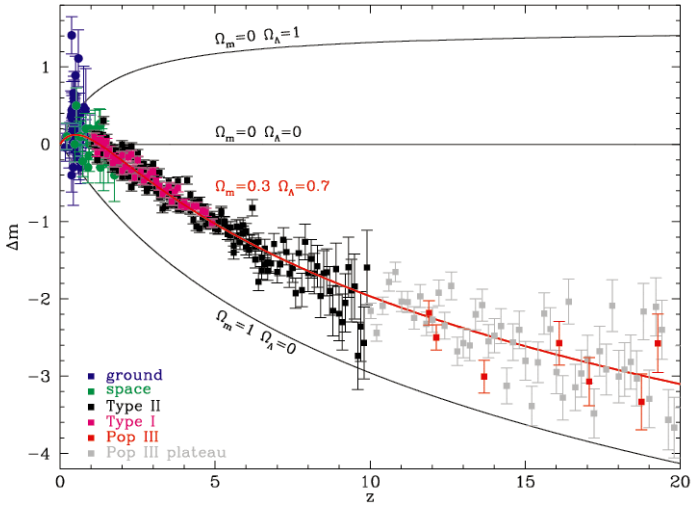


Fig. 6. Hubble diagram for the simulated ELT observations of SNe. Pink, black, grey dots represent type Ia, type II (+Ib/c) and SNe from Pop III stellar population (red dots are SNe from Pop III caught at maximum light). Blue and green dots are 'real' SNe observed from ground telescopes and HST, respectively.

6 Conclusions

In this paper we have argued that SNe can be used as profitable tracers of cosmic star formation for a number of reasons: *i)* Determinations of the SFR based on SN measurements are independent of other possible determinations, *ii)* SNe provide a more direct diagnostics than the UV luminosity or the Hα line emission because the IMF extrapolation is much smaller and *iii)* SNe are a more reliable source of information because it is based on a simple count of individual SN explosions rather than relying on identifying and measuring the source of ionization (if using H-alpha flux) or the source of UV continuum. In addition, by studying SNe at high redshifts *iv)* we can learn to what extent the IMF was more skewed toward massive stars (relatively to a normal Salpeter's) in low metallicity environments, and *v)* we can study the properties of the progenitors of the primordial Gamma Ray Bursts (=GRBs) (given the growing evidence for the existence of an association between core collapse SNe with the long duration GRBs, see [16] and references therein).

The results of our simulation point out that $\sim$ 400 SNe can be studied up to $z \sim 15$ within a reasonable amount of telescope time (about 160 nights). This pilot programme has been conceived to study the history of the cosmic star formation rate, nevertheless a number of important by-products are at hand: such as *vi)* to disentangle cosmological models alternative to Λ, *vii)* to clarify the nature of the progenitors of type Ia SNe *viii)* to probe the physical properties of

the ISM and IGM at $z > 10$ through high spectral resolution ($R \sim 10^4$) of Pop III SNe (feasible with 50–100 m telescope) *ix)* to explore the metal enrichment of the IGM at early epochs (up to $z \sim 4$) via observations of bright type II and Ia SNe at a resolution of $R \sim 1000$ (feasible with 50–100 m telescope).

References

1. G. Aldering, et al.: SPIE **4835**, 146 (2002)
2. R. Barbon, F. Ciatti, L. Rosino: A&A **25**, 241 (1973)
   A&A, 72, 287
3. A. Bressan, M. Della Valle, P. Marziani: MNRAS **331**, L25 (2002)
4. E. Cappellaro, M. Turatto, D.Yu. Tsvetkov, O.S. Bartunov, C. Pollas, R. Evans, M. Hamuy: A&A **322**, 431 (1997)
5. T. Dahlen, et al.: ApJ **614**, 189 (2004)
6. M. Della Valle, et al.: A&A **406**, L33 (2003)
7. M. Della Valle, et al.: ApJ, submitted (2004)
8. J.B. Doggett, D. Branch: AJ **90**, 2303 (1985)
9. M. Hamuy, et al.: ApJ **558**, 615 (2001)
10. M. Hamuy, P.H. Pinto: ApJ **566**, L63 (2002)
11. A. Heger, S.E. Woosley, I. Baraffe, T. Abel: 'Evolution and Explosion of Very Massive Primordial Stars'. In: *Lighthouses of the Universe: The Most Luminous Celestial Objects and their use for Cosmology*, Proc. of a MPA/ESO/MPE/USM Joint Astronomy Conference, eds. M. Gilfanov, R/ Sunyaev, E. Churazov (ESO, Garching 2002), p. 369
12. R.A. Knop, et al.: ApJ **598**, 102 (2003)
13. C. Leitherer, et al.: ApJS, **123**, 3 (1999)
14. P. Madau, M. Della Valle, N. Panagia: MNRAS **297**, L17 (1998)
15. R. Maiolino, et al.: A&A **389**, 84 (2002)
16. D. Malesani, et al.: ApJ **609**, L5 (2004)
17. F. Mannucci, et al.: A&A, submitted (2004)
18. F. Mannucci, M. Della Valle, N. Panagia: in preparation
19. J. Miralda-Escudé, M. Rees: ApJ **478**, L57 (1997)
20. N. Panagia: 'Ultraviolet Supernovae'. In: *Supernovae and Gamma-Ray Bursters*, ed. K.W. Weiler (Springer-Verlag LNP 598, Berlin 2003), pp. 113–144
21. N. Panagia, M. Stiavelli, H.C. Ferguson, H.S. Stockman: RevMexAA SC **17**, 230 (2003)
22. F. Patat, R. Barbon, E. Cappellaro, M. Turatto: A&A **282**, 731 (1994)
23. M.M. Phillips: ApJ **413**, L105 (1993)
24. S. Perlmutter, et al.:Nature **391**, 51 (1998)
25. S. Perlmutter, et al.: ApJ **517**, 565 (1999)
26. P. Podsiadlowski, et al.: ApJ **607**, L17 (2004)
27. A. Riess, et al.:AJ **116**, 1009 (1998)
28. A. Riess, et al.:ApJ **607**, 665 (2004)
29. A. Saha, et al.:ApJ **551**, 973 (2001)
30. L.G. Strogler, et al.: ApJ, in press, astro-ph/0406546 (2004)
31. J.L. Tonry, et al.: ApJ **594**, 1 (2003)
32. F. Zwicky: ApJ **88**, 529 (1938)

SKA and the Magnetic Universe

R. Beck[1], B. Gaensler[2], and L. Feretti[3]

[1] Max-Planck-Institut für Radioastronomie, Auf dem Hügel 69, 53121 Bonn, Germany
[2] Harvard-Smithsonian Center for Astrophysics, 60 Garden Street MS-6, Cambridge, MA 02138, USA
[3] Istituto di Radioastronomia CNR/INAF, Via Gobetti 101, 40129 Bologna, Italy

Abstract. The Square Kilometer Array (SKA) can deliver new data which will directly address currently unanswered issues concerning the origin and evolution of cosmic magnetism. An *all-sky survey of Faraday rotation measures* towards $> 10^7$ background sources will provide a dense grid for probing magnetism in the Milky Way, nearby galaxies, distant galaxies, clusters and in protogalaxies. Using these data, we can map out the evolution of magnetised structures from redshifts $z > 3$ to the present, can distinguish between different origins for seed magnetic fields in galaxies, and can develop a detailed model of the magnetic field geometry of the overall Universe.

1 Introduction

Magnetism is one of the four fundamental forces. Understanding the Universe is impossible without understanding magnetic fields. However, the origin of cosmic magnetic fields is an open problem in astrophysics and fundamental physics. When and how were the first fields generated? Are present-day magnetic fields the result of standard dynamos, or do they represent rapid or recent field amplification through some other process? What role do magnetic fields play in turbulence, cosmic ray acceleration, galaxy formation, and structure formation in the early Universe?

Most of what we know about astrophysical magnetic fields comes through the detection of radio waves, but our present knowledge is restricted to nearby or bright objects. With the unprecedented sensitivity, polarization purity and spectropolarimetric capability of the Square Kilometre Array (SKA) [2], the window to the Magnetic Universe can finally be opened.

2 An All-Sky Rotation Measure Survey with the SKA

Faraday rotation has been observed for ∼1200 extragalactic sources and ∼300 pulsars. The resulting rotation measures (RM) are useful probes of magnetic fields in the Milky Way [14], nearby galaxies [12], clusters [10], and in distant Lyα absorbers [29]. However, the sampling of RMs over the sky is very sparse.

A key platform on which to base the SKA's studies of cosmic magnetism will be to carry out an **all-sky RM survey** [9], in which spectropolarimetric continuum imaging of 10 000 deg^2 of the sky can yield RMs for approximately 2×10^4 pulsars and 2×10^7 compact polarized extragalactic sources in about a year of observing time. This data set will provide a grid of RMs at a mean spacing of $\sim 30'$ between pulsars and just $\sim 90''$ between extragalactic sources.

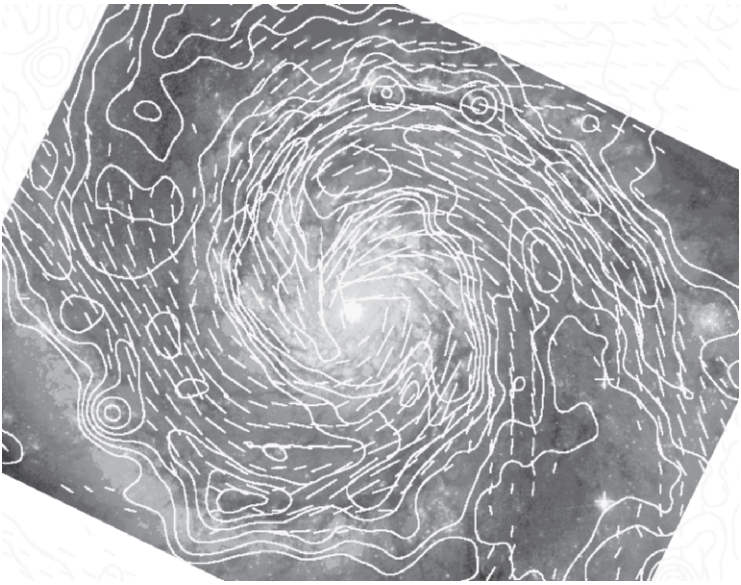


Fig. 1. The magnetic field of the grand design spiral galaxy M 51. The background optical image from the *HST* image is overlaid with contours of the radio total intensity at 5 GHz, combined from observations at the VLA and Effelsberg radio telescopes. The vectors show the orientation of the magnetic field, as determined from the 5 GHz linear polarization measurements (Faraday rotation is small at this frequency) [6].

3 Expected Results

3.1 Magnetic Fields in the Local Universe

For the Milky Way, nearby galaxies and clusters, high-sensitivity mapping with the SKA of polarized synchrotron emission, combined with determinations of RMs for extended emission, pulsars and background sources, will allow us to derive detailed three-dimensional maps of the magnetic fields in these sources. Of special interest are the turbulence spectrum, the number and location of magnetic reversals, the relation between magnetic and optical spiral arms, and the structure and extent of halo fields.

In our Milky Way, the large sample of pulsar RMs obtained with the SKA can be inverted to yield a complete delineation of the magnetic field in the spiral arms and disk on scales $\geq 100\,\mathrm{pc}$ [25]. Small-scale structure and turbulence can be probed using *Faraday tomography*, in which foreground ionised gas produces frequency-dependent Faraday features when viewed against diffuse Galactic polarized radio emission [8,13,27]. Magnetic field geometries in the Galactic halo and outer parts of the disk can be studied using the all-sky RM grid.

In external galaxies, magnetic fields can be directly traced by diffuse synchrotron emission and its polarization [1] (Fig. 1). The SKA will provide sufficient resolution and sensitivity to carry out Faraday tomography on the nearest

galaxies, allowing us to identify individual features and turbulent processes in the magneto-ionised ISM. Deep observations of nearby galaxies can provide $> 10^5$ background RMs and hence fantastically detailed maps of the magnetic structure, even in the outer disk and halo. The overall structure of galactic magnetic fields can be determined for a large sample of more distant galaxies, which will give an excellent data base to discriminate between dynamo and other mechanisms for the origin and sustainment of these fields [3].

In clusters of galaxies, magnetic fields play a critical role in regulating heat conduction [20], and may also both govern and trace cluster formation and evolution. With the SKA, the RM grid can provide ~ 1000 background RMs behind a typical nearby cluster; a comparable number of RMs can be obtained for a more distant cluster through a deep targeted observation [5]. These data will allow us to derive a detailed map of the field in *each* cluster. The field properties in various types of clusters (e.g., those showing cooling cores, or those with recent merger activity, etc.) at various distances can be obtained. Detailed comparisons between RM distributions and X-ray images of clusters will allow us to relate the efficiency of thermal conduction to the magnetic properties of different regions and to directly study the interplay between magnetic fields and hot gas.

3.2 Galaxies at Intermediate and High Redshifts

Measurements of the magnetic field in galaxies at intermediate redshifts ($0.1 \leq z \leq 2$) provide direct information on how magnetised structures evolve and amplify as galaxies mature. The linearly polarized emission from galaxies at these distances will often be too faint to detect directly; Faraday rotation thus holds the key to studying magnetism in these sources.

There are many distant *extended* polarized sources (e.g., many of the quasars and radio galaxies in the 3C catalogue), which provide ideal background illumination for probing Faraday rotation in galaxies which happen to lie along the same line of sight. These experiments can deliver maps of magnetic field structures in galaxies more than 100 times more distant than discussed above. We expect that a large number of the sources for which we measure RMs will be quasars showing foreground Lyα absorption; these absorption systems likely represent the progenitors of present-day galaxies. If a large enough sample of RMs for quasars at known redshift can be accumulated, a trend of RM vs z can potentially be identified. The form of this trend can then be used to distinguish between RMs resulting from magnetic fields in the quasars themselves and those produced by fields in foreground absorbing clouds [29]; detection of the latter effect would then directly trace the evolution of magnetic field in galaxies and their progenitors. This experiment has been attempted several times, but the existing data sets provide only marginal (if any) evidence for any evolution of RM with redshift [29,22,21]. With the SKA accurate RM measurements and precise foreground subtraction will allow us to reliably probe magnetic field to much higher redshifts than has been previously possible, and thus derive the field evolution as a function of the cosmic epoch.

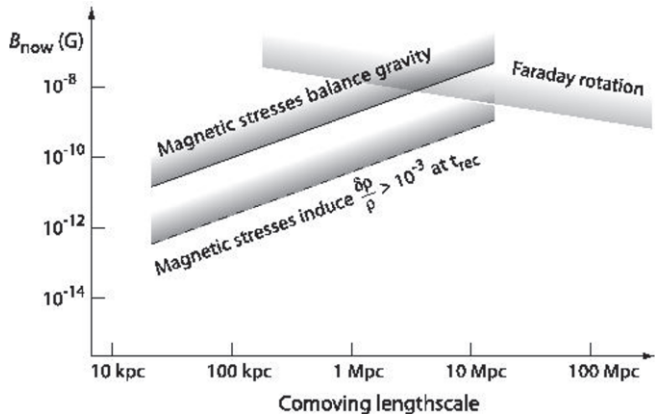


Fig. 2. Observational and theoretical constraints on the magnetic field on various length scales at the time of recombination, t_{rec}. A field is cosmogonically important if it can generate density perturbations of amplitude $\sim 10^{-3}$ at t_{rec}, since these would have developed into gravitationally bound systems by the present time [23].

At yet higher redshifts, we can take advantage of the sensitivity of the deepest SKA fields, in which we expect to detect the synchrotron emission from the youngest galaxies and proto-galaxies out to redshifts $z \geq 2$. Since standard dynamos need a few rotations or about 10^9 yr to build up a coherent field [3], detection of synchrotron emission in young galaxies at high z put constraints on the seed field which potentially challenge these models [22].

3.3 The Intergalactic Medium and Cosmic Field Geometry

Fundamental to all the issues discussed above is the search for magnetic fields in the IGM. All of "empty" space may be magnetised, either by outflows from galaxies [19], by relic lobes of radio galaxies, or as part of the "cosmic web" structure. Its role as the likely seed field for galaxies and clusters, plus the prospect that the IGM field might trace and regulate structure formation in the early Universe, places considerable importance on its discovery. To date there has been no detection of magnetic fields in the IGM; current upper limits on the strength of any such field suggest $|B_{\rm IGM}| \leq 10^{-8} - 10^{-9}$ G [18,4].

This all-pervading magnetic field can finally be identified through the all-sky RM grid (Sect. 2). The correlation function of the RM distribution provides the magnetic power spectrum of the IGM as a function of cosmic epoch [15,4]. Such measurements will allow us to develop a detailed model of the magnetic field geometry of the IGM and of the overall Universe. The required large sample of RMs from sources at known redshift should be obtainable by combining the SKA All-Sky RM grid with the spectroscopic data bases provided by SDSS and KAOS plus the all-sky multiband photometry of LSST and SkyMapper.

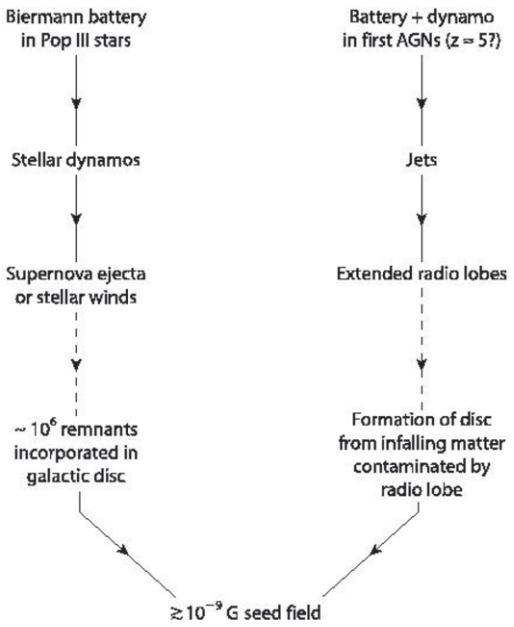


Fig. 3. Suggested mechanisms through which Population III stars and active galactic nuclei can both produce seed magnetic fields of strength $\geq 10^{-9}$ G [24].

3.4 Primordial Fields

A magnetic field already present at the recombination era might have affected the processes occurring at that epoch [26]. The constraints are summarised in Fig. 2, in terms of the field's characteristic length scale. A variety of cosmological processes can produce relatively high magnetic fields, of strength $10^{-10} - 10^{-9}$ G at $z \sim 5$ [11]. Active galactic nuclei and violent star-formation activity in young galaxies may be able to generate seed fields of similar strength [19,28,7] (Fig. 3). The dynamo mechanism may then have amplified the seed field to the microgauss strength observed in galaxies today. RM experiments with the SKA toward very high redshift sources (gamma-ray bursts, radio galaxies) might provide evidence for such fields. With the advent of projects such as *SWIFT* and LOFAR, it is virtually certain that the sample of such high redshift sources will soon greatly expand. With the high sensitivity of the SKA, linear polarization and Faraday rotation should be detectable from some of these sources.

Primordial fields induce Faraday rotation of the polarized CMB signals [17] and generate a characteristic peak in the power spectrum at small angular scales [16]. The detection needs an instrument with superb sensitivity like the SKA.

4 Conclusion

We have outlined the exciting new insights which the SKA can provide into the origin, evolution and structure of cosmic magnetic fields. The sheer weight of statistics of Faraday rotation measures which the SKA can accumulate, combined with deep polarimetric observations of individual sources, will allow us to characterise the geometry and evolution of magnetic fields in galaxies, in clusters and in the IGM from high redshifts through to the present. We may also be able to provide the first constraints on when and how the first magnetic fields in the Universe were generated. Apart from these experiments which we can conceive today, we also expect that the SKA will certainly discover new magnetic phenomena beyond what we can currently predict or even imagine.

References

1. R. Beck: Phil. Trans. R. Soc. Lond. A **358**, 777 (2000)
2. R. Beck, B.M. Gaensler: In: *Astrophysics with the Square Kilometer Array*, eds. C. Carilli & S. Rawlings, New Astronomy Reviews, astro-ph/0409368
3. R. Beck, A. Brandenburg, et al.: ARA&A **34**, 155 (1996)
4. P. Blasi, S. Burles, A.V. Olinto: ApJ **514**, L79 (1999)
5. L. Feretti, M. Johnston-Hollitt: In: *Astrophysics with the Square Kilometer Array*, eds. C. Carilli & S. Rawlings, New Astronomy Reviews, astro-ph/0409462
6. A. Fletcher, R. Beck, et al.: In: *How Does the Galaxy Work?*, eds. E.J. Alfaro et al. (Kluwer, Dordrecht 2004), 299
7. S.R. Furlanetto, A. Loeb: ApJ **556**, 619 (2001)
8. B.M. Gaensler, J.M. Dickey, et al.: ApJ **549**, 959 (2001)
9. B.M. Gaensler, R. Beck, L. Feretti: In: *Astrophysics with the Square Kilometer Array*, eds. C. Carilli & S. Rawlings, New Astronomy Reviews, astro-ph/0409100
10. F. Govoni, L. Feretti: Int. J. Mod. Phys. D, in press (2004), astro-ph/0410182
11. D. Grasso, H.R. Rubinstein: Phys. Rep. **348**, 163 (2001)
12. J.L. Han, R. Beck, E.M. Berkhuijsen: A&A **335**, 1117 (1998)
13. M. Haverkorn, P. Katgert, A.G. de Bruyn: A&A **403**, 1031 (2003)
14. C. Indrani, A.A. Deshpande: New Astronomy **4**, 33 (1998)
15. T. Kolatt: ApJ **495**, 564 (1998)
16. A. Kosowsky, T. Kahniashvili, et al.: astro-ph/0409767 (2004)
17. A. Kosowsky, A. Loeb: ApJ **469**, 1 (1996)
18. P.P. Kronberg: Rep. Prog. Phys. **57**, 325 (1994)
19. P.P. Kronberg, H. Lesch, U. Hopp: ApJ **511**, 56 (1999)
20. R. Narayan, M.V. Medvedev: ApJ **562**, L129 (2001)
21. A.L. Oren, A.M. Wolfe: ApJ **445**, 624 (1995)
22. J.J. Perry, A.M. Watson, P.P. Kronberg: ApJ **406**, 407 (1993)
23. M. Rees: *New Perspectives in Astrophysical Cosmology*, 2nd edition (Cambridge Univ. Press, Cambridge 2000)
24. M. Rees: In: *Cosmic Magnetic Fields*, ed. R. Wielebinski & R. Beck (Springer, Berlin 2005)
25. R. Stepanov, P. Frick, A. Shukurov, D. Sokoloff: A&A **391**, 361 (2002)
26. K. Subramanian, J.D. Barrow: Phys. Rev. Lett. **81**, 3575 (1998)
27. B. Uyanıker, T.L. Landecker, A.D. Gray, R. Kothes: ApJ **585**, 785 (2003)
28. H.J. Völk, A.M. Atoyan: ApJ **541**, 88 (2000)
29. G.L. Welter, J.J. Perry, P.P. Kronberg: ApJ **279**, 19 (1984)

SSF as a Manifestation of Protoobjects in the Dark Ages Epoch: Theory and Experiment

V.K. Dubrovich[1], A.T. Bajkova[2], and V.B. Khaikin[1]

[1] Special Astrophysical Observatory of RAS, St.Petersburg, Russia (1)
[2] Main Astronomical Observatory of RAS, St.Petersburg, Russia (2)

Abstract. Spectral Special Fluctuations (SSF) of CMBR temperature as manifestation of protoobjects in Dark Ages epoch are considered. Expected values of $\Delta T/T$ are $\sim 10^{-5}$–10^{-6} and the bandwidth of the lines is 0.1–3% depending on the scale of protoobjects and redshifts. Simulation of the experiment is made for MSRT (Tuorla Observatory, Finland) equipped by a 7x4 beam cryo-microbolometer array with a chopping flat and frequency multiplexer providing 7 spectral channels in each beam (88–100 GHz). Expected upper limit of $\Delta T/T$ in the experiment is $2 \cdot 10^{-5}$ with angular resolution $6'$–$7'$ that may be enough to detect large scale SSF with $l = 1200$–1500 at $z = 20$–30. Such an experiment sets upper limits of SSF in MM band and allows us to prepare future SSF observations.

Observational effects caused by primordial molecules seem to be most promising in investigating Dark Ages epoch of the Universe. In fact, SSF are manifestations of the proto-objects in Dark Ages epoch at redshifts $10 < z < 300$. We consider LiH, H_2D^+, HeH^+ as the basic molecules at high z [1,2]. The basic properties of molecules are discrete narrow lines and high efficiency of their interaction with CMBR. This leads to forming SSF of CMBR temperature due to protoobjects motion with peculiar velocities V_p relative to CMBR. As shown in [2], the cosmological molecules LiH and HeH^+ can exist at $10 < z < 200$. The interval of wavelengths for LiH spectral lines in this condition lies between 7.5 cm ($z = 100$ and $i = 1$) and 7.3 mm ($z = 10$ and $i = 1$). For HeH^+ it spreads from 1.5 cm to 1.5 mm.

First attempts of SSF observations were made in 1992 at IRAM MM radio telescope, yielding an upper limit of $\Delta T/T = 2 \cdot 10^{-3}$ at 1.3 mm [3] and in 2001 at RATAN-600, giving an upper limit of $\Delta T/T = 10^{-3}$ at 6 cm [4]. In this paper we have simulated an experiment reaching an upper limit of $\Delta T/T = 2 \cdot 10^{-5}$ for MSRT, Tuorla Observatory, Finland equipped by 7×4 beam cryo-microblometer array at 3 mm with a chopping flat and RF multiplexer providing 7 spectral channels in each beam. MSRT resolution at 88 GHz–100 GHz is $6'$–$7'$, which corresponds to $l = 1200$–1500 depending on CMBR map size and wavelength. We plan to fix MSRT central beam near North Celestial Pole (NCP) at $\delta = 86°$ to increase cosmic source passing time via the beam up to 348–402 s and to observe the strip preferably in low culmination from $\alpha = 8^h00^m$ to 16^h00^m at high Galactic latitudes. A cryo-microbolometer array at 88–100 GHz with the physical temperature of 0.3 K and expected NEP $= 1.5 \cdot 10^{-17}$ W/Hz$^{1/2}$ may give us $\sigma = 1.0$–2.0 mK s$^{1/2}$ sensitivity per beam per channel (2 GHz bandwidth) in the

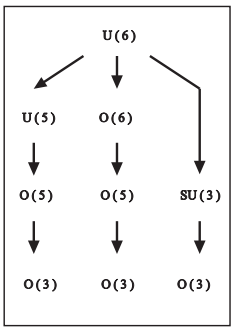


Fig. 1. Initial single frequency CMBR maps 15°x15° (128x128 pixels) (up), difference maps (down), power spectrum corresponding to ΛCDM model for initial (solid line) and differential (dashed line) CMBR maps (right)

best atmospheric conditions with $T_{atm} < 20$ K [5]. Ten to twenty identical maps are to be summed for 10-20 cold clear nights in order to reach a thermal noise level $\sigma = 30\,\mu$K in the averaged single frequency maps. We expect contribution of non thermal instrumental noise, atmosphere and foregrounds in differential maps up to $30\,\mu$K as well and the total $\sigma = 50$–$55\,\mu$K in differential maps. The special ground screen (height up to 3 m) is to be installed near the radio telescope to avoid contribution of the hot atmosphere and ground via sidelobes and scattering background.

To search for the SSF, CMBR maps obtained in neighbouring narrow spectral channels must be studied and then processed using the special difference method [6]. Our simulation includes convolution of simulated CMBR maps with a simulated radio telescope beam and obtaining differential maps. We used ΛCDM CMBR model with $\Omega_b * h^2$=0.2 ($h = H_0/100\,\mathrm{km\,s^{-1}\,Mpc^{-1}}$, $H_0 = 65\,\mathrm{km\,s^{-1}\,Mpc^{-1}}$), $\Omega_\lambda = 0.65$, $\Omega_M = 0.3$, $n = 1$, $h = 0.65$ parameters. The value of l_{max} was limited in simulation by $l = 1036$. Initial single frequency and differential CMBR maps are given in Fig. 1. The simulated CMBR maps do not include noise but it was shown in [6] that the difference method is rather stable to noise up to S/N=1.44. Most of foregrounds and systematic effects are to be significantly reduced in differential maps. The simulation shows that we can achieve $\Delta T/T = 2 \cdot 10^{-5}$ in this experiment.

References

1. V.K. Dubrovich: Astron. Lett. **3**, 66 (1977)
2. V.K. Dubrovich: A&A **324**, 27 (1997)
3. P. De Bernardis, V. Dubrovich, et al.: A&A **269**, 1 (1993).
4. I.V. Gosachinskii, V.K. Dubrovich, et al.: Astron. Rep. **46**, 7 (2002)
5. V.B. Khaikin, A. Luukanen, V.K. Dubrovich: Gravitation and Cosmology, in press (2005)
6. V.K. Dubrovich, A.T. Bajkova: Astron. Lett. **20** 9, (2003).

Cosmic Ray Astrophysics with AMS-02

E. Lanciotti[1] on behalf of the AMS collaboration

CIEMAT, Avenida Complutense 22, 28040, Madrid, Spain

Abstract. The Antimatter Magnetic Spectrometer (AMS) is a particle physics experiment designed to operate in space. AMS consists of a magnetic spectrometer, equipped with several sub-detectors which provide a very precise particle identification as well as redundant measurement of its energy, velocity and electric charge.

AMS will detect cosmic ray (CR) nuclei with an unprecedented statistics during a 3 year mission on the International Space Station (ISS). The very precise measurement of CR elements and isotopes and their energy flux will set stringent constraints on parameters of propagation models (PM).

1 Cosmic Rays and Propagation Models

CR are high energy particles of extraterrestrial origin. Their flux is isotropic and constant for all species. The flux consists mainly of ionized nuclei (of which about 90 % are protons, 10 % Helium and a small fraction of heavier nuclei) and $\sim 1\%$ of electrons. In addition to this isotropic flux, γ rays and neutrinos also contribute to the cosmic radiation.

The CR spectrum covers a very extended energy range ($10^8 - 10^{20}$ eV) and follows a power law decreasing with energy: $N(E) \propto kE^{-\gamma}$. CR of energy up to E=$10^{14}$ eV are believed to be of galactic origin, therefore the study of their production and propagation can yield crucial information about matter content and magneto-hydrodynamical properties of the Galaxy.

The aim of PMs is to provide a complete description of the production and propagation of CR from the source to the detection site. They start from a set of galactic parameters, spallation cross sections and CR spectral composition at the sources and try to reproduce some observed quantities such as the particle flux and the secondary to primary ratio. Precise measurements of these quantities are required in order to tune the PM free parameters and to improve our knowledge of galactic processes.

2 The AMS Experiment

The main structure of the AMS spectrometer [1] consists of a cylindrical superconducting magnet which bends the charged particle trajectory, a Silicon Tracker Detector (STD) which measures the particle rigidity (p/Z) with a resolution of 1.5% at 10 GeV, and a Time of Flight (TOF) system giving a velocity measurement with a 3% resolution. In addition to this, an Electromagnetic Calorimeter

and a Transition Radiation detector give an efficient hadron/lepton discrimination. Finally, the electric charge is determined by a combined measurement of the deposited energy in the TOF and STD planes and by the Cherenkov light detected in a Ring Imaging Cherenkov detector (RICH). The same RICH will also provide a very precise velocity measurement, of order of 1 per mil, for particles above its threshold. Thanks to its large acceptance and excellent particle identification AMS will reach an unprecedented sensitivity for CR measurement.

3 AMS-02 Expected Performances

The issues about antimatter and dark matter search are discussed in [2]. Here we focus on the astrophysically relevant measurements, which can be itemized in three points, as shown in Table 1:

- The precise measurements of primary spectra (p, He, C, N ... up to Fe) in the energy range 0.1 GeV/n<E<1 TeV/n will improve the precision on the injection spectra used in PMs and put constraints on the acceleration mechanism.
- The determination of the secondary flux (like Boron) and secondary to primary ratio (B/C) is related to the quantity of material crossed by CR during their propagation.
- Finally, the ratio of unstable to stable isotopes (the most relevant case: ^{10}Be/^{9}Be) is used to estimate the confinement time of CR in the galaxy. AMS will collect a huge amount of ^{10}Be and will extend significantly the energy range of isotope separation; for instance ^{10}Be identification is expected to be extended up to 10 GeV/n.

Table 1. Expected capabilities for AMS-02 after three years on the ISS.

Measurement	Statistics	Energy Range	Physics
p	10^8	>100 GeV/A	primary spectra
He	10^7	>100 GeV/A	
C	10^5	>100 GeV/A	
B	10^4	> 100 GeV/A	secondary spectra
^{3}He	10^9	0.1–10 GeV/A	
^{10}Be	10^5	1–10 GeV/A	unstable isotopes

References

1. http://ams.cern.ch/AMS/AMS.pdf by AMS Collaboration, to be submitted to NIM.
2. G. Lamanna 'Astroparticle Physics with AMS-02', *ICRC 2003, Tokyo, Japan*, ed. by Universal Academy Press, pp. 1727–1731 (2003)

Studying the Nature of Dark Energy with Current and Future Instruments

T.H. Reiprich[1,2]

[1] Department of Astronomy, University of Virginia, Charlottesville, VA 22903, USA
[2] Institute for Astrophysics, University of Bonn, D-53121 Bonn, Germany, http://www.dark-energy.net

Abstract. Understanding the nature of dark energy is one of the most important quests in modern cosmology and fundamental physics. Observations of galaxy clusters at low and high redshifts can be used to place constraints on the equation of state of dark energy and its evolution. Here, we briefly illustrate an ongoing project to constrain dark energy using state-of-the-art X-ray and optical observatories.

Low Redshift Cluster Observations: Analysis of follow-up observations of a complete, low redshift, X-ray selected galaxy cluster sample (*HIFLUGCS* [1]) with Chandra and XMM-Newton is under way. Such detailed observations are necessary because, currently, systematic effects related to an incomplete understanding of cluster physics dominate the total error budget on cosmological parameter estimates from clusters. Because of its superb angular resolution, Chandra is ideally suited to study processes in cluster centers (Fig. 1; notice, e.g., A4038's depressions, "bubbles," in the X-ray surface brightness close to the central radio source and how well the X-ray and radio emission to the west of the center seem to be aligned) and XMM-Newton, because of its high throughput and larger field of view, is used to study effects in cluster outskirts (Fig. 2).

High Redshift Cluster Observations: Figure 3 illustrates how constraints on the equation of state of dark energy, w, can be obtained. Notice how the model mass functions split up at high redshift. Chandra and XMM-Newton observations of a complete sample of distant galaxy clusters are being proposed. Total masses will, additionally, be determined through optical, weak gravitational lensing observations. Megacam, a new 36-CCD wide field camera at the MMT 6.5m telescope on Mt. Hopkins in Arizona, is being used for the weak lensing observations of the distant clusters (first run completed, second run scheduled).

In the near future, the X-ray missions ROSITA and DUO (1), XEUS and Constellation-X (2) will be vital because they will allow to construct much larger statistical distant cluster samples (1) and to study the individual distant clusters in much more detail (2), allowing to tighten dark energy constraints.

THR ackowledges support by the F.H. Levinson Fund of the Peninsula Community Foundation through a Post-Doctoral Fellowship.

References

1. T.H. Reiprich, H. Böhringer: ApJ **567**, 716 (2002)
2. T.H. Reiprich, C.L. S¡arazin, J.C. Kempner, E. Tittley: ApJ **608**, 179 (2004)

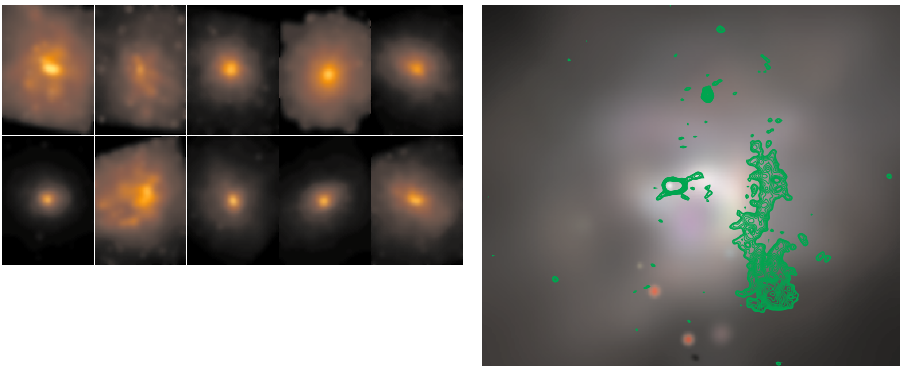


Fig. 1. (**a**) Adaptively smoothed central X-ray surface brightness distributions for ten HIFLUGCS clusters observed recently with Chandra. (**b**) Adaptively smoothed X-ray false color image of the very center of Abell 4038. Red corresponds to soft, green to intermediate, and blue to hard emission.Overlaid in green are 1.4 GHz VLA radio contours (provided by T. Clarke)

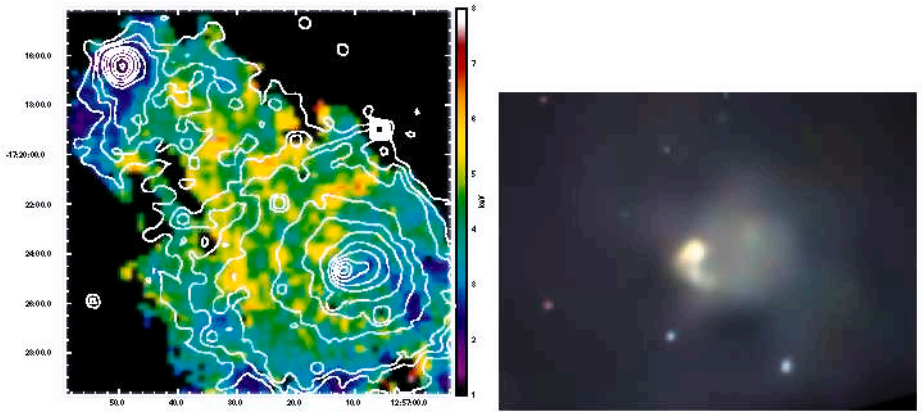


Fig. 2. (**a**) X-ray gas temperature map of Abell 1644 obtained with XMM-Newton [2]. Overlaid are X-ray surface brightness contours. Notice the two sub clusters with cool (blue) cores. The northern sub cluster appears to be leaving a trail of cooler gas behind. (**b**) Chandra false color image of the center of the southern sub cluster. One notes that the complexity of this exceptional system, apparent on large scales, continues down to the very center.

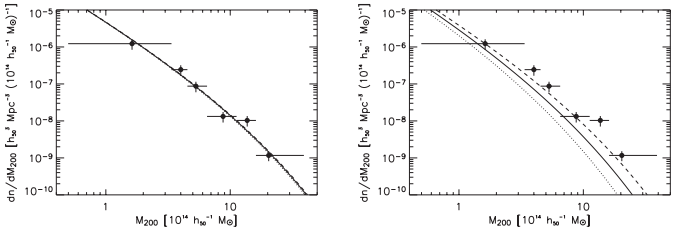


Fig. 3. Shown are galaxy cluster mass functions (number densities as functions of mass) at (**a**) low redshift ($z = 0.05$) and (**b**) high redshift ($z = 0.61$). Solid lines assume $w = -1$, dashed lines $w = -0.5$, and dotted lines $w = -1.25$.

Project ASTRAL: All-sky Space Telescope to Record Afterglow Locations

G. Tsarevsky[1,2], G. Bisnovaty-Kogan[3,7], A. Pozanenko[3], G.M. Beskin[4], S. Bondar[5], and V. Rumyantsev[6]

[1] Australia Telescope National Facility, CSIRO, PO Box 76, Epping NSW, Australia
[2] Astro Space Center, 84/32 Profsoyuznaya St, 117997 Moscow, Russia
[3] Space Research Institute, 84/32 Profsoyuznaya St, 117997 Moscow, Russia
[4] Special Astrophysical Observatory, Karachai-Cherkessia, Russia
[5] Kosmoten Observatory, Karachai-Cherkessia, Russia
[6] Crimean Astrophysical Observatory, Ukraine
[7] Joint Institute of Nuclear Researches, Dubna, Russia

Abstract. ASTRAL is a project incorporating wide-field optical telescopes on board a small satellite (FedSat or SMEX type) dedicated to the whole-sky detection of a variety of rapid astronomical phenomena, particularly optical flashes associated with gamma ray bursts (GRB). Those flashes only visible optically (so called *orphans*), as well as those which could precede associated GRBs, cannot be detected in the current triggering mode of the world wide GRB Coordinates Network (GCN). Hence ASTRAL would have a unique opportunity to trigger a follow-up multi-frequency study via GCN. ASTRAL consists of a set of 13 wide-field cameras, each with FOV $= 70^\circ$, equipped with 4096×4096 CCDs. The detection method is based on comparison of sky images with the reference image. Supernovae, novae and nova-like explosions, fast variable AGNs, flare stars, and even new comets would be promptly detected as well. Thus ASTRAL would be an original working prototype of the prospective major space mission to monitor on-line all the sky, a high priority instrument of 21st Century astrophysics. See http://www.atnf.csiro.au/people/Gregory.Tsarevsky for details.

1 Introduction

It recently became evident that the Gamma-ray burst (GRB) could appear to the observer only in optics (so called *orphan*, see [5]), or optical flash could even precede GRB [2,3]. Such optical flash associated with GRB can not be picked up by the current GRB Coordinates Network (GCN) and even forthcoming Swift mission. This way we possibly miss a clue to resolve the mystery of GRB, the most powerful and extraordinary fast exposition in the Universe.

So a problem is to build up an optical telescope which catches an optical transient (OT) and trigger other observatories in the GCN like way. It preferably should be an all-sky system, independent of the weather, day/night and light pollution, thence a space based. A probative ground-based system, which watches a FOV $= 17^\circ \times 20^\circ$ synchronously with HETE-2, was recently installed [4], but it evidently has severe restrictions mentioned above. We propose here project ASTRAL - a space system, which, being compact and cheap, provide an independent and early detection of various optical flashes on the whole sky sending an instant alert to other multiwavelength observatories including the gamma-ray ones.

2 Motivations and Scientific Objectives

MOTIVATION 1: The total number of GRBs studied optically remains small. Moreover, for the short GRBs (with T $<$ 2 s) there is no detection of optical afterglow at all. In fact, there is still only one detection - the truly spectacular optical flash detected by ROTSE - a unique detection of GRB 990123 in optical with the following characteristics: delay 22 s; initial detection: $11.7^{\rm m}$ V; Max: $8.9^{\rm m}$ V; the power law decline down to detection limit $14.3^{\rm m}$ V [1]. The detection level of GRB 990123 was chosen as a detection ability of ASTRAL).

MOTIVATION 2: If the ultrarelativistic bulk flow is a collimated jet, radiation at wavelengths longer than gamma-rays will be emitted through a larger solid angle [5]. This suggests a population of bright *orphans* - optical bursts with timescales similar to GRBs but more frequent and with no gamma-ray signature.

MOTIVATION 3: A search for optical flashes independent of GRB triggers, particularly those which could *precede* GRBs and thus would provide important diagnostics for the GRBs and their environments [2,3].

In brief, scientific objectives of ASTRAL are to monitor in the whole sky and to detect promptly a wide variety of rapid astronomical phenomena (fast transients and outbursts) that last from less than a day to as short as a second. A full list of them is in the web page indicated above.

3 Payload Description (in brief):

3.1. Detection concept: Blink Comparator Method, with well calibrated reference image, and an on-line frame processing.
3.2. Optical system design: 13 wide field cameras covering all sky (with some overlap); a *hedgehog* like design.
3.3. Optical Unit (OU):
  3.3.1. A wide-field camera with FOV = 70°.
  3.3.2. CCD unit: 4096 × 4096 matrix, 60 × 60 cm, 15 micron pixels.
3.4. Modes of observations: detection; monitoring.
3.5. Limiting magnitude: $12^{\rm m}$ in detection mode.
3.6. Timing resolution: 30 s in detection, and up to 1 s in monitoring mode.
3.7. Orbit: Elliptical with an apogee up to 40,000 km.
3.8. Stabilization/Pointing: The solar oriented 3-axis stabilization with calibrated pointing knowledge 6-10 arcsec. Re-pointing rate: Nil !
3.9. On-board computer: CPU 2Gb memory; 13 microprocessors, one per OU.
3.10. Telemetry: Uplink 4 kb/s. Downlink: alert 4 kb/s; data transfer 1 Mb/s.
3.11. Power & Weight & Cost Budget: 20 Wt &150 kg & $30 M (est. totals).

References

1. C. Akerlof, et al.: Nature **398**, 400 (1999)
2. A. Beloborodov: ApJ **565**, 808 (2001)
3. B. Paczynski: astro-ph/0108522 (2001)
4. Pozanenko A., Beskin G., Bondar S. et al. In: AIP727 *Gamma-Ray Bursts: 30 Years of Discovery*, eds E.E. Fenimore, M. Galassi, p. 757 (2004)
5. J. Rhoads: In: *Gamma-Ray Bursts*, 4th Huntsville Symp., p. 699 (1998)





Brotherhoods of the rings





Coffee break discussions

Part III

High-redshift Universe, Galaxies, Galaxy Evolution

Overview of the Science Case for a 50–100 m Extremely Large Telescope

I. Hook[1] and The OPTICON ELT Science Working Group[2]

[1] University of Oxford, Keble Road, Oxford OX1 3RH, U.K.
[2] see http://www-astro.physics.ox.ac.uk/∼imh/ELT/ for a list of participants.

Abstract. We present an overview of the science case for a 50–100 m Extremely Large Telescope. A summary of the potential performance in terms of angular resolution and depth is given. Selected science drivers are then discussed including terrestrial planets in extra-solar systems; stellar populations across the Universe; the first objects and reionization structure of the Universe. Although by no means an exhaustive list, these cases provide examples where an ELT can make a dramatic advance in our understanding of the Universe around us.

1 Expected Performance of ELTs

Current AO systems on 8-m class telescopes have recently demonstrated performance close to the theoretical diffraction limit. Figure 1 shows the diffraction limits for 8 m, 30 m and 100 m telescopes compared to the typical sizes of astronomical objects. While 8 m telescopes can resolve large regions within galaxies (between 300 and 1000 pc in size) at redshifts around unity, Extremely Large telescopes (ELTs) can, in principle, resolve structures of a few tens of pc in size (the approx size of a globular cluster) at similar redshifts.

The smaller diffraction limit combined with increased light-collecting aperture translates into great gains in sensitivity as telescope diameter is increased, particularly for point sources. This is largely because of the reduced contribution from sky noise when the size of the image is reduced. For example a 100 m ELT with perfect diffraction-limited images would reach about 8.4 magnitudes fainter for point sources than an 8 m telescope that delivers 0.5 arcsec images (for the same signal-to-noise and exposure time in the J band). In this simple scaling argument, we have assumed perfect diffraction-limited images (Strehl = 1). However, more realistic cases are also encouraging - for example the magnitude gain is decreased by only 0.5 mag for Strehl of 0.6. Even with a moderate AO correction that results in the majority of the light falling inside a 0.1 arcsec aperture, a 100 m telescope would give a gain of 4.5 magnitudes for point sources compared to an 8 m telescope producing 0.5 arcsec images.

2 Highlights from the Science Case for a 50–100 m ELT

The science case for a 50–100 m ELT has been the subject of a series of meetings held in Europe, the most recent of which was held in Marseilles in November 2003. Several key scientific themes were identified by the participants, and

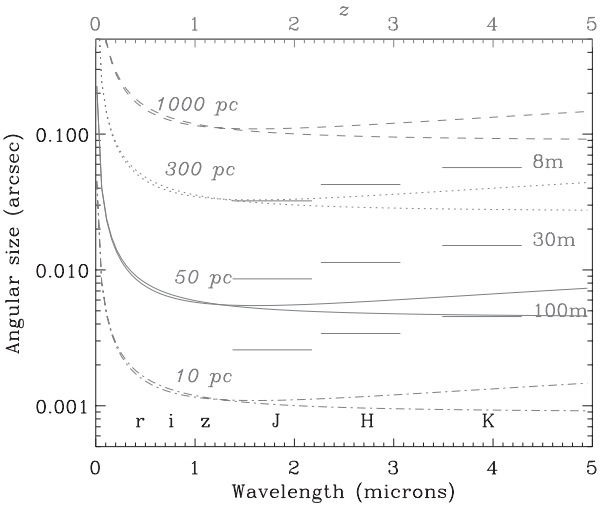


Fig. 1. The theoretical diffraction limits (λ/D) for 8m, 30m and 100 m telescopes are plotted at three wavelength values corresponding approximately to the J, H and K infrared bands (horizontal bars). Also plotted are curves of projected angular size as a function of redshift for objects of various physical sizes (10 pc, 50 pc, 300 pc and 1 kpc) for two sets of cosmological parameters : ($\Omega_{\rm m}$, Ω_Λ)=(0,0) and (0.3,0.7) for the lower and upper curves respectively.

various presentations at this meeting have described these in detail (see presentations by O. Hainaut, M. Della Valle, and M.N. Bremer). Here we give a very brief overview of some highlights from the science case for a 50–100 m ELT.

2.1 Terrestrial Planets in Extra-Solar Systems

Although over a hundred extra-solar planets are now known to exist, none has ever been imaged directly. Furthermore the inferred properties of known exoplanets are unlike those of planets in our solar system. To understand how common systems like our own are, and begin to answer fundamental questions such as "how common are the conditions required to support life?" requires finding and studying a significant sample of planets like our own.

In the next ten years, astronomers using current 8-10 m class telescopes expect to perform the first direct detections of gaseous giant planets. It is the next generation of 50–100 m ELTs, however, that will address critical issues associated with details of gas giants similar to our own Jupiter and Saturn, and, importantly, questions about terrestrial (Earth-like) planets. Only these giant telescopes will have the light collecting power and the resolution (suppression levels of up to 10^{10}) required to search many hundreds of nearby stars for the light from faint terrestrial planets.

Assuming that $\sim 1\%$ of stars may have terrestrial planets in orbits undisrupted by eccentric gas-giant companions, an ELT must be capable of searching stars as distant as 30 pc for terrestrial planets in order to produce a meaningfully large sample of detections. Ultimately, a 100 m class ELT would allow us to obtain spectra from terrestrial planets in order to examine their possible atmospheres. This will provide vital information on the habitability, and indeed the presence of biospheres, of terrestrial planets.

2.2 Formation of Stars Across the Universe

When did stars form? Current methods to measure the star-formation history of the universe often rely on measurements of ultraviolet emission from stars or optical emission lines (such as H-alpha), which are produced by only the most massive stars, larger than about 40 solar masses. However measuring the rate of supernova explosions is a direct way to determine when stars form and in what quantities, and is also sensitive to more normal-mass stars which make up the majority. Simulations show that a supernova sample measured with a 100 m class ELT could provide a direct measurement of the star formation rate up to $z \sim 10$ (see presentation by M. Della Valle).

2.3 Resolved Stellar Populations in a Representative Sample of the Universe

It is now believed likely that mergers between galaxies play an important part in the build-up of the galaxies we see today. Recent studies of individual stars in our own Milky Way galaxy have revealed populations of stars with distinct ages and composition. These are thought to be remnants of previous mergers, and give clues as to the timing of the main mergers in the Milky-Way's history. Until now these studies have been limited to our own Galaxy and its satellites but it is unknown whether these are special cases and whether the merger history is similar for all galaxy types. In particular, our own galaxy is a spiral galaxy, and no examples of large elliptical galaxies are within reach of current telescopes for this type of study.

To study a representative section of the Universe requires reaching at least the nearest large galaxy clusters which contain large elliptical galaxies, i.e. the Virgo or Fornax clusters at distances of 16 or 20 megaparsecs respectively. Individual stars at these distances appear very faint (about V=35 magnitudes) and must be individually resolved from each other in order to determine their ages and chemical composition. Simulations by P. Linde and by C. Frayn [1] demonstrate the accuracy with which 50 m and 100 m ground-based telescopes respectively are able to recover the colour magnitude diagram of individual stars observed in distant galaxies. Although a 30 m telescope could detect the main-sequence turnoff at Virgo distances for the youngest stars, to observe the main-sequence turnoff in populations of any age requires a larger, 100 m telescope.

2.4 The First Objects and the Reionization Structure of the Universe

A key goal of astrophysics is to understand how and when the first objects in the universe formed, the nature of these objects and how they contributed to ionizing and enriching the gas that pervades the Universe. The combination of results from WMAP with observations of the highest redshift quasars known today have raised the most tantalising question of how the reionization of the universe proceeded. Possibilities include two reionization epochs, the first due to the first generation of massive stars and the second from the first quasars and galaxies. Alternatively there may have been a slower, highly inhomogeneous reionization period.

The first "fairly bright" objects are not only markers of the beginning of the reionization epoch, but are also crucial for probing the inhomogeneous structure and metal enrichment of the intergalactic medium (IGM) from metal absorption lines in their spectra. The short-lived gamma-ray bursts (GRBs) are an obvious population that can be detected up to $z \sim 15$–20. Explosions of population III stars (events fainter than GRBs) can be used to probe the IGM at $z \sim 12$. Although the epoch of quasar formation is an open question, the existence of the luminous SLOAN quasars at redshifts around 6 implies that intermediate mass black holes (corresponding to quasars of intermediate luminosity) must exist up to at least redshifts of about 10. Probing the physics of the IGM at redshifts from 10 to 20 requires intermediate/high resolution spectroscopy in the near IR, which can only be carried out with telescopes of the 50–100 m class due to the predicted low fluxes of these first "background" objects.

The first galaxies compete with the first quasars for the reionization of the IGM. Although less luminous than quasars, they are far more numerous and can be directly investigated with ELTs. Candidate star-forming galaxies out to redshift about 6 have already been discovered and a few have been confirmed spectroscopically. Identical objects at z=9 and 16 would be detectable with JWST by broad-band photometric Lyman-Break techniques. However, only a 100m-class ELT can provide key diagnostics of both the inter-stellar medium and stellar populations in these galaxies by intermediate resolution spectroscopy in the near IR to $z \sim 15 - 17$ (see presentation by M.N. Bremer).

Acknowledgements

The European ELT science working group is supported by the Optical Infrared Coordination Network (OPTICON).

References

1. C. Frayn: PhD thesis, University of Cambridge, Cambridge (2003)

Distant Galaxies and Extremely Large Telescopes

M.N. Bremer[1] and M.D. Lehnert[2]

[1] H.H. Wills Physics Laboratory, University of Bristol, UK
[2] Max-Planck-Institut für extraterrestrische Physik, Garching bei München, Germany

Abstract. We review the properties of Lyman break galaxies at $z \geq 5$ and use them to explore prospects for observations of such galaxies at $z = 5, 10$ and beyond with 30-100m optical/near-IR ground-based telescopes.

1 Introduction

Driven initially by the possible discovery of Gunn-Peterson troughs in the spectra of $z > 6$ SDSS quasars [1], a large number of searches for very high redshift galaxies have taken place in the past two years in the hope of identifying the earliest generations of galaxies. Until now, two main methods have been used to identify the earliest galaxies. The first is an extension of the Lyman Break technique to redder bands ($V-$ and $R-$band dropouts identify $4 < z < 5.8$ galaxies, *e.g.*, [2,3] and $I-$band dropouts identify galaxies at $z > 5.8$, *e.g.*, [4]. The second is searching for Lyα emitters in narrow band imaging or spectroscopy (*e.g.*, [5]). This tends to identify sources with very faint continuum $M_{AB} > 27$ and large emission line equivalent widths, possibly galaxies caught in a very early starburst phase. Although important in their own right, such sources probably represent only a small fraction of the parent population of Lyman break galaxies (LBGs), and are not considered here.

In the following, we first describe the properties of $z > 5$ LBGs discovered using 8m-class telescopes and then explore how these properties shape potential observations of distant galaxies with the largest future optical/near-IR ground-based telescopes. As examples we concentrate on $V-$ and $R-$band dropouts from our work, although the properties of $I-$band dropouts studied by others are comparable.

2 Properties of $z > 5$ LBGs

2.1 Morphologies

HST imaging of $V-$dropout LBGs in the ACS GOODS [3] and UDF [6] data sets allow us to determine the range of morphologies exhibited by these galaxies. In general, these sources are resolved (in continuum at least) with half-light radii of $\sim 0.1 - 0.2$ arcsec (1-2 kpc). A significant minority of these sources appear double or triple, with several components of size 0.1-0.2 kpc separated by less

than 1 arcsec and sometimes showing tails of lower surface brightness emission between or beyond the components. In general these sources are a factor ~ 2 smaller than sources at $z \sim 3$, indicating that LBGs get smaller with increasing lookback time.

2.2 Surface Densities

In our original study [2] covering ~ 44 arcmin^2 we photometrically identified 13 R-drop LBG candidates (with $25 < I < 26.3$, $R - I > 1.5$, all magnitudes in AB). Six of these were spectroscopically confirmed as having $4.8 < z < 5.8$, the rest showed no spectroscopic evidence for any particular redshift. We have now enlarged our survey to ~ 170 arcmin^2 and analysed a further ~ 44 arcmin^2 of spectroscopy. Over the whole area we photometrically identified ~ 50 LBGs, with the new spectroscopy identifying a comparable number of $z > 4.8$ LBGs as in our original study (see [7] for an initial report). All of this points to an average source density of $\sim 0.25 - 0.3$ arcmin^{-2} for $4.8 < z < 5.8$ sources with $I < 26.3$. Douglas et al. [8] select R-drop LBGs in an analogous manner to those in [2] from ten widely-separated fields (totalling over 400 arcmin^2) and find a similar average source density, but find that this can vary by factors of ∼few on scales of 10-20 arcmin^2 in a minority of the fields

Using the HST UDF, we can select V-drop LBGs to $I > 28$ with essentially no incompleteness correction. In the ~ 11 arcmin^2 of the UDF, photometrically selecting sources with $V - I > 2$ and $26 < I < 28$, excluding point sources and those with half light radii larger than~ 0.5 arcsec we obtain a source density of ~ 2.3 arcmin^{-2}. This photometric selection identifies galaxies over a redshift range of 0.5-1 out to $z \sim 5.8$.

2.3 Line Fluxes, Luminosities and Widths

The spectroscopically-confirmed $z > 5$ LBGs in Lehnert & Bremer have Lyα line fluxes of $2 \times 10^{-18} - 2 \times 10^{-17}$ erg s^1 cm^{-2}, with luminosities between $\sim 5 \times 10^{41}$ and 10^{43} erg s^{-1}. The $I-$band magnitudes of $I \sim 26$ give absolute magnitudes of M(1700 Å)~ -20.5 to ~ -22, and lead to equivalent widths for the lines of 30-50 Å rest-frame and 2–300 Å observed. The emission lines have the characteristic shape of an outflowing wind: a sharp rise in the blue (caused by absorption by the Lyα forest) with a extended tail or "shoulder" in the red. Lines have a typical FWHM of $\sim 3 - 500$ km s^{-1}

3 Implications for 100m-class Studies

3.1 Studies of $z \sim 5 - 6$ Galaxies

The best 8m-class spectroscopy (with exposures 4-8 hrs) of $z \sim 5$ galaxies with $I_{AB} < 26$ allows us to study the shape of the Lyα line for the brightest sources and confirm the continuum break across the line. In ≥ 100 hr 8 m exposures

we could identify UV interstellar and ISM absorption lines in the most luminous sources using medium resolution spectroscopy, but with no spatial resolution (*e.g.* see the composite spectrum in [9]). HST imaging indicates that these sources are resolved on scales of 0.1-0.2 arcsec. Given the surface brightness of the objects, spectral studies of the continuum with 30–100 m telescopes could not fully exploit the diffraction limit of the telescope. However, with good adaptive correction, an IFU spectrum on a 30 m could make a 3 by 3 spatial pixel data cube in 100 hrs with sufficient signal-to-noise to trace UV absorption line dynamics. An IFU on a 100 m could split the same galaxy into 10 by 10 independent spatial pixels.

Lyα emission could be probed at even higher spatial resolution given its higher surface brightness. Given the complicated radiative transfer of this line, the morphology of the emission is likely to be clumpier than the continuum. Only the largest individual HII regions would be resolvable by a 100 m at its diffraction limit. The brightest individual HII regions found in the present-day Universe have Hα luminosities of $\sim 10^{39}$ erg s^{-1}. Optimistically assuming Case-B recombination and no dust extinction, these could have Lyα luminosities close to 1 per cent that of the $z > 5$ galaxies in [2] and therefore would be detectable by a 50–100 m telescope at the diffraction limit. Typical HII regions are two orders of magnitude fainter, and therefore cannot be individually detected. The [OII] line is redshifted into the $H-$ or $K-$band and could be a factor of 10 fainter, depending upon metallicity. Though more difficult, spatially resolved detections of the line will be possible, depending upon the exact redshift of the source.

The source density on the sky is such that in a 10 arcminute diameter field, deployable IFUs could target up to 30 such sources per unit redshift, though only about a third will have strong enough Lyα emission to trace individual star forming regions. Additionally, 30–100 m telescopes could routinely carry out redshift surveys similar to those in, *e.g.*, [2] to I =28 and 29 magnitude in a few hours per pointing. Given the source density at these levels it will be straightforward to trace the large-scale structure or cosmic web at $5 < z < 6$. The surface density of the brighter sources would seem to make relatively fine-scale tomography of intervening absorbers possible. However, these studies will be complicated by the continuum in the sources being resolved on scales of 1-2 kpc at these redshifts.

3.2 Higher Redshift Galaxies

In the absence of evolution of the luminosity function between $z = 5$ and 10, the source surface densities at $z \sim 9 - 10$ should be ~ 1 per 5-10 arcminute^2 at $J_{AB} = 27$. Multiple studies have shown that the luminosity function of LBGs evolves between $z = 3$ and $z = 6$, such that the sources are become rarer with increasing redshift, with the most luminous sources evolving fastest (*e.g.*, [2]). This is consistent with the expectations of hierarchical structure formation scenarios, the more massive (and luminous) systems form later than smaller systems. Consequently, the above extrapolated surface density is probably an upper limit on the true value.

A significant challenge for studies at $z \geq 10$ is the increase in sky brightness between the optical and near-IR bands. For example, the combined effect of the change in sky brightness and increased luminosity distance between $z = 5$ and $z = 10$ is an effective ~ 3 magnitude decrease in sensitivity for observations of the rest-frame 1200-1500 Å spectral region. The kind of extremely sensitive spatially-resolved study described above for a typical $I = 26$ galaxy at $z = 5$ would be impossible for an identically luminous source at $z = 10$. For the sources with the brightest Lyα emission, and assuming that the IGM at $z \sim 10$ is not completely opaque to the line, the morphology of the emission could be traced at a similar resolution to those of $z = 5$ galaxies.

Assuming evolution in the luminosity function does not dramatically decrease the surface density of sources, even with the increased difficulty of working in the near-IR, 50–100 m telescopes could carry out imaging and low-resolution spectroscopic surveys for z=10 sources similar in scope and fidelity to the current 8 m $z = 5$ surveys. However, such surveys will no doubt be carried out by JWST. A 50–100 m telescope should be as sensitive as JWST at low spectral resolution out to the $J-$band. Whether such surveys are worthwhile will depend on the relative timescales for JWST and 50–100 m telescope operation, the details of the evolution of the luminosity function out to $z = 10$ and the maximum field-of-view possible for the ground-based telescope, obviously the larger the better. At even higher redshift, JWST will have the advantage over ground-based telescopes at low spectral resolution because of the increasing ground-based sky brightness longward of J, apart from studies of sources or source components smaller than the diffraction limit of the ground-based telescope.

All of this assumes that the properties of $z \sim 10$ galaxies are comparable to those at $z = 5$. Given these two redshifts are only 0.5 Gyr apart, this is a reasonable assumption, although the possibility of a separate radically different UV-bright population existing at higher redshifts cannot be excluded (especially if reionization began at $z > 10$, *e.g.*, [10]).

References

1. R. Becker et al.: AJ **122**, 2850 (2001)
2. M.D. Lehnert, M.N. Bremer: ApJ **593**, 630 (2003)
3. M.N. Bremer, M.D. Lehnert, I. Waddington, M.J. Hardcastle, P.J. Boyce, S. Phillipps: MNRAS **347**, 7, (2004)
4. E. Stanway, A. Bunker, R.G. McMahon, R.S. Ellis, T. Treu, P.J. McCarthy: ApJ **607**, 704 (2004)
5. J.E. Rhoads et al.: AJ **125**, 1006 (2003)
6. M.N. Bremer, M.D. Lehnert, L. Douglas: in prep (2005)
7. M.D. Lehnert, M.N. Bremer: Messenger **115**, 27 (2004)
8. L. Douglas et al.: in prep (2005)
9. M. Ando, K. Ohta, I Iwata, C. Watanabe, N. Tamura, M Akiyama, K. Aoki: ApJ **610**, 635 (2004)
10. A. Kogut et al.: ApJS **148**, 161 (2003)

Extragalactic Science with the Allen Telescope Array

G.C. Bower

Radio Astronomy Lab, University of California, Berkeley, CA 94720, USA

Abstract. The ATA is a new radio telescope operating at centimeter wavelengths. Its wide field of view and continuous frequency coverage make it an excellent instrument for surveys of both continuum and line sources. I discuss in detail two goals of the ATA in extragalactic science: an HI counterpart to the Sloane Digital Sky Survey; and surveys for transient sources.

1 The Allen Telescope Array

The Allen Telescope Array (ATA) is a new radio telescope designed to operate at centimeter wavelengths [1]. Currently under construction at Hat Creek, CA, the ATA is the prototype of the large N-small D concept for the Square Kilometer Array. Ultimately, the ATA will rival the Very Large Array in sensitivity and will exceed by an order of magnitude its survey capability.

The basic element of the ATA is a 6.1m off-axis Gregorian antenna. This small diameter dish gives a very large field of view, 2.5 degrees at a frequency of 1.4 GHz. The ATA will achieve its sensitivity and image fidelity through the use of a large number of elements. Current plans are that we will have 32 functioning antennas by mid-2005 and ultimately 350 antennas following that. Since survey speed is proportional to ND, where N is number of elements and D is element diameter, the ATA with even 32 antennas will compare well with the 305-m single dish at Arecibo in its survey capability.

The ATA employs several other novel characteristics that will serve its scientific capabilities. The ATA feed is a log-periodic antenna that is continuously sensitive from 500 MHz to 11 GHz, permitting observations outside of the standard radio frequency bands. Additionally, the ATA digital processing system consists of multiple backends that can be used simultaneously. With this system, one astronomer can map extragalactic HI with the correlator while a pulsar observer times her favorite object and while a SETI observer searches for pulsed signals from a nearby star. In fact, the system will produce 16 phased array beams in addition to the correlator output.

We describe here two of the many science projects that the ATA will engage in. Both of these projects will have a substantial impact on the science that will be done with the Square Kilometer Array.

2 An HI Counterpart to the SDSS

The Sloane Digital Sky Survey will cover 10^4 square degrees of sky and detect normal galaxies out to a typical redshift of $z \sim 0.2$, revealing unprecedented information about the stellar content of the local universe [2]. The ATA will produce a similar survey of the neutral gas component of the local universe to a redshift $z \sim 0.2$. This survey is motivated to some extent by the discovery of HI objects that have no apparent stellar counterpart [3]. The survey is made possible by the large field of view, the broad frequency coverage and the multiple backend capability of the ATA.

An $L*$ galaxy has $2 \times 10^9\,\mathrm{M}_\odot$ of atomic hydrogen. With a channel width of 200km s^{-1} and an integration time of 4 hours, the 350-element ATA can detect at 5σ an $L*$ galaxy at $z \sim 0.16$. A full year of integration will permit coverage of 10^4 square degrees to these limits, fully complementing the SDSS.

In addition to producing the largest catalog of extragalactic HI, the ATA survey will also be an important pre-cursor to an SKA survey designed to detect all HI to $z \sim 2$ in order to constrain parameters related to dark energy. The ATA survey will give the most complete look at potential systematic issues affecting a survey of this kind.

3 Transient Radio Sources

Transients represent one of the most important understudied class of radio source. For the most part, radio transients have been studied through follow-up of high energy and optical transients. Gamma-ray burst afterglows and supernovae are clear examples of this phenomena [4]. Much of this science is quite mature.

On the other hand, blind surveys for radio transients are in their early stages. Surveys that have been conducted to this point have been limited in frequency range, time resolution, sensitivity and/or solid angle coverage so that discoveries have been limited. *The parameter space for transient discovery is almost completely unexplored.* Just below current limits, there are a number of phenomena awaiting detection (Fig. 1). These include orphan gamma-ray burst afterglows (OGRBAs) and flares from stars undergoing tidal disruption by massive black holes. Some phenomena are inherently long wavelength (such as coherent emission processes) while others are short wavelength phenomena (such as OGRBAs which produce self-absorbed synchrotron spectra). The ultimate goal, of course, is discovery of new phenomena through serendipity.

Given its powerful survey capabilities, the ATA will dramatically influence what we know about the transient sky. Surveys with a wide range of characteristics will be made. At one extreme, we hope to be able to survey $\sim 10^4$ square degrees daily at a frequency of 700 MHz to a sensitivity of ~ 1 mJy. Surveys that are sensitive to timescales of months will be powerful for finding phenomena that radiate through synchrotron self-absorption.

We have constructed a deep, small solid-angle survey using archival Very Large Array data at 5 GHz. These data consist of 20 epochs spread over 10

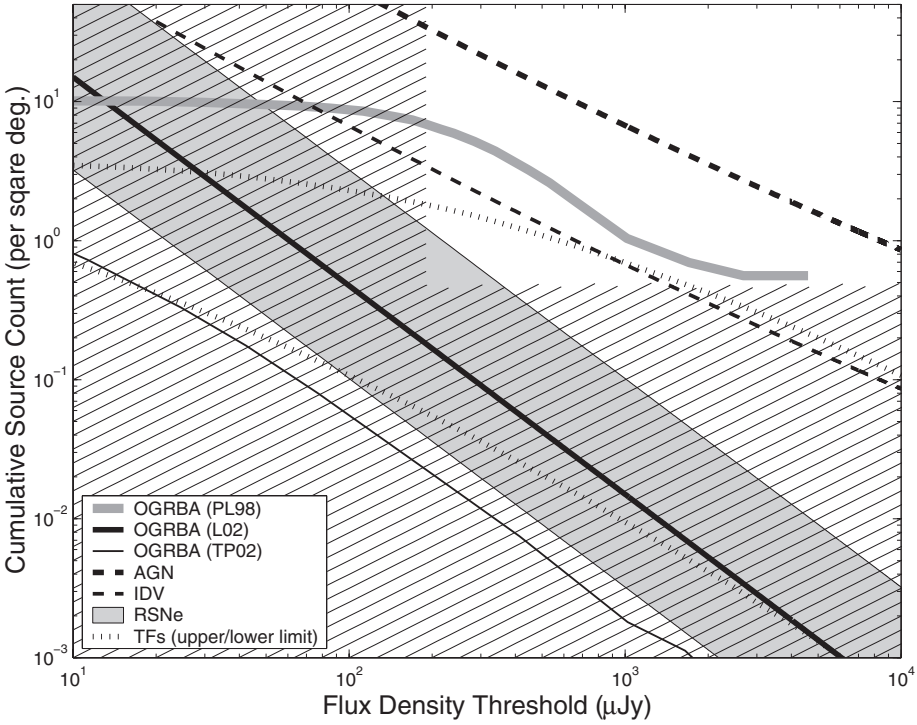


Fig. 1. Predictions for transient source counts in an extragalactic field. AGN including those showing intra-day variability (IDV) are likely to dominate the counts. The expected number of orphan gamma-ray burst afterglows (OGRBAs) is widely uncertain, as are the numbers for radio supernovae (RSNe) and tidal flare (TFs). OGRBA models are PL98 [5], L02 [6] and TP02 [7]. The unshaded area is the area of parameter space accessible to the VLA at 5 GHz with 200 hours of integration per epoch. The ATA will cover an order of magnitude more solid angle to the same flux density threshold in the same integration time

years with a typical rms of 20 μJy. We find 20 sources suitable for transient study of which one appears in only a single epoch and not in the image made from combining all epochs (Fig. 2). The source is ~ 80 μJy and is detected at 4.9σ, placing it on the edge of viability. The combined image has an rms of < 5 μJy, meaning that if the source is real, it has faded by more than a factor of 5 from its peak. There is no known optical or X-ray counterpart to this object.

4 Summary

The ATA will open new windows for extragalactic science driven primarily by the wide field of view of the telescope, the multiple backend design and the broad frequency coverage. We have outlined two of these: a 10^4 square degree

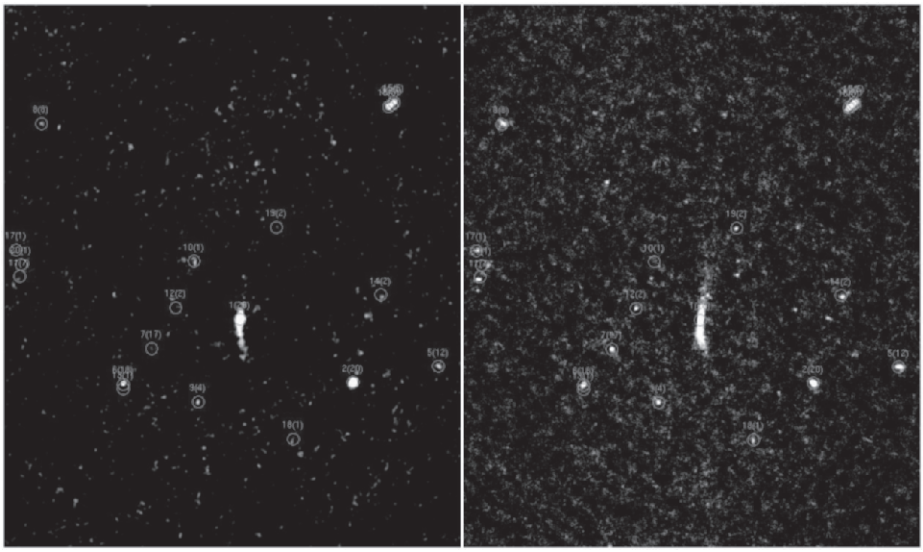


Fig. 2. VLA images of a deep field from epoch 1983 March 24 (left) and from all epochs combined (right). A potential transient source is circled in the single epoch image and labeled 10. This is the only source detected in a single epoch that does not appear in another image or in the combined image

HI survey to $z \sim 0.2$ and blind surveys for radio transients. These experiments will be pathfinders for future SKA experiments.

References

1. D. DeBoer, et al.: Proc. SPIE **5489**, in press (2004)
2. C. Stoughton, et al.: AJ **123**, 485 (2002)
3. T. Robishaw, J.D. Simon, L. Blitz: ApJL **580**, 129 (2002)
4. K.W. Weiler, N. Panagia, M.J. Montes, R.A. Sramek: ARA&A **40**, 387 (2002)
5. R. Perna, A. Loeb: ApJL **509**, 85 (1998)
6. A. Levinson, E.O. Ofek, E. Waxman, A. Gal-Yam: ApJ **576**, 923 (2002)
7. T. Totani, A. Panaitescu: ApJ **576**, 120 (2002)

Spectral Aging in the Relic Radio Galaxy B2 0924+30

L. Gregorini[1], M. Jamrozy[2], U. Klein[2], K.-H. Mack[1,2], and P. Parma[1]

[1] Istituto di Radioastronomia, Via P. Gobetti 101, I-40129 Bologna, Italy
[2] Radioastronomisches Institut der Universität Bonn, Auf dem Hügel 71, D-53121 Bonn, Germany

Relic radio sources (for the nomenclature see [1]) are extinct or dying active galactic nuclei (AGN). These sources bear importance to the understanding of radio source evolution, in particular to the late phase of exhaustion of the central energy source, the AGN. The few existing candidate sources provide the (almost) unique opportunity to estimate at least the duration of the decline of the lobe brightness, owing to the pronounced spectral steepening which they are characterized by. Another essential condition that features them is the absence of any central source and of any coherent jet structure, both of which would hint at ongoing activity and transport of energy and momentum out into the lobes.

Here we present B2 0924+30, associated with the luminous E/S0 galaxy IC 2476, which may be considered a prototypical relic galaxy (see, in Fig. 1a, the map at 49 cm madoe from a WSRT observation). The radio spectrum is investigated using integrated flux densities between 0.151 and 10.6 GHz, as well as maps at 0.325, 0.609, 1.400 and 4.750 GHz. The integral spectrum, shown in Fig. 1b, presents a pronounced steepening beyond 2 GHz: the spectral index is -0.89 between 151 and 408 MHz, while it is -2.25 between 4.75 and 10.55 GHz (defined as $S \propto \nu^{\alpha}$). The spectral index distribution across B2 0924+30, using the available maps, is rather steep. The high-frequency spectral index map (presented in Fig. 1c) shows values of -1.4 with further steepening to -1.7 around the host galaxy IC 2476 (marked in Figs. 1a and 1c by a cross). No significant asymmetry of the lobe spectrum is evident. An even more pronounced steepening of the spectrum is seen away from the major axis, where the spectrum reaches values of about -1.7. Both the integrated spectrum as well as its spectral index distribution have been analysed in order to determine the characteristic break frequency of the synchrotron emission and corresponding particle ages, assuming that synchrotron and inverse Compton losses are at work. For an obviously aged source like B2 0924+30, expansion losses can be ruled out. The lack of any central source and hot spots suggests that particle acceleration is no longer taking place. Therefore, we have excluded a model describing continuous injection and we favour the model of Jaffe & Perola [2] (hereafter JP), which allows for permanent pitch angle isotropisation. Using the SYNAGE package [3], we have performed a fit to the entire source spectrum and compute the break frequency. To derive the synchrotron age of the relic source the strength of the magnetic field, inferred from the usual equipartition arguments, is used. The best fit to the JP model (see Fig. 1b) was obtained for a break frequency of about 7.0 GHz and an injection spectral index of -0.87. Applying the equation given in [4] the

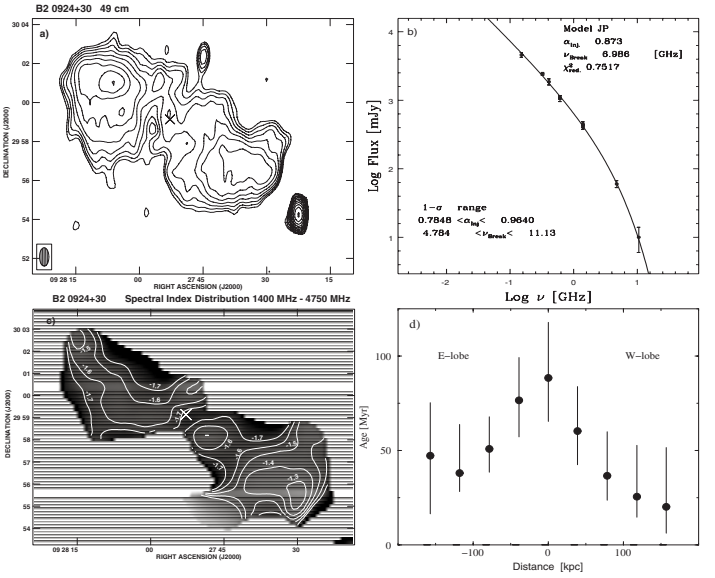


Fig. 1. a) map at 49 cm; b) integral radio spectrum; c) spectral index distribution between 1400 MHz and 4750 MHz; d) distribution of the synchrotron age measured along the source major axis

average particle age is about 54 Myrs. Using the maps at 6.3, 21, 49 and 92 cm wavelength we have determined the spectrum at different positions along the major axis of the source, and with the SYNAGE software we have obtained the following results for the JP model: i) in the central part of the source the break frequency is around 2.5 GHz, implying a particle age of about 90 Myrs; ii) away from the centre the break frequency is around 30 GHz and the particle age is about 26 Myrs (see Fig. 1d), the corresponding particle advance speed is of the order of 2000 km/s.

With the relatively low particle age since switch-off inferred from this study, aged radio sources would easily escape detection in the GHz-frequency range. It is therefore important to search for such objects in the low-frequency radio continuum surveys. In the not too far future, the Low Frequency Array (LOFAR [5]) will provide the tool to search for exhausted radio galaxies and quasars, thus gaining a more complete census of AGN in the universe.

References

1. J.C. Kempner et al.: In http://www.astro.virginia.edu/coolflow (2003)
2. W.J. Jaffe, G.C. Perola: A&A **26**, 423 (1973)
3. M. Murgia: Laurea Thesis, University of Bologna, Bologna (1996)
4. P. Alexander, J.P. Leahy: MNRAS **255**, 1 (1987)
5. H. Röttgering: New Astron. Rev. **47**, 405 (2003)

Extragalactic Sources with Extended Radio Emission

M. Jamrozy[1], U. Klein[1], and K.-H. Mack[2,1]

[1] Radioastronomisches Institut der Universität Bonn, Auf dem Hügel 71, D-53121 Bonn, Germany
[2] Istituto di Radioastronomia, Via P. Gobetti 101, I-40129 Bologna, Italy

1 Giant Radio Galaxies

Galaxies (and quasars) hosting active galactic nuclei (AGN) are usually powerful radio sources which produce jets and extended radio emitting regions (lobes) of plasma. There is a huge range from less than 100 pc up to few Mpc in linear extent of the radio galaxies (RGs). RGs with sizes over more than one Mpc represent the biggest single objects in the Universe. The most extreme of those is 3C236 which has a projected linear size of 4.2 Mpc ($H_0 = 71$ km s^{-1} Mpc^{-1}, $\Omega = 1$). Another example of a giant radio galaxy (GRG) B0503-286 is shown in Fig. 1. The very large angular sizes (up to several dozens of arcminutes) of GRGs on the sky give an excellent opportunity to study the nature of AGNs and provide important constraints on the evolution of galaxies. Because of their sizes and luminosities GRGs have significant influence on the intergalactic medium (IGM). The total energy delivered into the IGM by the twin jets of a GRG is about 10^{54} J, which is a significant fraction of the gravitational energy released during the formation of a supermassive black hole in the centre of an AGN's parent galaxy. On the other hand, GRGs possess low equipartition magnetic field strengths and energy densities of their cocoons. This matches the statement of Colgate & Li [1] who affirm that for most radio sources located in a low-density environment only a small fraction of the magnetic energy is dissipated in the form of synchrotron radiation while the bulk of the magnetic energy is deposited in the walls and voids of the Universe. Kronberg et al. [2] suggest that the magnetic energy which originates from AGN outflows and which is stored in the intergalactic magnetic field has a major influence on the evolution of galaxies and visible structure formation on scales of up to $\sim$1 Mpc.

2 Necessity of Low-Frequency Radio Observations

Although significant progress has been made in our understanding of the evolution of radio sources, it is not clear yet what conditions lead to the formation of a GRG. The possibilities discussed in the literature include a low-density IGM and higher ages. Because GRGs possess steep radio spectra and a low surface brightness only a small fraction of the expected faint GRGs have been detected and mapped at high (> 1 GHz) radio frequencies so far. Candidates for new GRGs are usually selected by apparent angular separation between the brightest regions (hot spots) of a radio source (e.g., [3]). However, objects with relatively

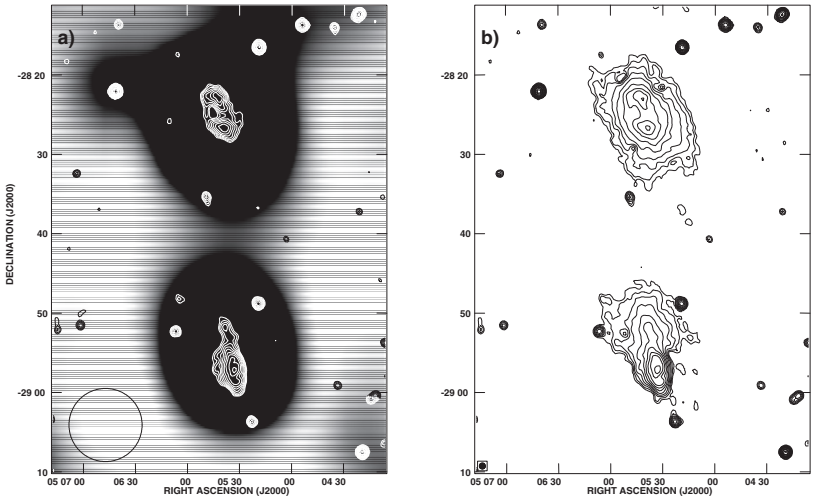


Fig. 1. 1.4-GHz total intensity images of the 1.8 Mpc GRG B0503-286. (**a**) Contours are taken from the VLA survey [4] and the gray-scales are the Effelsberg 100-m antenna measurements. (**b**) Contours of the combined single-dish and interferometer data which are shown in the left panel. In both panels, the contour levels are separated by a factor of $\sqrt{2}$ and the lowest contours are drawn at 1.95 mJy/beam. The beam sizes of the Effelsberg antenna and the VLA are marked by the circles in the lower left corners of each panel.

faint hot spots and without radio emission (radio bridge) between them are very hard to recognise in high-frequency maps. The still limited number of known ($\sim$ 130) and well-studied GRGs is a reason for the existence of a gap in the picture of RGs evolution and the phenomenon of GRGs is still open for further research. Therefore it is important to search for GRGs in low-frequency continuum radio surveys with high sensitivity and angular resolution. The proposed Low-Frequency Array (LOFAR) and the Square Kilometre Array (SKA) will be excellent tools to investigate GRGs.

Acknowledgements

MJ acknowledges the Deutsche Forschungsgemeinschaft for the award of a postdoctoral fellowship (GRK 787).

References

1. S.A. Colgate, H. Li, 'The Magnetic Fields of the Universe and Their Origin'. In: *Highly Energetic Physical Processes and Mechanisms for Emission from Astrophysical Plasmas, IAU Symposium 195*, ed. by P.C.H. Martens, S. Tsuruta, M.A. Weber (Astronomical Society of the Pacific, San Francisco 2000) pp.255–264
2. P.P. Kronberg, Q.W. Dufton, H. Li, S.A. Colgate: ApJ **560**, 178 (2001)
3. J. Machalski, M. Jamrozy, S. Zola: A&A **371**, 445 (2001)
4. J.J Condon, W.D. Cotton, E.W. Greisen, Q.F. Yin, et al.: AJ **115**, 1693 (1998)

The B3 VLA Sample at Low Frequencies: Results from a Survey at 74 MHz

K.-H. Mack[1,2], M. Vigotti[1], L. Gregorini[1], U. Klein[2], W. Tschager[3], R.T. Schilizzi[4,3], and I.A.G. Snellen[5]

[1] Istituto di Radioastronomia del CNR, Via P. Gobetti 101, I-40129 Bologna, Italy
[2] Radioastronomisches Institut der Universität Bonn, Auf dem Hügel 71, D-53121 Bonn, Germany
[3] Sterrewacht Leiden, PO Box 9513, NL-2300 RA Leiden, The Netherlands
[4] Int. SKA Project Office, Postbus 2, NL-7990 AA Dwingeloo, The Netherlands
[5] Institute for Astronomy, Royal Observatory, Blackford Hill, Edinburgh, EH9 3HJ, United Kingdom

The low-frequency (< 150 MHz) region is among the most poorly explored of the entire radio spectrum despite the many unique astrophysical questions that can be addressed with observations in these bands. In the framework of our on-going study of the radio continuum spectra of the B3 VLA survey we have used observations of Tschager et al. [1] obtained with the VLA in A-array at 74 MHz to extend our database towards lower frequencies – with a resolution of about a factor of 3 higher than the upcoming VLA Low-frequency Sky Survey (VLSS, [2]). For about a third of the sample (~ 360 radio sources) we have now 6 or more measurements in the range between 74 MHz and 10.5 GHz. This unique frequency coverage allows consistency checks of the new 74 MHz flux densities and provides the comparison data to test the influence of various observational effects at such low frequencies. We have performed a spectral analysis to determine particular features like low-frequency turn-overs caused by synchrotron self-absorption or free-free absorption. Some radio sources show extended and complex morphologies not seen at higher frequencies, indicating the presence of diffuse structures with very steep spectra. Our project is an example of a typical application of the future LOFAR telescope in the field of source evolution.

The observations were done with the VLA in its A-array at six pointings between $08^{\rm h} < \mathrm{RA} < 17^{\rm h}$ and $37° < \mathrm{DEC} < 43°$. The formal beam size is $24''$. Starting from the calibrated radio maps we have used AIPS tasks IMFIT and TVSTAT to obtain the integrated flux densities at the positions of the B3 VLA sources up to a distance from the phase centre of 11° (i.e. at a primary beam attenuation of 70%). Taking into account that Tschager et al. have found a significant decrease of the source density at distances larger than 3° from the phase centre we have performed several tests to assure the quality of the extracted flux densities. We managed to diminish the calibration error to some 18% across the entire primary beam area, although the ionosphere still causes considerable artifacts. In this way, flux densities for 297 and upper limits for 68 sources were obtained. The well-known spectral shape of the B3 VLA sources allowed us to extrapolate the 74 MHz flux densities and to evaluate its deviation of the measured value.

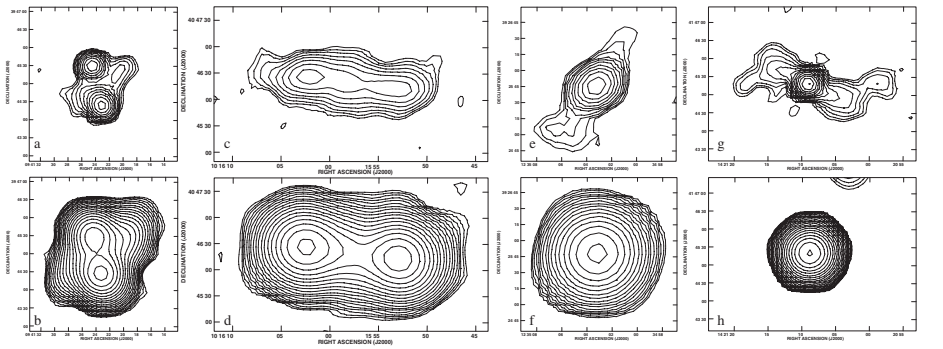


Fig. 1. a) B3 0938+399B at 74 MHz: levels: 65 mJy $\times 2^{\frac{n}{2}}$; b) B3 0938+399B at 1.4 GHz (NVSS): levels: 0.56 mJy $\times 2^{\frac{n}{2}}$; c) B3 1013+410 at 74 MHz: levels: 60 mJy $\times 2^{\frac{n}{2}}$; d) B3 1013+410 at 1.4 GHz (NVSS): levels: 0.39 $\times 2^{\frac{n}{2}}$; e) B3 1232+397B at 74 MHz: levels: 71 mJy $\times 2^{\frac{n}{2}}$; f) B3 1232+397B at 1.4 GHz (NVSS): levels: 0.50 mJy $\times 2^{\frac{n}{2}}$; g)B3 1419+419 at 74 MHz: levels: 90 mJy $\times 2^{\frac{n}{2}}$; B3 1419+419 at 1.4 GHz (NVSS): levels: 0.11 mJy$\times 2^{\frac{n}{2}}$

A visual inspection of the images revealed 19 sources with significantly extended morphology, of which we show four examples, together with the corresponding NVSS images.

In the X-shaped source B3 0938+399B the presumed relic emission of the secondary lobe system is still well visible. B3 1013+410 shows an increased core-lobe emission ratio (compared to the 1.4-GHz data) which implies a steep spectrum, indicative of a complex interior structure. The sources B3 1232+397B and B3 1419+419 – compact at 1.4 GHz – disclose extended diffuse emission which could be explained as remainders of a previous activity period. B3 1419+419 (3C 299) has been classified as a Compact Steep Spectrum source by various authors.

We have identified a number of sources exhibiting extended emission, which in some cases is not seen at higher frequencies. It is here that the potential power of low-frequency radio astronomy is revealed: future observations with LOFAR will bring a rich harvest of diffuse, extended radio continuum structures not visible at cm wavelengths. This implies that we are dealing with aged synchrotron emitters, such as quenched radio galaxies or relics. However, it must be pointed out that the detection of diffuse low-frequency radio continuum structures requires excellent imaging which clearly necessitates new calibration and imaging strategies.

References

1. W. Tschager, R.T. Schilizzi, H.J.A. Röttgering, I.A.G. Snellen, G.K. Miley, R.A. Perley: A&A **402**, 171 (2003)
2. R.A. Perley, N.E. Kassim: *VLSS: The VLA Low-frequency Sky Survey*, URL: http://lwa.nrl.navy.mil/VLSS/

Modeling the Faint Radio Population: The NanoJY Radio Sky

I. Prandoni[1], H.R. de Ruiter[2], and P. Parma[1]

[1] Istituto di Radioastronomia - INAF - Bologna, Italy
[2] Osservatorio Astronomico di Bologna - INAF - Bologna, Italy

Abstract. The apparent change in the composition of the parent optical objects of radio sources around 1 mJy (at 1.4 GHz) is now well established, although there is still some debate about the relative importance of classical radio galaxies and star-forming galaxies at sub-mJy levels (see e.g. Gruppioni et al. 1999, MNRAS, 304, 199; Prandoni et al. 2001, A&A, 369, 787). It is clear, however, that at μJy levels star-forming galaxies are dominant (see Fomalont et al. 1997, ApJ, 475, L5; Haarsma et al. 2000, ApJ, 544, 641).

Does this mean that SKA will basically tell us more about the history of star formation than about the space density (and its cosmological evolution) of active galactic nuclei?

Using current best estimates of luminosity functions (and their evolution) of various classes of objects, we show that the increasing dominance of star-forming galaxies below 1 mJy is a natural consequence of the different luminosity functions, but that this does not at all mean that star-forming galaxies do necessarily dominate at all sub-mJy flux levels and all redshifts.

1 Models and Comparison Samples

In order to have an idea on the types of objects we can expect at flux levels accessible with SKA we have modeled the main classes of sources detected at mJy and sub-mJy levels: steep AGNs (Radio Galaxies) modeled following Dunlop & Peacock (1990, MNRAS, 247, 19); flat AGNs (Sy1 and QSO), for which we have assumed the quasar optical LF and evolution (Boyle et al 1988, MNRAS, 235, 935; 1991, ASP Conf. Ser. 21, p. 191; Schmidt et al 1995, AJ, 109, 473); the star-forming galaxies (RLF from Sadler et al 2002, MNRAS, 329, 227) composed by a fraction (assumed 50%) of non-evolving normal spirals and a fraction (50%) of evolving starburst galaxies ($L \sim (1+z)^3$). Passive optical evolution has been assumed whenever necessary (Poggianti 1997, A&AS, 122, 399).

A number of available surveys at the mJy, sub-mJy and μJy level can provide important boundary conditions to any modelling of the radio sky. The radio counts are constrained by using all the samples available in the literature, while we focused on samples with optical spectroscopy follow-up to get constraints on the redshift and magnitude distributions of the sources. In particular we refer to the following samples: FIRST (Magliocchetti et al. 2000, MNRAS, 318, 1047), ATESP-EIS (Prandoni et al. 2001), PDF (Phoenix Deep Field, Georgakakis et al. 1999, MNRAS, 306, 708), MF (Marano Field, Gruppioni et al. 1999), B93 (sample collection studied by Benn et al. 1993, MNRAS, 263, 98), H00 (collection studied by Haarsma et al. 2000).

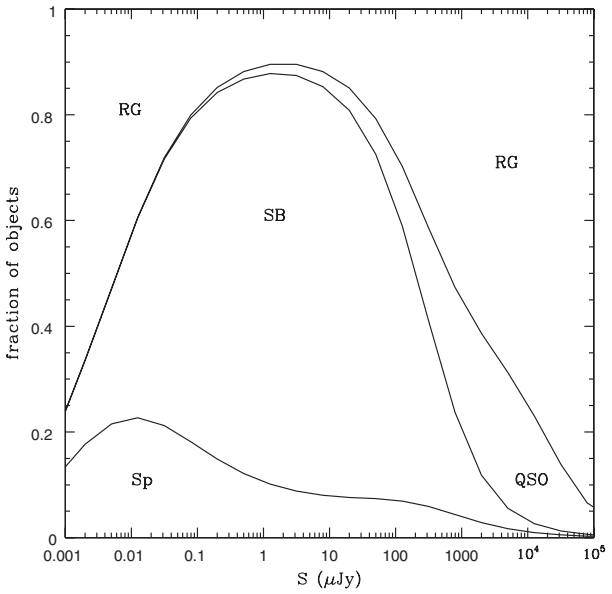


Fig. 1. Summed contribution of different kinds of sources as a function of flux. Regions separated by solid lines correspond to: steep-spectrum sources (RG), flat-spectrum sources (QSO), normal non-evolving spirals (Sp) and starbursts (SB).

The models used here provide a good fit to the observed number counts along the entire flux range spanned by the counts (40 μJy – 1 Jy) and can reproduce the total number of sources in the comparison samples within a factor of 2. The models can trace with good accuracy both the magnitude and the redshift distributions of the sources in the given samples.

2 The Composition of the Nanojy Radio Sky

The models above have been used to simulate the radio sky at fainter flux levels than reached by the current surveys. The composition of the radio sky changes with flux as shown in Figure 1. The figure clearly shows that radio galaxies, which dominate (together with QSO) the mJy population, reappear in large proportions going to nanoJy levels ($> 50\%$ at $S < 10$ nJy)!

On the other hand, starburst galaxies and their evolution can be suitably studied with less sensitive surveys (e.g. $S > 10 - 100$ nJy). The other main population at nanoJy level is represented by non-evolving spirals, whose contribution shows a bump (mainly due to $z > 1$ galaxies) in the range $1 < S < 100$ nJy.

This work demonstrates that nuclear activity could be important at nanoJy flux levels. Deeper data are strongly needed to better constrain the models and provide more reliable simulations. This kind of analysis can provide very useful constraints to the design of SKA.

Radio View of Merging Clusters of Galaxies

T. Venturi[1], S. Bardelli[2], D. Dallacasa[3], S. Giacintucci[2], P. Rao[4], and E. Zucca[2]

[1] IRA–CNR, Via Gobetti 101, 40129 Bologna, Italy
[2] INAF–Bo, Via Ranzani 1, 40127 Bologna, Italy
[3] Astronomy Department, Bologna University, Via Ranzani 1, 40127 Bologna, Italy
[4] NCRA, Pune University Campus, Pune, India

Abstract. We present radio observations at 610 MHz, 330 MHz and 235 MHz, carried out with the Giant Metrewave Radio Telescope (GMRT, Pune, India) of three clusters of galaxies at different merging stages. The purpose of our work is to investigate the connection between cluster merger parameters (i.e. masses, ages, impact parameter) and the formation of radio halos and relic sources.

1 Scientific Background

The radio emission is one of the distinctive features of clusters of galaxies, together with the thermal X–ray emission from the intergalactic gas. It may be associated with individual cluster galaxies, and with the cluster as a whole, in the form of radio halos and relics [4]. There is now widely accepted evidence in favour of the connection between the presence of radio halos and relics, and the cluster connection and evolution via *cluster mergers* [1]. However, while all clusters containing a radio halo and/or relic show evidence of a merger event, not all merging clusters host a halo/relic source. In this paper we will briefly show three different cases of merging clusters, with different properties with respect to the existence of extended cluster radio emission.

2 GMRT Radio Observations

We observed the three merging clusters A2061, A3528 and A3562 with the Giant Metrewave Radio Telescope, in the frequency range 1.4 GHz - 235 MHz.The sensitivity (1σ level) of our images ranges between 0.1 and 0.5 mJy/beam.

2.1 A2061

This cluster (z=0.0784) shows a bimodal distribution of the X–ray emission and it is most likely an early merger. It hosts a peripheral radio source, first spotted on the WENSS and NVSS [5]. Our very sensitive GMRT observations confirm the existence of this relic, located at the border of the X–ray emission and perpendicular to it [6] (see Fig. 1).

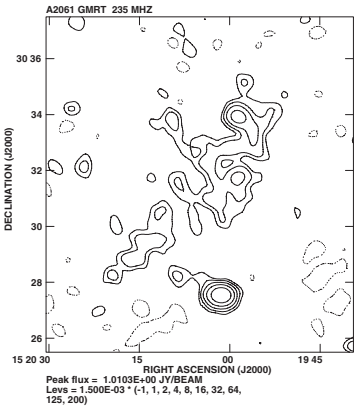


Fig. 1. 235 MHz GMRT image of the peripheral relic in A2061. The resolution is 34.2×29.2 asec^2.The lowest contour is 1.5 mJy/beam.

2.2 A3528

This cluster (z=0.053) has a bimodal X–ray emission and it is located in the central region of the Shapley Concentration. It is now believed to be the result of an off–axis post–merger event [2]. It hosts an impressive number (five) of extended radio galaxies with double and/or distorted morphology, but there is no evidence of radio halo/relic to the sensitivity level of $\sim 100\mu$Jy/b.

2.3 A3562

This cluster (z=0.048) is located in the A3558 cluster complex, at the centre of the Shapley Concentration. A wealth of data over many bands supports the idea that it is a violent on–axis advanced merger. The cluster hosts a small and faint radio halo [7], whose observed properties are consistent with the idea that it is just being formed [3].

References

1. G. Brunetti: In: *Outskirts of Galaxy Clusters: intense life in the suburbs*, IAU Coll. 195, ed. A. Diaferio, in press (astro–ph/0404507)
2. F. Gastaldello, S. Ettori, S. Molendi et al.: 2003, A&A 411, 21
3. S. Giacintucci, T. Venturi, S. Bardelli, et al.: In: *Outskirts of Galaxy Clusters: intense life in the suburbs*, IAU Coll. 195, ed. A. Diaferio, 2004, in press (astro–ph/0404498)
4. G. Giovannini, L. Feretti: in *Merging Processes in Clusters of Galaxies*, ed. by L. Feretti, I.M. Gioia, G. Giovannini, (Kluwer, Dordrecht 2002) ASSL, Vol. 272, p. 197
5. J.C. Kempner, C.L. Sarazin: ApJ **548**, 639 (2001)
6. E. Marini, S. Bardelli, E. Zucca, et al.: MNRAS, in press (astro–ph/0406538)
7. T. Venturi, S. Bardelli, D. Dallacasa, et al.: A&A **402**, 913 (2003)





Setting the stage for the conference dinner





Proceeding with the ceremony

Part IV

AGN and Compact Objects

Active Galactic Nuclei at the Crossroads of Astrophysics

A. Lobanov and J.A. Zensus

Max-Planck-Institut für Radioastronomie, Auf dem Hügel 69, 53121 Bonn, Germany

Abstract. Over the last five decades, AGN studies have produced a number of spectacular examples of synergies and multifaceted approaches in astrophysics. The field of AGN research now spans the entire spectral range and covers more than twelve orders of magnitude in the spatial and temporal domains. The next generation of astrophysical facilities will open up new possibilities for AGN studies, especially in the areas of high-resolution and high-fidelity imaging and spectroscopy of nuclear regions in the X-ray, optical, and radio bands. These studies will address in detail a number of critical issues in AGN research such as processes in the immediate vicinity of supermassive black holes, physical conditions of broad-line and narrow-line regions, formation and evolution of accretion disks and relativistic outflows, and the connection between nuclear activity and galaxy evolution.

1 Nuclear Activity in Galaxies

Recent years have witnessed substantial progress in studies of active galactic nuclei (AGN). Activity is observed in galaxies throughout the entire range of the electromagnetic spectrum [35]. It is manifested on spatial and temporal scales that span over 12 orders of magnitude, ranging from several Schwarzschild radii to megaparsecs and from minutes to millions of years [141]. On the surface, the activity of galactic nuclei comes in many faces, outlined by the uncomfortably large number of the AGN classes — yet the underlying mechanism and physical conditions in the nuclear regions of all galaxies are probably more similar than may appear at first glance [4,53,178]. Last but not least, AGN are now detected at redshifts of 6 and beyond [40], and they may be closely connected to the formation and evolution of the large-scale structure [124] and to the epoch of reionization of the Universe [39,113,151].

There is growing acceptance of ubiquity of the nuclear activity in galaxies and its connection to the presence of supermassive black holes (SMBH) in the centres of all massive galaxies [3,57,74,75]. Observations in the infrared [52] and sub-millimetre bands [124] indicate that almost every galaxy exhibits certain characteristics previously thought to be related only to a much narrower class of powerful AGN. This implies that virtually all massive galaxies may go through a strong AGN phase in the course of their cosmological evolution. Historically, observational studies of AGN have been concentrated largely within six broadly defined areas.

1. Surveys have been used effectively, first in the optical and radio domains and later throughout much of the electromagnetic spectrum, to find correlations

between different types of AGN and to trace their cosmological evolution. The databases provided by the ROSAT, IRAS, ISO, SIRTF and VLA (FIRST [7] and NVSS [21]) surveys have become the true cornerstones of AGN research, as well as the HST and Chandra deep field observations. These efforts will be taken further by the ongoing SDSS survey [1] and the Spitzer surveys [41]. The Spitzer data have already yielded a fundamental result on the obscuration in AGN, indicating that as much as three quarters of all AGN are likely to be obscured at all redshifts [176], which implies that the number of active galaxies may be much higher than was thought. AGN studies in the next decade will also benefit from multi-wavelength surveys such as the great observatories origins deep survey (GOODS [56]) which addresses AGN structure and demographics [66], unification scheme and and AGN–SMBH co-evolution [53,176]. A number of ground and space VLBI surveys undertaken in the radio in the centimetre [43,47,70,72,88,98,137,143,168–170,186] and millimetre [109,110,149] domains have revealed a wealth of information about morphology [76,94,193], kinematics [87] and evolution of radio-emitting material in the nuclear regions and relativistic outflows in AGN on scales down to fractions of a parsec. VLBI surveys have also been used effectively for addressing a variety of general astrophysical problems including AGN evolution [161] and population modelling [97,100], jet formation [109], fundamental astrophysical emission processes [86,99], and cosmology [60].

2. Morphological studies of AGN have been done extensively in the radio [84,136], optical [139] and X-ray regimes [118,119], recovering large-scale structures produced by AGN. Circumnuclear disks and tori have been revealed conclusively in recent optical, near-infrared and radio observations [79,91,128,183] (Fig. 1). Most spectacularly, recent X-ray images obtained with Chandra have shown the shocks and ripples in the intergalactic medium excited by the central engine in NGC 1275 [38].

3. Variability studies of long- and short-term changes of continuum and line emission have enabled detailed investigations of non-stationary processes in the immediate vicinity of the SMBH and understanding better the physics of nuclear regions of AGN [174]. Timescales probed by these studies range from hours to several decades [2,6,141,159,165,181,194]. The variable continuum flux is believed to be responsible for ionizing the cloud material in the broad-line region (BLR). Optical spectral line and continuum variability data have been combined to model the BLR [83,141,142], which provided a reliable method for estimating the mass of the central black holes in a number of AGN [141]. In radio-quiet AGN, short-term variations of the continuum X-ray emission [5,14] are most likely connected with processes occurring the accretion disk at distances of $\sim$ 10–100 $R_{\rm g}$ ($R_{\rm g} = G\,M_{\rm bh}/c^2$ is the gravitational radius for a black hole of mass $M_{\rm bh}$, where G is the Newtonian gravitational constant) from the black hole [130]. This conclusion is contested by multi-wavelength monitoring observations [24,141] showing no apparent time delay between flux variations in the ultraviolet (UV) and optical continua, which indicates that instabilities in the accretion disk or random fluctuation in the accretion rate alone cannot explain

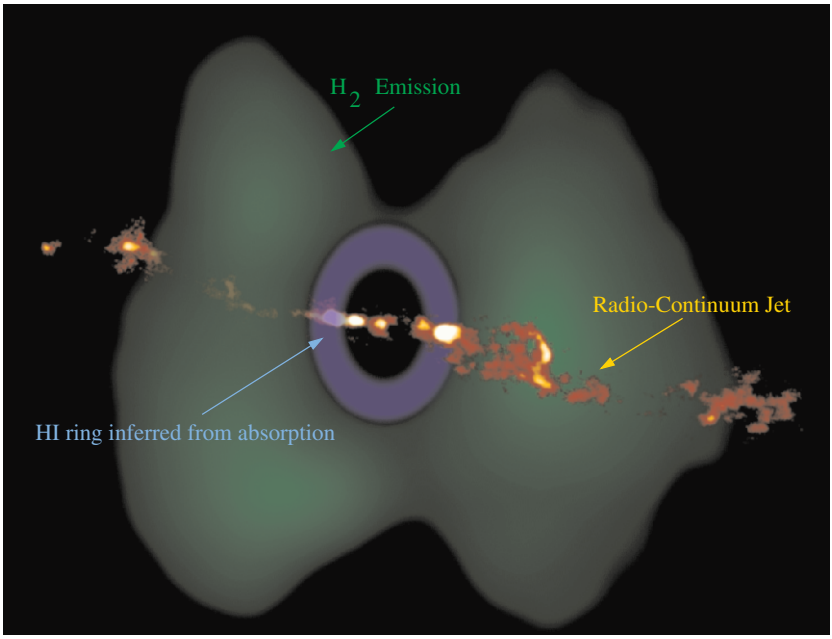


Fig. 1. Montage of the inner 250 pc of NGC 4151. The H_2 emission traces a torus, the H I absorption comes from a ring inside the torus. Ionized gas (black) is assumed to fill the torus inside the H I ring [128].

the continuum variability [141]. In radio-loud AGN, continuum emission from the relativistic plasma in the jet dominates at all energies [175,185], swamping the X-ray emission associated with the accretion flow. Hence, the continuum variability in radio-loud AGN may be related to both the jet and the instabilities of accretion flows [130,175] near the central engine.

Long-term variability of X-ray [119,126,160] and radio emission [2] probably reflects instabilities developing in the disk [105] and shocks propagating in the relativistic jet [45]. Ejections of new jet components have been reported to occur after minima in the X-ray light curve [119], suggesting that the jet is fed by the material falling onto the black hole from inner radii of the accretion disk. No observational evidence has been reported so far for a link between optical/UV continuum variability and the compact radio jet.

Intraday variations observed in the radio [95,180], optical [67], IR [59], and X-ray domains [5] most likely reflect processes in the immediate vicinity of the central engine and in internal shocks developing in relativistic outflows [156,162,163]. In this respect, intraday variability in AGN may be similar to quasi-periodic oscillations observed in Galactic X-ray binaries. Interstellar scintillations are also likely to play a role in the intraday variations observed in the radio regime [10,150].

4. Multifrequency campaigns, albeit proven difficult to organize, have yielded accurate broad-band spectra of AGN [116,172] and have enabled detailed in-

vestigations of physical processes governing the production of the non-thermal continuum emission from circumnuclear regions in AGN [64,173]. Multifrequency data were used to determine the spectral energy distribution in AGN in the quiescent and flaring stages [48,121,158] and to characterize the properties of the synchrotron emission in relativistic outflows [26,102].

5. Spectroscopic studies in the optical [8,58,120,184] infrared [111] radio [104], and increasingly also in the X-ray domain [34,37,115,131,132,135,157,167,187] have provided measurements of the gas and stellar kinematics near the central black hole [189], in the broad and narrow line regions of galactic nuclei. These studies will be greatly enhanced with the systematic spectroscopy provided by the SDSS data and with the high-energy spectroscopy data from the existing and planned X-ray missions.

6. Dedicated monitoring programs have been employed successfully virtually in all observational domains to study in detail the dynamics and physical conditions in the nuclear regions of a number of prominent AGN. Structure of the nuclear regions has been imaged extensively with high resolution radio interferometry, uncovering the evolution of radio emitting plasma on linear scales from $\approx 100R_{\rm g}$ [80,96] to $\approx 1\,{\rm kpc}$ [182,191,192]. Radio monitoring programs are now reaching timescales of several decades [22,106,105]. Radio frequency observations of maser emission have been used to probe the presence of accretion disks [71,127] and molecular tori [90] around putative black holes in the centres of AGN. Extragalactic maser emission has provided direct evidence of interaction between the dense molecular material and the ionization cones [50] or nuclear jets [20,138]. Properties of relativistic outflows have been connected to the physical conditions in the nuclear regions [81,101] and used for identifying possible binary systems of SMBH in AGN [19,105,152].

High-resolution radio observations of Seyfert galaxies have offered an opportunity to study the optical emission from the immediate vicinity of the central engine of AGN, on scales comparable to the largest extent of the BLR. Optical observations of broad emission lines have been instrumental for understanding the structure and dynamics of the circumnuclear gas, and they have yielded an attractive concept of a disk-like morphology of the BLR [146]. The detection and modelling of several double-peaked Balmer lines has further supported this idea. In most cases, the double-peaked emission lines can be explained with line emission that originates in the disk [33]. There are, however, two very notable exceptions among the radio-quiet AGN. The core of the broad double-peaked emission lines in RX J1042+1212 [148] and Ark 120 [145] is most likely to originate from an outflow-related component of the BLR (Fig. 2). It is possible that this component is indeed related to an interaction between the relativistically moving plasma and high-velocity clouds situated in a sub-relativistic outflow/wind surrounding the jet [32,129,147]. In this case, the broad-line emitting region associated with the jet/outflow can be located at a significant distance from the nucleus, perhaps as large as $\sim 1\,{\rm pc}$. Verifying the existence of the outflow-related component of the BLR and testing the putative connection between the BLR and relativistic

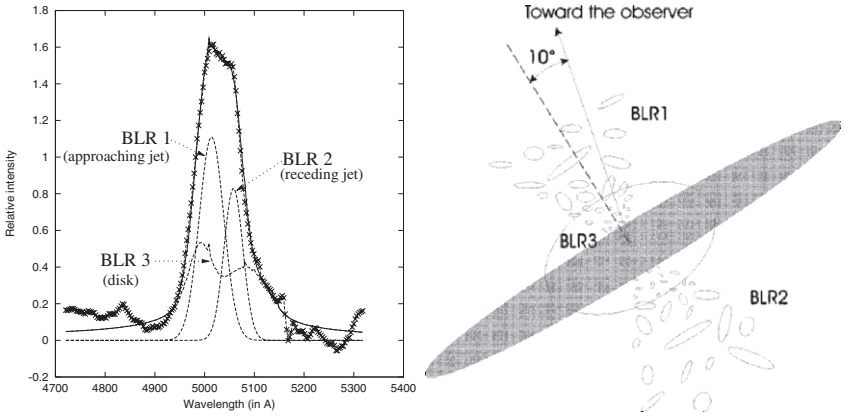


Fig. 2. Left: The observed H_β line of Ark 120 fitted by the two-component model (solid line): a disk (in the line wings) plus an outflow-related component of the BLR (the core of the line). The two components in the core correspond to the line emission generated in the approaching (left) and receding (right) part of a bipolar outflow. **Right**: The scheme of the proposed BLR model for Ark 120 [145].

outflows in Seyfert galaxies can therefore be viewed as critical experiments that may advance our understanding of the nuclear activity in galaxies.

2 A Synthetic View of AGN

The nuclear environment in active galaxies hosts a variety of physical phenomena on scales ranging from $\sim$1–2 $R_{\rm g}$ to $\sim$ 100 parsecs. Table 1 lists most important components of the nuclear regions in galaxies. They cover over seven and ten orders of magnitude in linear and temporal scales, respectively. This presents a serious challenge to any attempt of creating a single framework for describing all aspects of nuclear activity. The key constituents of the nuclear environment can be divided into six broad categories:

Accretion disks and infalling material producing strong continuum and line emission in the high-energy (X-ray and possibly even Γ-ray) regime [5,78], and often exhibiting maser lines in the radio regime [71].

Broad-line and narrow-line regions detected in the line emission and absorption in the optical regime [141].

Obscuring torus composed of clouds of gas and dust [4] and manifested by emission and absorption, primarily in the optical [177], infrared [179] and radio domains [128].

Bipolar outflows detected in continuum emission throughout much of the electromagnetic spectrum. Sub-relativistic outflows are also manifested by the optical absorption lines (BAL outflows [32,49])

Table 1. Characteristic scales in the nuclear regions in active galaxies

	l [R_g]	l_8 [pc]	θ_{Gpc} [mas]	τ_c [yr]	τ_{orb} [yr]
Event horizon:	1–2	10^{-5}	5×10^{-6}	0.0001	0.001
Ergosphere:	1–2	10^{-5}	5×10^{-6}	0.0001	0.001
Accretion disk:	10^1–10^3	10^{-4}–10^{-2}	0.005	0.001–0.1	0.2–15
Corona:	10^2–10^3	10^{-3}–10^{-2}	5×10^{-3}	0.01–0.1	0.5–15
Broad line region:	10^2–10^5	10^{-3}–1	0.05	0.01–10	0.5–15000
Molecular torus:	$>10^5$	>1	>0.5	>10	>15000
Narrow line region:	$>10^6$	>10	>5	>100	>500000
Jet formation:	$>10^2$	$>10^{-3}$	$>5 \times 10^{-4}$	>0.01	>0.5
Jet visible in the radio:	$>10^3$	$>10^{-2}$	>0.005	>0.1	>15

Column designation: l – dimensionless scale in units of the gravitational radius, $G\,M/c^2$; l_8 – corresponding linear scale, for a black hole with a mass of $5 \times 10^8\,M_\odot$; θ_{Gpc} – corresponding largest angular scale at 1 Gpc distance; τ_c – rest frame light crossing time; τ_{orb} – rest frame orbital period, for a circular Keplerian orbit.

Nuclear stellar population detected in the optical through near IR regimes via velocity dispersion or individual stellar proper motions in the nearest AGN in Sgr A* [31,54].

Secondary black holes in multiple black hole systems, which can be inferred from characteristic emission and structural variability in the X-ray through radio regimes [19,105,155].

The AGN studies outlined in the previous section have provided substantial knowledge about each of these aspects of nuclear activity. This has enabled the construction of a synthetic, "unified" picture of active galaxies, in which the entire spectrum of galactic activity is described as an intricate interplay between the physical conditions and orientation of individual constituents of an active nucleus [4,53]. In the current AGN paradigm, several key components, including the accretion disk, the broad-line region and the relativistic outflow (jet), play major roles [35], together with the putative central SMBH (Fig. 3). A fraction of the infalling material forms an outflow along the rotational axis of the SMBH [11,12,45,129] and a strong, compact source of continuum radiation that ionizes the material in the BLR. The nature of the continuum source and its relation to the BLR and the jet remain unclear. The continuum source can be located in the accretion disk [46] or in the hot corona at 200-1000 R_g above the accretion disk [36,144]. A contribution from the jet cannot be excluded [42]. The BLR is often assumed to have an ellipsoidal shape, with at least a fraction of the BLR clouds interacting with the jet plasma. There is also growing evidence for the presence of a conical BLR component [145] associated with a slower, sub-relativistic outflow originating in outer regions of the accretion disk [145]. The sub-relativistic outflow is believed to be responsible also for the broad absorption lines (BAL) observed in a number of quasars [32,49]. The disk, the BLR, and the outflows must be closely connected, producing the bulk of the AGN power.

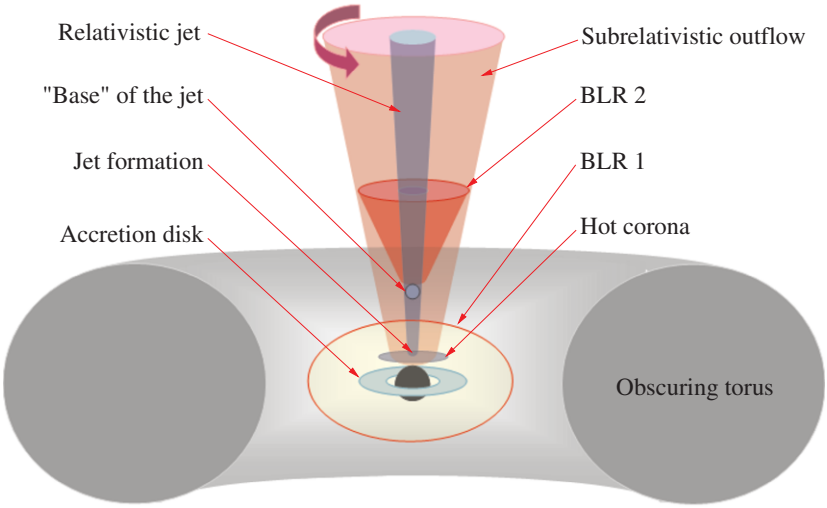


Fig. 3. A sketch of the nuclear region in an active galaxy (the drawing is made not to scale and shows only the approaching jet). The broad-line emission is likely to be generated both near the disk [141] (an ellipsoidal BLR 1, ionized by the emission from a hot corona [36,144] or the accretion disk [46]) and in a rotating subrelativistic outflow [32,129,147] surrounding the jet (a conically-shaped BLR 2, ionized by the emission from the relativistic plasma in the jet). BLR 2 is evident in the broad-line emission when the jet emission dominates the optical continuum. BLR 1 may be manifested in the broad-line emission when the jet contribution to the ionizing continuum is small.

Reconstructing the physical mechanism behind this connection is pivotal for understanding the AGN phenomenon in general.

3 Zooming on the Central Engine

The central engine, presumed to contain a SMBH, is an elusive formation. Direct detection and imaging of the event horizon of a black hole cannot be done with present instruments. The presence of SMBH in galactic centres has been inferred so far only on the basis of circumstantial evidence obtained from observations in the X-ray, optical, near infrared, and radio domains.

X-ray observations have revealed relativistically broadened line profiles indicative of motions at speeds exceeding 10^5 km/s (Fig. 4). The X-ray emission generated above the accretion disk interacts with the disk material and produces the iron fluorescence line [37,38,126]. Observed line profiles show relativistic speeds, Doppler shifts and gravitational redshift. Modelling of the line

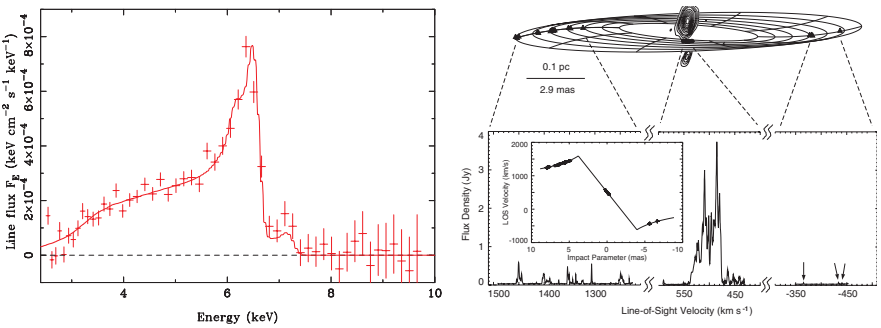


Fig. 4. Left: Relativistic Fe Kα line profile in a Seyfert 1 galaxy MCG-6-30-15 obtained from a joint *XMM-Newton* and *Beppo-SAX* dataset [37]. The crosses mark the data points and the solid line marks the model in which the emission is generated in an accretion disk accretion and the inner radius of the emission is at $\approx 2\,R_{\rm g}$. **Right:** H_2O masers in NGC 4258. Top panel: actual maser positions (filled triangles and circles) superimposed on the radio-continuum emission (contours) and approximated by a model of warped disk. The filled square marks the best-fit location of the centre of the disk. Bottom panel: total spectrum of the maser emission and line of sigh velocities of individual spots fitted by a Keplerian disk model. The high-velocity masers trace a Keplerian curve to better than 1%. Observations of H_2O masers in NGC 4258 have allowed to infer a geometric distance of 7.2 ± 0.3 Mpc to the galaxy from the direct measurement of orbital motions in the maser spots. The motions imply a central object with a mass of $(3.9 \pm 0.1) \times 10^7\,{\rm M}_\odot$ [71].

profiles constrains the disk inclination and spin of the SMBH, which can be used to distinguish between rotating and non-rotating black holes [188].

Optical spectroscopy has revealed the Doppler shift caused by the fast Keplerian rotation of material in the accretion disk implying masses of $1.5 \times 10^9\,{\rm M}_\odot$ in M 84 [13] and $2.5 \times 10^9\,{\rm M}_\odot$ in M 87 [112].

Near-infrared observations of the nucleus of our own Galaxy show the proper motion of stars there [31,54]. This motion implies a mass of $\approx 3.7 \times 10^6\,{\rm M}_\odot$ enclosed within 45 AU distance from the Galactic Centre [55].

Radio observations of maser lines in NGC 4258 (Fig. 4) have yielded the most accurate measure of distance and black hole mass in an external galaxy [71]. High-resolution radio observations of M 87 have probed directly scales as small as $100\,R_{\rm g}$ [80,96]. The presence of supermassive black holes in galactic centres is also implied indirectly by the exceptional stability of jet direction [136,139] and apparent superluminal motions that require highly relativistic flows [191,192].

3.1 Physics of Relativistic Outflows from SMBH

The activity of the central engine is accompanied by highly-relativistic collimated outflows (jets) of plasma material formed and accelerated in the vicinity of the black hole [45,92,123]. Inhomogeneities in the jet plasma appear as a series of compact radio knots (jet components) observed on scales ranging from several light weeks to about a kiloparsec [191,192]. The kinematics and

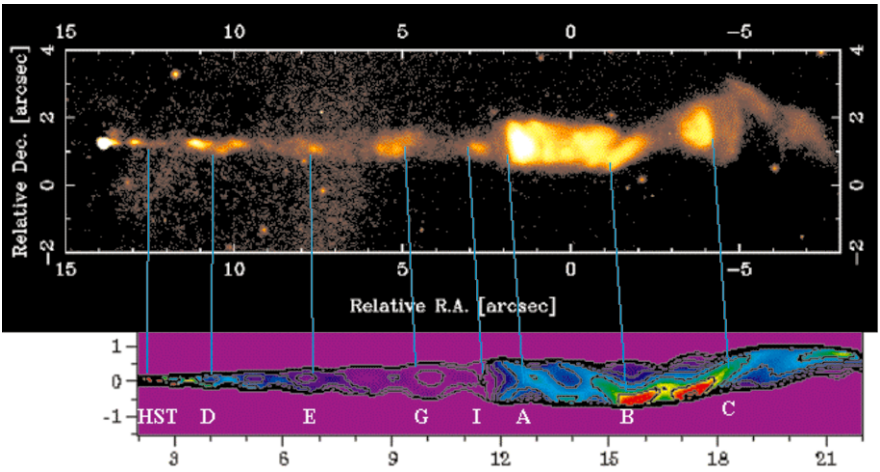


Fig. 5. Top: HST image of M 87 [139]. Botom: Line-of-sight synchrotron intensity image and contours at $\theta = 40°$ calculated from an analytical model of the internal structure of the jet using Kelvin-Helmholtz instability. Connecting lines illustrate the correspondence between the two images. The model represent well the brightness distribution in the jet on scales larger than 1 kpc [108].

spectral evolution of the knots are determined by relativistic shocks [106] and plasma instabilities [102,107,108]. Strong relativistic shocks tend to dissipate on scales of ~ 10 pc [106] and internal structure of large-scale jets is dominated by Kelvin-Helmholtz instability (Fig. 5). Close to the central engine, the kinematic and emission changes can reflect the dynamics in the central engine, and this can be used effectively for estimating the properties of the binary systems of SMBH [19,105].

4 SMBH in a Larger Context

Supermassive black holes have now become the centrepiece of the modern AGN paradigm. They are expected to form in the early Universe, in the course of multiple mergers of dark matter halos (hierarchical structure formation, [85]). SMBH are probably present in all (or almost all) galaxies [93,114] and their masses are correlated with the velocity dispersion in galactic bulges [44,51,114,171]. SMBH are closely related to just about every aspect of galactic activity, and may be one of the most significant energy sources in the Universe. Strength of the AGN activity depends critically on the dynamic properties of gas and stars in the nuclear region [29,30,77], and may be connected to the presence of multiple SMBH in the host galaxy [103,153–155].

Most of the energy in the vicinity of SMBH is created through accretion, which ultimately releases the gravitational energy of infalling matter and possibly mediates the process of releasing the rotational energy of the SMBH it-

self [18]. However, the dominating mechanism and detailed physics of the energy release are still not well understood — it could be the ionizing continuum from the accretion disk, the kinetic energy of the outflow [11], a magnetohydrodynamic mechanism [122,123] or perhaps even a purely electromagnetic process [12]. A detailed picture of physical conditions in the immediate vicinity of SMBH is required for attempting to understand the mechanism for production, conversion and transport of the gravitational energy of the infalling material.

The most straightforward approach to studies of SMBH — probing their environment via direct imaging — is still out of reach because of extremely challenging requirements posed by this task on resolution and dynamic range of observations [9,166]. Direct detection and imaging of the event horizon of a black hole may become possible with the future interferometric missions planned in the X-ray [16,17] and radio [190] domains.

In this situation, physical properties of SMBH can be presently constrained from detailed studies of their environment on scales readily accessible for modern astrophysical instruments. Most important effects of SMBH on their environment are: 1) strong relativistic effects in the immediate vicinity of the event horizon, providing characteristic distortion of background line and continuum radiation [9,27,28,82,188,166]; 2) processing of the galactic gas and shaping the mass distribution and dynamics of gas and stars in the central regions of galaxies [77]; 3) energy and matter release into the ISM and IGM via outflows and emission (both substantially non-isotropic) during galaxy formation and evolution [25,68]; 4) stellar disruptions and other recurrent events of energy release (flares) [63,134]. Further detailed studies of these effects will be instrumental for understanding the physics of SMBH and their role in active galactic nuclei.

5 Cosmological Co-evolution of AGN and SMBH

Recent years have seen an impressive progress in our understanding of cosmological co-evolution of active galaxies and supermassive black holes at their centres. The "demographics" of black holes can now be studied in detail, using the celebrated $M_{\rm bh}$–$\sigma_{\rm bulge}$ relation [89,171] and its derivatives connecting black hole masses in galaxies to observable properties of their nuclear emission. Evidence accumulates for SMBH to be residing practically in every galaxy with a nuclear bulge [61]. The black hole growth via accretion correlates with the bulge growth via star formation [85], which results in a tight correlation between the masses of bulges and central black holes [62]. The mass ratio $M_{\rm bh}/M_{\rm bulge}$ is likely to be higher at $z = 2$–3, implying that black hole growth may induce the formation of galactic bulges. More massive galaxies and SMBH form at earlier cosmological epochs [65]. Initial assembly of SMBH in most powerful AGN begins at $z > 10$ [15], and primordial SMBH in AGN are likely to contribute to reionization of the Universe [113]. The cosmological growth of SMBH is regulated by accretion, black hole mergers and stellar disruption events. The evolutionary sequence of AGN can be roughly outlined within four basic stages: manifestations of nuclear activity start from extremely obscured objects with a prominent sub-

millimetre excess [111,124], then proceed to mainstream QSO stage, followed by an extremely red object (ERO) stage, and finally turning into "normal", "inactive" elliptical and spiral galaxies [23].

During the entire course of their evolution, AGN have a significant impact on the interstellar and intergalactic medium [25,38]. The radiative and kinetic feedback from AGN deposits vast quantities of energy into the environment on scales reaching several megaparsecs. The kinetic feedback from jets and BAL outflows reaches energies of $\sim 0.01\, M_{\rm bh}\, c^2$ [69]. The radiative feedback influences strongly the SMBH growth in galaxies [25,164].

Galactic mergers and binary black holes are probably pivotal for the cosmological evolution of active galaxies. Powerful AGN are most likely produced in the course of galactic mergers [61], with every merger inducing two main episodes of accretion and star formation: at the first contact and at the final coalescence of two galaxies [25]. The nuclear activity is reduced when a loss cone is formed and most of nuclear gas is accreted onto SMBH [30,77], but it can be maintained at a relatively high level in the presence of a secondary black hole [29,125]. It is possible that the nuclear activity is closely related to dynamic evolution of binary SMBH in the centres of active galaxies [103]. Observational investigations of binary black hole systems in galaxies will be crucial for understanding the connection between SMBH and AGN.

6 Fundamental Questions

Despite recent substantial advances in the field of AGN research, nuclear activity in galaxies still holds a number of puzzling questions that can only be answered with the next generation instruments which would provide orders of magnitude increases in sensitivity and resolution in just about every domain of astrophysical observations.

Accretion of galactic gas, stars, and (possibly) dark matter on supermassive black holes is now widely recognized as the most plausible mechanism of maintaining the black hole growth and nuclear activity in galaxies on cosmologically significant timescales. The gravitational potential energy of the infalling material and the rotational energy of the black hole are probably the primary sources of the AGN power. There is, however, a number of poorly understood fundamental issues connecting the observed manifestations of nuclear activity to the accretion process and physics of black holes. We still do not know the exact mechanism by which the gravitational and rotation energy is extracted and converted into emission and kinetic energy of relativistic plasma ejected from the nucleus. We need to understand how the mechanism and efficiency of the energy release is connected to the state of the SMBH (mass, spin, presence of a secondary SMBH in the nucleus) and physical conditions in the nuclear region. It is critical to understand whether and how these properties differ in the objects with and without powerful outflows. In a broader scope, putting these properties in the cosmological context would help attempting to reconstruct the pace of cosmological growth of SMBH and the evolution of their environment.

Resolving these fundamental issues should provide a sufficient basis for answering at least some of the "eternal" questions about galactic activity. Is there a unified model for all of the different types of AGN? Can we draw an evolutionary diagram for AGN? What is the relationship between the SMBH and the host galaxy? Do all galaxies have SMBH? Were black hole seeds or by-products of galaxy formation? How important is the feedback from supermassive black holes for the structure formation in the Universe? What is the role of accreting black holes in the reionization of the Universe? What causes the activity phase in a galaxy and sets its lifetime? How are AGN jets produced and collimated? How do they interact with, and affect, the host galaxy. How is the SMBH activity connected to galaxy mergers and central starbursts? Are multiple SMBH common in AGN, and how do they form and evolve? These are some of the problems that will hopefully be understood and resolved in the next decades with the help of the new generation of astrophysical facilities.

References

1. K. Abazajian, J.K. Adelman-McCarthy, M.A. Agüeros, et al.: AJ **126**, 2081 (2003)
2. M.F. Aller, H.D. Aller, P.A. Hughes: ApJ **586**, 33 (2003)
3. J.M. Anderson, J.S. Ulvestad, L.C. Ho: ApJ **603**, 42 (2004)
4. R. Antonucci: Ann. Rev Astron. & Astroph. **31**, 473 (1993)
5. P. Arévalo, I. Papadakis, B. Kuhlbrodt, W. Brinkmann: A&A **430**, 435 (2005)
6. D.R. Ballantyne, S. Vaughan, A.C. Fabian: MNRAS **342**, 239 (2003)
7. R.H. Becker, R.L. White, D.J. Helfand: ApJ **450**, 559 (1995)
8. R.H. Becker, R.L. White, M.D. Gregg, et al.: ApJS **135**, 227 (2001)
9. K. Beckwith, C. Done: MNRAS **359**, 1217 (2005)
10. H.E. Bignall, D.L. Jauncey, L.L. Kedziora-Chudczer, et al.: PASA **19**, 29 (2002)
11. R.D. Blandford, D.G. Payne: MNRAS **199**, 883 (1982)
12. R.D. Blandford, R.L. Znajek: MNRAS **179**, 433 (1976)
13. G.A. Bower, R.F. Green, A. Danks, et al.: ApJ **492**, 111 (1998)
14. W. Brinkmann, P. Arévalo, M. Gliozzi, E. Ferrero: A&A **415**, 959 (2004)
15. V. Bromm, A. Loeb: ApJ **596**, 34 (2003)
16. W. Cash: Adv. Space Res. **35**, 122 (2005)
17. W. Cash, A. Shipley, S. Osterman, J. Marshall: Nature **407**, 160 (2000)
18. M. Camenzind, R. Khanna: Il Nuovo Cimento **115 B**, 815 (2000)
19. A. Caproni, Z. Abraham: ApJ **602**, 625 (2004)
20. M.J. Claussen, P.J. Diamond, J.A. Braatz, A.S. Wilson, C. Henkel: ApJ **500**, 129 (1998)
21. J.J. Condon, W.D. Cotton, E.W. Greisen, et al.: AJ **115**, 1693 (1998)
22. T. Courvoisier: A&A Reviews **9**, 1 (1998)
23. L.Danese, F. Shankar, G.L. Granato, et al.: in *Growing Black Holes: Accretion in a Cosmological Context*, ESO Astrophysics Symposia Series, ed. S. Nayakshin, A. Merloni, R.A. Sunyaev (Springer-Verlag: Heidelberg 2005) p. 60
24. M. Dietrich, B.M. Peterson, P. Albrecht, et al.: ApJSS **115**, 185 (1998)
25. T. Di Matteo, V. Springel, L. Hernquist: Nature **433**, 604 (2005)
26. R. Dodson, P.G. Edwards, H. Hirabyashi: PASJ, *subm.* (2005)
27. M. Dovčiak, S. Bianchi, M. Guainazzi, V. Karas, G. Matt: MNRAS **350**, 745 (2004)
28. M. Dovčiak, V. Karas, G. Matt: MNRAS **355**, 1005 (2004)

29. V.I. Dokuchaev: Sov. Astron. Lett. **15**, 167 (1989)
30. V.I. Dokuchaev: MNRAS **251**, 564 (1991)
31. A. Eckart, R. Genzel, T. Ott, R. Schödel: MNRAS **331**, 917 (2002)
32. M. Elvis: ApJ **545**, 63 (2000)
33. M. Eracleous, J.P. Halpern: ApJ **599**, 886 (2003)
34. A.C. Fabian, K. Nandra, C.S. Reynolds, et al.: MNRAS **342**, 1325 (1995)
35. A.C. Fabian: Proc. Natl. Acad. Sci. USA **96**, 4749 (1999)
36. A.C. Fabian: astro-ph/0412224 (2004)
37. A.C. Fabian, S. Vaughan, K. Nandra, et al.: MNRAS **335**, L1 (2002)
38. A.C. Fabian, J.S. Sanders, S.W. Allen, et al.: MNRAS **344**, 43 (2003)
39. X. Fan, V.K. Narayan, M.A. Strauss, et al.: AJ **123**, 1247 (2002)
40. X. Fan, M.A. Strauss, D.P. Schneider, et al.: AJ **125**, 1649 (2003)
41. D. Fadda, B.T. Januzzi, A. Ford, L.S. Storie-Lombardi: AJ **128**, 1 (2004)
42. H. Falcke, S. Markoff: A&A **362**, 113 (2000)
43. A.L. Fey, P. Charlot: ApJS **128**, 17 (2000)
44. L. Ferrarese, D. Merritt: ApJ **539**, L9 (2000)
45. A. Ferrari: ARA&A **36**, 539 (1998)
46. G.B. Field, R.D. Rogers: ApJ **403**, 94 (1993)
47. E.B. Fomalont, S. Frey, Z. Paragi, et al.: ApJS, **131**, 95 (2000)
48. G. Fossati, L. Maraschi, A. Celotti, A. Comastri, G. Ghisellini: MNRAS **299**, 433 (1998)
49. S.C. Gallagher, W.N. Brandt, G. Chartas, G.P. Garmire, R.M. Sambruna: Adv. Space Res. **34**, 2594 (2004)
50. J.F. Gallimore, S.A. Baum, C.P. O'Dea, E. Brinks, A. Pedlar: ApJ **462**, 740 (1996)
51. K. Gebhardt, R. Bender, G. Bower, et al.: ApJ **539**, L13 (2000)
52. R. Genzel, C.J. Cesarsky: Ann. Rev. Astron. & Astroph. **38**, 761 (2000)
53. M. Georganopoulos, A.P. Marscher: ApJ **506**, 621 (1998)
54. A.M. Ghez, M. Morris, E.E. Becklin, A. Tanner, T. Kremenek: Nature **407**, 349 (2000)
55. A.M. Ghez, S. Salim, S.D. Hornstein, et al.: ApJ **620**, 744 (2005)
56. M. Giavalisco, H.C. Ferguson, A.M. Koekemoer, et al: ApJ **600**, L93 (2004)
57. J.E. Greene, L.C. Ho: ApJ **610**, 722 (2004)
58. M.D. Gregg, R.H. Becker, R.L. White, D.J. Helfand, R.G. McMahon, I.M. Hook: AJ **112**, 407 (1996)
59. A.C. Gupta, D.P.K. Banerjee, N.M. Ashok, U.C. Joshi: A&A **422**, 505 (2004)
60. L.I. Gurvits, K.I. Kellermann, S. Frey: A&A **342**, 378 (1999)
61. M.G. Haehnelt, G. Kauffmann: MNRAS **318**, 35 (2000)
62. N. Häring, H.-W. Rix: ApJ **604**, 89 (2004)
63. J.P. Halpern, S. Gezari, S. Komossa: ApJ **604**, 572 (2004)
64. M.C. Hartmann, M. Bötcher, G. Aldering, et al.: ApJ **553**, 683 (2001)
65. G. Hasinger: in *Growing Black Holes: Accretion in a Cosmological Context*, ESO Astrophysics Symposia Series, ed. S.Nayakshin, A. Merloni, R.A. Sunyaev (Springer-Verlag: Heidelberg 2005) p. 418
66. T.M. Heckman, G. Kauffmann, J. Brinchman, S. Charlot, C. Tremonti, S.D.M. White: ApJ **613**, 109 (2004)
67. J. Heidt, S.J. Wagner: A&A **305**, 42 (1996)
68. S. Heinz, R.A. Sunyaev: MNRAS **343**, 59 (2003)
69. S. Heinz, R.A. Sunyaev, A.Merloni, T. Di Matteo: *Growing Black Holes: Accretion in a Cosmological Context*, ESO Astrophysics Symposia Series, ed. S.Nayakshin, A. Merloni, R.A. Sunyaev (Springer-Verlag: Heidelberg 2005) p. 371

70. D.R. Henstock, I.W.A. Browne, P.N. Wilkinson, et al.: ApJS **100**, 1 (1995)
71. J.R. Herrnstein, J.M. Moran, L.J. Greenhill, et al.: Nature **400**, 539 (1999)
72. H. Hirabayashi, E.B. Fomalont, S. Horiuchi, J.E.J. Lovell, G.A. Moellenbrock: PASJ **52**, 997 (2000)
73. L.C. Ho: in *Observational Evidence for the Black Holes in the Universe*, ed. S.K. Chakrabarti (Kluwer, Dordrecht 1999) p. 157
74. L.C. Ho: Adv. Space. Res. **23**, 816 (1999)
75. L.C. Ho: ApJ **510**, 631 (1999)
76. S. Horiuchi, E.B. Fomalont, W.K. Scott, et al.: ApJ, **616**, 110 (2004)
77. P.B. Ivanov, A.G. Polnarev, P.Saha: MNRAS **358**, 1361 (2005)
78. K. Iwasawa, A.C. Fabian, C. Reynolds, et al.: MNRAS **282**, 1038 (1996)
79. W. Jaffe, K. Meisenheimer, H.J.A. Röttgering, et al.: Nature **429**, 47 (2004)
80. W. Junor, J.A. Biretta, M. Livio: Nature **401**, 891 (1999)
81. M. Kadler, E. Ros, A.P. Lobanov, H. Falcke, J.A. Zensus: A&A **426**, 481 (2004)
82. V. Karas, D. Vokrouhlicky, A.G. Polnarev: MNRAS **259**, 569 (1992)
83. S. Kaspi, P.S. Smith, H. Netzer, D. Maoz, B.T. Jannuzi, U. Giveon: ApJ **533**, 631 (2000)
84. N.E. Kassim, R.A. Perley, W.S. Erikson, K.S. Dwarakanath: AJ **106**, 2218 (1993)
85. G. Kauffmann, M.G. Haehnelt: MNRAS **311**, 576 (2000)
86. K.I. Kellermann: PASA **19**, 77 (2002)
87. K.I. Kellermann, M.L. Lister, D.C. Homan, et al.: AJ, **609**, 539 (2004)
88. K.I. Kellermann, R.C. Vermeulen, J.A. Zensus, M.H. Cohen: AJ **115**, 1295 (1998)
89. A. King: ApJ **593**, 184 (2003)
90. H.-R. Klöckner, W.A. Baan: A&A **419**, 887 (2004)
91. H.R. Klöckner, W.A. Baan, M.A. Garrett: Nature, **421**, 821 (2003)
92. S. Koide, K. Shibata, T. Kudoh, D.L. Meier: Science **295**, 1688 (2002)
93. J. Kormendy, D.O. Richstone: Ann. Rev. Astron. & Astroph. **33** 581 (1995)
94. Y. Kovalev, K.I. Kellermann, M.L. Lister, et al.: AJ **130**, 2473 (2005)
95. A. Kraus, T.P. Krichbaum, R. Wegner, et al.: A&A **401**, 161 (2003)
96. T.P. Krichbaum, D. Graham, W. Alef, et al.: in *New Developments in VLBI Science and Technology*, ed. E. Ros R.W. Porcas, A.P. Lobanov, J.A. Zensus (MPIfR: Bonn 2002) p. 125
97. M.L. Lister: ApJ **599**, 105 (2003)
98. M.L. Lister: astro-ph/0309413 (2003)
99. M.L. Lister, A.P. Marscher: Astroparticle Physics **11**, 65 (1999)
100. M.L. Lister, P.S. Smith: ApJ **541**, 66 (2000)
101. A.P. Lobanov: A&A **390**, 79 (1998)
102. A.P. Lobanov: A&AS **132**, 261 (1998)
103. A.P. Lobanov: in *Growing Black Holes: Accretion in a Cosmological Context*, ESO Astrophysics Symposia Series, ed. S.Nayakshin, A. Merloni, R.A. Sunyaev (Springer-Verlag: Heidelberg 2005) p. 354
104. A.P. Lobanov: MemSAItS **7**, 12 (2005)
105. A.P. Lobanov, J. Roland: A&A **431**, 831 (2005)
106. A.P. Lobanov, J.A. Zensus: ApJ **509**, 521 (1999)
107. A.P. Lobanov, J.A. Zensus: Science **294**, 128 (2001)
108. A.P. Lobanov, P.E. Hardee, J.A. Eilek: New Astronomy **47**, 629 (2003)
109. A.P. Lobanov, T.P. Krichbaum, D.A. Graham, et al.: A&A **364**, 391 (2000)
110. C.J. Lonsdale, S.S. Doeleman, R.B. Phillips: AJ, **116**, 8 (1998)
111. D. Lutz, E. Sturm, T. Alexander, et al.: in *ISO Survey of a Dusty Universe*, ed. D. Lemke, M. Stickel, K. Wilke, Lecture Notes in Physics, v. 548 (Springer-Verlag: Heidelberg 2000) p. 209

112. F. Macchetto, A. Marconi, D.J. Axon, A. Capetti, W. Sparks, P. Crane: ApJ **489**, 579 (1997)
113. P. Madau, M.J. Rees, M. Volonteri, F. Haardt, S.P. Oh: ApJ **604**, 484 (2004)
114. J. Magorrian, S. Tremaine, D.O. Richstone, et al: AJ **115**, 2285 (1998)
115. A. Malizia, L. Bassani, J.B. Stephen, G. Malaguti, G.G.C. Palumbo: ApJS **113**, 311 (1997)
116. L. Maraschi, P. Grandi, C.M. Urry, et al.: ApJ **435**, 91 (1994)
117. A.P. Marscher, S.G. Jorstad, J.L. Gómez, et al.: Nature **417**, 625 (2002)
118. H.L. Marshall, D.E. Harris, J.P. Grimes, et al.: ApJ **549**, 167 (2001)
119. H.L. Marshall, B.P. Miller, D.S. Davis, et al.: ApJ **564**, 683 (2002)
120. P. Marciano, J.W. Sulentic, R. Zamanov, et al.: ApJSS **149**, 199 (2003)
121. G. Matt: Nuclear Physics B Proceedings Supplements **132**, 97 (2004)
122. D.L. Meier: ApJ **548**, 9 (2001)
123. D.L. Meier, S. Koide, Y. Uchida: Science **291**, 84 (2001)
124. K. Menten, F. Bertoldi: Rev. Mod. Astron. **13**, 229 (2000)
125. D. Merritt: in *Coevolution of Black Holes and Galaxies*, Carnegie Observatories Astrophysics Series, ed. L.C. Ho (CUP: Cambridge 2004) p. 264
126. G. Miniutti, A.C. Fabian, R. Goyder, A.N. Lasenby: MNRAS **344**, 22 (2003)
127. M. Miyoshi, J. Moran, J. Herrnstein, et al.: Nature **373**, 127 (1995)
128. C.G. Mundell, J.M. Wrobel, A. Pedlar, J.F. Gallimore: ApJ **583**, 192 (2003)
129. N. Murray, J. Chiang: ApJ **474**, 91 (1997)
130. R.F. Mushotzky, C. Done, K.A. Pounds: ARA&A **31**, 717 (1993)
131. K. Nandra, I.M. George, R.F. Mushotzky: ApJ **476**, 70 (1997)
132. K. Nandra, I.M. George, R.F. Mushotzky: ApJ **477**, 602 (1997)
133. S. Nayakshin: MNRAS **359**, 545 (2005)
134. S. Nayakshin, J. Cuadra, R.A. Sunyaev: A&A **413**, 173 (2004)
135. P.M. Ogle, H.L. Marshall, J.C. Lee, C.R. Canizares: ApJ **545**, L81 (2000)
136. F.N. Owen, P.E. Hardee, T.J. Cornwell: ApJ **340**, 689 (1989)
137. T.J. Pearson, A.C.S. Readhead: ApJ **328**, 114 (1988)
138. A.B. Peck, C. Henkel, J.S. Ulvestad, et al.: ApJ **590**, 149 (2003)
139. E.S. Perlman, J.A. Biretta, F. Zhou, W.B. Sparks, F.D. Macchetto: AJ **117**, 2185 (1999)
140. E.S. Perlman, W.B. Sparks, J. Radomski, et al.: ApJ **561**, 51 (2001)
141. B.M. Peterson: in *Advanced Lectures on the Starburst-AGN Connection*, ed. by I. Aretxaga, D. Kunth, R. Mújica. (World Scientific: Singapore, 2001), p. 3
142. B.M. Peterson, P. Berlind, R. Bertram, et al.: ApJ **581**, 197 (2002)
143. A.G. Polatidis, P.N. Wilkinson, W. Xu., et al.: ApJS **98**, 33 (1995)
144. G. Ponti, M. Cappi, M. Dadina, G. Malaguti: A&A **417**, 451 (2004)
145. L.Č. Popović, N. Stanić, A. Kubičela, E. Bon: A&A **367**, 780 (2001)
146. L.Č. Popović, E. Mediavilla, E. Bon, D. Ilić: A&A **423**, 909 (2004)
147. D. Proga, J.M. Stone, T.R. Kallman: ApJ **543**, 686 (2000)
148. E.M. Puchnarewicz, K.O. Mason, F.J. Carrera: MNRAS **283**, 1311 (1996)
149. F.T. Rantakyrö, L.B. Bååth, D.C. Backer, et al.: A&AS **131**, 451 (1998)
150. B.J. Rickett, L. Kedziora-Chudczer, D.L. Jauncey: ApJ **581**, 103 (2002)
151. M. Ricotti, M.G. Haehnelt, M. Pettini, M.J. Rees: MNRAS **352**, 21 (2004)
152. G.E. Romero, L. Chajet, Z. Abraham, J.H. Fan: A&A **360**, 57 (2000)
153. N. Roos: A&A **104**, 218 (1981)
154. N. Roos: ApJ **294**, 479 (1985)
155. N. Roos: ApJ **294**, 486 (1985)
156. M. Salvati, M. Spada, F. Pacini: ApJ **495**, 19 (1998)

157. R.M. Sambruna, I.M. George, R.F. Mushotsky, K. Nandra, T.J. Turner: ApJ **495**, 749 (1998)
158. R.M. Sambruna, L. Maraschi, C.M. Urry: ApJ **463**, 444 (1996)
159. A.I. Shapovalova, A.N. Burenkov, L. Carrasco, et al.: A&A **376**, 775 (2001)
160. D.C. Shih, K. Iwasawa, A.C. Fabian: MNRAS **333**, 687 (2002)
161. P.A. Shaver, J.V. Wall, K.I. Kellermann, C.A. Jackson, M.R.S. Hawkins: Nature **384**, 439 (1996)
162. M. Spada, M. Salvati, F. Pacini: ApJ **511**, 136 (1999)
163. M. Spada, G. Ghisellini, D. Lazzati, A. Celotti: MNRAS **325**, 1559 (2001)
164. V. Springel, T. Di Matteo, L. Hernquist: MNRAS **361**, 776 (2005)
165. C.S. Stalin, Gopal Krishna, R. Sagar, P. Wiita: MNRAS **350**, 175 (2004)
166. R. Takahashi: PASJ **57**, 273 (2005)
167. Y. Tanaka, K. Nandra, A.C. Fabian, et al.: Nature **375**, 695 (1995)
168. G.B. Taylor, R.C. Vermeulen, T.J. Pearson, et al.: ApJS **95**, 345 (1994)
169. G.B. Taylor, R.C. Vermeulen, A.C.S. Readhead, et al.: ApJS **107**, 37 (1996)
170. D.D. Thakkar, W. Xu, A.C.S. Readhead, et al.: ApJS **98**, 33 (1995)
171. S. Tremaine, K. Gebhardt, R. Bender, et al.: ApJ **574**, 740 (2002)
172. M. Türler, S. Paltani, T.J-L. Courvoisier, et al.: A&AS **134**, 89 (1999)
173. M. Türler, T.J-L. Courvoisier, S. Paltani: A&A **361**, 850 (2000)
174. M.H. Ulrich: Rev. Mod. Astron.: **5**, 247 (1992)
175. M.H. Ulrich, L. Maraschi, C.M. Urry: ARA&A **35**, 445 (1997)
176. C.M. Urry, E.Treister: in *Growing Black Holes: Accretion in a Cosmological Context*, ESO Astrophysics Symposia Series, ed. S.Nayakshin, A. Merloni, R.A. Sunyaev (Springer-Verlag: Heidelberg 2005) p. 432
177. I.M. van Bemmel, C.P. Dullemond: A&A **404**, 1 (2003)
178. P. Véron, M.P. Véron-Cetty: Astron. & Astroph. Rev. **10**, 81 (2000)
179. B. Vollmer, T. Beckert, W.J. Duschl: A&A **413**, 949 (2004)
180. S.J. Wagner, A. Witzel: ARA&A **33**, 163 (1995)
181. W. Wamsteker, W. Ting-gui, N. Schartel, N., R. Vio: MNRAS **288**, 225 (1997)
182. P.J. Wiita: astro-ph/0103020 (2001)
183. G. Weigelt, M. Wittkowski, Y.Y. Balega, et al.: A&A **425**, 77 (2004)
184. R.L. White, R.H. Becker, M.D. Gregg, et al.: ApJS **126**, 133 (2000)
185. D. Worrall: MemSAIt **76**, 28 (2005)
186. W. Xu, A.C.S. Readhead, T.J. Pearson, A.G. Polatidis, P.N. Wilkinson: ApJS **99**, 297 (1995)
187. T. Yaqoob, I.M. George, K. Nandra, T.J. Turner, P.J. Serlemitsos, R.F. Mushotzky: ApJ **546**, 759 (2000)
188. A.F. Zakharov, S.V. Repin: Adv. Space Res. **34**, 2544 (2004)
189. A.F. Zakharov, N.S. Kardashev, V.N. Lukash, S.V. Repin: MNRAS **342**, 1325 (2003)
190. A.F. Zakharov, A.A. Nucita, F. Depaolis, G. Ingrosso: New Astronomy **10**, 479 (2005)
191. J.A. Zensus: Ann. Rev. Astron. Astrophys. **35**, 607 (1997)
192. J.A. Zensus, T.P. Krichbaum, A.P. Lobanov: Rev. Mod. Astron. **9**, 241 (1996)
193. J.A. Zensus, E. Ros, K.I. Kellermann, M.H. Cohen, R.C. Vermeulen, M. Kadler: AJ **124**, 662 (2002)
194. W. Zheng: AJ **111**, 1498 (1996)

New Frontiers in AGN Astrophysics: The X-ray Perspective

T. Boller and L. Gallo

Max-Planck-Institut für extraterrestrische Physik, Garching, Postfach 1312, 85741 Garching

Abstract. After four years of dedicated service from the new generation of X-ray telescopes, XMM-Newton and Chandra, as well as results obtained from various multiwavelength observations, we are at a good point to revisit the topic of AGN physics. This proceeding will review the basic open questions posed by earlier X-ray missions which have now been answered, as well as address new questions which still require further investigation. The topics critically discussed will include: the physics of the innermost region of AGN, the nature of sharp spectral drops in the high-energy spectra of NLS1s, as well as new aspects of Seyfert unification.

1 Theorem I: We have not Lost the Scattering from the Relativistic Accretion Disc

The Fe K line profiles observed in the majority of active galactic nuclei are narrow and unresolved, in contrast to the expectation of relativistically blurred and broadened lines. To address this basic scientific aspect we consider the following.

1.1 Individual XMM-Newton/Chandra Spectra

We have conducted a literature search of all AGN observed with XMM-Newton in the $2 - 10\,\mathrm{keV}$ band. Of about 60 objects which could potentially show a relativistic iron line, only 3 do so with relative confidence. The question arises: Why are the effects of relativistic motions in radio-quiet moderately luminous AGN not detectable in the XMM-Newton and Chandra spectra?

1.2 Fe K Line Simulations

We simulated Fe Kα emission under various condition to determine the likelihood of detecting the feature with a typical 40 ks XMM-Newton observation. First we considered a neutral accretion disc. Varying the observed flux from 10^{-11} down to 10^{-14}, and the equivalent width of the Fe Kα line from 400 down to 100 eV shows, that the relativistic line is clearly detected with XMM-Newton (c.f. Fig. 1).

We then considered if ionization plays a major role. We simulated accretion disc spectra for ionized discs and found that with relatively mildly ionization the effects of Compton broadening within the disc are already so strong that the line becomes undetectable for XMM-Newton. In Fig. 1 we show the resulting

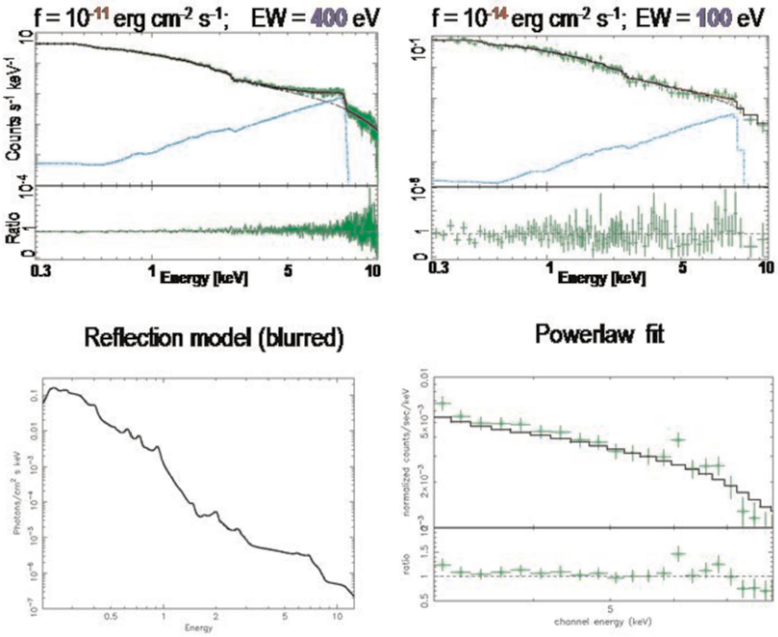


Fig. 1. Upper panels: XMM-Newton simulations of Fe Kα emission from a neutral accretion disc. By varying the observed flux and the equivalent width, we find that the relativistic line should be clearly detectable within a typical 40 ks observation. **Lower panels**: Same as the upper panel, but for an ionized accretion disc with an ionization parameter of 1000. The left panel shows the model (including strong Compton broadening effects and relativistic blurring) and the right panel the resulting XMM-Newton statistics. The relativistic Fe K line is undetectable.

simulation for an ionization parameter of 1000 [cgs]. The line is undetectable with XMM-Newton. We note that by folding the model through the XEUS response, results in a detectable feature; therefore the missing broad relativistic Fe K lines are most probably due to an ionized accretion disc.

1.3 The First Stacked XMM-Newton Spectrum of Type 1 AGN in the Local Universe

We have stacked 36 moderately luminous PG quasars which do not show any evidence of relativistic lines. In Fig. 2 we show the ratio plot of a power-law continuum fitted to the high-energy spectrum. A broad and significant Fe K line is clearly visible in the ratio plot, supporting the results from the simulations that XMM-Newton lacks the sensitive to detect relativistic lines in ionized accretion discs.

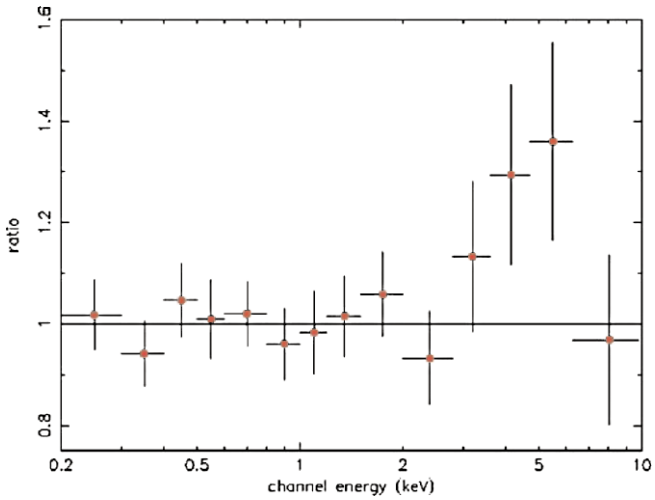


Fig. 2. Results from the stacking analysis of 36 PG quasars obtained from the XMM-Newton archive. Although none of the objects show a relativistic Fe K line, the improved statistics after applying a stacking analysis clearly indicates the presence of a strong relativistic Fe K lines.

2 Theorem II: Some Open Questions of Accreting Black Holes are Explained by Light Bending Effects

One of the challenges of recent years has been in understanding the apparent lack of response of the Fe Kα broad line flux to the varying X-ray continuum flux. This can now be explained by strong light bending effects occurring in the extreme Kerr black hole space time (e.g., [7]). In this scenario there is a compact region at some height above the accretion disc, emitting a power-law continuum. When the source height is small, then most of the photons are bent towards the disc and lost in the black hole reducing the power-law component at infinity. The observed spectrum is then reflection dominated. As the source height increases, then the gravitational potential that the power-law photons have to overcome is reduced, so that more continuum photons reach the observer. When the source height is very large, then light bending is not effective, and we have the standard picture: half of the continuum photons are intercepted by the disc and half reach the observer. The power-law component is now fully recovered. As the power-law component varies, the Fe K line/power-law flux-flux diagram shows three different regimes: (i) a correlation between the two fluxes for small source heights of the power-law component above the disc, (ii) a saturation phase, where the Fe K line flux is not responding to changes in the power-law continuum and (iii) an anti-correlation between the Fe K line flux and the power-law flux (see Fig. 2 in [8]). We note that the light bending model also explains the spectral variability of AGN in their low and high states.

3 Theorem III: The Unique Spectral and Timing Features of NLS1s Pose New Challenges for the Future

We have detected sharp spectral drops above 7 keV in the NLS1s 1H0707-495 [1,5] and IRAS 13224-3809 [2]. The nature of these features are still controversial discussed. Plausible scenarios include partial covering (e.g., [6]) or a reflection dominated spectrum (e.g., [4]). While the two theories manifest similar spectra as seen with XMM-Newton, the large collecting areas of future missions such as XEUS, will easily disentangle between the two.

4 Theorem IV: The Standard Seyfert 1 - Seyfert 2 Unification Scheme is Oversimplified

We have observed 1ES 1927+654 [3] and determined that the optical and X-ray properties do not fit into the standard Seyfert unification model. The X-ray observations obtained with ROSAT and Chandra reveal persistent, rapid and large scale variations, as well as steep 0.1–2.4 keV ($\Gamma = 2.6 \pm 0.3$) and 0.3–7.0 keV ($\Gamma = 2.7 \pm 0.2$) spectra. The measured intrinsic neutral X-ray column density is approximately $7{\cdot}10^{20}$ cm^{-2}. The X-ray timing properties indicate that the strong variations originate from a region, a few hundred light seconds from the central black hole, typical for type 1 AGN. However, high quality optical spectroscopy reveals a typical Seyfert 2 spectrum with some host galaxy contamination and no evidence of Fe II multiplets or broad hydrogen Balmer wings. The intrinsic optical extinction derived from the BLR and NLR are $A_V \geq 3.7$ and $A_V = 1.7$, respectively. The X-ray observations give an A_V value of less than 0.58, in contrast to the optical extinction values. Ideas to explain this apparent difference in classification include partial covering, an underluminous BLR, or a high dust to gas ratio.

References

1. Th. Boller, A.C. Fabian, R. Sunyaev, et al.: MNRAS **329**, 1 (2002)
2. Th. Boller, Y. Tanaka, A. Fabian, et al.: MNRAS **343**, 89 (2003)
3. Th. Boller, W. Voges, M. Dennefeld, et al.: A&A **397**, 557 (2003)
4. A. Fabian, D. Ballantyne, A. Merloni, et al.: MNRAS **331**, 35 (2002)
5. L. Gallo, Y. Tanaka, Th. Boller, et al.: MNRAS in press (astro-ph/0405159)
6. S. Holt, R. Mushotzky, E. Boldt, et al.: ApJ **241**, 13 (1981)
7. G. Miniutti, A. Fabian, R. Goyder, et al.: MNRAS **344**, 22 (2003)
8. G. Miniutti, A. Fabian: MNRAS **349**, 1435 (2004)

Deep Radio Source Surveys with the SKA

K.I. Kellermann

NRAO, 520 Edgemont Road, Charlottesville, VA 22903, USA

Abstract. We discuss the potential of the SKA for doing deep surveys considering the limitations of sensitivity and confusion resulting from the expected high source density and finite source size. Array dimensions of several thousand or more may be needed to reduce confusion below the thermal noise.

1 Deep Surveys

One of the first things that one thinks of doing with any new telescope, is a deep survey, both to reach to lower levels of the luminosity function and to extend the range of observable space at all levels of the luminosity function. Radio observations are important since they, a) give highly precise astrometry, which is important to identify optical, X-ray, and IR counterparts; b) can give very high angular resolution diffraction limited images needed to distinguish star formation in galaxies from AGN and to relate black hole formation to host galaxy properties; and c) can see through the gas and dust to the very central regions of galaxies that are obscurred or absorbed in other wavelength bands.

Using the VLA, radio galaxies, quasars, and other powerful AGN associated with massive black holes can be observed out to $z \gg 1$, and moderate star forming galaxies such as M82, LLAGN, and radio quiet quasars to $z \sim 1$. With the Expanded VLA (EVLA) it will be possible to observe star forming galaxies, radio quiet quasars, and LLAGN to $z > 1$.

With the SKA, it will be possible to push the sensitivity limits by nearly another two orders of magnitude so that even normal galaxies may be observed at cosmologically interesting redshifts. Radio astronomers can gain increased sensitivity by building arrays where the costs are approximately linear with collecting area, rather than by building costly complex monolithic structures. Optical astronomers are also developing arrays. But, only at radio wavelengths can we build low noise amplifiers and effectively share the signal without any loss of sensitivity, whereas optical interferometers must divide the photons among the individual elements, and thus are limited to relatively bright sources. Also, at radio wavelengths, it is possible to integrate for hundred of hours without suffering from systematic effects or non thermal noise contributions. It, remains to be seen however, whether this will be true for the SKA, where the thermal noise floor will be very low.

2 Current Deep Surveys

The most sensitive deep radio surveys have been made with the VLA which can reach an rms noise level of a few microJy with a resolution of a few arc seconds in a few hundred hours integration time corresponding to a source density of about 1 per square arcmin [1–4]. A combined VLA and MERLIN observation included 42 hours of VLA data and 18 days of MERLIN data to image the HDF with an angular resolution of a few tenths of an arcsec and rms noise of 3 microJy [5]. The microJy radio sources found in these deep surveys are associated with a variety of optical counterparts. Most are identified with galaxies which are brighter than $I = 25$ mag, but a few sources appear "optically quiet" and remain unidentified even to the limits of the HDF [6].

3 Deep surveys with the SKA

With its huge sensitivity, deep surveys with the SKA will be able to detect even normal galaxies at early cosmological epochs ($z \sim 1$) to trace the early history of the formation of stars and galaxies, as well as radio quiet quasars and LLAGN to $z \gg 1$ to trace the formation and evolution of massive black holes and to better understand the relation between black holes and star formation. Do black holes induce star formation? Does, star formation induce the creation of black holes? Or, is the formation of stars an black holes linked to some other underlying phenomena?

Perhaps more important, by time the SKA is built, many of the scientific problems which drive today's research will either have been solved or shown to be naive. If history is any example, the exiting thing about deep surveys made with the SKA will be the opportunity to discover new things which will raise new questions and problems, rather than just solve old problems.

4 Resolution Requirements for the SKA

With an integration time of a few hundred hours, SKA, images will have a thermal noise of only a few nanoJy, sufficient to detect sources as weak as 10 to 20 nanoJy, unless limited by confusion. We can only guess the source density at levels nearly three orders of magnitude weaker than the weakest radio sources currently detected. Extrapolating existing counts, Fig. 1a shows the angular resolution needed to keep confusion below the thermal noise based on the criteria that the source density should not exceed 20 beamwidths per source. Fig. 1b shows the corresponding array dimensions needed to reach this confusion level. This ranges from about 100 km at 4 cm to 1000 km at 20 cm to 10,000 km at 4 m wavelength.

We emphasize, however, that these numbers are very uncertain. Confusion could be less of a problem if the counts turn over at sub-microJy levels, or it could be worse if a previously unknown population appears. Some constraints exist from available data. Unless the centimeter counts turn over below about 30 nJy

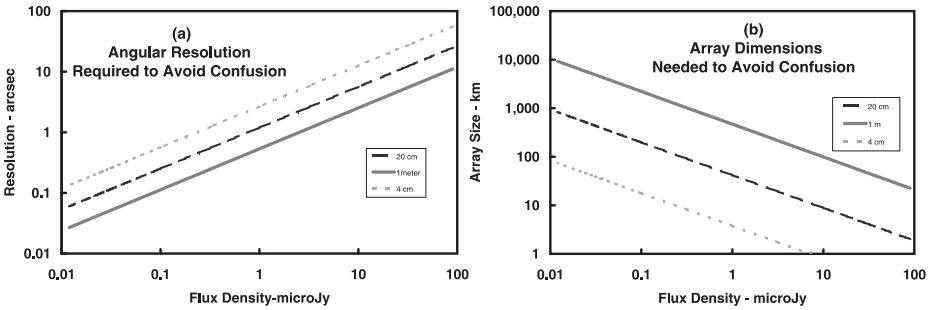


Fig. 1. a) Angular resolution required to keep confusion below a given flux density. b) corresponding array dimensions.

the combined contribution of weak sources would distort the CMB spectrum. A stronger constraint is obtained from the well established radio-FIR correlation which suggests that the observed 100 micron background would be exceeded if the counts do not turn over below about 100 nanoJy. But, this assumes that the radio – FIR correlation for star forming regions holds at these faint source levels and that the nanoJy population is due to star formation and not to a new population.

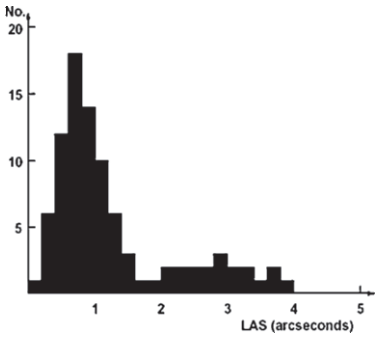


Fig. 2. Distribution of angular sizes in the HDF region

These estimates, however, assume point sources. If, instead, the nanoJy sources have finite angular extent, *natural confusion* may limit the sensitivity of the SKA, independent of the array dimensions. Fig. 2 shows the distribution of angular sizes for microJy radio sources found in a ten arcmin region around the HDF observed at 20 cm [5]. Nearly all sources are resolved by the 0.2 arcmin VLA plus MERLIN beam and have a median angular size about 0.6 arcsec [5]. If the nanoJy sources have comparable sizes to the microJy sources, they will begin to overlap below about 100 nanoJy and this *natural confusion* may limit the ability of the SKA to explore the nanoJy sky.

The EVLA will have up to an order of magnitude improvement in sensitivity over the current VLA, depending on wavelength, while both the EVLA and eMERLIN will give an order of magnitude improvement in resolution at all wavelengths. The EVLA will fill in the missing spacings between the VLA and the VLBA, and together with the VLBA will give continuous coverage of spacings between 30 m and 8000 km, comparable to what is being discussed for the SKA, albeit with much less sensitivity. Deep surveys of hundreds of hours with the EVLA will reach the 100 nanoJy level and give us a better feeling for the source density and angular size of the nanoJy population.

5 Summary

MicroJy radio sources are due to both star formation and AGN, which often appear to coexist in relatively bright galaxies suggesting a causal relation between star formation and the presence of massive black holes. The EVLA will have improved sensitivity and resolution and will begin to characterize the sub-microJy sky. Deep surveys made with the SKA will have sufficient sensitivity to observe radio galaxies, quasars, and active star forming galaxies anywhere in the Universe, and to observe normal galaxies such as the Milky Way out to $z \sim 1$. With more than an order of magnitude improvement in sensitivity over other radio telescopes, deep SKA surveys will have the potential for discovering new phenomena and to raise new questions. However, the SKA will need to have dimensions of at least one thousand to perhaps several thousand kilometers to keep confusion noise below the thermal noise, at least at the longer wavelengths. But, if the nanoJy radio sources have dimensions comparable with galaxies, natural confusion may limit the sensitivity that can be achieved in practice with the SKA. Deep surveys made with the EVLA will begin to probe the sub-microJy sky to better evaluate the potential confusion from both the high source density and finite source size expected at nanoJy levels.

The NRAO is operated by Associated Universities Inc., under a cooperative agreement with the NSF.

References

1. E.A. Richards, K.I. Kellermann, E.B. Fomalont, R.A. Windhorst, R.B. Partridge: AJ **116**, 1039 (1998)
2. E.A. Richards: PASP **112**, 1001 (2000)
3. E.B. Fomalont, K.I. Kellermann, R.B. Partridge, R.A. Windhorst, E.A. Richards: AJ, **123**, 2402 (2002)
4. E.B. Fomalont, K.I. Kellermann, R.B. Partridge, R.A. Windhorst, E.A. Richards: ApJS, in press (2004)
5. T.W.B. Muxlow et al.: MNRAS, in press (2004)
6. E.A. Richards, E.B. Fomalont, K.I. Kellermann, R.A. Windhorst, R.B. Partridge, L.L. Cowie, A.J. Barger: ApJL **526**, L73 (1999)

e-VLBI... a Wide-Field Imaging Instrument with Milliarcsecond Resolution & Microjy Sensitivity

M.A. Garrett

Joint Institute for VLBI in Europe (JIVE), Postbus 2, 7990 AA Dwingeloo, The Netherlands.

Abstract. The European VLBI Network (EVN) is in the process of establishing an e-VLBI array in which the radio telescopes and the EVN correlator at JIVE are connected in real-time, via high-speed national fibre optic networks and the pan-European research network, GÉANT. This paper reports on recent test results, including the production of the first real-time e-VLBI astronomical image. In a parallel and related development, the field-of-view of VLBI is also expanding by many orders of magnitude, and the first results of deep, wide-field surveys capable of detecting many sources simultaneously are summarised. The detection of sources as faint as 10 microJy should soon be possible in the era of "Mk5" and e-VLBI.

1 Introduction to e-VLBI

The application of fibre optic network technology to existing radio telescope facilities (e.g. EVLA & e-MERLIN), will permit these instruments to achieve sub-microJy continuum sensitivity noise levels in very modest integration times (e.g. 12-24 hours). In addition, new telescopes such as LOFAR will employ advanced digital processing techniques, in order to survey huge areas of the sky simultaneously via independently steerable, so-called "multiple" beams.

The VLBI community around the world is also engaged in the first attempts to connect VLBI antennas and correlator centres in real-time (*e-VLBI*) using commercial optical fibre networks (e.g., [2,3]). In addition, improvements in data storage media and the emergence of affordable PC clusters, are poised to transform VLBI into a wide-field, all-sky survey instrument. This paper presents some recent results in these areas, describing technical and scientific developments that are relevant to the SKA.

2 e-VLBI: The First Real-Time e-EVN Image

By definition, VLBI antennas and correlators are separated by many hundreds, indeed thousands of kilometers. Typically they are also located in remote areas, far from centres of population and network services. The goal of connecting together these antennas and correlators is therefore challenging, especially as it also requires connections to be made across national and international boundaries. Despite these difficulties, the prospect of achieving this goal is becoming an increasingly realistic proposition, as advanced national, continental and transcontinental research networks begin to interconnect across the globe.

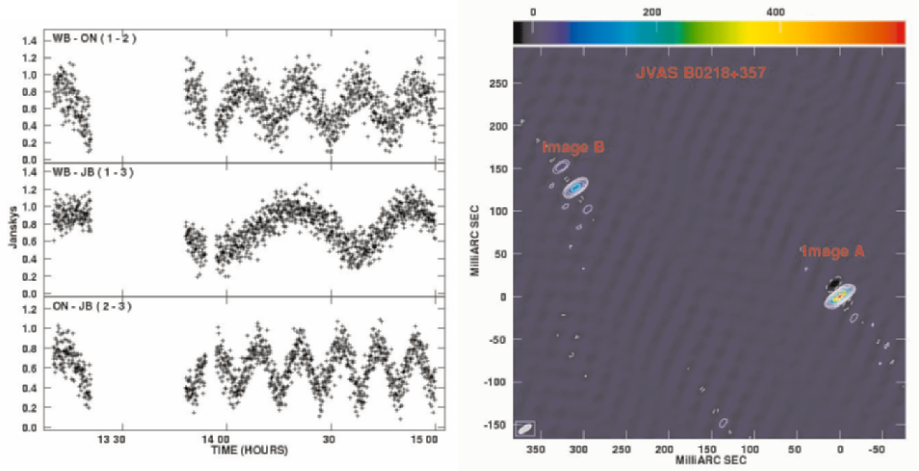


Fig. 1. The first real-time e-EVN image. The target source was the well-known, small-separation gravitational lens system, B0218+357. The lensed images are separated by $\sim$ 334 milliarcseconds.

In Europe, the EVN has entered into a collaboration with the major European National Research Networks (NRENs) and the pan-European research network GÉANT, operated by DANTE. Progress has been aided by the introduction of the new Mk5 PC-based recording systems [3] at the major telescopes across the EVN, including those with good network connections. The first eVLBI tests in Europe began in September 2002, and recently culminated in observations that have included three telescopes (Westerbork, Onsala & Jodrell Bank) simultaneously transmitting data at rates of 32 Mbps to the EVN correlator at JIVE. The first real-time e-VLBI image (see Fig. 1) was produced by this array in April 2004 [2], the data flowing without interruption from the telescopes to the correlator, where fringes were generated at JIVE in real-time. After real-time correlation, the data were automatically processed using the EVN data pipeline. Some plots of the visibility data and the pipelined image are presented in Fig. 1.

In terms of local logistics and network reliability, e-VLBI offers many advantages over conventional VLBI data transport systems. From the astronomers perspective, the prospect of immediate results and unlimited access to the high data rates (currently restricted by the available disk resources) are also important new features. Progress in this area continues as other EVN telescopes come "on-line", including the Torun and Medicina 32-m telescopes.

3 VLBI Sensitivity and Deep Wide-Field VLBI Surveys

The current sensitivity of existing VLBI arrays is "embarrassingly" good. The new Mk5 system currently being introduced across the EVN, permits data rates of 1 Gbps to be recorded robustly and without error. The expectation is that a

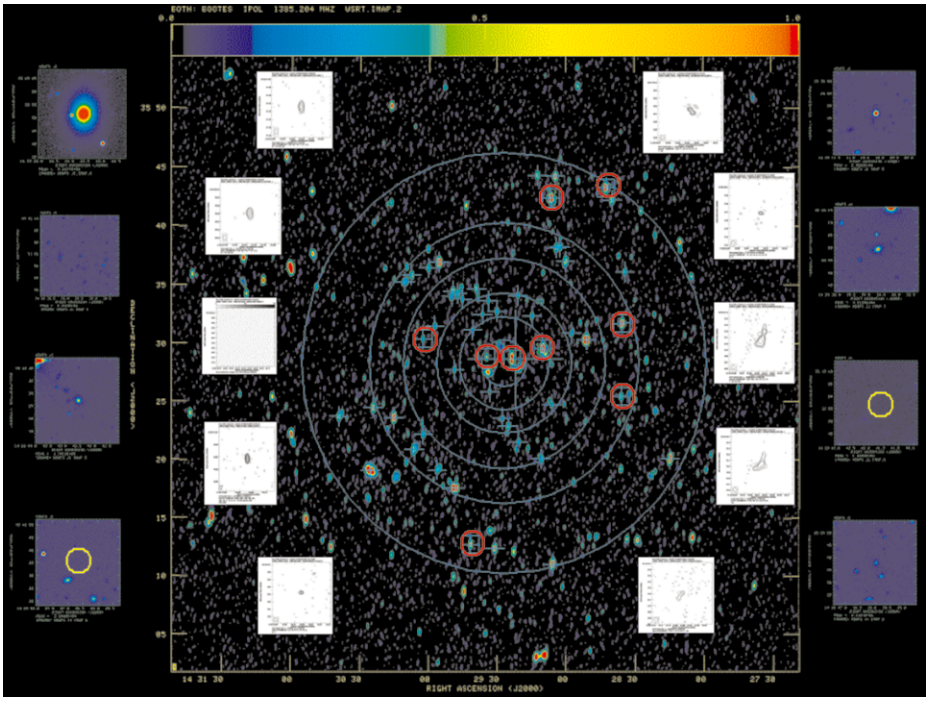


Fig. 2. A wide-field VLBA+GBT survey of part of the NOAO-N Deep Field region. With an r.m.s. noise level of 9 μJy, many sources are detected simultaneously. A significant fraction of radio sources are not detected in the optical images also presented.

global VLBI array, also equipped with Mk5, could achieve $1-\sigma$ r.m.s. noise levels better than a few microJy per beam for an on-source integration time of $\sim$ 24 hours. At these sensitivity levels, VLBI can expect to simultaneously detect many sources within the primary beam of an individual antenna (see Fig. 2). Currently deep, wide-field observations [1], achieve noise levels of 9 microJy/beam and are capable of detecting mJy, sub-mJy and microJy radio sources across the field. The first results indicate that the fraction of radio sources (AGN) detected by VLBI falls from $\sim$ 29% at mJy levels to only 8% at sub-mJy flux density levels. The results are in good agreement with less direct studies – these suggest the emergence of a dominant star-forming radio source population at these faint flux density levels.

Fig. 3 shows an example of the compact radio sources that might be simultaneously detected in a typical region of sky by a Mk5 equipped Global VLBI array, assuming the fractional detection rate of 8% (as observed for sub-mJy sources) is also appropriate for the microJy radio source population. Current and future wide-field VLBI surveys are likely to be highly efficient AGN detectors, and in addition, may be sensitive to cold, very high-redshift, dust-obscured systems that will be difficult to detect in other wave-bands.

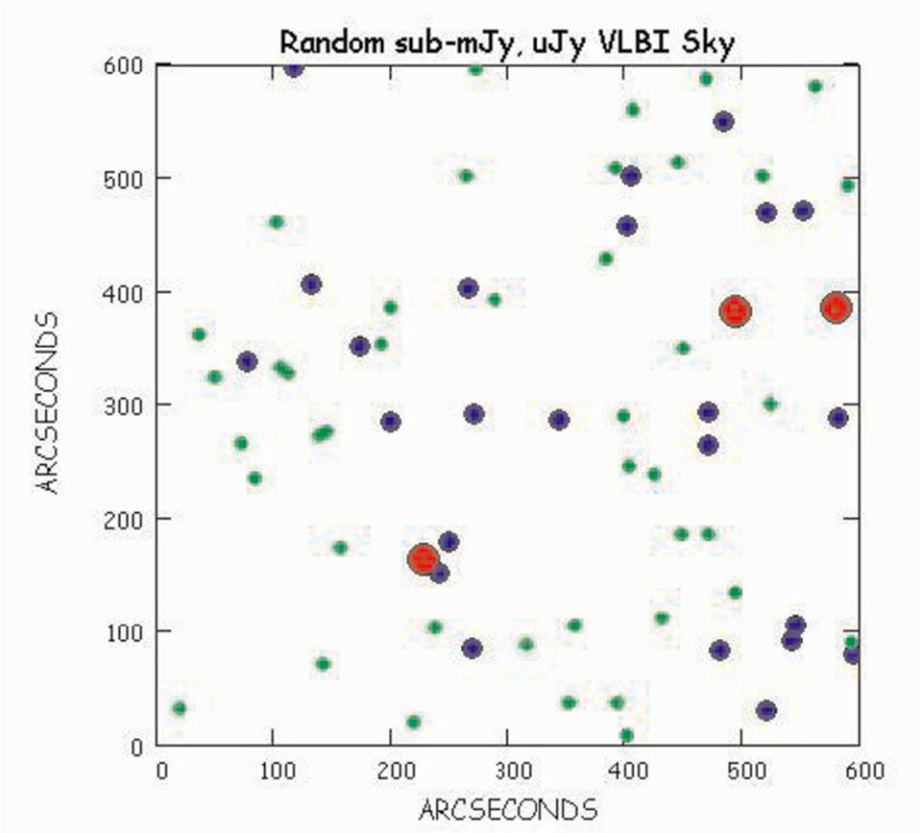


Fig. 3. A view of the faint but compact (AGN) radio sky as viewed by a wide-field global VLBI array. Representation: large dots ($S > 1$ mJy), medium dots ($S \sim 100 - 1000\mu$Jy) and small dots ($S \sim 10 - 100\mu$Jy).

References

1. M.A. Garrett, J.M. Wrobel, R. Morganti: ApJ, submitted (2004) (see also astro-ph/0403642 & astro-ph/0301465)
2. S. Parsley, et al.: IVS 2004 General Meeting Proceedings, edited by N. R. Vandenberg and K. D. Baver, NASA/CP-2004-212255 (2004)
3. A.R. Whitney: New Technologies for VLBI, ed. Y.C. Minh, ASP Conference Series **306**, 123 (2003)

Results from Observations of AGNs with the H·E·S·S· Telescope System and Future Plans

M. Punch for the H·E·S·S· Collaboration

Physique Corpusculaire et Cosmologie, IN2P3/CNRS, Collège de France,
11 Place Marcelin Berthelot, F-75231 Paris Cedex 05, France

Abstract. The H·E·S·S· (High Energy Stereoscopic System) Phase-I is comprised of four Imaging Atmospheric Cherenkov Telescopes (IACTs) for observation of galactic and cosmic sources of Very High Energy (VHE) gamma rays, with a significant improvement in sensitivity and a detection threshold below that of previous IACTs. Observations of Active Galactic Nuclei (AGNs) since the start of operations in June 2002 are presented, in particular for PKS 2155-304 and Mkn 421, along plans for Phase-II.

1 The H·E·S·S· Telescope System

The H·E·S·S· detector for observation of > 100 GeV γ-rays has been operating since June, 2002 in the Khomas highlands of Namibia (23°S, 15°E, 1.8 km a.s.l.). It captures the Cherenkov light emitted by cascades of particles in the atmosphere initiated by a γ-ray or charged cosmic ray incident on the atmosphere. The Cherenkov pulses ($\lambda \sim 350$ nm) are brief (few ns), faint, and illuminate a light-pool of diameter ~ 250 m on the ground for vertical cascades. The Cherenkov images of these cascades, roughly cometary in shape with an angular extent of a few mrad, can be seen by a detector anywhere in the light-pool equipped with a sufficiently fast and sensitive camera. This permits the estimation of the nature of the initiating particle (signal γ-ray or background cosmic-ray) and the measurement of its angular origin and energy. The Atmospheric Cherenkov technique intrinsically has a large (~ 50000 m^2) collection area, though with a small field of view (few degrees). Observations must take place on clear, moonless nights.

The detector, in its Phase-I, consists of four IACTs in a square of side 120 m. Each telescope mount has a tessellated mirror of 107 m^2 area with a camera in the focal plane at 15 m. The camera contains 960 photo-multipliers (PMs) with a $0\overset{\circ}{.}16$ pixel-size and a 5° field of view. The read-out electronics, all contained within the camera, is triggered when the signal from a number of PMs exceeds a trigger threshold in an effective ~ 1.3 ns trigger window. The PM signals, which are stored in an analogue memory while awaiting the trigger, are then read out, digitized, and integrated within a 16 ns window. The results are then sent from the camera's data-acquisition system to the control room via optical fibres.

Soon after the second telescope became operational in January 2003, a 'Stereo' central trigger was implemented (June 2003), by which events are only retained if multiple telescopes see the same cascade. This decreases the dead-time for the individual telescopes, allowing the trigger threshold to be decreased (thus decreasing detector's energy threshold), while the multiple images of each cascade

provide a increase in the background-rejection capability and the angular and energy resolution of the system.

The Phase-I of H·E·S·S· was completed in December, 2003, with the addition of the fourth telescope, since which time the system has been operating at its full sensitivity. The energy threshold of the system is ~ 120 GeV for sources close to Zenith after background rejection cuts (~ 400 GeV for single-telescope mode) with an angular resolution improved to $0.^{\circ}06$ (from $0.^{\circ}1$) and allowing spectral measurements with an energy resolution of $\simeq 15\%$. Observations of the Crab nebula have confirmed the system's performance, with a rate of 10.8 γ/minute and a detection significance of 26.6 $\sigma/\sqrt{\text{hr}}$, which when extrapolated for a sources close to Zenith give a 1 Crab-level sensitivity (5σ detection) in only 30 seconds (1% Crab in 25 hrs). See [1,2] for further details.

2 Observations of AGNs with H·E·S·S·

Since the first operation of the H·E·S·S· detector, many galactic and extragalactic sources have been studied. The observation of AGNs at the highest energies is a probe of the emission mechanisms in the jets of these sources, and studies of the their multi-wavelength spectral energy distributions (SEDs) and correlated variability over wavelength enable emission models (leptonic or hadronic) to be tested. In addition, as these VHE photons interact with the intergalactic Infra-Red (IIR) background (to give an electron-positron pair) and are thus absorbed, they can also serve as a probe of this background (resulting mainly from early star formation) which is difficult to measure by direct means. However, this absorption limits the distance at which we can see AGNs to a redshift 0.5 at the H·E·S·S· detector threshold energy. The large detection area of H·E·S·S· allows us to measure spectral and temporal characteristics on hour timescales (depending on the strength of flares) for the sources seen.

Among the extra-galactic targets (with observing time up to Summer, 2004 in parentheses) are: PKS 2155-304 (92h), PKS 2005-489 (52h), M87 (32h), NGC253 (34h). Here we present results from two AGNs: PKS 2155-304 and Mkn 421.

2.1 The AGN PKS 2155-304

PKS 2155-304 is the brightest AGN in the Southern Hemisphere, and has been well studied in many energy bands over the last 20 years. It has been previously detected at VHE energies [3]. With a redshift of $z = 0.117$ it is one of the most distant VHE blazars, and therefore of interest not only for studies of this class of object, but also for IIR studies.

Initial observations were taken over all the installation phase of H·E·S·S· Phase-I from July 2002 to October 2003, with an evolving detector threshold and sensitivity. Clear detections ($> 5\sigma$) are seen in each night's observations, and an overall signal of 44.9σ in 63.1 h of this mixed data, with ~ 1.2 γ/min, 10-60% Crab level, with variability on time-scales of months, days, and hours. The energy spectra are characterized by a steep power law with a time-averaged photon index of $\alpha = -3.31 \pm 0.06$.

Owing to a particularly high level seen by H·E·S·S· in October, 2003, we triggered our RXTE "target of opportunity" proposal on this source, enabling quasi-simultaneous observations to be taken between the two instruments. Short-term variations (< 30 min) are seen in both these datasets, and multi-wavelength correlations will be published in a forthcoming paper.

A H·E·S·S· multi-wavelength campaign with the PCA instrument on board the Rossi X-ray Timing Explorer (RXTE) has been successfully completed in August, 2004, with the full four-telescope Phase-I array, and therefore full sensitivity, and these data are under analysis. This intense study of this source should yield insights into its inner workings.

2.2 The AGN Mkn 421

Mkn 421 was the first extra-galactic source detected at VHE energies [4]. It is the closest such source (at $z = 0.03$) and so is little affected by IIR absorption. With a declination $\delta \sim 38°$, it is still accessible to H·E·S·S·, though culminating at a Zenith angle above 60°. Under these conditions, observations with the H·E·S·S· detector have a higher threshold, but a compensatory larger effective area (as the light-pool is geometrically larger for showers developing at a greater atmospheric slant distance), and so gives access to the highest energies of the spectrum.

In April of this year, a great increase in activity from this source was seen by the all-sky monitor aboard RXTE, reaching an historically-high level of 110 mCrab in mid-April. A multi-wavelength campaign was therefore triggered on this source, including other IACTs, radio and optical telescopes, and RXTE.

The H·E·S·S· observations, at an average Zenith angle of 62°, provided a very clear signal in April, with 66σ in 9.71 h of data, yielding ~ 5.1 γ/min, and an estimated 1-2 Crab level. The flux clearly increases from the January level (6σ in 2.12 h, ~ 0.8 γ/min, 10-50% Crab level), and was also seen by other IACTs in the Northern hemisphere (Whipple, MAGIC). Shorter-term variations and correlations with other energy domains are currently under study.

3 Future Plans for Expansion to H·E·S·S· Phase-II

Plans for Phase-II of the experiment are comprised of a large telescope in the centre of the current Phase-I (Fig. 1) providing a lowered threshold and increased sensitivity. This will provide access to a number of astrophysical phenomena, such as the spectral cut-offs in pulsars, microquasars, GRBs, and dark matter in the form of WIMPs. As concerns this paper, AGNs can be observed up to redshift of 2-3 with H·E·S·S· Phase-2 (vs. 0.5 with H·E·S·S·), provided that they are sufficiently bright, as the optical depth due to absorption in the intergalactic infra-red background is smaller at lower energies. With detections of a larger number of AGNs at varying redshifts, the effect of IIR absorption may be disentangled from the intrinsic spectra of the sources.

Technical plans for this very-large telescope are well advanced. The mount and dish structure (30m Ø) are well within the capabilities of industry, since



Fig. 1. Photo of the current four-telescope H·E·S·S· Phase-I array, with an artist's impression of the Phase-II 30m Ø telescope in the centre of the array superimposed.

much larger radio-telescopes have been built. The camera, using the same technology as Phase-I, with some improvements in order to decrease the dead-time and readout speed, will have ~ 2000 pixels of size $0.^{\circ}05$ ($\sim 3^{\circ}$field of view). An improved Analogue Memory ASIC (Application-Specific Integrated Circuit) is being prototyped, and the associated camera and read-out electronics are being designed, based on the experience gained with the Phase-I.

In operation with the four telescopes of Phase-I, Monte Carlo simulations indicate that, in coincidence mode the '4+1' system would have a detection threshold of $\sim$ 50GeV with fine-grained and photon-rich image in the central telescope providing improved background rejection and angular and energy resolution. In stand-alone mode, a threshold as low as $15-25$ GeV may be achieved, though with lower background-rejection capability.

4 Conclusions

Phase-I of H·E·S·S· has already provided many interesting new results, of which some of those from extra-galactic sources are presented here. Based on the experience gained with H·E·S·S· Phase-I, a Phase-II extension consisting of a very large Cherenkov Imaging Telescope is being designed, which will provide an unprecedentedly low threshold IACT, while greatly increasing the sensitivity at current energies. H·E·S·S· Phase-I will continue to provide exciting new results in the future, while the Phase-II is being designed and installed.

References

1. W. Hofmann et al.: *Proc. 28th ICRC* (Tsukuba) 2811 (2003)
2. P. Vincent et al.: *Proc. 28th ICRC* (Tsukuba) 2887 (2003)
3. P. Chadwick et al.: ApJ **513**, 161 (1999)
4. M. Punch et al.: Nature **358**, 477 (1992)

The Innermost Regions of AGN with Future mm-VLBI

I. Agudo[1], T.P. Krichbaum[1], U. Bach[1], A. Pagels[1], B.W. Sohn[1], D.A. Graham[1], A. Witzel[1], J.A. Zensus[1], J.L. Gómez[2,3], M. Bremer[4], and M. Grewing[4]

[1] MPIfR, Auf dem Hügel 69, 53121 Bonn, Germany
[2] IAA(CSIC), Apartado 3004, 18080 Granada, Spain
[3] IEEC/CSIC, Edifici Nexus, C/Gran Capità, 2-4, E-08034 Barcelona, Spain
[4] IRAM, Grenoble, 300 Rue de la Piscine, 38406 Saint Martin d'Hères, France

1 mm-VLBI: Astronomy at the Highest Resolution

More than 40 years since the discovery of the AGNs, there are still fundamental questions related to the nature of these intriguing objects. In particular, the accretion processes onto their super-massive black holes and the mechanisms through which their relativistic jets are formed, accelerated and collimated are still not well understood. Great effort has been made during the last decade to push the mm-VLBI technique to progressively shorter wavelengths, offering the best tool to observe the innermost regions of the jets and study the physics involved in their behaviour.

At present, the most sensitive mm-VLBI instrument is the Global mm-VLBI Array, composed of the Effelsberg, Plateau de Bure, Pico Veleta, Onsala and Metsähovi stations, in addition to eight of the ten VLBA antennas (for more details see *http://www.mpifr-bonn.mpg.de/div/vlbi/globalmm*). The Global mm-VLBI Array reaches a baseline sensitivity of 38 mJy (adopting 20 s coherence time, 100 s segmentation time and a sampling rate of 512 Mbps [2bits]). This yields an image sensitivity of ~ 0.85 mJy (for 12 h of observation and a duty cycle of 0.5). With these characteristics the number of sources which could be imaged with high dynamic ranges ($\geq$500:1) is nowadays larger than 100.

In an attempt to obtain a deeper knowledge of the physics in the innermost regions of jets in AGNs, we have started a VLBI monitoring, at 3mm, of some of the brighter-most sources. Fig. 1 represents some of the images from these observations (still in progress). The images demonstrate the capability of the Global mm-VLBI Array to study the innermost jet structures with an angular resolution better than 50 μas.

2 The Future: Higher Sensitivity and Image Fidelity

In order to achieve a better quality of images and increase the number of sources that can be observed, a further increase in sensitivity is still needed. To do that, the most direct way is to increase the collecting area of the present interferometer. For the near future, ALMA, the GBT, the LMT, CARMA, SRT, Yebes,

Nobeyama and Noto are some of the most sensitive stations suitable to participate in mm-VLBI. This future array, together with the present Global mm-VLBI Array, would achieve baseline sensitivities of up to 3 mJy (assuming 1 Gbps recording rate and 100 s segmented integration time), and an image sensitivity better than 0.07 mJy. These estimates predict a large increase, by a factor of 13, with respect to the present Global mm-VLBI Array levels of sensitivity. In addition, continuous development of VLBI will provide standard recording rates of at least 2 Gbps in the next years, which will increase the expected sensitivities by an extra factor $\geq \sqrt{2}$. Further significant improvements in coherence time can be reached by atmospheric phase correction methods.

But the proposed future array will not only influence the sensitivity. The new stations will also largely improve the UV-coverage, and so the image fidelity. The addition of ALMA will improve the UV-coverage for sources with low declination (less than 20°) and facilitate the VLBI imaging of the Galactic Centre source SgrA*. With these improvements, dynamic ranges of ≥1000:1 could be easily obtained. This will place mm-VLBI at comparable levels of sensitivity and image fidelity than present day cm-VLBI.

3 Science with Future mm-VLBI

The expected improvements in sensitivity and image fidelity would impact our knowledge of the physics of jets and central engines in AGNs. It would be possible to obtain high quality images of the innermost regions in the jets. This would facilitate, for several hundreds or even thousands of compact sources (i) to investigate the MHD physics in strong gravitational fields, (ii) to study the formation, initial acceleration and collimation of relativistic jets, (iii) to probe their initial magnetic field configurations (via polarimetry) and (iv) to infer the properties of the super-massive black holes and their immediate vicinity.

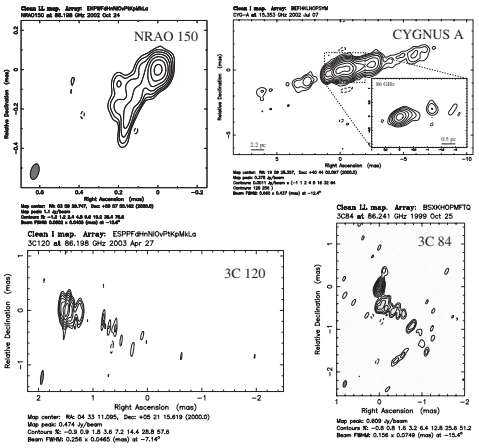


Fig. 1. 3mm-VLBI images of NRAO150, Cygnus A, 3C 120 and 3C 84.

Probing the Gravitational Redshift Effect from the Relativistic Jets of Compact AGN

T.G. Arshakian[1,⋆]

Max-Planck-Institut für Radioastronomie, Auf dem Hügel 69, 53121 Bonn, Germany

Abstract. I explore a possibility to measure the gravitational redshift (GR) effect in the gravitational field of massive central nuclei residing in active galaxies (AGN). The activity of central nuclei is associated with the bipolar jet ejection of relativistic plasma which produces strong radio emission. I consider the behavior of the flux density variations of the jet plasma as a result of GR effect, and I discuss possibilities to detect the GR effect from the relativistic jets of compact AGN with present and future radio facilities.

1 Introduction

Development of new astronomical facilities provides high resolution and sensitivity thus allowing one to reach the scales where the General Relativity effects can be tested. There is already compelling evidence that active galaxies host super massive black holes (SMBH) reaching up to $\sim 10^{10}$ solar masses. The central active nuclei are associated with the relativistic jets which originate near the central nuclei and move out with relativistic speeds exceeding $0.9\,c$. The jet plasma radiates strong synchrotron radio emission which is detectable on parsec-scales by very large baseline interferometry (VLBI). Here, we consider the flux-density variation of the jet plasma due to the GR effect, and the possibility of its detection by present and future radio-astronomical facilities.

2 Flux Variation of the Relativistic Jet

Suppose that the jet plasma component radiating a power law spectrum $F_{\rm e}(\nu) \sim \nu^{-\alpha}$ (α is the spectral index) moves in the gravitational field of SMBH with a speed β in a direction with an angle θ to the line of sight of the observer. Then the observed flux at a time t depends on the Doppler factor $\delta_{\rm t}(\beta;\theta)$ of the component and the distance of the component from the SMBH at t, $R_{\rm t}$,

$$F_{\rm t}(\nu) = k_{\rm t}^{3+\alpha}\, F_{\rm e}(\nu); \quad k_{\rm t} = \frac{\delta_{\rm t}}{1+z}\left(1-\frac{R_{\rm s}}{R_{\rm t}}\right)^{1/2}; \tag{1}$$

where $R_{\rm s}$ and z are the Schwarzschild radius of the SMBH and its redshift. The detected flux density may vary as a result of deceleration or acceleration of the jet component, bending of the jet and intrinsic or extrinsic variability of radio emission. To investigate the pure effect of the GR on the flux density variation, we assume, that the $F_{\rm e}(\nu)$ and $\delta_{\rm t}$ remain unchangeable in time. At a

⋆ On leave from Byurakan Astrophysical Observatory, Byurakan 378433, Armenia

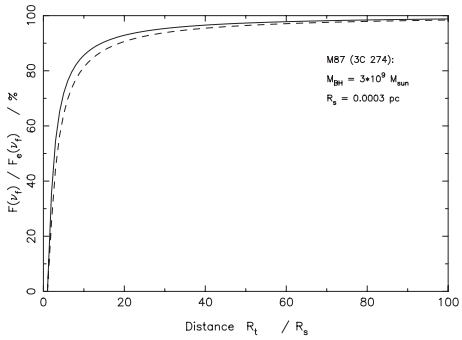


Fig. 1. The observed flux density normalized to the intrinsic flux density of the jet component versus its distance (in R_s units) from the SMBH. Amplification of the flux density due to GR effect is shown for a flat $\alpha = 0$ (solid line) and steep $\alpha = 1$ (dashed line) spectra.

fixed frequency ν_f, the detected flux density $F(\nu_\mathrm{f})$ of the jet component grows with R_t (Fig. 1) reaching up to 90 % of its intrinsic flux density at $\sim 20R_\mathrm{s}$, and then gradually approaches to ~ 100 % at $\sim 100R_\mathrm{s}$.

3 Prospects of Detecting the GR

Seven millimeter VLBI[1] (43 GHz) can achieve an angular resolution of $\sim 70\,\mu$as corresponding to a spatial resolution of $0.0058\,\mathrm{pc} \simeq 19R_\mathrm{s}$ for M87[2]. Full coverage global mm-VLBI imaging with more sensitive radio telescopes will allow even more detailed and better quality images[1]. Present high-resolution multi-epoch mm-VLBI imaging of M87 is capable of detecting ~ 10 % flux density variations (Fig. 1) from the relativistic jet plasma at $\sim$ (15 to 100)R_s due only to GR effect.

At lower frequency, a global VLBI array enhanced by the SKA will allow one to study the nearest weak AGN which previously were unreachable by VLBI due to their faintness. The next generation space-VLBI mission VSOP-2[3] will achieve the highest resolution of 38 μas at 43 GHz, which is twice as high ($\sim 10R_\mathrm{s}$ for M87) as the resolution of a present mm-VLBI. The resolution of a global sub-mm-VLBI[1] at 230 GHz will be $< 30\,\mu$as which is comparable with the resolution of future space-VLBI missions. The global sub-mm-VLBI combined with ALMA can achieve the unprecedented angular resolution of $\sim 10\,\mu$as ($\sim 3\,R_\mathrm{s}$ for M87!) allowing the gravitational effects to be tested in the vicinity of SMBH thus providing additional test for the theory of general relativity and a new method for measuring the masses of SMBH.

TGA is grateful to the AvH Foundation for a Humboldt Fellowship, and to Drs. T. Krichbaum, A. Lobanov and A. Polatidis for useful discussions.

[1] Krichbaum et al., these proceedings

[2] M87 (3C 274) has a radio bright core-jet structure, $z = 0.0044$ ($D \sim 17.1$ Mpc, for a flat cosmology with $H_0 = 70$ km s^{-1}Mpc^{-1}), $M_\mathrm{BH} \sim 3 \times 10^9\,M_\odot$ ($R_\mathrm{s} = 0.0003$ pc)

[3] Hirabayashi et al., these proceedings

VLBA Surveys and Preparation of the "RADIOASTRON" Mission

A. Chuprikov and I. Guirin

Astro Space Center of P.N.Lebedev Physical Institute, 117997, 84/32 Profsoyuznaya, Moscow, Russia

Abstract. Preparation of Space VLBI (SVLBI) mission titled RADIOASTRON (see *http://www.asc.rssi.ru/radioastron/index.html*) requires, particularly, the developing of new software methods for data processing. We present the *Multi Frequency Synthesis (MFS)* method. Maps of 2 sources from the RADIOASTRON listing had been observed with VLBA in 2 and 8 GHz bands simultaneously are demonstrated. We have used the MFS method to reconstruct 5 GHz images of these sources.

The orbit of RADIOASTRON has a period of 9.5 days and eccentricity to be equal to 0.853. Hence, the semi-major axis of this orbit is 189000 km. A very serious problem of high orbit SVLBI mission is a poor (u,v)-plane coverage. It is proposed to use a broad frequency band to solve this problem partially. Such MFS method is developed in our laboratory and has already been included into the software titled *Astro Space Locator (ASL for Windows)*. VLBA data are used to test this method. Fig. 1 demonstrates the reconstructed milliarcsecond scale images of two bright quasars, J0555+3948 and J0530+1331.

The current version of RADIOASTRON source listing consists of 209 sources. Many of them have been observed during the VLBA sessions titled RDV14 - RDV17 and also during VLBA session titled RDGEO. Processing of this data is being continued. Some results could be found in the following Internet site :

http://kenga.asc.rssi.ru/asl/index.asp.

Thus, we have good results of application of the MFS method to Ground VLBI data. Fig. 2 demonstrates the simulated MFS (u,v)-plane for SVLBI data. It is clear, that this coverage is improved due to usage of MFS method.

The ASL software is free and could be easily installed in any PC-computer. See *http://platon.asc.rssi.ru/DPD/ASL/asl.html*

Acknowledgments

We thank Leonid Petrov (Goddard Space Center, NASA, USA) for the permission to use his data. We express our gratitude to Dr. Nikolai Kardashev and to Dr. Sergey Likhachev (Astro Space Center) for extensive consultation.

This research is partially supported by the Russian Fund of Basic Research through the Grant No. 03-02-16580-a

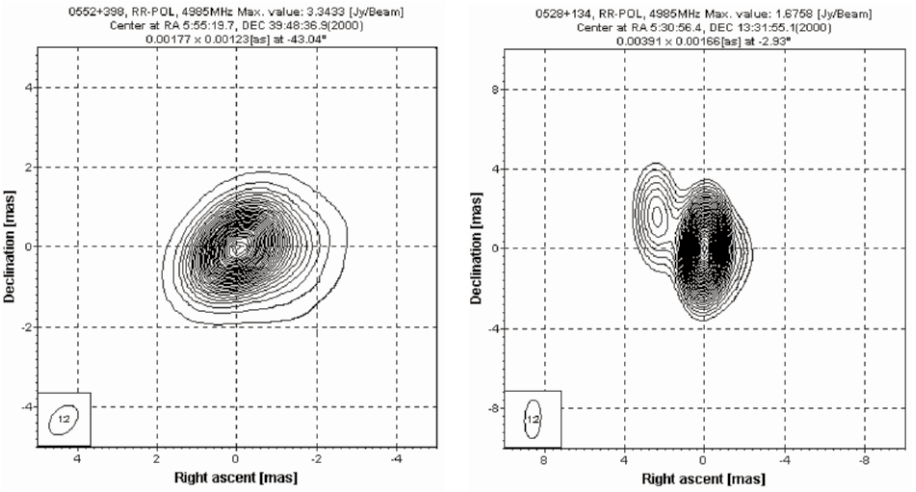


Fig. 1. Left: The reconstructed C-band MFS image of core of J0555+3948.RDGEO VLBA observational session. **Right:** The reconstructed C-band MFS image of core of J0530+1331. RDV14 VLBA observational session.

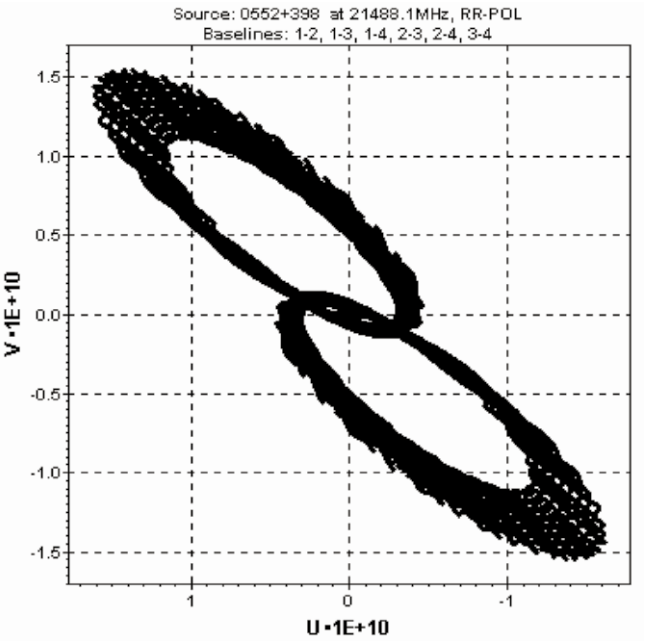


Fig. 2. The simulated K-band MFS (u,v)-plane for J0555+3948. Parameters of MFS procedure could be found in ASC site mentioned above

The Radio Properties of Low Power BL Lacs

M. Giroletti[1,2] and G. Giovannini[1,2]

[1] Istituto di Radioastronomia, via Gobetti 101, 40129, Bologna, Italy
[2] Dip. di Astronomia, Università di Bologna, via Ranzani 1, 40127 Bologna, Italy

We have selected a sample of nearby ($z < 0.2$) BL Lacs, in order to extend the current knowledge on radio loud AGN to low redshift, weak objects and to test the unified scheme in the low luminosity range. Hubble Space Telescope observations have been previously presented [2], as well as radio observations of a few well known objects. After collecting the main results from the literature, we have obtained new observations, resulting in a complete set of parsec and kiloparsec scale images of all the objects in the sample. From the analysis of these data, we obtain the following main results [1]:

Morphology on kpc scale: objects are typically dominated by a compact core, although not as extremely as other brighter samples. The mean core dominance parameter is $\langle R \rangle = 3.2$. Therefore, the core is frequently associated to a resolved radio morphology, including halos, secondary components, and symmetric two-sided jets; this suggests that kiloparsec scale jets may have different properties, being either non-relativistic or still mildly relativistic in different sources. This suggests that the decrease in jet velocity is related to the ISM properties, which can vary among galaxies. Finally, a few objects show a Head Tail morphology, suggesting that they are radio galaxies belonging to galaxy clusters.

Morphology on parsec scale: most of the arcsecond core flux density is present in our VLBA or EVN images, which implies that we have not missed considerable sub-arcsecond structure. The largest fraction of flux density is in a parsec scale core, occasionally associated to one-sided jets; many extremely weak objects possess however only a few mJy core. When a jet is present, it does not show evidence of large bending, although some remarkable exceptions do exist (e.g., Markarian 501 [3]). The kiloparsec scale structure is also quite well aligned with the inner direction, showing little or no bending (typically $< 30°$). This fact makes nearby BL Lacs quite different from, e.g., the objects in the 1 Jy sample.

Beaming factors and Parent population: radio emission presents the features characteristic of relativistic beaming; the study of the core dominance, jet/counter-jet ratio, SSC model yields consistent results, with Doppler factors in the range $1 < \delta < 10$. Given the observed radio properties, we conclude that our BL Lacs are clearly aligned objects, as expected by the unified schemes. De-beaming the observed radio power, and considering isotropic properties such as the low frequency radio power and host galaxy properties, we do not find any

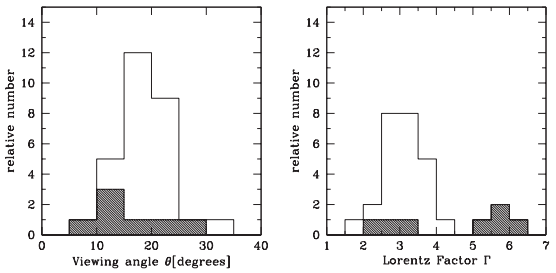


Fig. 1. Distribution of the resulting viewing angle θ and the Lorentz factor Γ, assuming $\Gamma \sim 1/\theta$; the shaded parts correspond to LBL only

difference with Fanaroff-Riley I radio galaxies [4]. None of our low redshift BL Lac requires an FR II as misaligned counterpart.

HBL and LBL: although our sample is mostly composed of High frequency peaked BL Lacs, it also contains seven Low frequency peaked objects, whose properties are slightly different; they are more powerful, core-dominated, and brighter. Under the assumption that all jets possess the same Lorentz factor (e.g. $\Gamma = 5$), LBL need to be oriented at smaller viewing angles than HBL; by contrast, if we allow both Γ and θ to vary, we derive similar orientation and a difference in velocity (see Fig. 1): interestingly, LBL would have larger bulk velocities (up to $\Gamma \sim 7$) than HBL, including TeV sources ($\langle\Gamma\rangle \sim 3$). In both cases, the Doppler factor of BL Lacs is considerably smaller in radio jets than in the γ-ray emitting region.

Future developments: the present work raises questions that can not be answered with the current data. Future instruments need to have better resolution and sensitivity, in order to address the following issues:

- How common is the presence of low brightness, extended emission regions? Are they halos, lobes, relics of previous phase of activity? What are the characteristics of the emitting particles (e.g. spectral age)?
- What are the physical properties of the inner jet? Do jets have dual velocity structure (e.g. fast spine and slow shear layer)?
- What happens on intermediate scale? Where and why does the jet lose its collimation?

References

1. M. Giroletti, et al.: ApJ, in press, astro-ph/0406255
2. R. Falomo, et al.: ApJ **542**, 731 (2000)
3. M. Giroletti, et al.: ApJ **600**, 127 (2004)
4. G. Giovannini, et al.: ApJ **552**, 508 (2001)

Probes of Jet-Disk-Coupling in AGN from Combined VLBI and X-Ray Observations

M. Kadler[1], J.Kerp[2], E. Ros[1], K.A. Weaver[3], and J.A. Zensus[1]

[1] Max-Planck-Institut für Radioastronomie, Auf dem Hügel 69, D-53121 Bonn, Germany
[2] Radioastronomisches Institut, Universität Bonn, Auf dem Hügel 71, D-53121 Bonn, Germany
[3] Laboratory for High Energy Astrophysics, NASA/Goddard Space Flight Center, Greenbelt, MD 20771, U.S.A.

Abstract. The formation of powerful extragalactic jets is not well understood at present as well as the associated key question:"What makes an AGN radio loud?". Here we discuss how the combination of VLBI and X-ray spectroscopic observations allows the inter-relation between the accretion flow and the formation of relativistic jets in AGN to be explored.

The Present: The nearby radio-loud core-dominated active galaxy NGC 1052 exhibits strong, relativistically broadened iron-line emission at X-ray frequencies [1]. Pronounced variability of the broad iron line was accompanied by an ejection of relativistic plasma into the radio jet in early 2000. This behaviour can be interpreted as an instability of the inner accretion disk around the central supermassive black hole, which triggered enhanced accretion onto the black hole, while a fraction of the inner-disk material was injected into the jet. The observations demonstrate that the combined analysis of VLBI and X-ray spectroscopic data allows the interplay of black hole accretion dynamics and jet production in active galaxies to be studied directly.

The Future: NGC 1052 is the only AGN with strong broad iron line emission and a bright, compact radio jet detected so far. This makes NGC 1052 the key object for future studies to address the open questions of black hole accretion and jet formation. A dedicated monitoring campaign of NGC 1052 with I) high frequency VLBI observations and II) high signal-to-noise X-ray spectroscopic observations provides a straightforward way to study the correlation between black-hole mass accretion and jet production.

The performance of VLBI observations is being continuously improved towards higher frequencies (yielding higher angular resolution) and higher sensitivities. Particularly, the upcoming Square Kilometer Array (SKA), if capable of operating at high frequencies with long baselines, will provide a breakthrough in sensitivity. This will allow a much larger number of AGNs, particularly some radio-quiet (i.e., weak) objects, to be studied.

A significant improvement of black-hole accretion and jet formation studies in AGN will come from future X-ray observatories. In Fig. 1, we show simulated

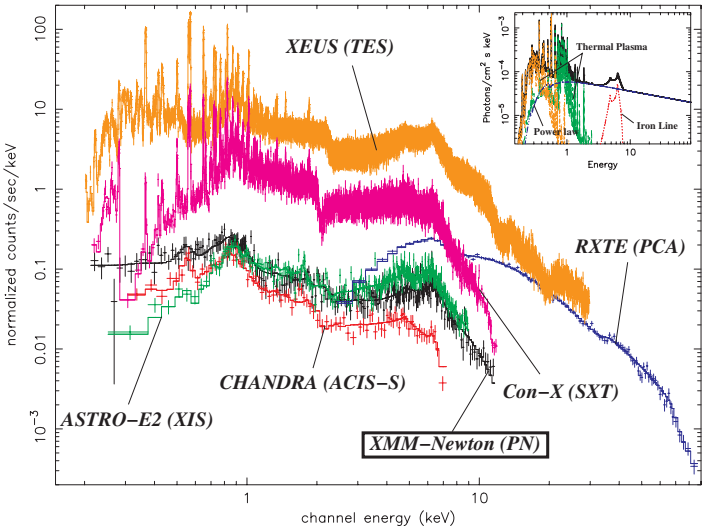


Fig. 1. The measured 13 ksec *XMM-Newton* spectrum of NGC 1052 (Kadler et al. 2004) and simulated 13 ksec spectra from *CHANDRA*, *RXTE*, *ASTRO-E2*, *XEUS*, and *Con-X*. The spectral model consisting of absorbed plasma, power-law, and iron-line emission is shown in the inset panel.

NGC 1052 X-ray spectra of current and future X-ray telescopes in comparison to a measured *XMM-Newton* spectrum [1]. *ASTRO-E2* (Hajime 2003), which will be launched in early 2005, will yield high X-ray spectral resolution throughout the iron line emission energy range. With *Constellation-X* [3] and *XEUS* [4] the sensitivity of broad iron line studies will increase dramatically. This will turn up other radio-loud AGN with considerable broad iron line emission. Direct comparison of the accretion flow properties in radio-loud and radio-quiet AGN will allow the unsolved mystery of the radio loud/quiet phenomenon to be attacked, or in other words to address the question: "What leads some supermassive black holes to launch powerful relativistic jets?"

References

1. M. Kadler, E. Ros, K.A. Weaver, J. Kerp, J.A. Zensus: BAAS **36**, No. 2, 823 (2004)
2. I. Hajime, *X-Ray and Gamma-Ray Telescopes and Instruments for Astronomy*, J. E. Truemper, H. D. Tananbaum (eds.), Proc. SPIE **4851**, 289 (2003)
3. N.E. White, H.D. Tananbaum: *X-Ray and Gamma-Ray Telescopes and Instruments for Astronomy*, J. E. Truemper, H. D. Tananbaum (eds.), Proc. SPIE **4851**, 293 (2003)
4. A. Parmar, G. Hasinger, M. Turner: *34th COSPAR Scientific Assembly, The Second World Space Congress, held 10-19 October, 2002 in Houston, TX, USA*, p. 2368 (2004)

Towards the Event Horizon: High Resolution VLBI Imaging of Nuclei of Active Galaxies

T.P. Krichbaum[1], D.A. Graham[1], A. Witzel[1], J.A. Zensus[1], A. Greve[2], M. Grewing[2], M. Bremer[2], S. Doeleman[3], R.B. Phillips[3], A.E.E. Rogers[3], H. Fagg[4], P. Strittmatter[4], and L. Ziurys[4]

[1] Max-Planck-Institut für Radioastronomie, Bonn, Germany
[2] Institut de Radioastronomie Millimétrique, Grenoble, France
[3] MIT-Haystack Observatory, Westford, MA, USA
[4] Steward Observatory, University of Arizona, Tucson, AZ, USA

1. Introduction

Very Long Baseline Interferometry at millimetre wavelengths (mm-VLBI) allows to image compact galactic and extragalactic radio sources with micro-arcsecond resolution, unreachable by other astronomical observing techniques. Future global VLBI at millimetre wavelengths therefore should allow to map,with a spatial resolution of only a few to a few ten gravitational radii, the direct vicinity of the Super Massive Black Holes (SMBH) located in the centres of nearby galaxies. With the reduced intrinsic self-absorption at short wavelengths, mm-VLBI opens a direct view onto the often jet-producing "central engine".

Here we report on new developments in mm-VLBI, with emphasis on experiments performed at the highest frequencies possible to date. We demonstrate that global VLBI at 150 and 230 GHz now is technically feasible and yields source detections with an angular resolution as high as 25–30 μas. The combination of the existing with future telescopes (e.g. CARMA, ALMA, LMT, etc.) will improve present day imaging capabilities by a large factor. Within the next decade, one therefore could expect direct images of galactic and extragalactic (super massive) Black Holes and their emanating outflows.

2. Imaging the Jet Base of M87 with 20 R_S

Since 2002, the Global mm-VLBI Array observes regularly at 86 GHz (URL: www.mpifr-bonn.mpg.de/globalmm, cf. Agudo et al., this conference). It combines the large European antennas (30 m Pico Veleta, 6x15 m Plateau de Bure, 100 m Effelsberg, etc.) with the VLBA, and offers a factor of $3-4$ higher sensitivity than the VLBA alone. As an example, we show in a new global-VLBI image of the inner jet of M87 at 86 GHz (Fig. 3). At a distance of 18.7 Mpc, the angular resolution of 300×60 μas corresponds to a spatial scale of 30×6 light days, or 100×20 Schwarzschild-radii (assuming 3×10^6 $M_\odot$ for the SMBH). The existence of a fully developed jet on such small spatial scales gives important new constraints for the theory of jet formation and may even indicate rotation of the central SMBH (via comparison with the width of the light cylinder).

3. Towards Shorter Wavelengths - VLBI at 2 and 1 mm

A convincing demonstration of the feasibility of VLBI at wavelengths shorter

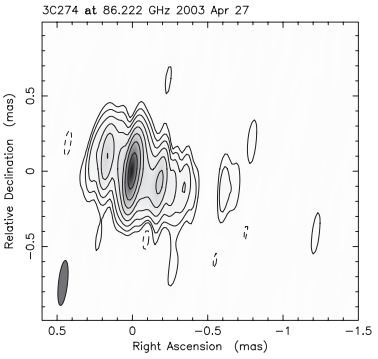


Fig. 1. VLBI image of M87 (3C 274) obtained in April 2003 at 86 GHz with the global mm-array. Contour levels are -0.5, 0.5, 1, 2, 4, 8, 16, 32, and 64 % of the peak flux of 0.79 Jy/beam. The beam size is 0.30 x 0.06 mas, pa=-6.3°. The identification of the easternmost jet component as VLBI core or as part of a counter-jet is still uncertain.

than 3 mm was made at 2 mm (147 GHz) in 2001 and 2002. These first 2 mm-VLBI experiments resulted in detections of about one dozen quasars on the short continental and long transatlantic baselines (participating telescopes: Pico Veleta - Spain; Metsähovi - Finland; Heinrich-Hertz and Kitt Peak telescope - Arizona, USA). A big success was the detection of 3 quasars on the 4.2 Gλ long transatlantic baseline between Pico Veleta and the Heinrich-Hertz Telescope: NRAO150 (SNR=7), 1633+382 (SNR=23) and 3C279 (SNR=75). Motivated by this success, the observations were repeated in April 2003, this time at 1.3 mm (230 GHz). Now also the phased IRAM interferometer on Plateau de Bure (France) participated. On the 1150 km long baseline between Pico Veleta and Plateau de Bure the following sources were detected: NRAO 150, 3C 120, 0420-014, 0736+017, 0716+714, OJ287, 3C 273, 3C 279, and BL Lac. On the 6.4 Gλ long transatlantic baseline between Europe and Arizona fringes for the quasar 3C454.3 (SNR=7.3) were clearly seen. For the BL Lac object 0716+714, however, only a marginal detection (SNR=6.8) was obtained. These transatlantic detections mark a new record in angular resolution in Astronomy (size $< 30\mu$as). They indicate the existence of ultra compact emission regions in AGN even at the highest frequencies (for 3C454.3 at z=0.859, the rest frame frequency is 428 GHz). So far, we find no evidence for a reduced brightness temperature of the VLBI-cores at mm-wavelengths, however some variability is possible.

4. Future Outlook

Good quality micro-arcsecond resolution VLBI images of the nuclei of galaxies will require an increased array sensitivity and better uv-coverage. The addition of large and sensitive mm-telescopes like CARMA, ALMA, the LMT, etc. to the existing VLBI antennas will be crucial for the future success of VLBI at and below 1 mm. The ongoing development towards observations with much larger larger bandwidths (several Gbits/s), and for instantaneous atmospheric phase corrections and coherence prolongation (e.g. via water vapor radiometry), will further enhance the sensitivity. Thus one can hope that within less than a decade from now, the detailed imaging of the 'event horizon' of SMBHs and a better understanding of the coupling between 'central engine' and jet will become possible.

Two-Component Model for the AGN Broad Line Region

L.Č. Popović[1,2]

[1] Astronomical Observatory Belgrade, Volgina 7, 11160 Belgrade, Serbia
[2] Astrophysikalisches Institut Potsdam, An der Sternwarte 16, 14482 Potsdam, Germany (Alexander von Humboldt Fellow)

Abstract. In order to explain the complex broad lines of AGNs, we apply the two-component model assuming that the line wings originated in a very broad line region (VBLR) and line core in an intermediate line region (ILR). The VBLR is assumed to be an accretion disk and ILR a spherical region. Such a model can very well fit complex broad lines of AGNs

1 Introduction

The motivations to develop a two-component model for Broad Line Regions (BLRs) of Active Galactic Nuclei (AGNs) are: (a) a statistically significant difference between the Full Width at Zero Intensity (FWZI) distributions of the Lyα and Hβ lines in QSO spectra [1] that provides additional evidence of an optically thin Very Broad Line Region (VBLR, which might be a disk or disk-like region) which contributes to the line wings. It is located interior to an Intermediate Line Region (ILR) which produces the profile cores; (b) a correlation weakness of the widths and asymmetries between the UV lines and the Hβ line, suggesting a stratified structure of the Broad Line Region (BLR), consistent with the variability studies of Seyfert 1 galaxies [2]; (c) from investigation of the physical processes in BLRs using a Boltzmann-plot method [3] it was found that probably physical conditions in the regions which contribute to the line core and line wings are different; (d) a smaller average FWHM value of the UV lines compared to the Hβ line indicates that they have a higher relative contribution of ILR emission, versus a more dominant VBLR component in the Balmer lines.

Here we present a two-component model for fitting the single peaked broad emission lines of AGNs – Sy1 and QSOs – in order to investigate the structure of emission line regions and to find evidence that suggests that the disk emission can contribute to the line emission (even if they have single-peaked line profiles).

2 The Model and Its Application

A two-component model can be represented by different geometries, here we choose the one with: a disk giving the wings of the lines, and a spherical medium giving the core of the lines.

For the disk we use the Keplerian relativistic model given in Ref. [4]. The emissivity of the disk as a function of radius, R, is given by $\epsilon = \epsilon_0 R^{-p}$. Since the

illumination is due to a point source radiating isotropically, located at the center of the disk, the flux in the outer disk at different radii should vary as r^{-3} [5,6]. Therefore we will start fitting by imposing the constraint $p = 3$.

The local broadening parameter (σ) and shift (z_l) within the disk have been taken into account as in [7], i.e. the δ function has been replaced by a Gaussian function:

$$\delta \rightarrow \exp \frac{(\lambda - \lambda_0 - z_l)^2}{2\sigma^2}.$$

On the other hand, we assume that the kinematics of the additional emission region can be described as the emission of a spherical region with an isotropic velocity distribution, i.e. with a local broadening w_G and shift z_G. Consequently, the emission line profile can be described by a Gaussian function. The whole line profile can be described by the relation:

$$I(\lambda) = I_{AD}(\lambda) + I_G(\lambda)$$

where $I_{AD}(\lambda)$, $I_G(\lambda)$ are the emissions of the relativistic accretion disk and of an additional region, respectively.

We applied the model to spectra of several AGNs, the model can well explain the complex Hα and Hβ line shapes. The results and more details about the model can be found in Refs. [8–11].

Acknowledgements

The work was supported by the Ministry of Science of Serbia through the project P1196 "Astrophysical Spectroscopy of Extragalactic Objects" and Alexander von Humboldt Foundation through the program for foreign scholars.

References

1. M. R. Corbin, T. A. Boroson: ApJS **107**, 69 (1996)
2. W. Kollatschny: A&A **407**, 461 (2003)
3. L. Č. Popović: ApJ **599**, 140 (2003)
4. K. Chen, J.P. Halpern, A.V. Filippenko: ApJ **339**, 742 (1989)
5. M. Eracleous, J.P. Halpern: ApJS **90**, 1 (1994)
6. M. Eracleous, J.P. Halpern: ApJ **599**, 886 (2003)
7. K. Chen, J.P. Halpern: ApJ **344**, 115 (1989)
8. L. Č. Popović, E.G. Mediavlilla, E. Bon, N. Stanić, A. Kubičela: ApJ **599**, 185 (2003)
9. L. Č. Popović, E.G. Mediavlilla, A. Kubičela, P. Jovanović: A&A **390**, 473 (2002)
10. L. Č. Popović, N. Stanić, E. Bon: A&A **367**, 780 (2001)
11. L. Č. Popović, E.G. Mediavlilla, E. Bon, D. Ilić: A&A, accepted (astro-ph/0405447)









Less formal dimensions of the conference dinner

Part V

ISM and Formation and Evolution of Stars

The Physics and Chemistry of High Mass Star Formation with ALMA

T.L. Wilson

European Southern Observatory, Garching, Germany

Abstract. The study of massive star formation is crucial for the understanding of the development of galaxies, as well as the Chemical Evolution of our galaxy. This study is at an early stage. The Atacama Large Millimeter Array (ALMA) will provide complete, high sensitivity, high angular resolution images of quasi-thermal dust and molecular line emission in protostellar objects. The data will have unprecedented quality, far exceeding what is now possible.

1 Inroduction

Stars with masses larger than 5 $M_\odot$ inject a disproportionate amount of turbulence in the ISM throughout their lives. If these objects end their lives as SNe, a large amount of heavier elements is injected in to the ISM [1]. Apparently formation involves groups of stars, and is probably the result of triggered star formation [2]. Near the Sun, there are hundreds of low mass stars for every high mass star [3]. Observationally, the study of high mass stars is attractive because these are bright sources associated with complex *Hot Core* chemistry [4]. Orion KL is the Hot Core closest to the Sun, at D=500 pc [5]. Another region, W3, at D=1.8 kpc, contains many stages of high mass star formation. Later stages include developed H II regions, compact, ultra-compact and hypercompact H II regions; earlier stages include molecular outflows, H_2O masers and sub-mm maxima [6]. With VLA images one measures the dynamics and distribution of ionized gas on sub-arcsecond scales. However, there are no comparable images of molecular line and dust continuum emission. In isolated sources, with increasing angular resolution, one finds evidence for fragmentation [7]. With subarcsecond resolution, we could measure quasi-thermal emission on linear scales of 10^3 Astronomical Units, so direct comparisons of dynamical and chemical processes with models are possible.

2 Models and Results

The present scheme of evolution of protostars is shown in Fig. 1. Although this scheme is specifically thought to apply to low mass star formation, it is also used as a working hypothesis for high mass star formation. A number of protostars or *Class 0* objects have been detected with bolometer surveys. In the next few years, the number of such candidates will certainly increase. Warmer regions, such as debris disks around more developed stars will certainly be found with

Spitzer. *SOFIA* will allow measurements not possible from the earth's surface. Later *Herschel* will allow measurements of spectral lines with resolutions to 13″. In order to provide inputs for models, however, one must have measurements on scales finer than 10^{16} cm or 670 AU. For sources at a distance of 500 pc from the Sun, such as Orion KL, this requires an angular resolution finer than 1.3″. Such a resolution can only be obtained with interferometry. The goal of such high resolution measurements will be a data set consisting of the distribution of thermal dust emission, as well as the column densities, linewidths and radial velocities of a large collection of gas phase molecular species. Only millimeter/sub-mm interferometers can provide such data. In addition one also requires short spacing interferometer and single dish measurements to insure that the results are complete, that is, not biased by missing Fourier components.

3 Probing Star Forming Regions with ALMA

Temperature sensitivity, ΔT, is an important limit to measurements of quasi-thermal emission from dust and molecular lines. This is the Rayleigh-Jeans criterion which relates flux density, S, to temperature, wavelength λ, and angle, θ: $\mathrm{S(mJy)}_\lambda = 73.6 \cdot \mathrm{T} \cdot \theta^2('')/\lambda^2(\mathrm{mm})$. The uncertainty in S is set by receiver noise, digitization and atmosphere. For a given uncertainty in S, the error in temperature varies as $1/\theta^2$, so an accurate measurement of cold regions with

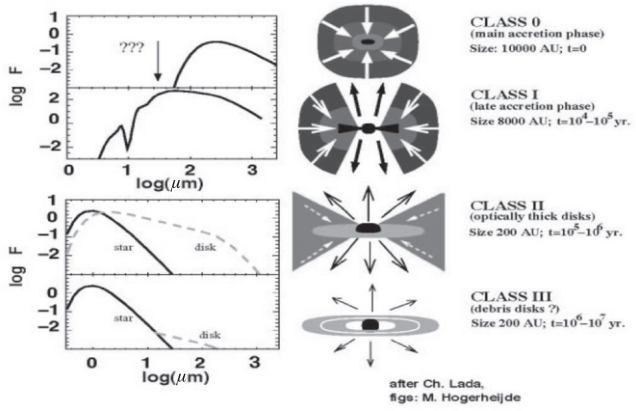


Fig. 1. Four stages in the development of a protostar, after C. Lada, adapted from [9]. In the uppermost panel and picture, the molecular cloud is collapsing. The material is cold, and most of the radiation peaks longward of 100 μm. In the next panel, a disk and core have formed, with an outflow perpendicular to the disk. Infall is still taking place. The peak of the radiation has shifted to shorter wavelengths; there is deep silicate absorption. In the next panel, the disk is well developed. Radiation arises from both the stellar core (peaking in the near infrared) and the disk (extending to the far IR). In the lowermost panel the radiation peaks in the near IR, while the disk contributes only a small amount of radiation in the far IR.

high angular resolution requires a small error in flux density; at shorter wavelengths, this error is lower [8]. In 2012, ALMA will come into full operation. ALMA will be the *ultimate* instrument for high resolution imaging of star forming regions; additional data will be obtained with SOFIA or satellites with lower resolution. The angular resolution of ALMA is: $\theta('') = 0.2\,\lambda(\mathrm{mm})/\mathrm{baseline(km)}$, where *baseline* is the maximum separation of antennas. The finest frequency resolution is 31 kHz. A sensitivity calculator is to be found at the following internet page: http://www.eso.org/projects/alma/bin/sensitivity.html. This website also gives the parameters of ALMA. The sensitivity calculator includes atmospheric effects, based on a model.

3.1 Examples of the use of ALMA

We now give examples taken from the *ALMA Design Reference Science Plan*, **DRSP**, which can be found via a link on the ESO website. The DRSP is meant to test the limits of the ALMA design. These should be considered as legacy-type programs, from the amount of time requested. These examples give estimates of integration times, calibration accuracies and noise limits. We have selected two proposals by Bacmann & Dutrey.

The first proposal, 2.1.4, is entitled *Density and Temperature Profile in High Mass Cores*. The goal is to measure the properties of sources similar to that in the uppermost panel of Fig. 1. The angular resolution is to be $0.5''$. The proposal includes measurements of 6 transitions of H_2CO at 0.8 mm to determine kinetic temperatures (T_{kin}), as well as measurements of broadband dust emission. The maximum line temperature is expected to be 7 K. The RMS noise in a 0.5 km s^{-1} spectral channel is 0.15 Kelvin. The RMS noise in a broadband continuum measurement is 0.03 Jy $beam^{-1}$. When combined with the T_{kin} values, a dust absorption coefficient and a dust-to-gas ratio, measurements of the broadband dust emission allow a determination of H_2 column densities and, with assumptions about geometry, local densities. From [8], for a dust temperature of 10K, the broadband continuum noise gives a limit to the H_2 column density of 10^{22} cm^{-2}. The sources are 1 to 10 kpc from the Sun. For one half of the sources, Dutrey & Bacmann require a 5 position by 5 position mosaic with 1.5 hours integration per field for the more distant, and for the others, a 3 position by 3 position mosaic with one hour of integration per field. The total time is 155 hours. For accurate images, one requires both single dish flux densities and also measurements with the ALMA Compact Array, ACA. We take a total velocity range of 10 km s^{-1}, and a total image size of $100''$ by $100''$.

Without the ACA or single dish data, each of these data sets has more than 6×10^7 values for the spectral lines alone. Such a data set cannot be compared to models without elaborate computer programs which optimize the fit by extensively (and intelligently) varying model parameters. The initial guesses for geometries must come from theory, and previous measurements in the IR.

In proposal 2.1.2, *Kinetics, Density and Temperature Profile in Pre-Stellar Cores*, the goal is to measure the $J = 2 - 1$ transitions in CO and isotopes, and the $J = 1{-}0$ transition of H_2D^+, as well as broadband continuum. Measurements

of the H_2D^+ molecule is very interesting since this appears not to deplete onto grains at high H_2 densities. The sources are 160 pc from the Sun, so the 1″angular resolution corresponds to 2.3 $\cdot 10^{15}$ cm, or 160 Astronomical Units. In addition to interferometer data, results from the ACA and single telescopes are required. The peak line temperatures will be ∼3 K for $C^{18}O$, 5 K for ^{13}CO and 0.1-1K for H_2D^+. From [8], for the optically thin line of $C^{18}O$, over a wide range of densities and kinetic temperatures, the RMS noise in a spectral channel gives a limit to the H_2 column density of 4 $\cdot 10^{21}$ cm^{-2}. The RMS noise in continuum measurements is 0.005 Jy beam^{-1}. From [8], this RMS noise gives an H_2 column density of $5 \cdot 10^{20}$ cm^{-2} if the dust temperature is 10 K. Since the $J = 1 - 0$ transition of H_2D^+, is absorbed in the atmosphere of the earth, 100 hours are needed for these measurements, while 25 hours are needed for measurements of the CO transitions.

For both programs, the absolute calibration accuracy should be better than 10% for continuum and spectral line measurements. The repeatability should be 3% and the relative calibration between receiver bands should be 3%.

I thank M. Zwaan (ESO) for checking the text.

References

1. D. Shepherd: 'The Energetics of Outflow and Infall from Low to High Mass YSOs'. In: *Galactic Star Formation Across the Stellar Mass Spectrum, ASP Conf. Series 287*, ed. J.M. De Buizer & N.S. van der Bliek, (ASP, San Francisco 2002), pp. 333–343
2. S.W. Stahler, F. Palla, P.T.P. Ho: 'The Formation of Massive Stars'. In: *Protostars and Planets IV*, ed V. Mannings, A.P. Boss, S. S. Russell (U. of Arizona Press, Tucson 2000) pp. 327–351
3. M. R. Meyer, F.C. Adams, L.A. Hillenbrand, J.M. Carpenter & R.B. Larson: 'The Stellar Initial Mass Function: Constraints From Young Clusters, and Theoretical Perspectives'. *ibid*, pp. 121–150
4. W.D. Langer, E.F. van Dishoeck, E.A. Bergin, G.A. Blake, A.G.G.M. Tielens, T. Velusamy, D.C.B. Whittet: 'Chemical Evolution of Protostellar Matter'. *ibid*, pp. 29–58
5. S. Kurz, R. Cesaroni, E. Churchwell, P. Hofner, C.M. Walmsley 'Hot Molecular Cores and the Earliest Phases of High Mass Star Formation'. *ibid* pp. 299–326
6. A. R. Tieftrunk, R.A. Gaume, M.J. Claussen, T.L. Wilson, K.J. Johnston: A&A **318**, 931 (1997)
7. H. Beuther, P. Schilke: Science **303**, 1167 (2004)
8. K. Rohlfs, T.L. Wilson: *Tools of Radio Astronomy* 4th edn. (Springer, Heidelberg 2003)
9. M. Hogerheijde: The Molecular Environment of low-mass protostars. PhD Thesis, Leiden University, Leiden, Netherlands (1998)

Building Complex Molecules During Star- and Planet Formation: Synergy of Infrared and Millimeter Observations

E.F. van Dishoeck[1]

Leiden Observatory, P.O. Box 9513, 2300 RA Leiden, The Netherlands

Abstract. The potential of current and future infrared and millimeter facilities to provide an inventory of the gases and solids during star- and planet formation is discussed, and the evolutionary pathways to complex, possibly prebiotic, species are described.

1 Introduction

The detection of exo-planetary systems and the quest to investigate the potential for life elsewhere in the Universe has provided renewed motivation for the study of the lifecycle of interstellar gas and dust. Simple and complex molecules are known to be present in diffuse interstellar clouds, in dense star-forming regions and in the envelopes around dying stars (e.g., [6]). Several of these species have now also been detected in cometary comae, with abundances that are in several cases remarkably similar to those found in interstellar ices [2]. Since impacts by comets and other icy bodies are one mechanism to deliver organic material and water to young planets, a study of the formation and evolution of interstellar molecules is highly relevant to studies of the conditions for life outside our own solar system.

Some of the main questions to be addressed with current and future instrumentation include: (i) What is the inventory of gases and solids at each stage of protostellar and protoplanetary evolution? What are the main reservoirs of the principle biogenic elements C, N, O, ...? (ii) How far does the chemical complexity go? Can the simplest building blocks of pre-biotic molecules such as sugars, amino acids and bases be formed under interstellar conditions? and (iii) Can we use some of these species as chemical diagnostics of different physical processes during star- and planet formation, for example heating, ultraviolet radiation, shocks etc.?

The principle wavelength regions to study gases and solids in obscured clouds are the millimeter (rotational transitions of gases) and infrared (vibrational transitions of gases and solids) regimes, making ALMA, Herschel, JWST and ELT's key facilities for further progress in this area. In this contribution, a few examples are given in the field of low-mass star formation.

2 Millimeter Versus Infrared Spectroscopy

Millimeter spectroscopy has several advantages compared with other wavelengths. First, the heterodyne technique naturally provides very high spectral resolving

power with $R = \lambda/\Delta\lambda > 10^6$, ensuring that the lines are spectrally resolved. This high resolution is essential to trace the kinematics of the gas to better than 0.1 km s^{-1}, and helps to associate different molecules with various physical components in protostellar environments such as outflows, rotating disks and infalling gas. Second, all gas-phase molecules with a permanent dipole moment can be searched down to abundances of at least 10^{-11} with respect to hydrogen, providing an enormous dynamic range. More than 120 different species (not including isotopes) have been found, including complex organic molecules like CH_3OH, CH_3OCH_3, $HCOOCH_3$, C_2H_5CN and the simplest sugar, CH_2OHCHO. The potential detection of interstellar glycine is still subject to discussion, however, and other prebiotic species like aziridine and pyrimidine have not yet been found [8]. Third, maps of the emission can be made, revealing chemical differentiation within protostellar regions and disks.

Infrared spectroscopy has the advantage that both gases and solids can be probed, including a rich variety of silicates, ices and polycyclic aromatic hydrocarbons (PAHs) seen by the ISO satellite (see review by van Dishoeck [11]). Gases without a permanent dipole moment such as H_2, CO_2 and organics like C_2H_2 and CH_4 —important building blocks of larger molecules— are uniquely probed through their infrared lines. These molecules are seen either in absorption along the line of sight to an infrared source (e.g., a protostar) or through their emission. Indeed, the recent images from the Spitzer Space Telescope beautifully reveal PAHs glowing throughout the local interstellar medium at 8 μm, and PAHs are even used to probe the most distant high-redshift galaxies.

3 Chemical Evolution During Star- and Planet Formation

Systematic studies of molecules in young stellar objects are starting to reveal the different chemical stages during star formation (e.g., [12]). The coldest pre-stellar cores are characterized by heavy freeze-out of virtually all gas-phase molecules onto the cold grains, where grain-surface chemistry can lead to more complex species. In particular, reactions with atomic H, which are very slow in the gas phase due to energy barriers, can proceed on the grains and lead to fully hydrogenated molecules such as H_2O, CH_4, NH_3 and CH_3OH. These are indeed the main ices observed in infrared spectra of both high- and low-mass YSOs, with up to 50% of the condensible oxygen and carbon locked up in ices (cf., [9,3] and Fig. 1. Thermal processing and reactions stimulated by ultraviolet radiation can lead to further complexity of molecules in ices.

Once the protostar starts to heat the envelope, the ices will evaporate in a sequence according to their sublimation temperatures, with the most volatile species like CO coming off at temperatures as low as 20 K and the most strongly bound species around 100 K. The evaporated ices subsequently drive a rapid gas-phase chemistry for a period of $10^4 - 10^5$ yr. In particular, reactions with evaporated CH_3OH are thought to lead to high abundances of CH_3OCH_3 and $HCOOCH_3$. These so-called 'hot cores' are signposts of the earliest stages of

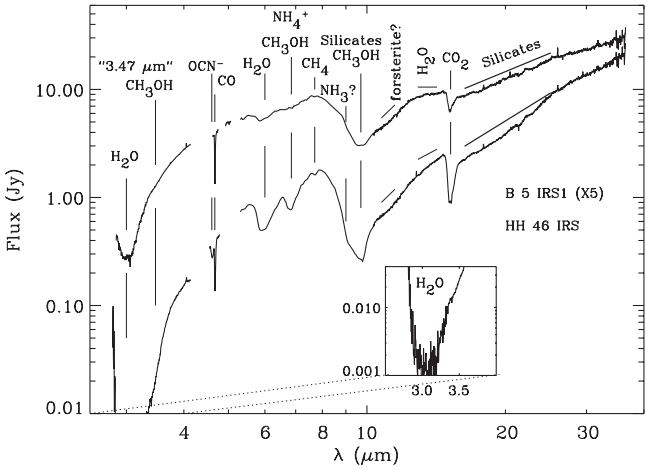


Fig. 1. Spitzer infrared spectra toward the low-mass protostars B5 IRS1 and HH 46 IRS by Boogert et al. [3], illustrating the presence of organic molecules in ices

high-mass star formation, and are now also found around some low-mass YSOs (Fig. 2).

A fraction of the envelope material —both ices and gases— will end up in the growing disk, where it becomes part of the material from which planetesimals and other planetary bodies are formed. Exactly how and where the material enters the disk and to what extent it is processed is currently unclear. Initial observations of simple molecules in disks show that their abundances are depleted compared with normal interstellar clouds (e.g., [5,10]) and that there are spatial variations in abundances in the disks (e.g., [7]). Models of flaring disks indicate that most of the active chemistry occurs in a warm layer at intermediate heights where the grains are warm enough to keep CO and related species in the gas but where the molecules are shielded from the stellar and interstellar radiation (e.g., [1]).

4 Future Instrumentation Needs

Using current millimeter and infrared facilities, inventories of the gases and solids are starting to be made in protostellar and protoplanetary regions which are thought to be representative of our own primitive solar system. The principle limitation at millimeter wavelengths is the low spatial resolution and sensitivity: most data are from single dish telescopes with beams of 10–20″ that encompass the entire envelope. Current interferometers can hardly resolve circumstellar disks. ALMA will be a tremendous leap forward in this field, with the capability and sensitivity to image molecules down to scales of tens of AU where planet formation takes place. Herschel-HIFI will be unique in providing information

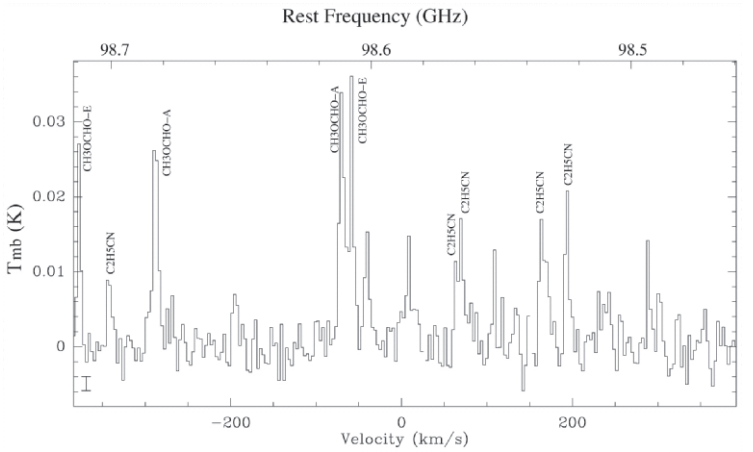


Fig. 2. Complex organic molecules detected toward the low-mass protobinary object IRAS16293 –2422 with the IRAM 30m at millimeter wavelengths by Cazaux et al. [4], illustrating their chemical richness

on a key chemical ingredient — H_2O, but future far-infrared interferometers in space are needed to spatially resolve the water emission.

At infrared wavelengths, Spitzer is opening up the study of ices in low-mass protostars and disks, but its modest spectral resolution ($R \leq 600$) prevents detection of minor ice species and most gas-phase molecules. High spectral resolution instruments with R up to 10^5 on 8m-class telescopes and ELTs will be essential to search for key organic molecules in atmospheric windows between 3 and 15 μm. Such instruments are an excellent complement to the medium resolution ($R \approx 3000$) spectrometers MIRI and NIRSPEC on JWST which will have unparalleled sensitivity at 3–28 μm to probe gases and solids.

References

1. Y. Aikawa, G.J. van Zadelhoff, E.F. van Dishoeck, E. Herbst: A&A **386**, 622 (2002)
2. D. Bockelée-Morvan, D.C. Lis, J.E. Wink, et al.: A&A **353**, 1101 (2000)
3. A.C.A. Boogert, K.M. Pontoppidan, F. Lahuis, et al.: ApJS **154**, 359 (2004)
4. S. Cazaux, A.G.G.M. Tielens, C. Ceccarelli, et al.: ApJ **593**, L51 (2003)
5. A. Dutrey, S. Guilloteau, M. Guélin: A&A **323**, 943 (1997)
6. P. Ehrenfreund, S.B. Charnley: ARA&A **38**, 427 (2000)
7. J.E. Kessler, C. Qi, G.A. Blake: In: *Chemistry as a Diagnostic of Star Formation*, ed. by C.L. Curry and M. Fich (NRC Press, Ottawa, Canada), pp.188–192 (2003)
8. Y-J. Kuan, S.B. Charnley, H-C. Huang, et al.: Adv. Space Res. **33**, 31 (2004)
9. K.M. Pontoppidan, E.F. van Dishoeck, E. Dartois: A&A, in press (2004)
10. W.F. Thi, G.J. van Zadelhoff, E.F. van Dishoeck: A&A, in press (2004)
11. E.F. van Dishoeck: ARA&A **42**, 119 (2004)
12. E.F. van Dishoeck, G.A. Blake: ARA&A **36**, 317 (1998)

GAIA: Composition, Formation and Evolution of Our Galaxy

G. Gilmore

Institute of Astronomy, Madingley Road, Cambridge CB3 0HA, UK

Abstract. GAIA will provide a multi-colour photometric and astrometric census of some one billion compact sources, complete to 20th magnitude. In addition, spectra for radial velocities will be obtained for about 30 million stars brighter than $V = 17$. The high spatial resolution and astrometric precision, 0.1 arcsec and 10 microarcsec to $V = 15$, will not only quantify the distribution of mass and the stellar populations in the Galaxy, but make major advances in fundamental physics, cosmology and solar system science. GAIA is an ESA mission, scheduled for launch in mid-2010. A full description of the GAIA project and science case, fairly crediting the hundreds of contributors, is available in the project 'Red Book' [1]. A brief overview is provided by Perryman, de Boer, Gilmore, et al. [2]. The www site is `http://www.rssd.esa.int/GAIA/`.

1 Introduction

Understanding the Galaxy in which we live is one of the great intellectual challenges facing modern science. The Milky Way contains a complex mix of stars, planets, interstellar gas and dust, radiation, and the ubiquitous dark matter. These components are widely distributed in age, reflecting their birth rate; in space, reflecting their birth places and subsequent motions; on varied orbits, determined by the gravitational force generated by their own and, more importantly, the dark mass; and with chemical element abundances, determined by the history of star formation, gas accretion, and mixing in the ISM prior to their formation. Astrophysics has now developed the tools to measure these distributions in space, kinematics, and chemical abundance, and to interpret the distribution functions to map, and to quantify, the formation, structure, evolution, and future of our entire Galaxy, given adequate data. This potential understanding is also of profound significance for quantitative studies of the high-redshift Universe: a well-studied nearby template underpins analysis of unresolved galaxies at early times.

1.1 Structure and Dynamics of the Galaxy

The primary objective of the GAIA mission is the Galaxy: to observe the physical characteristics, kinematics and distribution of stars over a large fraction of its volume, with the goal of achieving a full understanding of the Galaxy's dynamics and structure, and consequently its formation and history. GAIA will make this goal possible by providing, for the first time, a catalogue which will sample a large and well-defined fraction of the stellar distribution in phase space from which

significant conclusions can be drawn for the entire Galaxy. Hipparcos did this for one location in the Galaxy, the Solar neighbourhood; GAIA will accomplish this for a large fraction of the Galaxy.

2 Space Astrometry

The apparent motion of a star across the sky is dominated by proper motion, which reflects the relative motion of the star and the Sun on their Galactic orbits; parallax, which reflects the orbital motion of the earth around our Sun, and provides a fundamental metric calibration; and possible higher frequency terms which reflect perturbations of the orbital motion of the target star from any companions, such as planets. Since the amplitude of the earth's orbit is known, the observed parallax determination of the angular parallax may be converted into a metric distance. This however requires extremely precise measurement, with precisions of a few microarcseconds (pico-radians) required to probe beyond the immediate Solar neighbourhood. Such precision is attainable in orbit, free from atmospheric refractive problems, provided a suitably stable platform is attainable. The ability of space astrometry to provide global high-precision astrometry was proven by the ESA HIPPARCOS mission, one of the greatest astrophysical advances of recent times.

The GAIA solution to this technical challenge is to mount two imaging telescopes at a fixed angle on a single optical bench. Each telescope has a wide field of view, in which the relative positions of all sources are determinable. Since the telescopes are fixed on the same bench, the relative positions of all sources in each telescope are also determined relative to each other. As the satellite spins and precesses, drift-scanning the sky across the large (180 CCDs) focal plane, accurate relative positions of all objects are obtained. To fix the zero point of the coordinates, all the observed unresolved quasars are used to define a non-rotating (cosmological, Machian) reference grid. The whole sky is observed every 70 days, providing, over a 5-year operational mission, an average of over 120 observations of each source, sufficient data (4.6 Mb/s for 5 years, or 0.1 petabytes) to model all of proper motion, parallax and multiplicity for all one billion compact sources brighter than magnitude 20. That is one percent of the stars in the Galaxy.

2.1 Relativistic Astrometry

One of the more interesting aspects of precision measurement is that the largest signal observed is not stellar motion, but general relativistic distortion of the metric, even though GAIA will orbit at L2, and not observe close to a line of sight near the Sun.

Table 1 gives the magnitude of the deflection for the Sun and the major planets, at different values of the angular separation χ, for the monopole term and the quadrupole term. While χ is never smaller than 50° for the Sun (a constraint from GAIA's orbit), grazing incidence is possible for the planets. With the astrometric accuracy of a few μas, the magnitude of the expected effects is considerable for the Sun, and also for observations near planets.

Table 1. Light deflection by masses in the Solar system. The monopole effect dominates, and is summarized in the left columns for grazing incidence and for typical values of the angular separation. Columns $\chi_{\min}$ and $\chi_{\max}$ give results for the minimum and maximum angles accessible to GAIA. J_2 is the quadrupole moment. The magnitude of the quadrupole effect is given for grazing incidence, and for an angle of 1°. For GAIA this applies only to Jupiter and Saturn, as it will be located at L2, with minimum Sun/Earth avoidance angle of ∼50°.

Object	Monopole term					Quadrupole term		
	Grazing μas	$\chi_{\min}$ μas	$\chi = 45^\circ$ μas	$\chi = 90^\circ$ μas	$\chi_{\max}$ μas	J_2	Grazing μas	$\chi = 1^\circ$ μas
Sun	1750000	13000	10000	4100	2100	$\leq 10^{-7}$	0.3	–
Earth	500	3	2.5	1.1	0	0.001	1	–
Jupiter	16000	16000	2.0	0.7	0	0.015	500	7×10^{-5}
Saturn	6000	6000	0.3	0.1	0	0.016	200	3×10^{-6}

3 Summary of the GAIA Science Capabilities

Objectives: Galaxy origin and formation; physics of stars and their evolution; Galactic dynamics and distance scale; solar system census; large-scale detection of all classes of astrophysical objects including brown dwarfs, white dwarfs, and planetary systems; fundamental physics

Measurement Capabilities:

- **catalogue:** ∼ 1 billion stars; 0.34×10^6 to $V = 10$ mag; 26×10^6 to $V = 15$ mag; 250×10^6 to $V = 18$ mag; 1000×10^6 to $V = 20$ mag; completeness to about 20 mag
- **sky density:** mean density ∼ 25 000 stars deg^{-2}; maximum density ∼ 3×10^6 stars deg^{-2}
- **accuracies:** median parallax errors: 4 μas at 10 mag; 11 μas at 15 mag; 160 μas at 20 mag
- **distance accuracies:** from Galaxy models: 21 million better than 1 per cent; 46 million better than 2 per cent; 116 million better than 5 per cent; 220 million better than 10 per cent
- **tangential velocity accuracies:** from Galaxy models: 44 million better than 0.5 km s^{-1}; 85 million better than 1 km s^{-1}; 210 million better than 3 km s^{-1}; 300 million better than 5 km s^{-1}; 440 million better than 10 km s^{-1}
- **radial velocity accuracies:** 1–10 km s^{-1} to $V = 16 - 17$ mag, depending on spectral type
- **photometry:** to $V = 20$ mag in 4 broad and 11 medium bands

Scientific Goals:

- **the Galaxy:** origin and history of our Galaxy — tests of hierarchical structure formation theories — star formation history — chemical evolution — inner bulge/bar dynamics — disk/halo interactions — dynamical evolution — nature of the warp — star cluster disruption — dynamics of spiral structure — distribution of dust — distribution of invisible mass — detection of tidally disrupted debris — Galaxy rotation curve — disk mass profile
- **star formation and evolution:** *in situ* luminosity function — dynamics of star forming regions — luminosity function for pre-main sequence stars — detection and categorization of rapid evolutionary phases — complete and detailed local census down to single brown dwarfs — identification/dating of oldest halo white dwarfs — age census — census of binaries and multiple stars
- **distance scale and reference frame**: parallax calibration of all distance scale indicators — absolute luminosities of Cepheids — distance to the Magellanic Clouds — definition of the local, kinematically non-rotating metric
- **Local group and beyond:** rotational parallaxes for Local Group galaxies — kinematical separation of stellar populations — galaxy orbits and cosmological history — zero proper motion quasar survey — cosmological acceleration of Solar System — photometry of galaxies — detection of supernovae
- **Solar system:** deep and uniform detection of minor planets — taxonomy and evolution — inner Trojans — Kuiper Belt Objects — disruption of Oort Cloud
- **extra-solar planetary systems:** complete census of large planets to 200–500 pc — orbital characteristics of several thousand systems
- **fundamental physics:** γ to $\sim 5 \times 10^{-7}$; β to $3 \times 10^{-4} - 3 \times 10^{-5}$; solar J_2 to $10^{-7} - 10^{-8}$; $\dot{G}/G$ to $10^{-12} - 10^{-13}$ yr^{-1}; constraints on gravitational wave energy for $10^{-12} < f < 4 \times 10^{-9}$ Hz; constraints on $\Omega_{\rm M}$ and Ω_Λ from quasar microlensing
- **specific objects:** $10^6 - 10^7$ resolved galaxies; 10^5 extragalactic supernovae; 500 000 quasars; $10^5 - 10^6$ (new) solar system objects; $\sim 50\,000$ brown dwarfs; 30 000 extra-solar planets; 200 000 disk white dwarfs; 200 microlensed events; 10^7 resolved binaries within 250 pc

References

1. K. de Boer, G. Gilmore, E. Hog, M.G. Lattanzi, L. Lindegren, X. Luri, F. Mignard, O. Pace, M. Perryman, P.T. de Zeeuw (eds): *GAIA Concept and Technology Study Report (the 'Red Book')* ESA-SCI(2000), 4 (ESA: Paris), pp. 1–381 (2000)
2. M. Perryman, K.S. de Boer, G. Gilmore, E. Hog, M.G. Lattanzi, L. Lindegren, X. Luri, F. Mignard, O. Pace, P.T. Zeeuw: A&A **369**, 339 (2001)

Large–Scale Surveys with the Arecibo Multibeam System

P.F. Goldsmith

Department of Astronomy and National Astronomy and Ionosphere Center, Cornell University, Ithaca NY 14853

Abstract. The Arecibo 305 m antenna is the largest filled–aperture radio telescope in the world. As such, it has extraordinary potential for high–sensitivity surveys. A new 7–element, 1225–1525 MHz, dual–polarization focal plane array receiver was installed in April 2004. The Arecibo L–band Focal Plane Array (ALFA) increases mapping speeds and so enables large-scale surveys for galactic astronomy, including HI and recombination lines and continuum, extragalactic astronomy using HI, and pulsars. We discuss some key characteristics of the new systems and the surveys that are being proposed. Additional information on ALFA and associated scientific consortia is available at **http://alfa.naic.edu/**.

1 The Arecibo Gregorian System

A fundamental aspect of the Arecibo radio telescope is the use of a spherical primary reflector with a movable feed system to enable tracking sources to a maximum zenith distance of almost 20 degrees. A primary having this form produces spherical aberration. Historically, this has been dealt with by using line feeds, which collect the radiation heading generally towards the paraxial focus, but which would otherwise cross the focal line closer to the primary reflector than the paraxial focal point. To illuminate the full 305 m diameter of the primary requires a line feed over 29 m long. Such a full–sized line feed has been in operation for many years with a center frequency of 430 MHz, but with an important drawback characteristic of line feeds which is a very limited bandwidth, in this case $\simeq$ 20 MHz. This bandwidth is independent of frequency, and is a direct consequence of the requirement that the radiation collected along the entire length of the feed arrive in phase at the end leading to the receiver. Line feeds at higher frequencies have significant loss (per unit distance), and as the length of the line feed is fixed by the geometry of the telescope, the total signal attenuation becomes prohibitive at frequencies above a few GHz.

To extend the upper frequency limit of the Arecibo 305m telescope to $\geq$ 10 GHz and achieve large instantaneous bandwidths required replacing the line feeds which had been used to correct for the aberration produced by the spherical primary reflector. This was achieved in 1997 with the installation of a reflective feed system. The new optical system is called the "Gregorian" since it utilizes concave, albeit aspheric reflectors, to bring the radiation reflected by the spherical primary to a point focus [1]. Its operation is frequency independent. Through photogrammetry, the total primary reflector error has been reduced to

2 mm rms. Combined with the secondary and tertiary reflector errors (at present rss $\simeq$ 2.3 mm), the aggregate surface error of 3 mm has allowed operation to 9.5 GHz, albeit with modest efficiency [3]. Good antenna performance has been verified up to 6.6 GHz, with an antenna gain of 6.5 K/Jy. With completion of the primary surface alignment, a rss error less than 2 mm is expected, allowing, efficient operation at wavelengths as short as 3 cm (frequencies up to 10 GHz). The instantaneous bandwidth of the Gregorian system is now limited only by the receivers and IF system, with $\delta\nu = 1$ GHz already successfully employed [2].

2 The ALFA Receiver

Another feature of the Gregorian system is the possibility of using focal plane arrays, although the effective focal ratio is small (f/D $\simeq$ 0.43). Thus, the imaging capabilities are limited by coma that results when the feed is moved away from the on–axis focal point. Tradeoff studies considering system noise and gain indicated that a feedhorn diameter of 25 cm is optimum, and stepped TE_{11} mode feedhorns of this size have been utilized. The key parameters of the ALFA front end receiver are given in Table 1.

Table 1. Parameters of ALFA Front End Receiver

Number of Feedhorns	7 (Dual Linear Polarization)
Polarization	Dual Linear
Polarization Isolation	>20 dB
Amplifiers	3-stage HEMTs (14)
Frequency Range	1225–1525 MHz
Gain Variation over Band	$\pm$ 0.5 dB
Dewar Flange Input Noise Temperature	6–8 K Average
System Noise Temperature on Telescope	29–34 K
Sensivity of Central Pixel @ 1420 MHz	10 K/Jy
Sensitivity of Outer Pixels	7–9 K/Jy
Max. Sidelobe Level of Central Pixel	-13 dB
Max. Sidelobe Level of Outer Pixels	-8 dB
Beam Size	3.3' x 3.8'
Calibration Noise Source	Correlated Between Polarizations
Dewar Rotation	$\pm$ 100 $^\circ$
Weight	900 kg
Feedhorns	Stepped TE_{11}; ϕ 25cm S = 26cm

The ALFA front end receiver was installed on 21 April, 2004. At the present time (July 2004) system commissioning tests are well underway, and scientific observations are expected to begin during the Fall of this year.

3 ALFA Signal Processing Systems

The varied astronomical uses of ALFA dictate that several high performance systems for processing the signals from the 14 receiver channels are necessary.

The "first light" backend system is both an autocorrelation spectrometer and pulsar processor, based on a custom VLSI chip. Each unit covers 195 kHz to 100 MHz bandwidth in octave steps, with up to 16384 lags available, depending on operating mode (Stokes, dual polarization, single polarization, bandwidth). The maximum sampling rate is limited by transfer rate to the data storage computer and bit packing, but can be as short as 32 μs with 192 lags of 520 kHz bandwidth each. A similar with comparable characteristics but covering 300 MHz bandwidth is currently being developed, based on FPGA technology. This will also be very useful for continuum observations, and the channelization will facilitate interference excision. This system will be available at the end of 2005. A spectrometer dedicated to galactic spectroscopy is being developed by D. Werthimer and his group at the University of California, Berkeley, also using FPGA technology. Each polarization/pixel will be covered by a 10 MHz Fast Fourier Transform (FFT) spectrometer having 10 MHz bandwidth and 8192 frequency channels, together with 256 channels covering 100 MHz bandwidth. The latter will be used for precise determination of the telescope+receiver spectral baseline. This system should be available late in 2004.

4 ALFA Surveys

The general areas in which the Arecibo telescope equipped with ALFA can have a major scientific impact are **Galactic Astronomy**, **Pulsar Astronomy**, and **Extragalactic Astronomy**. Obviously, these are not entirely distinct since, e.g. pulsars are (to date) galactic objects and high velocity clouds may be considered to be either galactic or extragalactic. The Arecibo telescope offers two primary advantages: high sensitivity and (for a single antenna at L–band) a small beam size. Offsetting these are the relatively high sidelobe levels due to blockage by the suspended structure and coma lobes for off–axis pixels of ALFA. In each scientific area, there are some projects that are very much favored, and those which are made more difficult by these various features of the system performance. To obtain the maximum scientific benefit from ALFA, NAIC has encouraged the formation of *Consortia* to develop and carry out large–scale surveys with the new instrument. Three Consortia, **G-ALFA**, **P-ALFA**, and **E-ALFA**, for each of the areas listed above have been formed. Each is in the process of developing plans for surveys of various types, and the software for reducing the data. Membership in ALFA Consortia is open to astronomers on a worldwide basis who are interested in and willing to carry out observing and analysis activities.

4.1 Galactic Astronomy

The interest of galactic astronomy in ALFA includes spectroscopic HI and recombination line and continuum observations. These actually have very different requirements on signal processing and observing modes.

HI Astronomy Surveys of HI in the interstellar medium of the Milky Way include:

- Neutral hydrogen as a probe of the origin & evolution of molecular clouds
- Interstellar turbulence
- HI clouds in the galactic halo
- The disk–halo connection
- High–latitude line wings and turbulence
- High–latitude clouds
- HI self–absorption and kinematics
- Line wings at forbidden velocities

It is not possible here to discuss the exciting astronomy associated with each of these topics. But they connect with many of the most important problems of galactic astrophysics including the big picture of star formation, supernovae and their energy input to the interstellar medium, and the structure and kinematics of the galactic halo.

The G-ALFA surveys range from relatively limited areas (for studying the relationship between atomic and molecular clouds) and very large areas (for high velocity clouds). Most of the observations will be carried out in drift scan or related observing modes, with special attention given to obtaining good spectral baselines. A few hundred to several thousand hours of telescope time are required.

Radio Recombination Line Astronomy Twelve radio recombination lines (RRLs) of H, He, and C fall within the ALFA bandpass. All of these are important targets for a large–scale RRL survey that would give valuable information on the physical parameters of the ionized gas in HII regions and the diffuse interstellar medium. This would be valuable for elucidating the structure of the Milky Way and studies of galactic chemical evolution. The galactic diffuse medium (WIM) in the plane and the halo will be an important target, and the proposed ALFA study should help clarify the sources of ionization.

The ALFA-RRL study requires integration times of 300 seconds per pointing due to the faintness of the recombination lines. The signal processing system will ideally allow combination of several lines observed simultaneously to improve the sensitivity. The low-latitude RRL survey ($|b| \leq 5^\circ$), covering 400 square degrees, will require 2000 hours of telescope time.

Continuum Astronomy Although there have been many radio continuum surveys of the galaxy, the ALFA system offers some unique capabilities for new discoveries. One of the most exciting areas is that of **polarized** continuum emission, for which the confusion limit (20 μJy/beam) is much less than the sensitivity of an Arecibo rapid–scan survey (2 mJy/beam). The proposed survey has the advantage of relatively large fractional bandwidth ($\delta\nu/\nu \simeq 0.2$). This means

that Faraday rotation produces a significant shift of polarization angle across the band. Disentangling this effect ("Faraday Tomography") offers the possibility of major new insights into the structure of the magnetic field in the Milky Way. The GALFA continuum Survey will be carried out in a "basket–weaving" mode in which the telescope is rapidly scanned in elevation at a fixed azimuth angle. This reduces the systematic confusion due to sidelobes, and by slipping the time each day, the whole sky is gradually covered multiple times, if desired. The time required to cover the Arecibo sky at an elevation scan rate of 2.5 deg/min is 1000 hours.

4.2 Pulsar Astronomy

Pulsars are an ongoing source of new astronomy and physics. To expand the parameter space of pulsars and to fully sample the galaxy, extensive, deep pulsar surveys are planned, which will be sensitive to pulsars with periods from 5 s to less than 1 ms, and in orbits with periods as short as hours. Some of the science highlights of pulsar surveys are

- Neutron star physics
- Sub ms pulsars; neutron star–neutron star and ns–black hole binaries
- Magnetospheric physics (emission mechanisms)
- Probing the interstellar medium
- Orbital elements of binary pulsars and tests of gravitation theories
- Pulsars as gravitational wave detectors

Canonical pulsars are important for understanding population and stellar evolution issues, as well providing powerful probes of the magnetoionic intestellar medium. But probably of greatest interest are "extreme" pulsars, as exemplified by recently recycled pulsar PSR J1740-5340, having P = 3.6 ms, the "Black Widow" pulsar PSR 1957+20 with P = 1.6 ms, with companion that will evaporate in about 10^9 yr, and the fastest known rotator, PSR 1937+21, with P = 1.56 ms. The motivation for sub–ms pulsar searches are several, including limits on pulsar periods and masses, the equation of state of exotic matter, phase transitions in neutron stars, and the ground state of matter in the universe.

The ALFA galactic plane pulsar survey will cover the Arecibo sky at $|b| \leq 5°$, with 300 s integration per pointing, and will be able to see 2.5 to 5 times further than the Parkes Multibeam Survey. An anticipated yield of $\simeq$ 1000 new pulsars will have a major impact on pulsar statistics, but there is also the hope of serendipitous discovery of objects which really push the envelope, such as a pulsar in orbit around a black hole. The P-ALFA survey will mark a distinct step towards the science expected from the capabilities of the Square Kilometer Array (SKA).

The obvious similarity in observing requirements between this survey and the GALFA-RRL survey suggests that *commensal* observing with two separate signal processing systems will obviously be an effective strategy when several thousand hours of telescope time are at stake. This is also the case for other

combinations of ALFA surveys, e.g. extragalactic HI and high latitude galactic HI, and once the appropriate spectrometers are available, it is anticipated that commensal observing will become a standard mode of observations.

4.3 Extragalactic Astronomy

The scientific goals of the extragalactic ALFA (E-ALFA) consortium are to:

- Determine the local density dependence of the HI mass function (HIMF)
- Map the distribution of luminous and dark matter
- Investigate the faint end of the HI mass function
- Determine the gas–rich membership of nearby groups of galaxies
- Determine the population of gas–rich systems in the Local Group and periphery of the Milky Way (HVCs)
- Investigate connection with Lα absorbers via 21cm absorption
- Find (rare) OH megamasers near z = 0.25

At least four large–scale surveys are contemplated, which in addition to the above, are anticipated to yield a rich harvest of serendipitous discoveries. The surveys are:

1. All-Arecibo-Sky Fast ALFA Survey (ALFALFA) – 12000 square degrees in drift mode, with 50–100 MHz coverage; 2000 hours of telescope time
2. Very Deep Survey – 0.4 square degrees, 200 MHz coverage, 50–100 hours integration per pointing; $\simeq$ 1100 hours of telescope time
3. Medium–Deep (Virgo and other groups) Survey – Virgo and anti–Virgo (VAVA) will require 60 seconds integration per pointing and 5 passes; total of $\simeq$ 900 hours of telescope time
4. Zone of Avoidance (ZOA) Survey – 300 seconds per pointing on galactic plane visible from Arecibo with $|b| \leq 5^\circ$; the similarity with the pulsar and RRL surveys makes this a prime candidate for commensal observing.

Acknowledgements

A large number of individuals at NAIC have made critical contributions to the ALFA project, notably L. Baker, D. Campbell, E. Castro, G. Cortés-Medellín, A. Deshpande, R. Ganesan, J. Hagen, P. Perillat, and S. Torchinsky. The ALFA receiver was designed and built by the Australia Telescope National Facility of the CSIRO, Australia, with major contributions by T.Bird, G. Carrad, G. Moorey, and P. Sykes. The Arecibo Observatory is operated by Cornell University under a cooperative agreement with the National Science Foundation.

References

1. P.F. Goldsmith: IEEE Potentials **15(3)**, 38 (1996)
2. T.H. Hankins, J.S. Kern, J.C. Weatherall, J.A. Eilek: Nature **422**, 144 (2003)
3. S.V. Kalenskii, V.I. Slysh, P.F. Goldsmith, L.E.B. Johansson: ApJ **610** 329 (2004)

Preliminary Science Results from the Submillimeter Array

A.B. Peck[1] and the SMA Team[2,3]

[1] Harvard-Smithsonian CfA
[2] Smithsonian Astrophysical Observatory, USA
[3] Academia Sinica Institute for Astronomy & Astrophysics, Taiwan

Abstract. The Submillimeter Array (SMA) is nearing completion on the summit of Mauna Kea and has begun science operations. The completed instrument will consist of eight 6-m diameter elements in reconfigurable arrays providing baselines from 7 to 500 m and resolutions of about 0.1 to 5 arcseconds. The full array will cover the atmospheric windows around 230, 345, 460, 650 and 850 GHz (1.3 to 0.3 millimeter wavelength) with a total bandwidth of 2 GHz in each of 2 sidebands and high spectral resolution. The dedication took place in November 2003, and internal science proposals have been accepted for the 230 GHz and 345 GHz receivers since that time. We will report on exciting results that are becoming available as data using the 230 GHz and 345 GHz receivers during the commissioning phase of operations are reduced. The science topics explored with these early observations range from star formation and evolved stars in our Galaxy to imaging starburst regions in nearby galaxies and attempting to perform high precision astrometry on extremely high redshift submillimeter galaxies. In addition, phase closure at 682 GHz and 691 GHz was achieved in late 2002 using 3 antennas, and further test observations at these frequencies are ongoing.

1 The SMA

The Submillimeter Array (SMA) is a new interferometer dedicated to observations in millimeter and sub-millimeter wavelengths. It is located on Mauna Kea, Hawaii, near the CSO and JCMT facilities and was commissioned in November 2003. The array consists of eight 6-meter diameter antennas which can be configured in 4 tangential rings which approximate Reuleaux triangles, whose relative sizes allow for resolution increments of 2.7. Antennas are moved between the 24 pads using a 6 wheeled transporter that moves on dirt roads. This minimizes the impact of the observatory on the mountain, and allows up to 4 antennas to be moved in one day. All four configurations will soon be available with baselines ranging from 8 to 508 meters, producing a maximum angular resolution of $0\farcs1$. Each antenna is equipped with a cryostat at its Nasmyth focus which will accept eight receivers covering all useable bands from 175 to 920 GHz. The SMA receivers are double sideband, SIS mixer heterodyne systems. Pairs of receivers can be illuminated simultaneously, allowing either 2 frequency (for example 230 and 690 GHz) or dual polarization observations. At present (August 2004) all antennas have receivers at 230 and 345 GHz, and 6 of the 8 have receivers at 690 GHz. The highly flexible correlator will accept two channels of 2 GHz bandwidth from each antenna, making possible either dual polarization

or simultaneous dual frequency operation. The 2 GHz bandwidth in each sideband is divided into 24 "chunks", and allows mixed resolution within the band, allocating between 8 and 1024 channels per IF chunk.

A pilot program to include the 15m JCMT and 10.4m CSO as part of the SMA for certain periods each year will begin in 2005. This will increase the maximum baseline to 770 meters, as well as more than doubling the collecting area.

2 Science Results

In the space provided, we can obviously only showcase a very small selection of the results obtained at the SMA during our construction and commissioning phase. In Figs. 1–2, we show plots from only 4 of the 14 papers which will have been accepted for the special edition of *Astrophysical Journal Letters* expected to appear in late summer of 2004. We encourage interested readers to look to that volume for the full papers presenting the results of the ∼1.5 years of science observations made during the early days of the SMA telescope. At present, the SMA is in a fully operational mode, accepting proposals from the three "internal" institutions, SAO, ASIAA and IfA. Beginning in autumn 2004, the SMA will also make some fraction of its time available to users from the global astronomical community.

The SMA is a collaborative project of the Smithsonian Astrophysical Observatory and the Academia Sinica Institute of Astronomy & Astrophysics of Taiwan.

References

1. H. Beuther, Q. Zhang, T.R. Hunter, et al.: ApJL, *in press*, astro-ph/0406020 (2004)
2. P.T.P. Ho, J.M. Moran, K.Y. Lo: ApJL, *in press*, astro-ph/0406352 (2004)
3. D. Iono, P.T.P. Ho, M.S. Yun, et al.: ApJL, *in press*, astro-ph/0403429 (2004)
4. K. Sakamoto, S. Matsushita, A.B. Peck, M.C. Wiedner, D. Iono: ApJL, *in press*, astro-ph/0403145 (2004)
5. P.K. Sollins, T.R. Hunter, J. Battat, et al.: ApJL, in press, astro-ph/0403524 (2004)
6. D.O.S. Wood, E. Churchwell: ApJS **69**, 831 (1989)
7. M.S. Yun, N.Z. Scoville, R.A. Knop: ApJL **430**, 109 (1994)

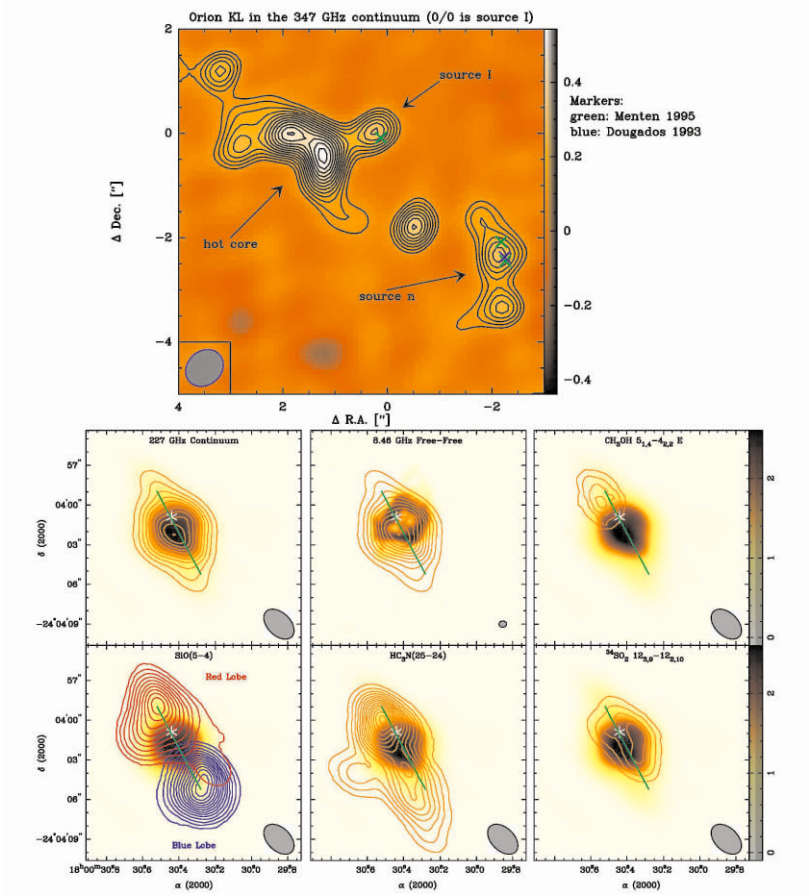


Fig. 1. a) This 347 GHz continuum image toward the Orion-KL region is the first sub-arcsecond resolution sub-mm continuum image ever observed. The light and dark crosses mark the radio and infrared positions, respectively. We clearly resolve the famous source I from the Orion hot core. Furthermore, the infrared and radio source n is detected in the sub-mm band. In addition we detect some more sources which were previously completely unknown [1]. **b)** The shell-like ultracompact H II region G5.89-0.39 was observed with the SMA in 2003 with five antennas, giving baselines with projected lengths ranging from 10.2 meters to 116 meters resulting in a $2\farcs8 \times 1\farcs8$ synthesized beam. The first panel of shows our 227 GHz continuum emission map. The second panel shows an 8.46 GHz continuum map [6] in grayscale overlaid with our 1.3 mm map in contours. In total we detected 9 spectral lines. SiO(5-4), $H_2S\ 2_{2,0} - 2_{1,1}$, HCCCN(25-24), $SO_2\ 22_{2,20} - 22_{1,21}$, and $^{34}SO_2\ 11_{1,11} - 10_{0,10}$ all show the outflow to varying degrees. $HC^{13}CCN$(24-23), $HCC^{13}CN$(24-23), and $CH_3OH\ 5_{1,4} - 4_{2,2}E$, show only marginally resolved emission all at the same location in the Northeast lobe of the outflow and all at the ambient velocity of v_{lsr}=10 km/s. DCN(3-2) was also detected but was difficult to map, probably due to missing flux. Our map of the integrated SiO(5-4) line emission in the lower left panel clearly resolves and separates the red- and blue-shifted lobes of the outflow [5].

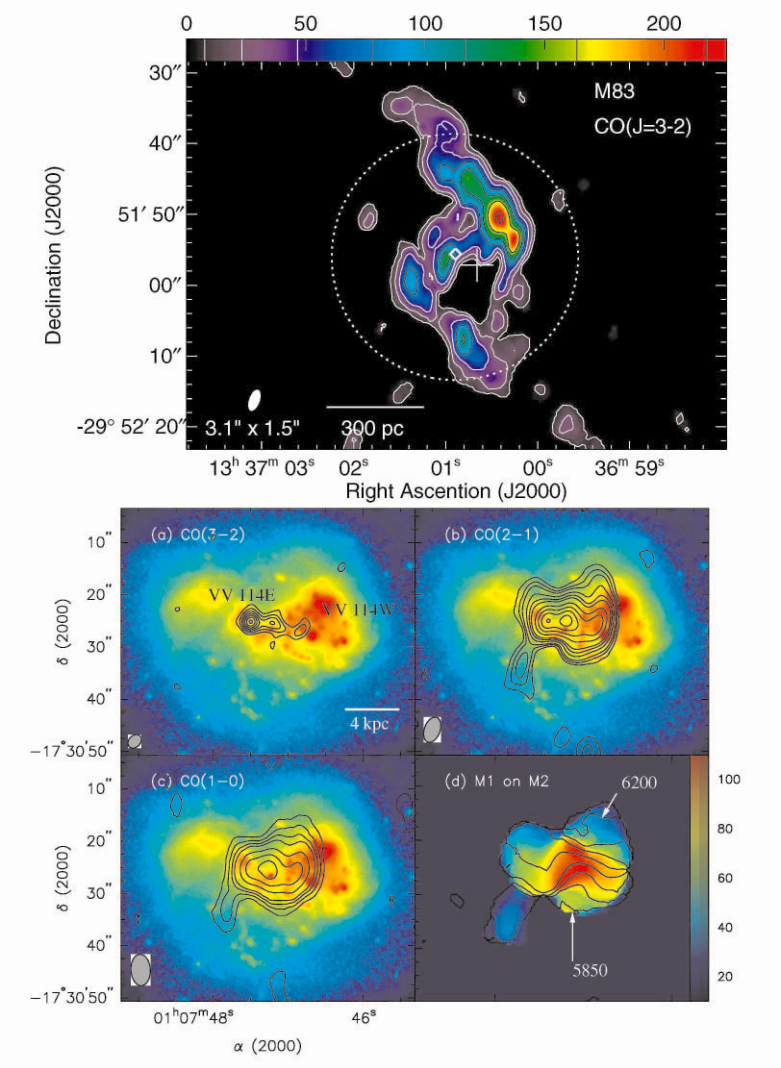


Fig. 2. a) Integrated intensity map of CO(3–2) in the center of M83. The diamond marks the visible nucleus and the cross is at the isophotal centroid in K band. The synthesized beam of $3\farcs1 \times 1\farcs5$ is shown at the bottom left corner. The unit of intensity is Jy beam^{-1} km s^{-1}. The dotted contour shows the half power width of the primary beam [4]. **b)** High resolution CO (3–2) interferometric map of the interacting galaxy system VV 114, revealing a substantial amount of warm and dense gas in the IR-bright but optically obscured galaxy, VV 114E, and the overlap region connecting the two nuclei. A 1.8×1.4 kpc concentration of CO (3–2) gas with a total mass of 4×10^9 $M_\odot$ coincides with the peaks of NIR, MIR, and radio continuum emission found previously by others, identifying the dense fuel for the AGN and/or the starburst activity there. Extensive CO (2–1) emission is also detected, and shows a similar morphology to the CO (1–0) results of Yun et al. [7] and Iono et al. [3].

On the Relevance and Future of UV Astronomy

A.I.G. de Castro[1,2]

Instituto de Astronomía y Geodesia (CSIC-UCM), Fac. de CC. Matemáticas, Univ. Complutense de Madrid, E-28040 Madrid, Spain

Abstract. The UV range supplies a richness of experimental data which is unmatched by any other spectral domain for the study of astrophysical plasmas since (1) almost all the resonance lines of all elements, covering plasmas from the coolest regimes (10-1000K) up to hot (some 10^5K) temperatures are observed in this range, (2)the electronic transitions of the most abundant molecules, such as H_2, are in the ultraviolet which is also the most sensitive to the presence of large molecules such as the PAHs and (3)the strong forbidden coronal lines produced at temperatures from 10^6K to 10^7K are also observed in this range. Amazingly enough, no firm plans exist for the future to maintain an Ultraviolet observing capability for Astrophysics. Only concerted efforts by the community will supply the information required to have the space agencies decide to release the funding needed for the support of these important Astrophysical study capabilities. For this purpose, the Network for UltraViolet Astrophysics (NUVA, `http://www.NUVA.ucm.es`) has been established within the OPTical Infrared COordination network for Astronomy (OPTICON). NUVA will assess the future needs and develop a perspective for the future on a European scale.

In this contribution, the relevance of the ultraviolet range for the progress of the science of astrophysics is outlined.

1 The Relevance of the UV Spectral Range for Astrophysics

Access to the ultraviolet range and, especially, high resolution spectroscopy (R$\geq 30,000$) is required to obtain detailed information of the physical properties, kinematics and velocity of the baryonic component that fills most of the volume of the Universe: diffuse gas. The richness of the UV spectral range (from 90 nm to 350 nm) cannot be matched by any other spectral range, unless for the high redshift Universe ($z > 3$) where the UV spectral tracers are detected in the optical range. The range $0 \leq z \leq 3$ represents an 80% of the cosmic time including the epoch $z = 1$ when the Universe expansion was accelerated through the action of a dark energy of still uncertain origin. Some key problems in modern astrophysics that can only be solved from the UV are:

1. The chemical evolution of the Universe during 80% of its lifetime (from the formation of the first galaxies until now). The UV will allow to study (and compare) the metallicity evolution in dense regions (star formation burst and HII regions) with that in the diffuse component (dark halos or gas clouds within the "voids" of the large scale structure). It will allow to determine the degree of disk-halo mixing and the role of magnetic buoyancy and supernovae explosions in the enrichment of the halo. In addition, the some 10^5–10^6 QSOs in the

magnitude range $18 < m_B < 20$ expected to be detected in the GALEX all-sky UV survey, will represent a complete set background sources to carry out for the first time, a comprehensive study of the InterGalactic Medium (IGM): the diffuse baryonic components that fills most of the volume of the Universe. High sensitivity UV spectroscopy will allow mapping the gas distribution, determining the characteristic sizes, topology, metallicity and ionization fraction of the IGM. The distribution of matter in the voids of the cosmic web will be studied.
2. The physics of accretion and outflow. This physics applies from the formation of the Solar System to cataclysmic variables, supernovae, novae, microquasars, Seyfert galaxies and quasars (i.e. over a range of 10^8 in mass). The transformation of gravitational energy into radiation and mechanical energy (outflow) is controlled by the interaction between the central object and the inner disk. The physics of this process is non-stationary and highly non-linear since magnetic fields and relativity are involved. Pre-Main Sequence stars are non-relativistic objects becoming ideal laboratories to test the numerical models; the radiative output from the disk-star interaction region comes in the UV. In addition, the reverberation of the variations observed in the UV spectrum of the Active Galactic Nuclei has been shown to be a powerful method to study the gas distribution around these sources.
3. The formation of planetary systems. Recent calculations show that planets begin to build-up as early as 10^{5-6} years after the formation of solar-like stars begins. At that time, the disk is irradiated by strong UV and X-ray radiation coming from the dissipation of magnetic energy in the interaction disk-star. This radiation will penetrate the disk giving rise to a very rich chemistry within the inner 2 AU, the area where terrestrial-like planets are expected to be formed. Ultraviolet radiation also plays a very important role in the evolution of the primary atmospheres of the planetary embryos.The electronic transitions of the most abundant molecules: CO, H_2, OH, CS, S_2, CO_2^+, C_2 are in the UV range. The huge effort run by the world-wide astronomical community to find other planetary systems will require follow-up missions to study and characterize the new planets. Access to the ultraviolet range will be instrumental for this purpose.
4. Gravitational effects on the fundamental constants around the epoch of the acceleration onset. The epoch around $z = 1$ is of prime importance for cosmology: at that epoch the expansion of the Universe was accelerated. The source of this acceleration is unclear: from a dark energy field where the Universe is embedded to a flux of gravity away from the 3D space... Detailed measurements of the α fine structure constant along line of sights crossing voids and galactic filaments will allow to study the role of gravity and "dark energy" in the acceleration. Theoretical estimates predict variations of $1/10^5$ in α; this precision can be achieved by observing the absorption of the IGM in some well known UV multiplets.

In fact, there are many fundamental astrophysical studies requiring access to the ultraviolet range to be properly studied. A short list of such studies, classified following the overall scheme of this Conference, is presented below.

1.1 Astrophysical Research Requiring Access to the Ultraviolet Range

Fundamental Physics and Cosmology. Variation of fundamental constants with the gravitational field and redshift. The properties of vacuum around z=1 (acceleration of the Universe expansion)
High-redshift Universe, Galaxies and Galaxy Evolution. Stellar metallicity ($0 < z < 2$). Star formation rates. Intergalactic medium: distribution,physical properties included metallicity. Galactic halos, high-velocity clouds, magnetic buoyancy in galactic disks, and disk-halo interaction.
AGN and Compact Objects. Accretion physics and disk instabilities. Reverberation mapping and gas distribution around AGN.
ISM and Formation and Evolution of Stars. Hot stars atmospheres (and abundance determination) from white dwarfs to hypergiants. Cool stars atmospheres and magnetic dissipation phenomena. Formation of stars (from the epoch of planet building-up) and accretion physics. Circumstellar material and shells in warm environments, jets, and shocks. Chemical abundances in supernovae remnants and in the early phases of supernovae explosions. The warm and hot components of the ISM.
Planets and the origin of life. Planetary atmospheres, auroral variability, comets. Circumstellar environment at the epoch of planet building-up. Chemistry in the Early Solar System.

2 The Future of UV Astronomy

The science outlined above includes some of the fundamental scientific problems that will be addressed by the major astronomical facilities in the next few decades. Henceforth, the access to the UV range is instrumental to guarantee that those objectives are fulfilled.

Presently, there are three major astronomical facilities working in the ultraviolet range: the *Hubble Space Telescope* (HST), the *Galaxy Evolution Explorer* (GALEX) and *Far Ultraviolet Spectroscopic Explorer* (FUSE). HST and FUSE are observatory missions while GALEX is mainly devoted to carry out the first all-sky UV survey in astronomy. The main characteristics of the UV instrumentation in these missions are summarized in Table 1. Unfortunately, FUSE is at the end of its nominal life-time (although new software has been recently implemented to allow FUSE working even without gyros but obviously with a rather limited performance) and the HST upgrade has been, *at the very least*, delayed after the cancellation of the the planned shuttle mission to service and upgrade the Hubble Space Telescope (SM-4). The non-availability of the WFPC3 and COS will have a very negative effect, not only through the absence of the observing capability by itself, but also because of the concurrency with the data from other spacecrafts. XMM-Newton, Integral, Chandra and Spitzer would, together with especially COS and HST, represent a unique capability to study a wide range of Astrophysics where the interactions between physical processes

have to be studied concurrently to establish the real nature and evolution of our Universe.

As for today, the future looks rather dark. The only main facility currently under study and/or development is the *World Space Observatory - Ultraviolet* (WSO/UV). Also a limited sky survey specifically oriented to interstellar absorption (TAUVEX) will be launched in 2005 under a collaboration between ISA and ISRO. If the policy of the Space Agencies does not change soon, the only available facility is going to be the *International Virtual Observatory* (IVO) providing quick and convenient access to the Archives of the old missions.

Table 1. The main UV facilities working in 2004

Facility (lifetime)	Type of Instrument	Spectral Range (nm)	Field of view (arcsec)	Spectral Resolution R	Spatial Resolution
HST (1990-...)	Imaging-ACS(HRC)	200-1100	26x29	Broad band filters (FWHM $\sim$ 40nm)	$0''.027$ pix^{-1}
	Imaging-ACS(SBC)	115-170	31x35		$0''.032$ pix^{-1}
	Imaging-STIS	115-$\sim$350	25x25	Lyα, CIII], MgII Continuum filters	$0''.0246$ pix^{-1}
	Spectroscopy-ACS	115-390	Grism	100	
	Spectroscopy-STIS	115-310	Long-Slit ($52''$)	$\sim$15000 $\sim$1000	$0''.03$ pix^{-1}
		115-315	(echelle)	140000 $\sim$50000	
FUSE (1999-...)	Spectroscopy	90.5-118.7		20000$\pm$2000	
GALEX (2003-2005)	Imaging	135-300	All-sky	Two broad bands: NUV(180-300) and FUV(135-180)	$3''$–$5''$
	Spectroscopy	135-300	(grism)	100	

Acknowledgements

I am indebted to my colleagues in the *Network for UltraViolet Astronomy* (NUVA) and in the *World Space Observatory* (WSO) Implementation Committee (WIC). We all share a common interest in the future of ultraviolet astronomy.

Interrelations Between Strömgren and Vilnius Photometric Systems: An Improvement of Stellar Classification

N. Kaltcheva[1] and J. Knude[2]

[1] University of Wisconsin Oshkosh, 800 Algoma Blvd., Oshkosh WI 54901, USA
[2] Niels Bohr Institute for Astronomy, Physics and Geophysics, Juliane Maries Vej 30, DK-2100 Copenhagen Ø, Denmark

1 Introduction

During recent years considerable efforts have been aimed at the development and use of photometric systems, applicable to very large samples of stars and under the constraints of space-based observations. These systems should be capable of recognizing stars of most spectral types and peculiarities in case of high and non-uniform values of interstellar absorption. In general, these are multi-color intermediate-band systems assuring stellar photometry of very high precision, robustness of the system transformability against different implementations and capability of determining stellar parameters precisely.

2 Results

Recently we presented a number of empirically derived relationships between Vilnius and Strömgren photometric quantities [1–3]. In particular we investigated interrelationships between quantities related to the Balmer discontinuity, metallicity and temperature and noticed significant differences in similar indices, apparently due to small deviations of central wavelength and band width. Using the largest data-base of near-IR Ca II triplet indices currently available [4–6], we demonstrated the influence of the Ca II stellar lines on the X magnitude of the Vilnius photometric system. This influence is significant for spectral classes later than G0, until mid K sub-class, where a linear relation exists between v-X difference and the strength of the infrared CaII triplet.

The strength of Ca II lines is a good luminosity indicator for G-K2 stars. Since most of the light from the galaxies is thought to come from G and K stars, the Ca II triplet is a useful discriminant for the dwarf-giant ratio of the light-dominant stellar population. A photometric index measuring the strength of the Ca II lines may likely find similar application. The further interpretation of the v-X index as a temperature, luminosity or metallicity indicator depends on the interpretation of the relation of the CaII lines strength to these stellar parameters. In general, a photometric index like v-X is virtually unaffected by the interstellar absorption and easily achievable observationally. It could be

developed to provide fast classification of stars of moderate and low surface temperature and may find applications for quick diagnostics of the stellar content of large samples of stars both in Milky Way and other galaxies.

3 Application

A medium-wide photometric band combination will be particularly useful for the ESA's Gaia mission since it may have both a wide band system for chromatic correction of the astrometry and a medium band system for astrophysical properties. If these systems are designed with a medium band located on some astrophysical interesting features (or spectral region) and a wide band with an identical central wavelength the reddening effect of the interstellar medium may be avoided to a large extent. An appropriate medium-wide index correlating well with astrophysical parameters in a simple way may be used for pre-classification the results of which could be fed into a neural network or some other classification procedure.

References

1. N. Kaltcheva, J. Knude: A&A **385**, 1107 (2002)
2. N. Kaltcheva, J. Knude, V. Georgiev: A&A **407**, 377 (2003)
3. J. Knude, N. Kaltcheva: Ap&SS **280**, 67 (2002)
4. A. J. Cenarro, N. Cardiel, J. Gorgas, et al.: MNRAS **326**, 959 (2001)
5. A. J. Cenarro, N. Cardiel, J. Gorgas, et al.: MNRAS **326**, 981 (2001)
6. A. J. Cenarro, J. Gorgas, N. Cardiel, A. Vazdekis, R. F. Peletier: MNRAS **329**, 863 (2002)

HH 110 Proper Motions

R. López[1], A. Riera[2,1], R. Estalella[1], and A.C. Raga[3]

[1] Departament d'Astronomia i Meteorologia, U. de Barcelona, Diagonal 647, E-08028, Spain.
[2] Departament de Física i Enginyeria Nuclear, U. Politècnica de Catalunya, Av. Víctor Balaguer s/n, E-08800 Vilanova i la Geltrú, Spain
[3] Instituto de Ciencias Nucleares, UNAM, PBox 70-543, 04510 México D.F., México

Abstract. The HH 110 jet presents a complex morphology in the optical images, with noticeable wiggles along the length of the jet. New proper motions have been calculated from [SII] CCD images obtained with a time baseline of ~ 15 yr. As a general trend, the HH 110 proper motions show a westward tilt with respect to the jet axis direction. Our results show evidence of an anomalously strong interaction between the outflow and the surrounding environment. These results reinforce the scenario proposed by several authors, in which HH 110 emerges as the result of a grazing collision of the HH 270 jet (another jet, at $3'$ to the NE of HH 110) with a dense clump of molecular gas.

1 Proper Motion Measurements

The HH 110 jet, discovered by Reipurth and Olberg [2], is a major jet (0.45 pc at 460 pc distance) in Orion. The jet presents a rather chaotic morphology in the optical images, its structure being reminiscent of a turbulent outflow. Any stellar source has been detected along the outflow suitable for powering the jet. Proper motions of the HH 110 knots have been determined from the five [SII] 6717+6731 CCD images listed in Table 1, following the method described in [1]. Results are shown in Figure 1 (right panel).

2 Conclusions

The proper motions of the knots show a westward tilt relative to the direction of the axis of the jet. This westward deviation tends to diminish as one goes southwards from knot A (the knot from which the HH 110 jet seems to emanate). Morphology of knot A appreciably changes with time: not only the peak of the emission clearly moves down, but also the structure develops a "tongue" of emitting material, extending along the outflow channel.

There is a region of $\sim 14''$ in length, that corresponds to the knots B and B$'$, which appears to be stationary.

Acknowledgements This work was supported by the MCyT grant AYA2002-00205, the CONACyT grants 36572-E and 41320, and the DGAPA grant IN 112602. ALFOSC is owned by Instituto de Astrofísica de Andalucía and operated at the Nordic Optical Telescope under an IAA-Astronomical Observatory of Copenhagen agreement.

Table 1. Log of the Data

Epoch	Telescope	Pix.scale(")	Exp.Time(s)	Reference
1987 Dec 18	1.5 m La Silla	0.35	3600	1
1988 Mar 5	3.6 m ESO	0.35	1800	1
1993 Dec 16	2.5 m INT	0.55	9000	2
1994 Jan 15	3.5 m NTT	0.35	1200	1
2002 Oct 24	2.6 m NOT	0.19	9000	3

References: (1) from Reipurth et al. 1996 [3]; (2) from Riera et al. 2003 [4]; (3) obtained by Gabriel Gómez through the NOT Service Time facility.

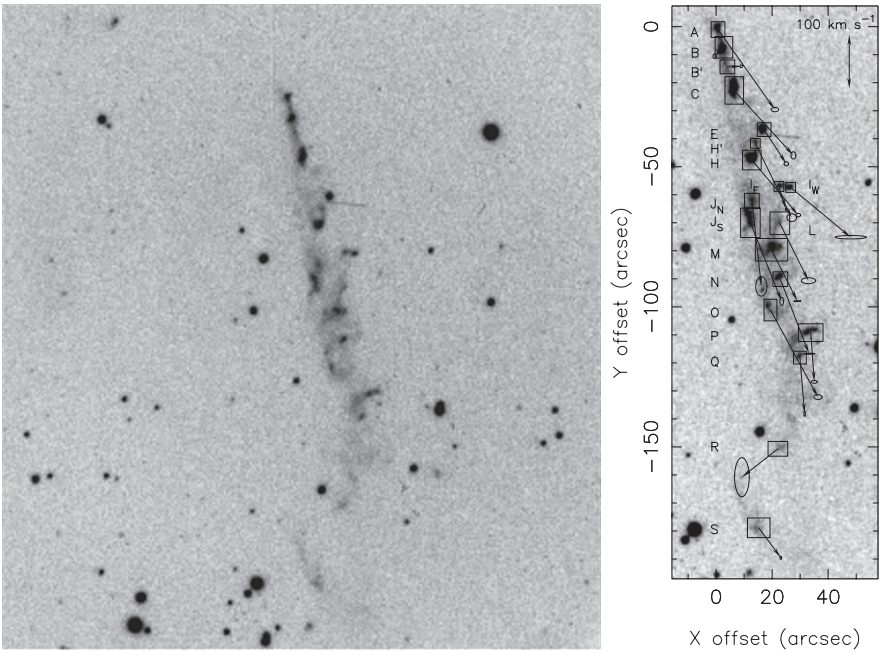


Fig. 1. Left panel:The [SII] 6717+6731 image of HH 110 obtained at the NOT with the ALFOSC camerea. Right panel: Proper motions of the HH 110 knots. Velocity of each knot is indicated by the corresponding arrow. Ellipses indicate the uncertainty in the components of velocity. Offsets are measured from the peak position of knot A. North is up and East is to the left.

References

1. R. López, R. Estalella, A.C. Raga, A. Riera, B. Reipurth, S. Heathcote: A&A, *submitted* (2004)
2. B. Reipurth, M. Olberg: A&A **246**, 535 (1991)
3. B. Reipurth, A.C. Raga, S. Heathcote: A&A **311**, 989 (1996)
4. A. Riera, R. López, A.C. Raga, R. Estalella, G. Anglada: A&A **400**, 213 (2003)

The Effect of the Galactic Gas Distribution on the Expected Cosmic Rays Spectrum

M. Mollá, M. Aguilar, J. Alcaraz, J. Berdugo, J. Casaus, C. Díaz, E. Lanciotti, C. Mañá, J. Marín, G. Martínez, C. Palomares, E. Sánchez, I. Sevilla, and A.S. Torrentó

CIEMAT, Avda. Complutense 22, 28040 Madrid (Spain)

1 Introduction

Cosmic ray (CR) nuclei are accelerated particles which move randomly through the interstellar medium (ISM), where they suffer scattering, reacceleration and energy loss processes before reaching Earth. Spallation processes also take place forming secondary nuclei by fragmentation of heavier ones. Due to the impossibility of observing directly their original direction, the determination of possible sources where these particles originated requires the use of codes to simulate the propagation of CR within the Galaxy. This consists of a spiral disk with a thickness of 2h $\sim$ 200 pc, where CR are created, and a halo with a height H, where they diffuse.

From the existing data, mostly ^{10}Be/^{9}Be and B/C, it is deduced that CR go through a mean density of ~ 0.3 cm^{-3} ([4,5]). Since the total density of the ISM is considered as 1 cm^{-3}, ($< n_{HI} > \sim 0.5\,\mathrm{cm}^{-3}$; [1,2,7,11]), a large effective halo and/or a local bubble or cavity of low density are required. This result is very dependent on the actual disk ISM density, largely uncertain. [6] have very recently obtained a new map of the diffuse gas distribution (Fig. 1), from which $< n_{HI} > \sim 0.2\,\mathrm{cm}^{-3}$, a factor of 2 lower than previous estimates.

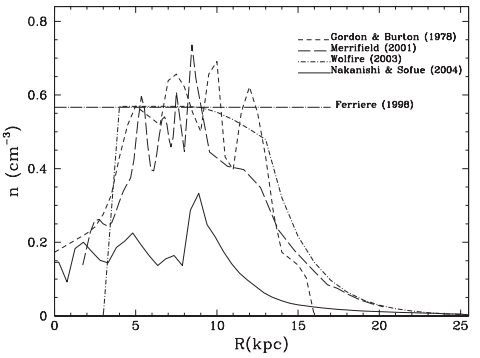


Fig. 1. The radial distribution of the diffuse gas atomic density as obtained from [6] compared with other author's distributions as labeled in the figure

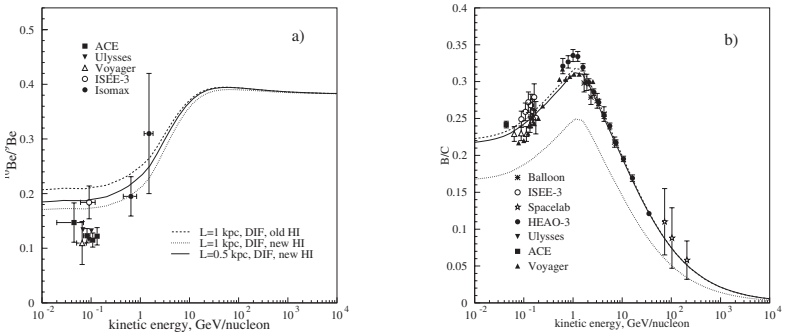


Fig. 2. The spectra of a) ^{10}Be/^{9}Be, and b) of B/C. Models are represented by lines as labeled

2 Computed Models and Results

We now use the GALPROP code, developed by [8,9], to compute how CR propagates. The model includes a realistic diffuse gas radial distribution ([3]). A halo height $H = 1 - 5\,\mathrm{kpc}$ is obtained, depending of the model. Results for ^{10}Be/^{9}Be and B/C are shown with dashed lines in Fig. 2 a) and b), respectively, for a diffusion model with $H = 1\,\mathrm{kpc}$.

We now change the old HI distribution with the new one. The dotted lines in Fig.2 represent the same model using this new distribution. It is evident that it is not yet valid. The solid lines correspond to a new good enough model, with a halo height H = 0.5 kpc. This implies that CR diffuse mostly in the disk closer to the sources than it was deduced before. This result agrees with [10] who obtain distances as short as 500 pc between the source and the Sun, from the ACE radionuclide measurements.

References

1. J.M. Dickey, F.J. Lockman: ARAA **28**, 215 (1990)
2. K. Ferriérre: ApJ **497**, 759 (1998)
3. M.A. Gordon, W.B. Burton: ApJ **208**, 346 (1976)
4. F.C. Jones, A. Lukasiak, V. Ptuskin, W. Webber: ApJ **547**, 264 (2001)
5. D. Maurin, F. Donato, R. Taillet, P. Salati: ApJ **555**, 585 (2001)
6. H. Nakanishi, Y. Sofue: PASJ **55**, 191 (2004)
7. R.P. Olling, M.R. Merrifield: MNRAS **326**, 164 (2001)
8. A.W. Strong, I.V. Moskalenko: ApJ **509**, 212 (1998)
9. A.W. Strong, I.V. Moskalenko: IRC Conf. **28**, 1921 (2003)
10. N.E. Yanasak, M.E. Wiedenbeck, R.A. Mewaldt, et al.: ApJ **563**, 768 (2001)
11. M.G. Wolfire, C.F. McKee, D. Hollenbach, et al.: ApJ **587**, 27 (2003)

Exploring Star Formation in the Galactic Centre Region: From ISO to ALMA

F. Schuller[1,2], F. Bertoldi[1], M. Felli[3], K.M. Menten[1], A. Omont[2], and L. Testi[3]

[1] MPI für Radioastronomie, Auf dem Hügel 69, D-53121 Bonn, Germany
[2] Institut d'Astrophysique de Paris - CNRS, 98 bis, bd Arago, F-75014 Paris, France
[3] Osservatorio Astronomico di Arcetri, Largo E. Fermi, 5, I-50125 Firenze, Italy

1 The ISOGAL YSO Candidates

ISOGAL is a 7 and 15 μm survey of the inner Galactic disk, combined with DENIS near-infrared data [4]. The observed area covers ∼16 deg^2 of the Galactic disk and bulge, with a sensitivity ∼10 mJy, nearly 100 times better than IRAS. A catalogue of ∼10^5 infrared point sources was extracted from these data [6]. Most of them are evolved stars on the asymptotic giant branch (AGB), but a few percent are interpreted as young stellar objects (YSO). In particular, this survey covers the inner Galactic bulge ($|l| \leq 1.5°$, $|b| \leq 0.5°$) almost completely.

In this peculiar region, we could identify most of the brightest ISOGAL sources with known objects. Within 1 deg around the Galactic Centre, 178 sources are matched with long period variable (LPV) stars [2]. Another few sources can be identified with higher mass-loss OH/IR stars or as probable LPV candidates. A total of 189 sources are associated with late-type evolved stars.

On the other hand, 13 sources in the same region can be associated with IRAS and/or radio continuum sources previously interpreted as ultra-compact HII regions. We will consider them as massive YSOs. Another 11 sources are associated with MSX sources (see Sect. 2) which have flux ratios between 21 μm and 15 μm greater than 2. We will consider them as good YSO candidates.

These two classes of objects show different properties at mid-infrared wavelengths: the YSOs have redder colours than late-type evolved stars (see also [1]), and appear slightly extended. This may indicate that the sources interpreted as YSOs are star forming regions containing clusters of young stars, while those associated with AGB stars are actually of stellar nature, and appear point-like.

Using both a colour and a spatial extension criterion, we have selected 300 candidate massive YSOs in the inner bulge from the ISOGAL database [5]. We *roughly* estimated their bolometric luminosities from their flux densities at 15 μm (see [1]). The total luminosity derived from this sample amounts to $\sim 5 \times 10^5$ $L_\odot$.

2 The MSX YSO Candidates

The MSX survey covers all of the Galactic Plane in the 8–21 μm range, with sensitivities of order 100 mJy at 8 μm and ∼1 Jy at longer wavelengths.

In the few regions of the inner Galactic bulge not covered by the ISOGAL observations, we have extracted YSO candidates from the MSX catalogue using

the simple colour criterion $F_{21\,\mu m}/F_{15\,\mu m} \geq 2$. We found 57 YSO candidates, with a total luminosity of $\sim 4.7 \times 10^5$ $L_\odot$.

Using the simple assumption that each source corresponds to a single zero age main sequence star, we can convert these luminosities to *approximate* masses. The observed distribution of masses seems to first order to be consistent with a Salpeter initial mass function (IMF). Finally, assuming that these sources are not older than 0.5 Myr (since they appear as bright mid-infrared sources) we can derive an order of magnitude of the average star formation rate in this region, using a Salpeter IMF to extrapolate our sample (complete above 10^5 $L_\odot$, or $\sim$25 $M_\odot$) to the lower masses. We find:

$$\mathrm{SFR}\,(0.1 - 120\,M_\odot) \approx 0.2 - 0.4\,M_\odot\,\mathrm{yr}^{-1} \quad (1)$$

3 Follow-up Projects

A subsample of 68 robust YSO candidates will be observed with the *IRS spectrometer* on board the *Spitzer Space Observatory*. Small regions (up to 90" extent) around the ISO detected sources will be mapped in the 5–38 μm range, with a moderate spectral resolution of order 100. The main goals are to derive the exact nature of these sources, and to better constrain their luminosities.

Several *large scale surveys* of the *Galactic plane* are currently being discussed, to be performed with upcoming facilities, such as the APEX telescope, equipped with a large (295 element) bolometer array camera operating at 870 μm [3], and the Herschel satellite (providing photometry between 60 and 600 μm). The combination of various wavelengths over the infrared to submillimeter range will allow very accurate assessments of the nature and properties of these objects.

Finally, starting in 2007, the *Atacama Large Millimeter Array (ALMA)* will interferometrically provide very high sensitivity and high spatial resolution, well suited for follow-up observations of a sample of selected targets.

4 Conclusion

Large-scale surveys at various wavelengths are obviously required to constrain the process of star formation in the complex environment of the Galactic Centre, and to better characterise the stellar populations.

References

1. M. Felli, L. Testi, F. Schuller, A. Omont: A&A **392**, 971 (2002)
2. I.S. Glass, S. Matsumoto, B.S. Carter, K. Sekiguchi: MNRAS, **321**, 77 (2001)
3. E. Kreysa, F. Bertoldi, H.-P. Gemuend, et al.: Proc. SPIE **4855**, 41 (2003)
4. A. Omont, G. Gilmore, C. Alard, et al.: A&A **403**, 975 (2003)
5. F. Schuller: The formation of massive stars in the Galaxy as seen by the ISOGAL survey. PhD Thesis, Paris VI University (2002)
6. F. Schuller, S. Ganesh, M. Messineo, et al.: A&A **403**, 955 (2003)

Future Observations of Cosmic Masers

V. Slysh

Astro Space Center, Lebedev Physical Institute, Profsoyuznaya 84/32, 117997 Moscow, Russia

Cosmic masers became a powerful tool for study of stellar evolution in the Galaxy, bursts of star-formation in external galaxies, and accretion disks around central black holes in active galaxies. Due to the small size and narrow line width of maser spots it is possible to measure transversal and radial velocity with high accuracy. Kinematics of the maser spots often reveals expansion and outflow of the matter from proto-stars and new-born stars, or rotation of circumstellar and circumnuclear disks. Stellar may disks contain proto-planets, and maser spots can trace their orbits. Parameters of the circumnuclear disks measured with maser spot motion are directly related to the mass of the central black hole. Another result of the study of maser kinematics is determination of distance to proto-stars and to galaxies. In the latter case the distance determination is independent of the red shift distance and may be used for the determination of the geometry of the Universe. The accuracy of the kinematic measurements of masers is limited by the available angular resolution, time span and sensitivity of VLBI systems used for such observations. The available time span is limited by the fast time variations of masers, especially variations in H_2O masers. Many of the masers studied with VLBI have unresolved maser spots, even at the highest resolution. Examples of OH masers unresolved on the space-ground baselines of the Japanese interferometer HALCA are given in [1,2]. In H_2O maser W3(OH) the fringe amplitude remains constant from zero baseline up to 635 $M\lambda$, which corresponds to the angular size of less than 0.06 milliarcsec [3]. High angular resolution images of methanol maser spots reveal presence of the position-velocity gradient across the spots from 3.3 to 50 AU/km s^{-1} . Bandwidth smearing of maser spot images may cause apparent increase of the size when measured with low spectral resolution. In NGC7538 0.1 km s^{-1} spectral resolution will cause increase of the angular size to 1.9 mas [4]. In W3(OH) the same spectral resolution will smear 12 GHz methanol maser spot images to the size from 0.15 to 2 mas [5]. Similar gradient may be present in OH and H_2O masers. It is interesting that the position-velocity gradient of the same magnitude is required by OH maser pump models in order to provide non-local overlap of far-infrared rotational lines [6]. VLBI observations with high spectral resolution like those described in [5] show that when the spectral resolution is sufficient to avoid bandwidth smearing the maser spots remain unresolved. Therefore more angular resolution is needed in order to image maser spots. For the masers the only way to increase angular resolution is to increase the baseline, up to the space baselines. The imaging of the maser spots is one of the goals of the space-ground interferometer RADIOASTRON.

Space-ground interferometer RADIOASTRON

- Ten-meter parabolic prime-focus antenna
- Four dual-polarization receivers at 0.3, 1.6, 4.8, and 22 GHz
- Simultaneous two-frequency or two-polarization operation
- Wide-band 128 Mb s^{-1} downlink
- Possibility to map 18-cm OH masers with angular resolution up to 0.1 milliarcsec, 1.35-cm H_2O masers, extragalactic H_2O megamasers with red shift up to 1500 km s^{-1}, with angular resolution up to 8 microarcsec.

Highly elongated elliptical orbit produces a fan beam for mapping maser spots. The orbit parameters are:

- Perigee 10,000 km
- Apogee 350,000 km
- Planned launch 2006

Prospects

- Sensitivity will be a factor of two higher compared to HALCA, which is still not sufficient for the high-dynamic range mapping of masers spots.
- Relative proper motion will be measured 25 times faster than with VLBA. This will enable proper motion measurements for highly variable short-lived H_2O masers.
- Real size of maser spots will be measured under condition of the very high (less than 0.01 km s^{-1}) spectral resolution in order to avoid bandwidth smearing. This reduces sensitivity by a factor of 3.

Available results of high angular resolution VLBI and space-VLBI maps of maser spots show a need for still higher angular resolution with better signal-to-noise ratio. The higher angular resolution will be achieved in future space VLBI mission Radioastron, but the sensitivity will be only a factor of two higher compared to HALCA. More sensitivity is needed in order to map maser spots with higher dynamic range and with high spectral resolution.

References

1. V.I. Slysh, M.A. Voronkov, V. Migenes, K.M. Shibata, T. Umemoto, V.I. Altunin, I.E. Val'tts et al.: MNRAS **320**, 217 (2001)
2. V.I Slysh, M.A. Voronkov, I.E. Val'tts, V. Migenes, K.M. Shibata, T. Umemoto, M. Inoue: 'Space-VLBI observations of OH masers'. In: *Cosmic Masers: From Protostars to Blackholes*, IAU Symposium No.206, eds. V.Migenes, M.J.Reid (ASP Conference Series) p.105 (2002)
3. V.I Slysh: 'Limit on Brightness Temperature in Cosmic Masers'. In: *Radio Astronomy on the Fringe*, eds. J.A. Zensus, M.H. Cohen, E. Ros. ASP Conference Series **300**, 239 (2003)
4. M.R Pestalozzi, M. Elitzur, J.E. Conway, R.S. Booth: ApJ **603**, L113 (2004)
5. L. Moscadelli, K.M. Menten, C.M. Walmsley, M.J. Reid: ApJ **583**, 776 (2003)
6. K.G. Pavlakis, N.D. Kylafis: ApJ **467**, 309 (1996)





Some of those who worked behind the scene, making it all happen





Wrapping up the symposium at the press-conference

Part VI

Planets and Origins of Life

Detection and Characterization of Extra-Solar Planets: Future Space Missions

M.A.C. Perryman[1,2]

[1] European Space Agency, ESTEC, Noordwijk 2200AG, The Netherlands
[2] Sterrewacht Leiden, Postbus 9513, Leiden 2300 RA, The Netherlands

Abstract. Various techniques are being used to search for extra-solar planetary signatures, including accurate measurement of positional (astrometric) displacements, gravitational microlensing, and photometric transits. Planned space experiments promise a huge increase in the detections and statistical knowledge arising from transit and astrometric measurements. Direct detection of even nearby Earth-mass planets in the habitable zone and the measurement of their spectral characteristics, typified by the TPF and Darwin missions, represents a considerable challenge. Beyond TPF/Darwin, Life Finder would aim to produce confirmatory evidence of the presence of life, while an Earth 'imager', some massive interferometric array providing resolved images of a distant Earth, appears only as a distant vision. A 10 nano-arcsec astrometric mission would detect 'Earths' systematically out to 100 pc.

1 Introduction

Many new results in the field of exoplanet detection and characterization from ground-based telescopes are expected over the coming years. Space experiments offer significant observational advantages which will be exploited by a series of planned and future missions, whose objectives focus on increasing our statistical knowledge in order to understand better the formation process, and detecting and characterizing habitable systems [1] (see Figures 1 and 2).

After summarising the status of the space-based transit and astrometry missions, the rest of this paper examines ideas extending beyond these accepted space missions. I have found no reference to transit missions beyond the planned Kepler and Eddington missions, and look first at a space-based lensing proposal, GEST, which expands on the parameter space for which statistical information on planet formation would be provided. Then I look at the various missions aiming at direct detection, including TPF/Darwin. The literature includes many ideas which fall under the category of scientific or technical precursors to TPF/Darwin, as well as some pointers to the missions which will follow a successful TPF/Darwin: 'life finders' and 'planet imagers'. I conclude with a look at nanoarcsec astrometry, which would have considerable discovery potential as well as demanding technology very similar to that of a 'mini-life finder' which has already been examined under NASA contract.

A convenient starting point for more information about each is contained in the ongoing programmes and future projects section of Jean Schneider's www page (http://www.obspm.fr/encycl/searches.html). I will not cover observations

of protostellar disks, and issues of the formation, evolution, migration and stability of systems, nor will I review the many ongoing ground-based surveys, which are limited in their search space due to the restrictions indicated in Figure 2. At the time of writing, this www page lists as either ongoing or planned: 18 radial velocity searches, 15 transit searches, 5 microlensing programmes, 10 imaging/direct detection programmes, 2 radio surveys, and 3 astrometric efforts.

This paper is an update of a similar presentation made in October 2003 at the Maryland Conference 'The Search for Other Worlds'.

2 Transits and Astrometry

First on the horizon of approved missions comes Kepler (NASA), due for launch around 2007. This should provide improved prospects for photometric transits following on from MOST (launched on 30 June 2003, and reportedly working well) and Corot (launch planned for June 2006). It focuses on the detection of Earth-size planets in the habitable zone, monitoring some 10^5 main-sequence stars. Detection of some 50–640 terrestrial inner-orbit planet transits are predicted, depending on whether their typical radii lie in the range $R \sim 1.0-2.2R_{\rm E}$. Eddington (ESA) was designed to monitor some 5×10^5 stars, and proposed for launch around 2008. It entered ESA's science programme as a 'reserve' mission, was approved in 2002, and cancelled in November 2003 (due to overall financial pressures), although studies continue in the context of future ESA options. Predictions are for some 20 000 planets with $R < 15R_{\rm E}$, some 2000 terrestrial planets, and perhaps some dozens of Earth-like planets in the habitable zone. An advance in transit statistics may also come from observations of the Galaxy bulge with HST in February 2004 by Kailash Sahu. Transit searches are particularly important since they open the possibility of determining physical diagnostics of the transiting planet, as has been demonstrated for HD 209458 with the detection of sodium [2], an extended hydrogen exosphere [3], oxygen and carbon [4], and the ongoing searches for CO and water.

Gaia (ESA) and SIM (NASA) are two very different approaches to space astrometry, both currently being developed for launch around 2010–12. Gaia is a scanning, survey-type instrument [5], contributing to the large-scale systematic detection of Jupiter-mass planets (or above) in Jupiter-period orbits (or smaller); some 10–20 000 detections out to 150–200 pc are expected [6,7], including most of the (longer-period) radial velocity detections known to date (see Figure 3). Planetary masses, M, rather than $M \sin i$, will be obtained, orbital parameters for some 5000 systems, and relative inclinations for multiple systems. Some 4–5000 transit systems, of the hot-Jupiter type, might also be detected [8]. Gaia might also detect a handful of protoplanetary collisions photometrically [9], although whether they might ever be recognised as such is a different matter.

SIM is a pointed interferometer with a launch around 2009 [10]: accuracies of a few microarcsec down to 20 mag are projected, but such faint observations will be expensive in observing time, and brighter target stars are likely to be the rule. In the field of exoplanets, SIM will excel in any accurate and frequent astro-

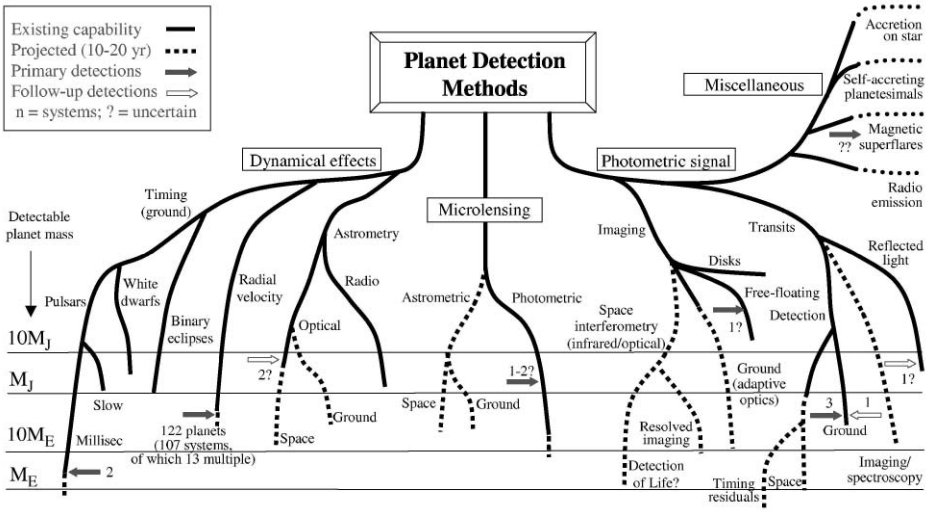


Fig. 1. Detection methods for extra-solar planets. The lower extent of the lines indicates, roughly, the detectable masses that are in principle within reach of present measurements (solid lines), and those that might be expected within the next 10–20 years (dashed). The (logarithmic) mass scale is shown at left. The miscellaneous signatures to the upper right are less well quantified in mass terms. Solid arrows indicate (original) detections according to approximate mass, while open arrows indicate further measurements of previously-detected systems. '?' indicates uncertain or unconfirmed detections. The figure takes no account of the numbers of planets that may be detectable by each method.

metric follow-up of previously-detected systems. The baselined planet detection program includes 50 separate epoch 1-hour observations of selected fields, with some 250 stars measured at 1 μas accuracies, and some 2000 stars at accuracies of about 4 μas.

While these transit and astrometric discovery predictions must be taken with certain caveats, most notably as a result of our uncertainty of the exoplanet population properties, they promise a major advance in the detection and knowledge of the statistical properties of a wide range of exoplanets: ranging from heavy (Jupiter-mass) planets in long-period (Jupiter-type) orbits via astrometry, through to Earth-mass planets in the habitable zone, and the occurrence and properties of multiple systems.

3 Lensing

Although primarily devoted to lensing searches, GEST (Galactic Exoplanet Survey Telescope [11]) is also sensitive to transits. GEST was proposed for a NASA mission in 2001–02 (a Survey for Terrestrial ExoPlanets (STEP) was also submitted to NASA's Extrasolar Planets Advanced Concepts Program at the same

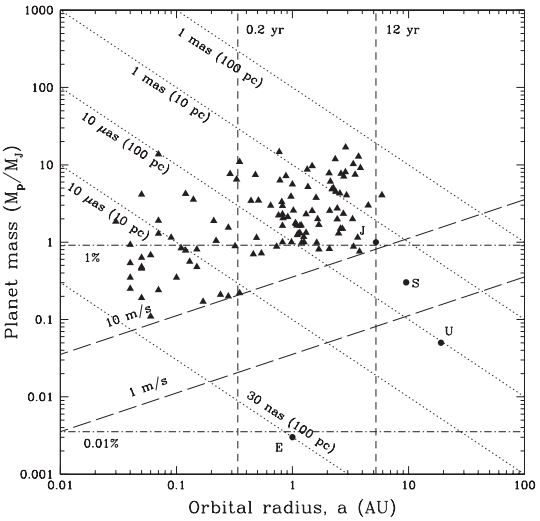


Fig. 2. Detection domains for methods exploiting planet orbital motion, as a function of planet mass and orbital radius, assuming $M_* = M_\odot$. Lines from top left to bottom right show the locus of astrometric signatures of 1 mas and 10 μarcsec at distances of 10 and 100 pc; a measurement accuracy 3–4 times better would be needed to detect a given value of α. Very short and very long period planets cannot be detected by planned astrometric space missions: vertical lines show limits corresponding to orbital periods of 0.2 and 12 years. Lines from top right to bottom left show radial velocities corresponding to $K = 10$ and $K = 1$ m s^{-1}; a measurement accuracy 3–4 times better would be needed to detect a given value of K. Horizontal lines indicate photometric detection thresholds for planetary transits, of 1% and 0.01%, corresponding roughly to Jupiter and Earth radius planets respectively (neglecting the effects of orbital inclination, which will diminish the probability of observing a transit as a increases). The positions of Earth (E), Jupiter (J), Saturn (S) and Uranus (U) are shown, as are the lower limits on the masses of known planetary systems (triangles).

time). A 1.2-m aperture telescope with a 2 deg^2 field of view continuously monitors 10^8 Galactic bulge main-sequence stars. Sources in the bulge are lensed by foreground (bulge or disk) stars which are accompanied by the planets being sought. GEST was not selected in 2002, but will be re-submitted during 2004 under the name of Microlensing Planet Finder (MPF), using HgCdTe and Si-PIN detectors in place of the earlier CCDs.

The sensitivity of such measurements is highest at orbital separations of 0.7–10 AU, but it will also detect systems with larger separations, masses as low as that of Mars, large moons of terrestrial planets, and some 50 000 giant planets via transits with orbital separations of up to 20 AU (the prime sensitivity of a transit survey extends inward from 1 AU, while the sensitivity of microlensing extends outwards). There are theoretical reasons to believe that free-floating

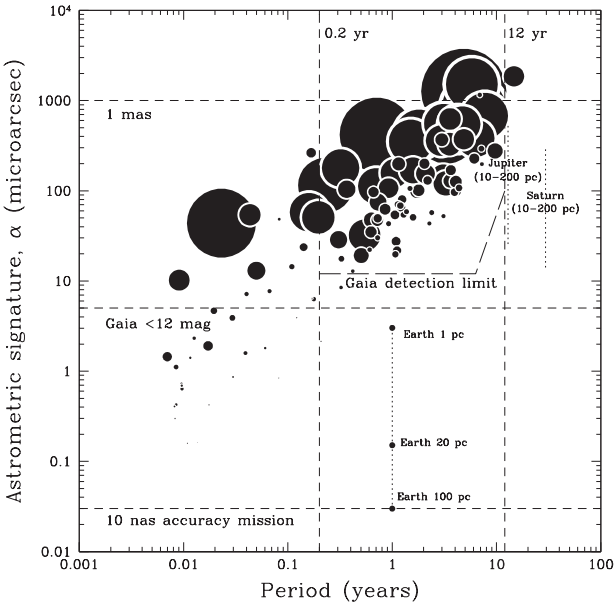


Fig. 3. Astrometric signature, α, induced on the parent star for the known planetary systems, as a function of orbital period. Circles are shown with a radius proportional to $M_p \sin i$. Astrometry at the milliarcsec level has negligible power in detecting these systems, while the situation changes dramatically for microarcsec measurements. Short-period systems to which radial velocity measurements are sensitive are difficult to detect astrometrically, while the longest period systems will be straightforward for microarcsec positional measurements. Effects of Earth, Jupiter, and Saturn are shown at the distances indicated.

planets may be abundant as a by-product of the planetary formation process and, uniquely, GEST will also be able to detect these.

The planetary lensing events have a typical duration of 2–20 hr (compared to the typical 1–2 month duration for lensing events due to stars), and must be sampled by photometry of $\sim 1\%$ accuracy several times per hour over a period of several days, and with high angular resolution because of the high density of bright main-sequence stars in the central bulge. The proposed polar orbit is oriented to keep the Galactic bulge in the continuous viewing zone.

Most of the multiple-planet detections in the simulations of [11] are systems in which both 'Jupiter' and 'Saturn' planets are detected (Figure 4). Since multiple orbits are generally stable only if they are close to circular, a microlensing survey will be able to provide information on the abundance of giant planets with nearly circular orbits by measuring the frequency of double-planet detections and the ratios of their separations.

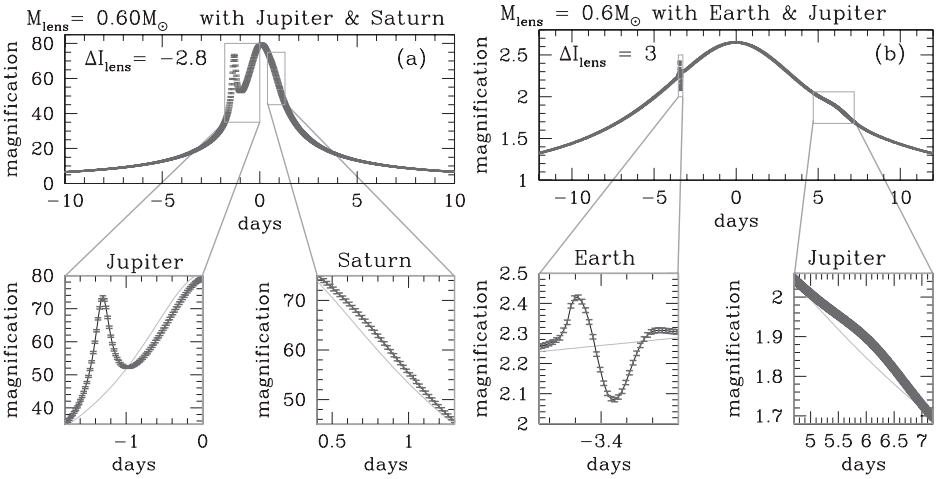


Fig. 4. Example multiple-planet light curves from the simulation of planetary systems with the same planetary mass ratios and separations as in our solar system (from [11]). Left: an example of a Jupiter/Saturn detections. Right: an example of the detection of Earth and a Jupiter.

Just over 100 Earths would be detected if each lens star has one in a 1 AU orbit. The peak sensitivity is at an orbital distance of 2.5 AU, with 230 expected detections if each lens star had a planet in such an orbit. Based on certain observational conditions and physical arguments, the data can provide the mass of the host star, the planetary mass, the distance to the host star, and the planet-star separation in the plane of the sky.

One of the disadvantages of lensing experiments is that a planet event, once observed, can never (in practice) be seen again – follow-up observations for further characterizations are not feasible (unlike the case for any of the other principal detection methods). Nevertheless, a mission like GEST will provide important observational and statistical data on the occurrence of low-mass planets, low-mass planets at larger orbital radii, multiple systems and, significantly, free-floating planets formed as a by-product of the system formation. Lensing experiments, like transit experiments, can never realize their full potential unless placed in space, so that a mission designed for both lensing and transit measurements should have a place in the armoury of space missions.

4 Direct Detection

The promised science and enabling technologies for high-contrast space imaging have been explored in the contexts of JWST, TPF/Darwin, and various NASA Explorer or Discovery class missions [12]. Very large ground-based telescope studies, in the 50–100 m class, consider the direct detection of exo-planet

systems high in their list of scientific priorities. The many possible solutions involve combinations of active wavefront correction, coronographs, apodization, interferometers, and large free-flying occulters. Table 1, from [13], is a summary of detection capabilities for an Earth at 10 pc for various experiments being studied, and shows that even for the most ambitious projects being planned at present, direct detection of even a nearby Earth represents a huge challenge.

TPF has been conceived as either a coronograph operating at visible wavelengths or a large-baseline interferometer operating in the infrared. There are two aspects of this choice which should be distinguished: (a) the scientific aspect: is reflected (visible and near IR) light or thermal emission (mid-IR) the best regime to characterize planets (albedo, temperature, colour, etc; see [14] for a recent discussion); (b) the instrumental aspects: is an interferometer or a coronograph the best? Here, the NASA Technology Plan for TPF stated that 'Technology readiness, rather than a scientific preference for any wavelength region, will probably be the determining factor in the selection of a final architecture'. In May 2002, two architectural concepts were selected for further evaluation: an infrared interferometer (multiple small telescopes on a fixed structure or on separated spacecraft flying in precision formation and utilizing nulling), and a visible light coronograph (utilizing a large optical telescope, with a mirror three to four times bigger and at least 10 times more precise in WFE than the Hubble Space Telescope). In April 2004, NASA announced that it would embark on a 6×3.5 m visual coronograph in 2014 (TPF-C), targeting a full search of 32 nearby stars and an incomplete search for 130 stars; and that a free-flying interferometer, in collaboration with ESA, would be considered before 2020 (TPF-I).

A visible light system can be smaller (some 10 m aperture) than a comparable interferometer, however advances in mirror technology are required: mirrors must be ultra-smooth ($\sim \lambda/15\,000$) to minimize scattered light, and in addition active optics would be needed to maintain low and mid-spatial frequency mirror structure at acceptable levels. IR interferometry would require either large boom technology or formation flying, typically with separation accuracies at the cm-level with short internal delay lines. For the detection of ozone at distances of 15 pc and S/N$\sim$25, apertures of about 40 m^2, and observing times of 2–8 weeks per object, are indicated.

The ESA effort is focussed on an interferometer: Darwin is a presently considered as a flotilla of eight spacecraft (6 telescopes, one beam combination unit, and one communication unit) that will survey 1000 of the closest stars in the infrared, searching for Earth-like planets and analyzing their atmospheres for the chemical signature of life [15], scientific objects in common with those of TPF. The system is presently planned for an L2 orbit, and a single Ariane launch. Specific precursor efforts include GENIE, a nulling interferometer prototype under development by ESA and ESO for the VLTI, and the space mission Smart-3, not yet approved, but included within the Darwin concept plans to demonstrate the concept of formation flying for two or three satellites. GENIE could use either the VLT UTs or ATs, at a wavelength of 3.6 μm, and will be considered by the ESA Council late in 2004.

Table 1. Detection capabilities: Earth at 10 pc (from [13]). $\Delta\theta = 0.1$ arcsec, $t_{\rm int} = 24$ hr, QE = 0.2, $\Delta\lambda/\lambda = 0.2$. Mode = N corresponds to a nulling system, C to a coronograph. The ground-based results assume that long-term averaging is realistic, with fast atmospheric correction.

Telescope	Size (m)	λ(μm)	Mode	S/N	Comment
Darwin/TPF-I	4×2	11	N	8	
TPF-C	3.5	0.5	C	11	Typical launcher diameter
”	7	0.8	C	5–34	
Antarctic	21	11	N	0.5	
”		0.8	C	6	
CELT, GMT	30	11	N	0.3	30 m [C] too small at 11 μm
”		0.8	C	4	
OWL	100	11	C	4	Large Φ [C] for IR suppression
”		0.8	C	46	Optical spectroscopy possible
Antarctic OWL	100	11	C	17	Comparable to Darwin/TPF
”		0.8	C	90	Water bands at 1.1–1.4 μm

4.1 Precursors: Interferometers, Coronographs and Apodizers

The McKee-Taylor Decadal Survey Committee [16] qualified its endorsement of the TPF mission with the condition that the abundance of Earth-size planets be determined prior to the start of the TPF mission. In these sections we look at ideas which have not (yet) been approved, and which may fall somewhere between scientific and technological precursors for TPF. Some are concepts, while some are specific mission proposals.

Eclipse (coronography) is a proposed NASA Discovery-class mission to perform a direct imaging survey of nearby planetary systems, including a complete survey for Jovian-sized planets orbiting 5 AU from all stars of spectral types A–K within 15 pc of the Sun [17]. Its optical design incorporates a telescope with an unobscured aperture of 1.8 m, a coronographic camera for suppression of diffracted light, and precision active optical correction for suppression of scattered light, and imaging/spectroscopy. A three-year science mission would provide a survey of the nearby stars accessible to TPF. Eclipse may be resubmitted for NASA's next Discovery round in 2004.

Jovian Planet Finder (JPF) was a MIDEX proposal to directly image Jupiter-like planets around some 40 nearby stars using a 1.5-m optical imaging telescope and coronographic system, originally on the International Space Station (ISS) [18]. Its sensitivity results from super-smooth optical polishing, and should be sensitive to Jovian planets at typical distances of 2–20 AU from the parent star, and imaging of their dusty disks – potentially solar system analogues. A 3-yr mission lifetime is proposed. Some successor to JPF may be resubmitted for NASA's next Discovery round in 2004, probably through a merging with ESPI ('EPIC', Clampin, private communication).

Extra-Solar Planet Imager (ESPI) is another proposed precursor to TPF [19]. Originally proposed as a NASA Midex mission as a 1.5×1.5 m^2 apodized square aperture telescope, reducing the diffracted light from a bright central source, and making possible observations down to 0.3 arcsec from the central star. Jupiter-like planets could be detected around 160–175 stars out to 16 pc, with S/N > 5 in observations lasting up to 100 hours. Spectroscopic follow-up of the brightest discoveries would be made. The Extrasolar Planet Observatory (ExPO) is a similar concept proposed as a Discovery-class mission [20].

Self-luminous Planet Finder (SPF) is a further TPF precursor under study by N. Woolf and colleagues, aiming at the search for younger or more massive giant planets in Jupiter/Saturn like orbits, where they will be highly self-luminous and bright at wavelengths of 5–10 μm, where neither local nor solar system zodiacal glow will limit observations. SPF will demonstrate the key technologies of passive cooling associated with interferometric nulling and truss operation that are required for a TPF mission. SPF targets young Jupiter-like planets both around nearby stars such as ϵ Eri, and around A and early F stars.

The Fourier-Kelvin Stellar Interferometer (FKSI) is a concept under study at NASA GSFC [21]. It is a space-based mid-infrared imaging interferometer mission concept being developed as a precursor for TPF. It aims to provide 3 times the angular resolution of JWST and to demonstrate the principles of interferometry in space. In its minimum configuration, it uses two 0.5-m apertures on a 12.5-m baseline, and predicts that some 7 known exoplanets will be directly detectable in this configuration, with low-resolution spectroscopy ($R \sim 20$) being possible in the most favorable cases.

Optical Planet Discoverer (OPD) is a concept midway between coronography and Bracewell nulling [22].

Phase-Induced Amplitude Apodization (PIAA [23]) is an alternative to classical pupil apodization techniques (using an amplitude pupil mask). An achromatic apodized pupil is obtained by reflection of an unapodized flat wavefront on two mirrors. By carefully choosing the shape of these two mirrors, it is possible to obtain a contrast better than 10^9 at a distance smaller than $2\lambda/d$ from the optical axis. The technique preserves both the angular resolution and light-gathering capabilities of the unapodized pupil, and aims for efficient detection of terrestrial planets with a 1.5-m telescope in the visible.

4.2 Free-Flying Occulters

Occulting masks are another approach to tackle in a conceptually simple manner the basic problem of how to separate dim sources from bright ones, although interest in this approach at NASA level currently appears limited. The history of free-flying occulters to search for extra-solar planets goes back to at least the early 1960s, with ideas by Robert Danielson, Lyman Spitzer, Gordon Woodcock, and Christian Marchal (who found that the screen's efficiency can be enhanced by choosing complex shapes). Occulters have also been considered as precursor missions to TPF/Darwin.

UMBRAS (Umbral Missions Blocking Radiating Astronomical Sources) refers to a class of missions, currently designed around a 4-m telescope and a 10-m occulter, with earlier concepts including a 5–8 m screen (CORVET), or as NOME (Nexus Occulting Mission Extension) a modification to Nexus, itself foreseen as an engineering test of key technologies for JWST, cancelled in 2000.

BOSS (Big Occulting Steerable Satellite [24]) consists of a large occulting mask, typically a 70×70 m^2 transparent square with a 35 m radius, and a radially-dependent, circular transmission function inscribed, supported by a framework of inflatable or deployable struts. The mask is used by appropriately aligning it with a ground- or space-based observing telescope. In combination with JWST, for example, both would be in a Lissajous-type orbit around the Sun-Earth Lagrange point L2, with the mask steered to observe a selected object using a combination of solar sailing and ion or chemical propulsion. Thermal emissivity, reflection, and scattering properties of the screen have also been considered. All but about 4×10^{-5} of the light at 1 μm would be blocked in the region of interest around a star selected for exoplanet observations (since occultation occurs outside the telescope, scattering inside the telescope does not degrade this performance). Their predictions suggest that planets separated by as little as 0.1–0.2 arcsec from their parent star could be seen down to a relative intensity of 1×10^{-9} for a magnitude 8 star. Their simulations indicate that for systems mimicking our solar system, Earth and Venus would be visible for stars out to 5 pc, with Jupiter and Saturn remaining visible out to about 20 pc (Figure 5).

5 Beyond TPF/Darwin

Within NASA's Origins Program HST, SIRTF and others are referred to as 'precursor missions', with SIM and JWST as 'First Generation Missions' leading to the 'Second Generation Mission' TPF which will begin to examine the existence of life beyond our Solar System. Once habitable planets are identified, a 'Life Finder' type of mission would expand on the TPF principles to detect the chemicals that reveal biological activities. And once a planet with life is found, 'Planet Imager' would be needed to observe it. These 'Third Generation Missions', Life Finder and Planet Imager, are currently just visions because the required technology is not on the immediate horizon.

Life Finder Taking pictures of the nearest planetary system (TPF/Darwin) is considered to be a reasonable goal on a 10-year timescale, with low-quality spectra a realistic by-product. Life Finder, which would only be considered after TPF/Darwin results are available, and once oxygen or ozone has been discovered in the atmosphere, would aim to produce confirmatory evidence of the presence of life, searching for an atmosphere significantly out of chemical equilibrium, for example through its oxygen (20% abundance on Earth) and methane (10^{-6} abundance on Earth). Some pointers to the technology requirements and complexity of Life Finder have been described in the 'Path to Life Finder' [25].

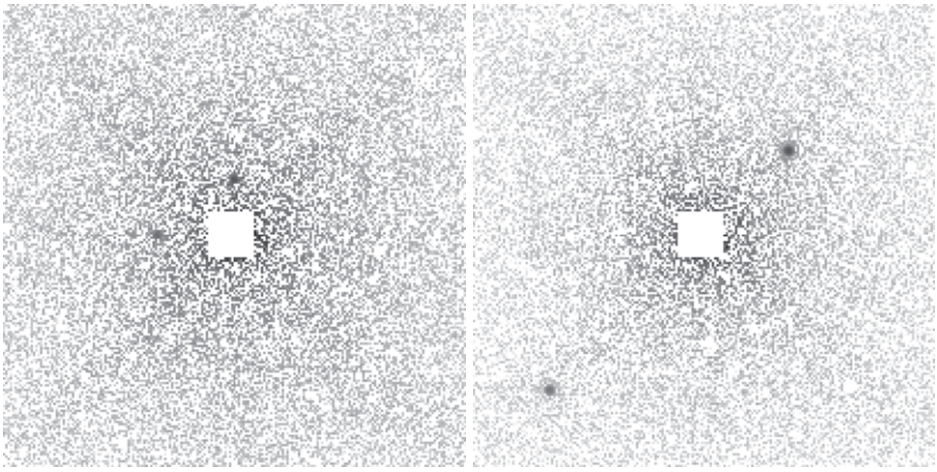


Fig. 5. Left: a 2×2 arcsec^2 image of the log intensity of our solar system at 3 pc from BOSS observed at 1 μm by an 8-m space telescope in a 3000 s exposure. The Sun is located at the centre, with the central 0.2 arcsec square, corresponding to BOSS, cut out of the image. Both Venus (above) and Earth (left) are observable. Right: as viewed from 10 pc. Venus and Earth are now occulted, and Jupiter (upper right) and Saturn (lower left) are visible.

Given that TPF/Darwin will take low-resolution low-S/N spectra, a large area high-angular resolution telescope will be needed for detailed spectral study in order to confirm the presence of life. Recalling that the target objects will be as faint as the Hubble Deep Field galaxies, buried in the glare of their parent star some 0.05–0.1 arcsec away, the light collecting area of Life Finder will have to be substantially larger than TPF's 50 m^2: a useful target is 500–5000 m^2. One of the primary technical challenges will be to produce such a collecting area at affordable cost and mass.

The required development of new low mass and better wavefront optics, coronography versus nulling, pointing control by solar radiation pressure, sunshield, vibration damping, and space assembly, were addressed in [25]. According to their study, a 'mini-Life Finder' might be a 50×10 m^2 telescope, made with 12 segments of 8.3×5 m^2, made of 5 kg m^{-2} glass, piezo-electric controlled adaptive optics, and a total mass (optics and structure) of about 10 tons. Cooling would be by an attached sunshade also used for solar pressure pointing, in a 'sun orbiting fall away' orbit to avoid the generation of thruster heat needed to maintain the L2-type orbit. There are still unsolved complexities underlying the actual science case for Life Finder: if the goal is to detect the 7.6 μm methane feature — which is not definitively the relevant goal; see, for example discussions of the use of the 'vegetation signature' in [26] — the required collecting area accelerates from a plausible 220 m^2 (four or five 8-m telescopes) for a planet at 3.5 pc, to a mighty 4000 m^2 (eighty 8-m telescopes) even at only 15 pc. A new

proposal to study Life Finder has recently been submitted to NASA by Shao, Traub, Danchi & Woolf (N. Woolf, private communication). Various reports on related studies can be found under NASA's Institute for Advanced Concepts (NIAC) www pages (http://www.niac.usra.edu/) including 'Very large optics for the study of Extrasolar Terrestrial Planets' (N. Woolf); and 'A structureless extremely large yet very lightweight swarm array space telescope' (I. Bekey). The former includes an outline technology development plan for Life Finder, with costs simply stated as $\gg$\$2 billion.

Planet Imager TPF aims to image a reflected point-source image of a planet. Resolving the surface of a planet is, at best, a far future goal requiring huge technology development that is not yet even in planning. Much longer baselines will be required, from tens to hundreds of km in extent. Formation flying of these systems will require technology development well beyond even the daunting technologies of TPF/Darwin – complex control systems, ranging and metrology, wavefront sensing, optical control and on-board computing. Having accepted that we are now peering into a much more distant and uncertain future, we can examine some of the ideas which are being discussed.

Life Finder studies [25] have been used to evaluate the requirements for Planet Imager which, they consider, would require some 50–100 Life Finder telescopes used together in an interferometric array. Their conclusions were that *'the scientific benefit from this monstrously difficult task does not seem commensurate with the difficulty'*. This echoes the conclusions of [27] who undertook a partial design of a separated spacecraft interferometer which could achieve visible light images with 10×10 resolution elements across an Earth-like planet at 10 pc. This called for 15–25 telescopes of 10-m aperture, spread over 200 km baselines. Reaching 100×100 resolution elements would require 150–200 spacecraft distributed over 2000 km baselines, and an observation time of 10 years per planet. These authors noted that the resources they identified would dwarf those of the Apollo Program or the Space Station, concluding that it was *'difficult to see how such a program could be justified'*. The effects of planetary rotation on the time variability of the spectral features observed by an imager, complicates the imaging task although may be tractable, while more erratic time variability (climatic, cloud coverage, etc.) will greatly exacerbate any imaging attempts.

OVLA Parallel to the Planet Imager studies in the US, in Europe the LISE group (Laboratoire d'Interférométrie Stellaire et Exo-planétaire) carries out research in the area of high-resolution astronomical imaging, including imaging extra-solar planets. The group is studying several complementary projects for 'hypertelescopes' on Earth and in space [28,29]. The steps needed to reach this goal are set out as requiring: (1) a hypertelescope on Earth – the OVLA (Optical Very Large Array); (2) a 100-m precursor geostationary version in space; (3) a km-scale version in a higher orbital location; (4) a 100 km version, including dozens of mirrors of typically 3 m aperture. Labeyrie et al. proposed the mission 'Epicurus', an extrasolar earth imager, to ESA in 1999 in response to the F2/F3 call for mission proposals.

Their basic 'hypertelescope' design involves a dilute array of smaller apertures (an imaging interferometer) having a 'densified' exit pupil, meaning that the exit pupil has sub-pupils having a larger relative size than the corresponding sub-apertures in the entrance pupil. Their applicability extends to observing methods highly sensitive to the exit pupil shape, such as phase-mask coronography.

In more recent published studies [28] the hypertelescope is combined with such a coronograph to yield attenuations at levels of 10^{-8}. Simulations of 37 telescopes of 60 cm aperture distributed over a baseline of 80 m in the IR, observing the 389 Hipparcos M5–F0 stars out to 25 pc (with simulated contributions from zodiacal and exo-zodiacal background) yields 10-hour snapshot images in which an Earth-like planet is detectable around 73% of the stars. Gains of a factor 20–30 with respect to a simple Bracewell nulling interferometer are reported.

In space, the plans call for a flotilla of dozens or hundreds of small elements, deployed in the form of a large dilute mosaic mirror. Pointing is achievable by globally rotating the array, which is slowly steerable with small solar sails attached to each element. A 'moth-eye' version allows full sky coverage with fixed elements, using several moving focal stations [30,31]. The geostationary precursor hypertelescope could be a possible version of Terrestrial Planet Finder (TPF). An exo-Earth discoverer would require a 100–1000 m hypertelescope with coronograph, while an exo-Earth imager would require a 150 km hypertelescope with coronograph. In the approach of [31] a 30-min exposure using a hypertelescope comprising 150 3-m diameter mirrors in space with separations up to 150 km, would be sufficient to detect 'green' spots similar to the Earth's Amazon basin on a planet at a distance of 10 light-years (although these vegetation features are more prominent in the infrared, e.g., citeperryman:26).

6 Nanoarcsec Astrometry

The ambitious technological nature of the imaging exoplanet missions being considered, as well as the subject of this review, offers an opportunity for some speculation about astrometry at the nas (nanoarcsec) levels. Earth-mass perturbations around a solar-mass star are 300 nas at 10 pc, or 30 nas at 100 pc, the latter requiring an instantaneous measurement accuracy a factor 3 better, i.e. 10 nas at, say, 12 mag. This is a factor of some 1000 improvement with respect to Gaia. Keeping all other mission parameters (efficiency, transverse field of view, mission duration, total observing time per star, and image pixel sampling, etc.) unchanged, we can consider reaching this accuracy simply through a scaling up of the primary mirror size. The Gaia primary mirror has an along-scan dimension $D = 1.4$ m and a transverse dimension $H = 0.5$ m; the final accuracy scales as $\sigma \propto D^{-3/2} H^{-1/2}$. These desired accuracies would therefore require a primary mirror size of order 50×12 m^2, and a focal length (scaling with D) of about 1600 m. Interestingly, this is the scale of the optics derived for the mini-version of Life Finder (Figure 6). Such a system would provide sub-microarcsec accuracies on all objects to 20 mag out to 100 pc, independent of *a priori* knowledge.

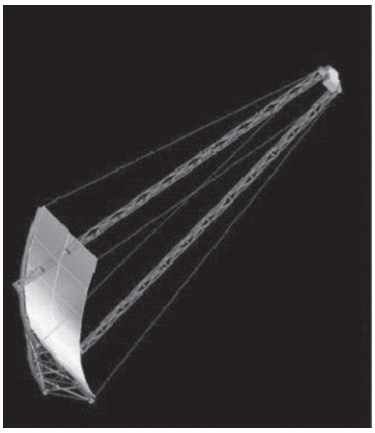


Fig. 6. The 50×10 m^2 telescope of a mini-life finder, from [25], also suitable for nano-arcsec level astrometry for the detection of Earths out to 100 pc.

Accuracy levels of $\sim$ 10 nas are still above the noise floors due to interplanetary and interstellar scintillation in the optical, or stochastic gravitational wave noise, although this does not consider whether an Earth signature can be extracted from that from other planets in the system. Aside from many other domains of interest at 1–10 nas, geometric cosmology becomes accessible.

7 Discussion

Kepler (and, if approved, Eddington) will provide a huge improvement in the statistical knowledge of exoplanet formation and distributions through photometric transits, around the end of this decade, detecting several thousand planetary systems, with perhaps several hundred in the habitable zone. Gaia will detect 10–20 000 Jupiter-type systems through astrometric perturbations, revealing evidence for potential Solar System like systems. The proposed mission GEST would provide statistical information through microlensing, including the distribution of free-floating systems. TPF/Darwin aim at the first direct detection of specific systems which are potentially habitable, and should be undertaken in the second half of the next decade. They will be challenging projects, and with a detection horizon of around 20 pc a key question is, of course, are there any Earth-like systems within their detectability domain. The investigations already carried out into Life Finder and Planet Imager provide an insight into the technology required to meet these ambitious goals, but again they will have to be underpinned by a clear and robust scientific judgment on the observational evidence that is needed to qualify the existence of life beyond our Solar System.

References

1. M.A.C. Perryman: Rep. Prog. Phys. **63**, 1209 (2000)
2. D. Charbonneau, T.M. Brown, R.W. Noyes, R.L. Gilliland: Detection of an Extrasolar Planet Atmosphere, ApJ **568**, 377 (2002)
3. A. Vidal-Madjar, A. Lecavelier des Etangs, J.M. Désert, et al.: An extended upper atmosphere around the extrasolar planet HD 209458b, Nature **422**, 143 (2003)
4. A. Vidal-Madjar, J.M. Désert, A. Lecavelier des Etangs, et al.: Detection of Oxygen and Carbon in the Hydrodynamically Escaping Atmosphere of the Extrasolar Planet HD 209458b, ApJ **604**, L69 (2004)
5. M.A.C. Perryman, K.S. de Boer, G. Gilmore, et al.: GAIA, Composition, Formation and Evolution of the Galaxy, A&A **369**, 339 (2001)
6. M.G. Lattanzi, A. Spagna, A. Sozzetti, S. Casertano: Space-Borne Global Astrometric Surveys: The Hunt for Extra-Solar Planets, MNRAS **317**, 211 (2000)
7. A. Sozzetti, S. Casertano, M.G. Lattanzi, A. Spagna: Detection and Measurement of Planetary Systems with Gaia, A&A **373**, L21 (2001)
8. N. Robichon: Detection of transits of extra-solar planets with Gaia, in O Bienaymé & C Turon, eds., Proc. Les Houches Summer School on Gaia, pp. 215–221 (2002)
9. B. Zhang, S. Sigurdsson: Electromagnetic Signals from Planetary Collisions, ApJ **596**, L95 (2003)
10. R. Danner, S. Unwin: SIM, Taking the Measure of the Universe, NASA/JPL (1999)
11. D.P. Bennett, S.H. Rhie: Simulation of a space-based microlensing survey for terrestrial extrasolar planets, ApJ **574**, 985 (2002)
12. C. Beichman: Recommended Architectures for the Terrestrial Planet Finder, Proc. ASP 291, 101 (2003)
13. R. Angel: Direct detection of terrestrial exoplanets: comparing the potential for space and ground telescopes, ESA SP-539: Earths: DARWIN/TPF and the Search for Extrasolar Terrestrial Planets, p. 221 (2003)
14. J. Schneider: Biosignatures and Extrasolar Planet Characterization: Visible versus Infrared, in Proc. Heidelberg Conference, ESA SP-339 (2003)
15. C.V.M. Fridlund: Darwin, the Infrared Space Interferometer, in Darwin and Astronomy, 11–18 ESA SP–451 (2000)
16. C.F. McKee, J.H. Taylor: Astronomy and Astrophysics in the New Millennium, Washington DC, National Academy Press (2000)
17. J. Trauger, A. Hull, D. Backman, et al.: Eclipse: A Mission Concept for a Coronographic Imaging Survey of Nearby Planetary Systems, 35th meeting DPS September (2003)
18. M. Clampin, H.C. Ford, G. Illingworth, et al.: Jovian Planet Finder: Imaging Extra-Solar Planets, AAS 199th meeting Washington (2002)
19. R.G. Lyon, D.Y. Gezari, G.J. Melnick, et al.: Extrasolar planet imager (ESPI) for space-based Jovian planetary detection, Proc SPIE **4860**, 45 (2003)
20. D.Y. Gezari, P. Nisenson, et al.: ExPO: a Discovery-class apodized square aperture exo-planet imaging space telescope concept, Proc SPIE **4860**, 302 (2003)
21. W.C. Danchi, D. Deming, M.J. Kuchner, et al.: Detection of close-in extrasolar giant planets using the Fourier-Kelvin stellar interferometer, ApJ **597**, L57 (2003)
22. B. Mennesson, M. Shao, E. Serabyn, et al.: Optical Planet Discoverer: how to turn a 1.5-m class space telescope into a powerful exo-planetary systems imager, Proc SPIE **4860** (2003)
23. O. Guyon: Phase-induced amplitude apodization of telescope pupils for extrasolar terrestrial planet imaging, A&A **404**, 379 (2003)

24. C.J. Copi, G.D. Starkman: The Big Occulting Steerable Satellite (BOSS), ApJ **532**, 581 (2000)
25. N. Woolf, et al.: Path to Life Finder, NASA Institute for Advanced Concepts (2001)
26. L. Arnold, S. Gillet, O. Lardière, et al.: A test for the search for life on extrasolar planets: Looking for the terrestrial vegetation signal in the Earthshine spectrum, A&A **392**, 231 (2002)
27. P.L. Bender, R.T. Stebbins: Multiresolution-Element Imaging of Extrasolar Earth-Like Planets, JGR **101(E4)**, 9309 (1996)
28. P. Riaud, A. Boccaletti, S. Gillet, et al.: Coronographic search for exo-planets with a hypertelescope I. In the thermal IR, A&A **396**, 345 (2002)
29. S. Gillet, P. Riaud, O. Lardière, et al.: Imaging capabilities of hypertelescopes with a pair of micro-lens arrays, A&A **400**, 393 (2003)
30. A. Labeyrie: Exo-Earth Imager for Exoplanet Snapshots with Resolved Detail, in Working on the Fringe: Optical and IR Interferometry from Ground and Space, ASP Conf. Ser. 194, 7 (1999a)
31. A. Labeyrie: Snapshots of Alien Worlds: The Future of Interferometry, Science **285**, 1864 (199b)

Down to Earths, with OWL

O.R. Hainaut, F. Rahoui, and R. Gilmozzi

European Southern Observatory, Casilla 19001, Santiago, Chile

Abstract. Realistic models of Extremely Large Telescopes (ELTs), including adaptive optics system and segmented mirrors, ranging from 10 to 100 m diameter have been used to simulate observations of extra-solar systems. It appears from these simulations that a 100 m diameter OWL will permit detailed observations of a large number of Extra Solar Planets (ESPs), including Earth-like, a 60 m would be much more limited, and a 30 m could observe ESPs only if we are lucky enough to find such objects in the very near neighborhood.

1 Introduction

Currently, about 120 ESPs have been discovered by radial velocity methods, and a few additional ones by transits, demonstrating that the planetary systems are more common and diverse than suspected earlier. It is expected that thousands of planetary systems, with broad mass and orbit distributions, will be discovered within 10-15 yrs (see [1,2] for reviews). By that time, some Extremely Large Telescopes (ELTs) should have become available. We study here the capabilities of these telescopes for performing physical studies of the ESPs.

2 Observational Challenges

The magnitude of an earth at 100 pc is $V \sim 32$ and the separation from its star is $0\farcs010$. This range of magnitudes is well within the reach of OWL (both for photometry and spectroscopy), and that the separations between the star and the planet are not particularly challenging. These, however, combined with the magnitude contrast between the planet and its star, makes ESPs a challenge for the instrumentation.

While the instrument modeled in this paper is a simple AO system, it is expected that planetary observations will make use of contrast enhancing methods, which are currently either already available, or are under development. As of today, the most promising are the following.

- Classic coronography: a focal mask stops the light from the star, and a Lyot pupil stop decreases the light diffracted by the spider and the mirror edges.
- Nulling interferometry: the coherent light from the star is split in two beams that interfere destructively, while the light from the planet (not coherent with the star light) does not interfere.

- Extreme Adaptive Optics (xAO, which correct many more aberrations than current AO systems), possibly combined with Multi-Conjugated Adaptive Optics (MCAO, several natural and laser reference stars are analyzed to re-build and correct the 3D turbulence profile).
- Simultaneous Differential Imaging: the target is observed simultaneously at two (or more) nearby wavelengths, between which it presents a very strong contrast (e.g. in and out the CH4 bands for a Jupiter-like planet). As the images are obtained simultaneously, the PSF –including the speckles– are identical and subtract perfectly. This method is already in use on NaCo at the VLT [3]. More advanced implementations will image the target at multiple wavelengths, and can make use of the polarization of the target.

3 Observations

ESO's OWL design [4] is used as template telescope. The ESO Adaptive Optics (AO) team generated a set of realistic Point Spread Functions (PSF) using a full model of the telescope [5], including segmented primary and secondary mirror, atmosphere turbulence, and an model AO system with one single deformable mirror, such as one we would be able to build today. We select the most appropriate PSF from these, and perform the following steps.

- The PSF is scaled to the considered wavelength and telescope diameter. The broad wing profile is modified in order to obtain the desired Strehl ratio.
- Copies of the resulting PSF are normalized to the flux of the Sun, Jupiter and the Earth at the considered distance, geometric parameters and wavelength. All the results described in this paper refer to the maximal elongation, i.e a 50% flux decrease, in the geometric approximation.
- The PSFs are shifted to match the angular distance between the star and the planets and are co-added, and a sky background is added, resulting in a noise-less image. The planet positions are recorded.
- Poissonian photon noise is added to the frame, resulting in a realistic image as would be produced by the telescope. The noise actually added is multiplied by 2 in order to account for the effect of a PSF subtraction and residual flat-fielding error. Such an image is presented at Fig. 1
- The flux and noise at the position of the planet are measured (flux in a $1.22\lambda/D$ diaphragm, noise in a sky annulus) and recorded.
- The parameter space is then scanned: images are generated and analyzed for different telescope sizes, Strehl ratio, planet distances, wavelengths, etc.

4 Results

Figure 2 displays the SNR variations with the planet distance and the strehl ratio $s = 0.7$ in the V band, for three telescope diameters. The total exposure time was set to 100 ks, which is the practical limit for a ground based telescope

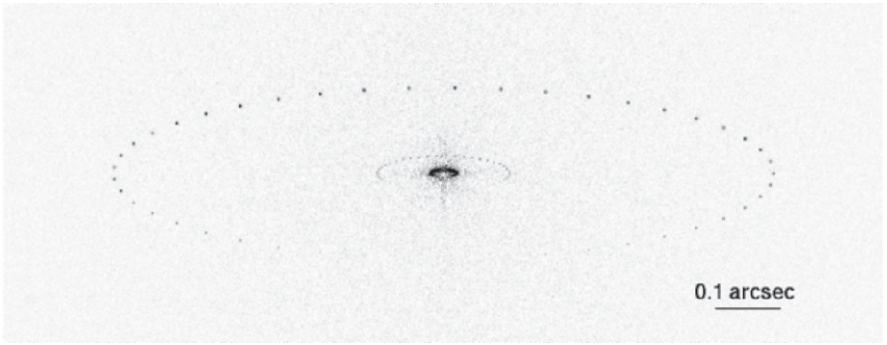


Fig. 1. A PSF-subtracted, 100 ks exposure with a 100 m OWL, on an hypothetical system at 10 pc. A jupiter and an earth have been put at several positions on their 15^0 obliquity orbit in order to illustrate the phase effect.

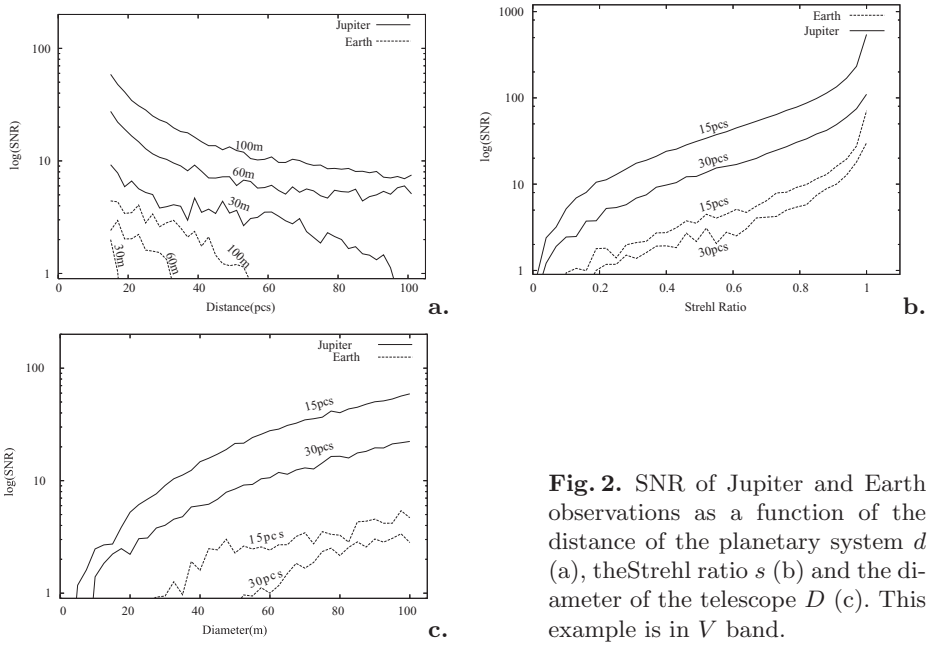


Fig. 2. SNR of Jupiter and Earth observations as a function of the distance of the planetary system d (a), theStrehl ratio s (b) and the diameter of the telescope D (c). This example is in V band.

(corresponding typically to 3n of observations). The noisy aspect of the curves reflect the fact that they present real measurement of noisy data, and not an analytical model

For positional measurements, simple detections are sufficient (SNR $\sim$ 3). However, other methods are likely to provide the planet orbital parameters. For photometric measurements, the SNR should be of the order of a few units (5-10 minimum), while to permit low resolution spectroscopic measurements to be performed, equivalent imaging SNR must be of at least a few tens. Table 1

Table 1. Limit distance for planet observations and corresponding number of observable stars. Exposure time is 100 ks, with $s = 0.7$, except for the earth spectroscopy, which are obtained with $s = 0.9$.

Telescope	Jupiter Spectroscopy		Earth Photometry		Earth Spectroscopy	
D	d	N.stars	d	N.stars	d	N.stars
100 m	60 pc	800	50 pc	460	28 pc	81
60 m	35 pc	150	27 pc	72	7 pc	3
30 m	15 pc	12	15 pc	12	1 pc	-

summarizes the limit distance at which measurements are possible. It is interesting to see that the SNR values obtained by Angel [6], from a detailed analytical analysis of the same problems, are comparable to ours.

An important parameter is the number of stars that will be observable within these SNR-driven distant constraints. Indeed, at this point, we have no valid statistic for the frequency of planets. It is therefore critical that a large number of stars be observable in order to have a chance to have some targets to study. In order to quantify this, the distribution of single G-stars has been extrapolated from various catalogs of nearby stars. In what follows, we consider a telescope located at the latitude giving the largest sample, i.e around 20–30^0South. Table 1 lists the number of stars reachable for the various types of observations. It appears that a 100 m telescope will give access to a large enough sample of stars to perform a comfortably statistically significant contribution to the study of ESPs. On the other hand, for a 30 m telescope to observe ESPs would imply that we would need to be very lucky to have some very nearby planets. It is also interesting to note that the simulation indicates that the SNR varies as D^2 when the planet appears very close to the star (i.e. in the inner PSF), while this drops to D when the planet appears in the outer wings. Consequently, the exposure time required to reach a given SNR will grow as D^4 for inner planets: a $D = 100$ m OWL will detect the same planet 120 times faster than a 30 m telescope. More detailed results and simulations will be presented in [7].

References

1. M. Perryman, *this volume*
2. M. Perryman: Rep. Prog. Phys. **63**, 1209 (2000)
3. M. Hartung, L. Close and R. Lenzen: *ESO Press Release 09/04* (2004)
4. E. Brunetto, P. Dierickx, G. Gilmozzi, M. Le Louarn, F. Koch, L. Noethe, Ch. Vérinaud and N. Yaitskova: 'Progress of ESO's 100-m OWL optical telescope design'. In: *Proceedings 2nd Bäckaskog Workshop on ELTs* (2004)
5. M. Le Louarn, Ch. Verinaud and N.Yaiskova: *priv.comm.* (2004)
6. R. Angel: ASP Conf. Series, **294**, eds. E. Deming S. Seager, p. 543 (2003)
7. O.R. Hainaut, F. Rahoui and R. Gilmozzi: *in prep.* (2004)

High-Precision Radio Astrometry: The Search for Extrasolar Planets

J.C. Guirado[1] and E. Ros[2]

[1] Departamento de Astronomía, Universidad de Valencia, 46100 Burjassot, Valencia, Spain
[2] Max-Planck-Institut für Radioastronomie, Auf dem Hügel 69, 53121 Bonn, Germany

Abstract. High-precision astrometry, applied to extrasolar planet detection, promises to be the most suitable technique to complement the increasing population of exoplanets detected by radial velocity surveys. At radio-wavelengths, present ground-based arrays already provide astrometric precisions at μas levels, comparable to those planned by future space-based instruments. The necessary boost in sensitivity will come from future instruments, such as the Square Kilometer Array, which will provide both the sensitivity and resolution needed for a survey of stars to contribute significantly to the planetary search.

1 Introduction

Radial velocity techniques, accurate to $3\,\mathrm{m\,s^{-1}}$ [2], have proved to be extraordinarily effective in detecting very low mass objects orbiting nearby stars. At the time of writing, the number of stars with planetary companions is over 120 [11], a remarkable number, especially when compared with the fewer detections resulting from other methods. Among these methods, high-precision astrometry promises to be a powerful technique that necessarily will contribute significantly to increase the census of exoplanets. Astrometry is the only technique that provides the mass of the companion without coupling with the orbit inclination; further, in contrast to radial velocity measurements, astrometry favors the detection of planets with longer periods and larger distances from the host star (orbits similar to those in our solar system) filling regions of the orbital space not reachable by Doppler techniques. If radial velocity is the technique of the present for detecting planets, the expected μas-precision of future astrometric space-based projects such as SIM [14] or GAIA (Gilmore, this volume) gives support to the idea that astrometry will be the technique of the future.

2 Radio Astrometry: High-Precision vs Sensitivity

Ground-based astrometry at radio wavelengths provides comparable precisions to those planned by the above-mentioned space missions. For twenty years, very long baseline interferometry (VLBI) techniques have been able to determine the positions of celestial bodies with μas precision (Marcaide & Shapiro 1983). Accordingly, a number of astronomical events have been discovered/tested via

radio astrometry (see [10] for a review of recent achievements), including: the relativistic displacement of a distant star due to Jupiter gravitational deflection [13], the proper motion and parallax of pulsars and the Galactic Center [9], the absolute kinematics of extragalactic radio sources [1], [8], [3], or the establishment of a link between the HIPPARCOS and radio reference frames [7].

The high precision of VLB interferometers is related to their high resolution by the following expression (e.g., [6]):

$$\sigma = \frac{1}{2\pi}\frac{1}{\mathrm{SNR}}\frac{\lambda}{D}$$

where SNR is the signal-to-noise ratio of the observed source, λ is the observing wavelength, and D is the interferometer baseline length. Even for a modest detection of SNR$\sim$15 on a modest baseline of $D = 3000\,\mathrm{km}$, the resolution is below $10\,\mu\mathrm{as}$ at $\lambda = 1.3\,\mathrm{cm}$.

However, there are some caveats that prevent VLBI astrometry achieving such high precisions for planetary searches. First, the poor radio emission of the stars, in general much below the sensitivity limit of most of interferometers. Hence, candidate stars for extrasolar planets at radio wavelengths are scarce. Second, the theoretical precision given above is hardly achieved; some undesired contributions (namely, imperfect time-extrapolation of the interferometric phases, unmodelled contribution of the troposphere and ionosphere, and variable structure of the target and reference source) affect the interferometric phases which, in turn, degrade the precision by, typically, one order of magnitude.

VLBI phase-reference techniques (e.g., [6]) overcome partially this situation; by interleaving observations of an angularly nearby strong extragalactic source, the coherent integration time on the radio star increases from minutes to hours, with a corresponding improvement in sensitivity. In addition, since the main observable used is the interferometric differential phase, systematic effects are partially cancelled out.

Using this technique, and with present VLBI resources, a long-term astrometric program was initiated to refine the kinematics of nearby, single, flare stars, and reveal possible motions resulting from the gravitational interaction of unseen low mass companions [5]. From the very active, well-known flare M dwarfs, these authors selected those placed within 10pc of the Sun, detected previously at least with connected interferometers at a flux density of 1 mJy or more. The VLBI array used was largely dominated by the baseline DSS63-Effelsberg, which provides a sensitivity of 0.4 mJy (5hr integration time at 8.4 GHz) and an astrometric precision of $\sim$0.3 mas. Multi-epoch detections of some of the stars of the sample, such as EV Lacertae, show the feasibility of this program to detect companions down to 1 Jupiter mass. Orbital motions smaller than $\sim$1 mas amplitude are not expected to be detectable due to instabilities of the surface of these flare stars. In practice, this fluctuating error will dominate the standard deviation of the relative position of the radio star. The use of short arrays for radio star astrometry already provided the detection of a previously unseen low-mass object around the star AB Doradus [4].

3 The Contribution of New Instruments

Further improvements in stellar astrometry are limited by sensitivity, rather than by resolution. New instruments at radio wavelengths, such as the planned Square Kilometer Array (SKA; see Ekers, this volume), will boost the sensitivity far below the μJy level, to the order of tens of nJy using phase-referencing (see Fig. 1). With this sensitivity, the number of radio stars detected will increase from hundreds to millions. In particular, the thermal emission of solar-type stars within tens of parsecs, preferred targets for extrasolar planets, could be detected.

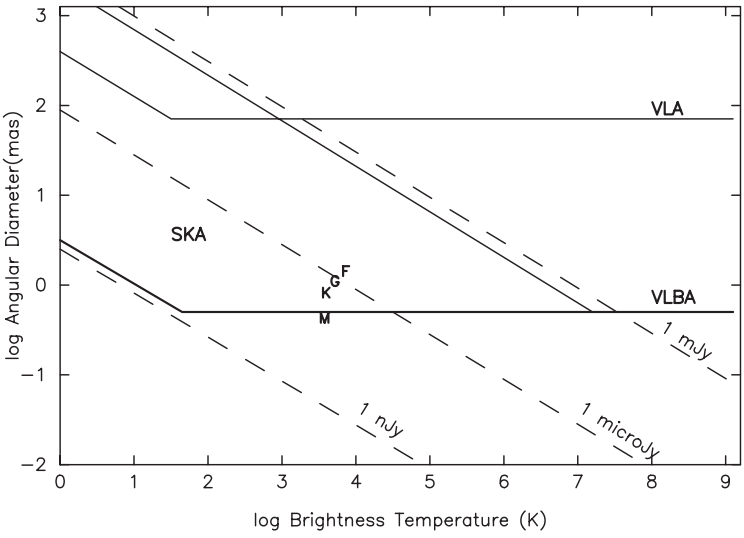


Fig. 1. 20 GHz sensitivity and resolution of interferometers as a function of the brightness temperature. Note the position of the radio emission of FGKM-type stars, if placed at 10 pc. Thermal emission of solar-types stars can be detected to within tens of parsecs (after [12]).

For a significant contribution to the astrometric search for exoplanets, the precision of the differential measurements should be at the μas level. This goal is achievable for new instruments, if they can reach intercontinental resolution, matching the present VLBI capabilities; also, multiple fields of view will be necessary to make simultaneous observations of the target star and the reference source, which will result in a complete cancellation of unmodelled (time-dependent) atmospheric effects (emulating μas-precise in-beam astrometry carried out with present VLBI arrays). Thermal emission from the stars is much more centered, and stable, on the star position than the flaring emission, avoiding the dominating source of fluctuating errors in the astrometric determinations. The combination of all items above will ensure μas-precise star positions.

Finally, although the cooperation of different techniques (radial velocity, ground-based, and space-based astrometry) will be essential for bona-fide planet detections, ground-based projects, such as SKA, are extremely important to keep monitoring the orbit of planet candidates, especially given the shorter lifetime of space projects.

References

1. N. Bartel, T.A. Herring, M.I. Ratner, M.I., et al.: Nature **319**, 733 (1986)
2. R.B. Butler, G.W. Marcy, E. Williams, et al.: PASP **108**, 500 (1996)
3. J.C. Guirado, J.M. Marcaide, A. Alberdi, et al.: AJ **110**, 2586 (1995)
4. J.C. Guirado, J.E. Reynolds, J.-F. Lestrade, et al.: ApJ **490**, 835 (1997)
5. J.C. Guirado, E. Ros, D.L. Jones, et al.: 'Searching for low mass objects around nearby dMe radio stars'. In: *Proceedings of the 6th EVN Symposium*, E. Ros et al. (eds.) (Bonn, Germany: MPIfR), pp. 255–258 (2002)
6. J.-F. Lestrade, A.E.E. Rogers, A.R. Whitney, et al.: AJ **99**, 1663 (1990)
7. J.-F. Lestrade, R.A. Preston, D.L. Jones, et al.: A&A **344**, 1014 (1999)
8. J.M. Marcaide, I.I. Shapiro: AJ **88**, 1133 (1983)
9. M.J. Reid, A.C.S. Readhead, R.C. Vermeulen, R.N. Treuhaft: ApJ **524**, 816 (1999)
10. E. Ros: 'High Precision Astrometry'. In: *Future directions in high resolution astronomy: A Celebration of the 10th Anniversary of the VLBA*, eds. J.D. Romney and M.J. Reid (San Francisco: ASP) in press (2004) [arxiv:astro-ph/0308265]
11. J. Schneider: *The Extrasolar Planets Encyclopaedia*, http://www.obspm.fr/encycl/encycl.html
12. A.R. Taylor: In: *Sub-arcosecond Radio Astronomy*, eds. R.J. Davis, R.S. Booth, (Cambridge: CUP), p. 1 (1993)
13. R.N. Treuhaft, S.T. Lowe: AJ **102**, 1879 (1991)
14. S.C. Unwin, M. Shao: SPIE **4006**, 754 (2000)

The CHEOPS Project: Characterizing Exoplanets by Opto-infrared Polarimetry and Spectroscopy

M. Feldt[1], R. Gratton[2], S. Hippler[1], H.M. Schmid[3], M. Turatto[2], R. Waters[4], and T. Henning[1]

[1] Max-Planck-Institut für Astronomie, Königstuhl 17, D-69117 Heidelberg, Germany
[2] Osservatorio Astronomico di Padova, Vicolo dell'Osservatorio 5, I-35122 Padova, Italy
[3] Institut für Astronomie, ETH Zentrum, CH-8092 Zürich, Switzerland
[4] Sterrenkundig Instituut "Anton Pannekoek", Universiteit van Amsterdam, Kruislaan 403, NL-1098 SJ Amsterdam, the Netherlands

Abstract. We are currently investigating the possibilities for a high-contrast, adaptive optics assisted instrument to be placed as a 2nd-generation instrument on ESO's VLT. This instrument will consist of an "extreme-ao" system capable of producing very high Strehl ratios, a contrast-enhancing device and an integral-field spectroscopic detection system. It will be designed directly take images of sub-stellar companions of nearby ($< 100\,\mathrm{pc}$) stars. We will present our current design study for such an instrument and discuss the various ways to tell stellar from companion photons. Results of our latest simulations regarding the instrument will be presented and the expected performance discussed. Derived from the simulated performance we will also give details about the expected science impact of the planet finder. This will comprise the chances of finding different types of exo-planets, the scientific return of such detections and follow-up examinations, as well as other topics like star-formation, debris disks, and planetary nebulae.

1 Introduction

The success story of the VLT/VLTI on Cerro Paranal in Chile encouraged ESO to set out on even more ambitious missions with a set of 2nd-generation instruments. One of these instruments is to become the VLT "Planet Finder", which aims at the direct detection of extra-solar planets. With this instrument, the key questions of the search for other planetary systems, evidence for the existence of exo-planets in habitable zones, and the fundamental understanding of how planets form can for the first time be answered by a direct observation.

After a call for preliminary proposals issued on November 15th 2001 by ESO, the CHEOPS consortium formed and responded with a preliminary proposal by February 2002. A second proposal for such an instrument was submitted by a team led by the Laboratoire d'Astrophysique de l'Observatoire de Grenoble. In May 2003, 2 contracts were signed with ESO, launching two parallel 18 month phase-A studies for a planet finder instrument at the VLT. This presentation will briefly summarize the phase-A result of the CHEOPS team.

2 Science Case

In the view of the consortium, CHEOPS (CHaracterizing Exo-planets by Opto-infrared Polarimetry and Spectroscopy) is an integrated project that contains the development of the instrument, and the preparation and execution of a dedicated science programme, aimed at the direct detection of several planets in each of three distinct age groups (few 10^7 yr, few 10^8 yr, and $> 10^9$ yr). The science programme is planned to be executed partly in GTO awarded to the consortium as compensation for building the instrument. Due to the large number of targets required for the detection of a statistically relevant sample of planets, the CHEOPS group will support a wider, comprehensive ESO survey of several hundred targets.

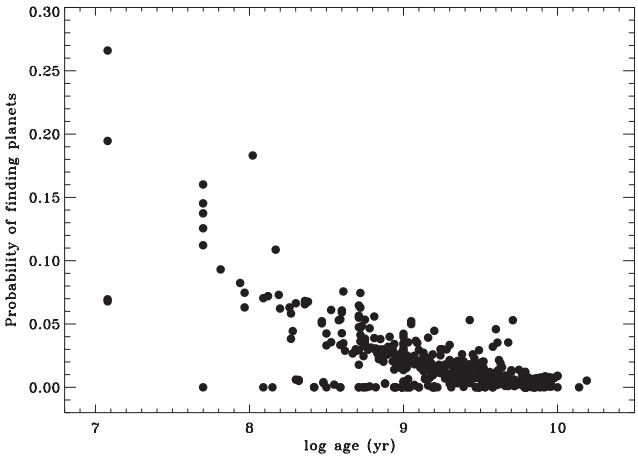


Fig. 1. Probability of finding a planet around a star from our current target sample versus the age of that star.

Detailed simulations were performed to asses the probability of planet detection using CHEOPS (see Fig. 1), considering the observed frequency of planets and the distribution of mass, orbital period, eccentricity of the planets resulting from radial velocity surveys, the luminosity contrast from theoretical models, and the detectability relation for CHEOPS derived from instrumental simulations. The simulation is performed for each star in the preliminary database of potential targets, with the goals to select the best targets and evaluate the properties of planets detectable with CHEOPS. Both IFS and ZIMPOL channel were considered. These simulations show that we can expect the detection of three planets in the three age bins defined above. The overall probability to detect at least one planet in the GTO survey is 95%.

The instrument optimized to achieve these goals will of course produce an enormous amount of data for faint objects and structures close to bright stars.

This is particularly true for brown dwarfs, jets, and accretion and debris disks - the latter one being a prerequisite for the Darwin mission.

3 Instrument Concept

The instrument concept is based upon the principles of maximum stability, simplicity, modularity and upgradeability. Three basic modules will be mounted at the Nasmyth focus of the VLT: The common fore optics that contains an extreme AO system and stabilizes the total instrumental polarization below 1%, and the two differential imagers, ZIMPOL and the IFS. The AO is extreme only in terms of actuator number and speed ($\sim$ 1600 actuators operating at 2 kHz). This otherwise standard-design system will deliver Strehl ratios between 0.4 and 0.85, depending on wavelength, conditions, and observing mode. ZIMPOL is an imaging polarimeter working between 0.65 µm and 0.95 µm. Due to its innovative lock-in technique – using a fast modulation of the polarization signal and a corresponding, on-chip de-modulation, it can achieve polarimetric precisions better than 10^{-5} on a localized signal measured differentially against a semi-smooth background. The IFS is a low-resolution integral field spectrograph working from 0.95 µm to 1.7 µm. Longer wavelengths have been excluded since they do not promise to increase the chances of detection. This simplifies the optical and mechanical design considerably.

All three modules are located on a common bench, fixed to the Nasmyth platform to ensure maximum mechanical stability. Detailed optical and mechanical designs of all three modules, plus the instrument electronics and software demonstrate that the instrument is feasible with current day technology and can easily be integrated into the existing VLT environment.

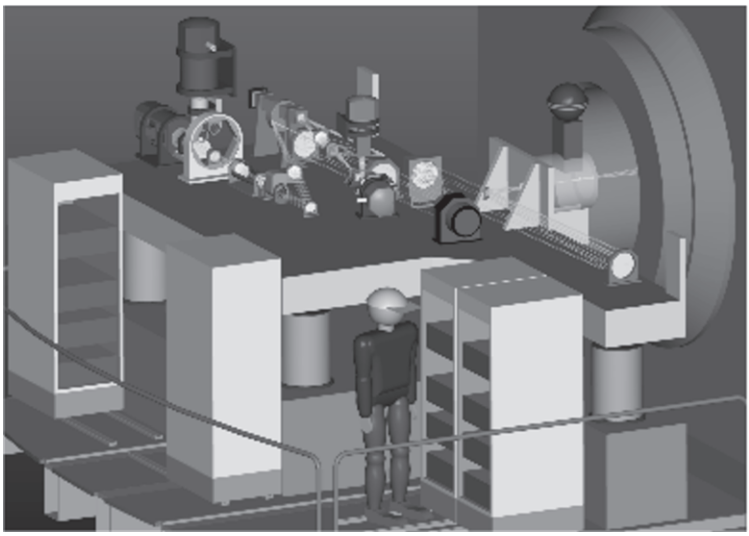


Fig. 2. Concept of CHEOPS at the VLT Nasmyth focus.

4 Performance

Our comprehensive analysis shows that critical issues and components can be controlled. It arrives at detailed end-to-end simulations of planet detections as shown in Fig. 3. This figure shows that the IFS channel of CHEOPS will be able to detect intermediate age planets around solar-type stars at orbits with radii greater than $r > 24$ AU out to 40 pc. It also shows that ZIMPOL observing Jupiter in orbit around α Cen can reach very high signal-to-noise ratios and could in fact detect planets of a few Earth masses around that star. There is also no doubt that the planet around ϵ Eri can be detected by both channels – IFS and ZIMPOL – at high SNR.

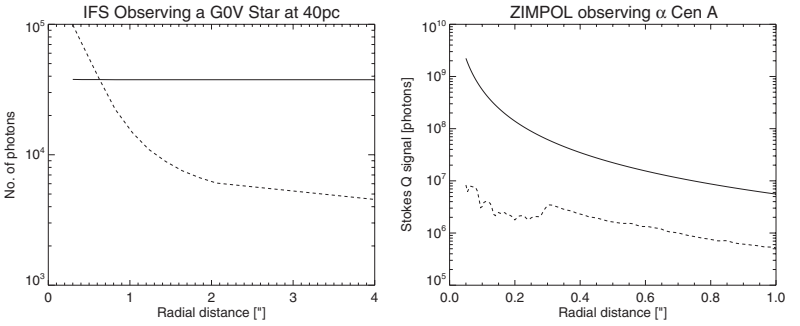


Fig. 3. Planet signal and residual noise curves. **Left:** IFS, the solid curve gives the planetary signal, the dashed curve gives 5 times the predicted residual noise. The planet of age 1 Million years can be detected from $\sim 0\farcs6$. **Right:** ZIMPOL observing α Cen A. Again the solid curve represents the planetary signal and the dashed curve the residual noise. The planet size corresponds to that of Jupiter, the assumed polarization is $P(80^\circ) = 0.5$.

5 Project Plan

The project plan currently foresees a start of phase B of the CHEOPS project in May 2005, and commissioning of the instrument on Paranal in late 2009. This period is followed by a four-year core survey by the CHEOPS consortium lasting until 2013. The consortium comprises the Max Planck Institute for Astronomy in Heidelberg as the P.I. institute, Padova Observatory (INAF-OPD), the Institute for Astronomy at ETH Zurich, and the University of Amsterdam (UvA). The total hardware costs are estimated to be 5 M€, the total manpower at about 1,300 person months.

Towards High-Precision Astrometry: Differential Delay Lines for PRIMA@VLTI

R. Launhardt[1], Th. Henning[1], D. Queloz[2], and A. Quirrenbach[3]

[1] Max Planck Institut für Astronomie, Königstuhl 17, D-69117 Heidelberg, Germany
[2] Observatoire de Genève, 51 Ch. des Maillettes, CH-1290 Sauverny, Switzerland
[3] Sterrewacht Leiden, P.O. Box 9513, NL-2300 RA Leiden, The Netherlands

Abstract. Deriving orbital parameters and masses of extrasolar planets by means of measuring the variation of the host star positions requires an astrometric accuracy of 10 microarcsec. To achieve this goal, a consortium with partners from Germany, the Netherlands, and Switzerland, in agreement with ESO, will enhance the PRIMA facility at the VLTI with Differential Delay Lines (DDLs). We give an overview of the PRIMA-DDL project, which consists of developing hardware, astrometric operation tools, and data reduction software, and outline the anticipated astrometric planet search program to be carried out with this facility.

1 Narrow-angle Astrometry with the VLTI

PRIMA, the instrument for Phase Referenced Imaging and Micro-arcsecond Astrometry is currently being developed at ESO. PRIMA will implement the dual-feed capability at the VLTI for both UTs and ATs to enable simultaneous interferometric observations of two objects that are separated by up to 1 arcmin, without requiring a large continuous field of view. PRIMA will be composed of four major sub-systems: Star Separators, Differential Delay Lines (DDLs), a laser metrology system, and Fringe Sensor Units (FSU). The system is designed to perform high-accuracy (10 μas) narrow-angle differential astrometry in K-band with two FSUs and, with one FSU in combination with AMBER or MIDI, phase-referenced aperture synthesis imaging. The purpose of the DDLs in differential astrometry is to increase the astrometric accuracy by separating the large OPD correction terms which are common for the two stars from the small differential terms, and to increase the sensitivity by stabilizing the fringe pattern (in a closed loop with the laser metrology) and thus allow for longer integrations.

2 DDLs and Astrometric Software for PRIMA

In order to speed up the full implementation of the 10 μas astrometric capability of the VLTI and to carry out a large astrometric planet search program, a consortium lead by the Observatoire de Genève (Switzerland), the Max Planck Institute for Astronomy in Heidelberg (Germany), and the University of Leiden/NOVA (The Netherlands) agreed with ESO to build and deliver the Differential Delay Lines for PRIMA (see Fig. 1) and to provide all necessary operation

and software tools to perform narrow-angle astrometry at the 10 μas level. This includes developing and building all the DDL hardware, the construction and analysis of an astrometric error budget, the establishment of an operations and calibration strategy, and the development of observation preparation and data reduction software:

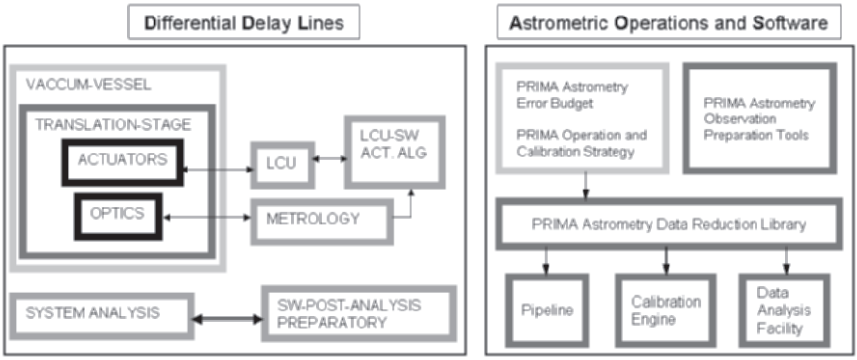


Fig. 1. The PRIMA-DDL project: breakdown of hard and software components

3 The Astrometric Planet Search Program

When completed in 2007, we will use the upgraded PRIMA facility to detect and characterize extra-solar planets through the reflex motions of their host stars in the plane of the sky. Two core programs are planned to be carried out over a duration of at least three years:

1) Observe all stars with known radial-velocity planets that are in reach of the VLTI and have a suitable phase reference star. We will resolve the $\sin i$ uncertainty of the planet masses and thus constrain the uncertain upper end of the planetary mass function. For stars with multiple planetary systems we will derive the relative inclination of the orbits. We will follow up long-term radial velocity trends and search for new planets in longer-period orbits for which astrometry is more sensitive than the radial velocity method.

2) Planet search around stars of different mass and evolutionary status without known planets. The search for planets by the radial-velocity technique is restricted to stars with narrow and stable spectral lines, thus excluding A and most F stars with their broad spectral lines as well as pre-main sequence stars. Our astrometric planet search program will explicitly include such stars. For nearby (< 20 pc) late-type (F-M) main sequence stars, the primary new discovery space opened by such an astrometric facility would be Saturn down to Uranus-mass planets with orbital periods of a few years ($a = 1$–5 AU).

Author Index

Ade, P. 45
Agudo, I. **179**
Aguillar, M. 227
Alcaraza, J. 227
Allen, M.G. 81
AMS Collaboration 111
Arshakian, T.G. **181**
Asaki, Y. 37
AstroGrid Team 81
Atkinson, D. 45
Audley, M. **45**
AVO Team 81

Bach, U. 179
Bachiller, R. **35**
Bajkova, A.T. 109
Balega, Y. 63
Bardelli, S. 141
Baruffolo, A. 59
Bastien, P. 45
Beck, R. **103**
Beckert, T. 63
Berdugo, J. 227
Bergeron, J. 95
Bertoldi, F. 229
Beskin, G.M. 115
Bintley, D. 45
Bisnovaty-Kogan, G. 115
Boller, T. **163**
Bondar, S. 115
Bower, G. **129**
Bremer, M. 179, 189
Bremer, M.N. **125**
Brigida, M. **65**, **67**
Brinks, E. 47
Brožek, V. 75

Carrasco, L. 47
Casaus, J. 227
Cernicharo, J. 53
Chuprikov, A. **183**
Cliffe, M. 45
Cresci, G. 59
Curran, S. **91**

Dallacasa, D. 141
Della Valle, M. **95**
de Ruiter, H.R. 139
Díaz, C. 227
Dierickx, P. 19, 95
Diolaiti, E. 59
Doeleman, S. 189
Doriese, R. 45
Driebe, T. 63
Dubrovich, V.K. **109**
Dunare, C. 45
Duncan, W. 45

Edwards, P.G. 37
Ekers, R.D. **3**
Ekkart, A. 51, 55
Ellis, M. 45
ESPRIT Team 53
Estalella, R. 225

Fagg, H. 189
Falomo, R. 59
Falvard, A. 69

Favuzzi, C. 65, 67
Feldt, M. **261**
Felli, M. 229
Feretti, L. 103
Fich, M. 45
Fusco, P.G. 65, 67

Gaensler, B. 103
Gaessler, W. **55**, 59
Gallo, L. 163
Gannaway, F. 45
Gao, X. 45
Gargano, F. 65, 67
Garrett, M. **171**
Garrington, S.T. 81
Giacintucci, S. 141
Giglietto, N. 65, 67
Gilmore, G. **205**
Gilmozzi, R. **19**, 95, 253
Giordano, F. 65, 67
Giovannini, G. 187
Giraud, E. **69**
Giroletti, M. **187**
GLAST LAT Collaboration 77
Goldsmith, P.F. **209**
Gómez, J.L. 179
Gómez de Castro, A.I. **219**
Gostick, D. 45
Graham, D.A. 179, 189
Gratton, R. 261
Gregorini, L. **133**, 137
Greve, A. 189
Grewing, M. 179
Guirado, J.C. **257**
Guirin, I. 183
Gurvits, L.I. 37

Hainaut, O.R. **253**
Halpern, M. 45
Han, S.-T. 41
Harrison, P.A. 81
Hengstebeck, T. **71**
Henning, Th. 261, 265
Herbst, T.M. 55
HESS Collaboration 175
Hilton, G. 45
Hippler, S. 261
Hirabayashi, H. **37**
Hodson, T. 45
Hofman, K.-H. 63
Holland, W. 45
Hook, I. **121**
Hudec, R. **73**, **75**, **79**
Hunt, C. 45

Inneman, A. 73, 75
Inoue, M. 37
Irwin, K. 45

Jamrozy, M. 133, 135

Kadler, M. **187**
Kalekin, O. 71
Kaltcheva, N. **223**
Kameno, S. 37
Kellermann, K.I. **167**
Kelly, D. 45
Kelz, A. **57**
Kerp, J. 187
Khaikin, V.B. 109
Kim, H.-G. **41**
Klein, U. 133, 135, 137
Knude, J. 223
Kramer, M. **87**
Kycia, J. 45

Lamb, R. 81
Lanciotti, E. 111, 227
Launhardt, R. **265**
Lavalle, J. 69
Lehnert, M.D. 125
LINC-NIRVANA Team 55
Lobanov, A.P. 37, **39**, **147**
Lombini, M. **59**
Loparco, F. 65, 67
López, R. **225**

MacIntocsh, M. 45
Mack, K.-H. 133, 135, **137**
Madau, P. 95

Mañá, C. 227
Mannucci, F. 59
Marangelli, B. 65, 67
Marín, J. 227
Martínez, G. 227
Mazziotta, M.N. 65, 67
McGregor, 45
Menten, K.M. 229
Merck, M. 71
Mirizzi, N. 65, 67
Mirzoyan, R. 71
Mitchell, G. 45
Mochizuki, N. 37
Mollá, M. **227**
Montgomery, D. 45
Mountain, M. 19
Murata, Y. 37
MUSE Coonsortium 57
Muxlow, T.W.B. 81

Naylor, D. 45

OAN Staff 35
Ohnaka, K. 63
Omont, A. 229
OPTICON ELT SWG 121

Padovani, P. 81
Pagels, A. 179
Palomares, C. 227
Panagia, N. 19, 95
Parkes, W. 45
Parma, P. 133, 139
Pavel, N. 71
Peck, A. **49**, **215**
Perryman, M.A.C. **237**
Phillips, R.B. 189
Pina, L. 73, 75
Pisano, G. 45
Popović, L.Č. **191**
Power, R. 81
Prandoni, I. **139**
Preibisch, T. 63
Punch, M. **175**

Queloz, D. 265
Quirrenbach, A. **61**, 265

Raga, A.C. 225
Ragazzoni, R. 55, 59
Rahoui, F. 253
Rainó, S. 65, 67
Rao, P. 141
Reimer, O. **77**
Reintsema, C. 45
Reiprich, T. **113**
Richards, A.M.S. **81**
Riera, A. 225
Robson, I. 45
Rogers, A.E.E. 189
Ros, E. 187, 257
Roth, M.M. 57
Rumyantsev, V. 115

Sadler, E.M. **139**
Sajjad, S. 69
Sánchez, E. 227
Schertl, D. 63
Schieder, R. 51
Schilizzi, R.T. 137
Schinkel, A. 49
Schloerb, F.P. **47**
Schmid, H.M. 261
Schuller, F. **229**
Schweizer, T. 71
Sevilia, I. 227
Shayduk, M. 71
Slysh, V. **231**
SMA Team 49, 215
Smith, I. 45
Snellen, I.A.G. 137
Sohn, B.W. 41
Sonnabend, G. 51
Sornig, S. 51
Spinelli, P. 65, 67
Spyromilio, J. 95
Steinmetz, M. 57
Stirling, A. 81
Straubmeier, C. **51**
Strittmatter, P. 189

Sudivala, R. 45
Sveda, L. 73

Testi, L. 229
Torrentó, A.S. 227
Tsarevsky, G. **115**
Tschager, W. 137
Turatto, M. 261

Ullom, J. 45
Umemoto, T. 37

Vale, L. 45
van Dishoeck, E.F. **201**
van Driel, W. **43**
Vasileiadis, G. 69
Venema, L. 53
Venturi, T. 81, **141**
Vernet, E. 59
Vernet, J. 59
Vetterle, V. 51
Vigotti, M. 137
Vollmer, B. 81

Walker, I. 45
Walton, A. 45
Walton, N.A. 81
Waters, R. 261
Weaver, K.A. 187
Weigelt, G. 55, **63**
Wild, W. **53**
Wilson, T.L. **197**
Winstanley, N. 81
Wirtz, D. 51
Wittkovski, M. 63
Witzel, A. 179, 189
Woodcraft, A. 45

Xompero, M. 59

Zensus, J.A. 147, 179, 187, 189
Zucca, E. 141



ESO ASTROPHYSICS SYMPOSIA
European Southern Observatory

Series Editor: Bruno Leibundgut

L. Kaper, A.W. Fullerton (Eds.),
Cyclical Variability in Stellar Winds
Proceedings, 1997. XXII, 415 pages. 1998.

R. Morganti, W.J. Couch (Eds.),
Looking Deep in the Southern Sky
Proceedings, 1997. XXIII 336 pages. 1999.

J.R. Walsh, M.R. Rosa (Eds.),
Chemical Evolution from Zero to High Redshift
Proceedings, 1998. XVIII, 312 pages. 1999.

J. Bergeron, A. Renzini (Eds.),
From Extrasolar Planets to Cosmology: The VLT Opening Symposium
Proceedings, 1999. XXVIII, 575 pages. 2000.

A. Weiss, T.G. Abel, V. Hill (Eds.),
The First Stars
Proceedings, 1999. XIII, 355 pages. 2000.

A. Fitzsimmons, D. Jewitt, R.M. West (Eds.),
Minor Bodies in the Outer Solar System
Proceedings, 1998. XV, 192 pages. 2000.

L. Kaper, E.P.J. van den Heuvel, P.A. Woudt (Eds.),
Black Holes in Binaries and Galactic Nuclei: Diagnostics, Demography and Formation
Proceedings, 1999. XXIII, 378 pages. 2001.

G. Setti, J.-P. Swings (Eds.)
Quasars, AGNs and Related Research Across 2000
Proceedings, 2000. XVII, 220 pages. 2001.

A.J. Banday, S. Zaroubi, M. Bartelmann (Eds.),
Mining the Sky
Proceedings, 2000. XV, 705 pages. 2001.

E. Costa, F. Frontera, J. Hjorth (Eds.),
Gamma-Ray Bursts in the Afterglow Era
Proceedings, 2000. XIX, 459 pages. 2001.

S. Cristiani, A. Renzini, R.E. Williams (Eds.),
Deep Fields
Proceedings, 2000. XXVI, 379 pages. 2001.

J.F. Alves, M.J. McCaughrean (Eds.),
The Origins of Stars and Planets: The VLT View
Proceedings, 2001. XXVII, 515 pages. 2002.

J. Bergeron, G. Monnet (Eds.),
Scientific Drivers for ESO Future VLT/VLTI Instrumentation
Proceedings, 2001. XVII, 356 pages. 2002.

M. Gilfanov, R. Sunyaev, E. Churazov (Eds.),
Lighthouses of the Universe: The Most Luminous Celestial Objects and Their Use for Cosmology
Proceedings, 2001. XIV, 618 pages. 2002.

R. Bender, A. Renzini (Eds.),
The Mass of Galaxies at Low and High Redshift
Proceedings, 2001. XXII, 363 pages. 2003.

W. Hillebrandt, B. Leibundgut (Eds.),
From Twilight to Highlight: The Physics of Supernovae
Proceedings, 2002. XVII, 414 pages. 2003.

P.A. Shaver, L. DiLella, A. Giménez (Eds.),
Astronomy, Cosmology and Fundamental Physics
Proceedings, 2002. XXI, 501 pages. 2003.

M. Kissler-Patig (Ed.),
Extragalactic Globular Cluster Systems
Proceedings, 2002. XVI, 356 pages. 2003.

P.J. Quinn, K.M. Górski (Eds.),
Toward an International Virtual Observatory
Proceedings, 2002. XXVII, 341 pages. 2004.

W. Brander, M. Kasper (Eds.),
Science with Adaptive Optics
Proceedings, 2003. XX, 387 pages. 2005.

A. Merloni, S. Nayakshin, R.A. Sunyaev (Eds.),
Growing Black Holes: Accretion in a Cosmological Context
Proceedings, 2004. XIV, 506 pages. 2005.

L. Stanghellini, J.R. Walsh, N.G. Douglas (Eds.)
Planetary Nebulae Beyond the Milky Way
Proceedings, 2004. XVI, 372 pages. 2006.

S. Randich, L. Pasquini (Eds.)
Chemical Abundances and Mixing in Stars in the Milky Way and its Satellites
Proceedings, 2004. XXIV, 411 pages. 2006.

A.P. Lobanov, J.A. Zensus, C. Cesarsky, P.J. Diamond (Eds.)
Exploring the Cosmic Frontier
Astrophysical Instruments for the 21st Century.
XXVI, 270 pages. 2006.